LBL-6703

RAMAN SIDESCATTER INSTABILITY IN A NONUNIFORM PLASMA*

Michael Alan Mostrom

Lawrence Berkeley Laboratory
University of California, Berkeley, California 94720

July 15, 1977

ABSTRACT

In the various laser-fusion concepts, an intense electromagnetic wave (the laser) must propagate through an underdense plasma region where it could decay, via the stimulated Raman instability, into a Langmuir plasma wave and a scattered electromagnetic wave. This process could, therefore, scatter a significant fraction of the laser energy before it could be deposited in the plasma. A density gradient, in the direction of laser incidence, localizes the instability to a narrow resonance zone where the local plasma wave frequency approximately equals the difference-frequency between the incident and scattered electromagnetic waves. The narrowness of this zone can strongly inhibit the growth of back- or oblique-scattered electromagnetic waves since they quickly propagate out of their resonance region; however, the density gradient has a much weaker effect on side-scattered waves (which propagate perpendicular to the density gradient) since they remain in their resonance zone until refraction bends them out or they exit through the side of the finite diameter laser beam. Thus, we place particular emphasis on evaluating, in a manner valid for the side scattered electromagnetic waves (which are

at their turning point), the level of exponentiation at which the growth is linearly saturated due to convection of the waves out of their resonance zone. We also determine the general nature and propagation of the scattered electromagnetic waves and obtain approximate values for the resonance zone size and the time required for the above saturation.

Our results are obtained by evaluating the "Green's function" response in time and space for the scattered electromagnetic waves assuming they are initiated by a "delta-function" source. We consider the case where the temporal growth dominates the plasma wave convection. Then the scattered electromagnetic waves are governed by a single second-order Helmholtz differential equation, in the position variable along the density gradient, with a complex potential having two simple zeros (turning points) and one simple pole. The relative position of these three transition points depends on the wave-vector perpendicular to the gradient and the complex frequency of the scattered electromagnetic waves. Using phase-integral (WKBJ) techniques, we obtain for the above differential equation two approximate solutions valid throughout the complex position plane except near the three transition points. These two solutions are used to obtain the spatial response at a given frequency; evaluating the proper inverse Fourier transform of this (in the complex frequency space) then gives the temporal evolution. Although by this method we generally cannot look too close to the turning point, we can

nevertheless follow the temporal evolution of the side-scattered waves before and after they encounter their turning point and, thereby, obtain the net growth.

The resulting Green's function response consists of two parts: (1) propagating and refracting wave-packets growing only while they are in their resonance zone; (2) eigenmodes localized along the density gradient and growing in time. The eigenmodes do not dominate the response until after the side-scattered wave-packets have saturated their growth by refraction out of their resonance zone. By taking into account the convection of the waves perpendicular to the density gradient, we show that the finite laser diameter can typically force an early saturation with the eigenmodes never appearing. This may explain the lack of experimental evidence for Raman side-scattering as opposed to its clear observation in computer simulations with periodic boundary conditions (i.e., infinitely wide laser diameter).

TABLE OF CONTENTS

I. INTRODUCTION

A. Past Work on Raman Instability

1. General Orientation

There are two general approaches toward controlled thermonuclear fusion which involve the use of lasers: (1) laser-pellet fusion where lasers are used to heat and compress a solid fuel pellet; (2) laser heating of a magnetically confined plasma. Several reviews of these approaches are listed under Ref. sec. A. In each approach, the intention is for the incident laser to propagate into the plasma and deposit its energy. In the first case above, the absorption takes place primarily in the denser regions of the plasma via classical inverse bremsstrahlung, resonant absorption, or nonlinear absorptive instabilities - the plasmon-ion decay instability, the oscillating two-stream instability, and the two-plasmon instability. For the second case above, the plasma typically remains far underdense (to the laser), and classical inverse bremsstrahlung is thought to dominate the absorption. However, an intense electromagnetic wave (the laser) propagating through a plasma is known to be subject to two reflective instabilities - stimulated Raman and Brillouin scattering - which could scatter a significant fraction of the incident laser energy before it could be deposited in the plasma. The density regions associated with these processes are shown in Fig. I.1. We will restrict ourselves here to the density region below the quarter critical density point, at which the incident wave frequency

ω_o is twice the local plasma frequency ω_p. Ignoring the forward-scattering modulational instabilities (filamentation, self-focusing), we are left to consider stimulated Raman and Brillouin scattering.

Raman and Brillouin scattering derive their names from the corresponding processes in solid state physics. The electromagnetic pump wave scatters off an ionic disturbance into another electromagnetic wave in Brillouin scattering (Ref. sec. B). If the disturbance is electronic, rather than ionic, we have Raman scattering (Ref. sec. C). Extended to a plasma, the above disturbance becomes an ion-acoustic wave (Ref. sec. D) or a Langmuir electron-plasma wave (Ref. sec. E), respectively.

Brillouin scattering is usually considered to be the most important (and most worried about) reflective instability for laser-fusion experiments due to its theoretically high linear (i. e., convective) and nonlinear saturation amplitudes (Refs. D V; G II, VII; K I, II). However, laser plasma experiments have yet to observe this as a dominant effect (Ref. sec. H), and several proposals have been offered to explain this (Refs. A IV; D IV, VI). Raman scattering has a higher threshold but also a larger growth rate than Brillouin scattering and therefore appears first in typical simulations where both thresholds are exceeded (Refs. K I, III). After nonlinear saturation of the Raman instability by pump depletion and electron trapping (leading to non-Maxwellian tail formation), the Brillouin scattering dominates the simulation until it in turn is nonlinearly

saturated (Refs. D V; G VII; K I-III). However, if this above-mentioned nonlinear pump depletion is due to scattering, and not absorption, then this is not a desirable means of saturating the instability. Furthermore, saturation by Landau damping of the plasma wave (from the Raman decay of the incident wave) would require an electron temperature $T_e \sim 30$ KeV (see Refs. A IV; D V) or equivalently an electron thermal velocity $v_{th}/c \sim 1/4$, and electron trapping would generate electron velocities up to $v/c \sim 1/2$ (see Ref. K II). Thus, both of these latter saturation mechanisms would lead to suprathermal electrons which can detrimentally preheat the core of a pellet (Ref. J I). Hence, a linear (i. e., convective) saturation mechanism would be desirable. In the following work we will concentrate on Raman scattering and several problems that have arisen concerning it. We note, however, that in certain parameter regimes the equations describing Brillouin scattering take on the same mathematical form as the equations used in the Raman analysis (Refs. F VII; G IX) and, therefore, many of our results can be extended to the Brillouin case.

To provide the background for our work on the Raman instability, we first review in detail what is already known (see Ref. sec. E) about the instability in a uniform plasma (sec. I A 2) and how a density gradient alters the behavior (sec. I A 3). For instance, it is known (see Ref. secs. F, G) that a density gradient, in the direction of laser incidence, localizes the instability to a narrow resonance zone where the local plasma wave frequency approximately equals the

difference-frequency between the incident and scattered electromagnetic waves. The narrowness of this zone can strongly inhibit the growth of back- or oblique-scattered electromagnetic waves since they quickly propagate out of their resonance zone (position of zone depends on the frequency of the scattered electromagnetic wave); however, the density gradient has a much weaker effect on side-scattered waves (which propagate perpendicular to the density gradient) since they remain in their resonance zone (position of this zone depends on the wavenumber, perpendicular to the density gradient, of the side-scattered wave) until refraction bends them out or they exit through the side of the finite diameter laser beam. Thus, a density gradient may not provide a sufficiently strong linear (i. e., convective) saturation mechanism for keeping the side-scattered waves under control, and this explains the attention we have given this particular case (e. g., note the title of this paper) even though our work here is valid also for back- and oblique-scattered electromagnetic waves.

To motivate our work on the Raman instability, we next (sec. I B) point out some problem areas (also discussed in sec. I A 3b) where further work - our work here - was necessary for a more complete understanding. To answer the questions we raise in sec. I B, we place particular emphasis on evaluating, in a manner valid for the side-scattered electromagnetic waves (which are at their turning point), the level of exponentiation at which the growth is linearly saturated due to convection of the waves out of their resonance zone. We also determine the general nature and propagation behavior of the

scattered electromagnetic waves and obtain approximate values for the resonance zone size and the time required for the above saturation. We require (and later find, in secs. III, V) that our results correctly reduce to the appropriate known results in the limits of early time (before refraction can become important), zero pump strength (i. e., laser intensity), or infinite nonuniformity scale-length.

In sec. I C, we discuss the physical process behind the Raman instability and the particular model (e. g., linear density profile, fixed ions, no static magnetic field) we have assumed in studying it. A nonuniform static magnetic field, varying along the density gradient but directed along the laser polarization direction, could be included with no change in the basic mathematical form of the equations we solve; however, this is not done here (it was felt to be too distracting) but rather is postponed till a later paper. We further limit our problem (to something manageable) by considering only the case where the plasma wave convection is negligible (e. g., compared with the temporal growth). Then, the scattered electromagnetic waves are governed by a single Helmholtz (or Schrödinger) differential equation, in the position variable along the density gradient, with a complex potential having two simple zeros (i. e., turning points) and one simple pole (see Refs. F VII; G XIII). This differential equation is also discussed in secs. I A 3b, II. The relative position of these three complex transition points depends on the wave-vector perpendicular to the density gradient and the complex frequency of the scattered electromagnetic waves and also on the pump strength

(i. e., laser intensity). One of the zeros corresponds to the usual turning point for electromagnetic waves travelling in a nonuniform plasma; the second turning point and the pole are introduced by the presence of the pump (i. e., laser).

In sec. I D, we describe the mathematical procedure we follow in the rest of this paper. Our results are obtained by evaluating the "Green's function" response in time and space for the scattered electromagnetic waves assuming they are initiated by a "delta-function" source. Using phase-integral (WKBJ) techniques (except in the special cases treated in sec. III, like no pump or a uniform plasma, where exact solutions are available), we obtain for the above differential equation two approximate solutions that are valid throughout the complex position plane except near the three transition points. These two solutions are used to obtain the spatial response at a given frequency; evaluating the proper inverse Fourier transform of this (in the complex frequency space) then gives the temporal evolution. Although by this method we generally cannot look too close to the turning point, we can nevertheless follow the temporal evolution of the side-scattered waves before and after they encounter their turning point and, thereby, obtain the net growth.

In sec. IV, we review and summarize phase-integral theory (Ref. sec. T) and present (in an easy-to-follow pictorial fashion) a set of rules that one can use in applying this approximation technique. We also obtain (modified from Ref. T III) here the

Stokes constant for a pole-zero combination as required for the solution in sec. V.

In sec. V, we show that the resulting Green's function response consists of two parts: (1) propagating and refracting wave-packets growing only while they are in their resonance zone; (2) eigenmodes (first discovered in Ref. F VII) localized along the density gradient and growing in time (as discussed also in sec. I A 3b). The eigenmodes do not dominate the response until after the side-scattered wave-packets have saturated their growth by refraction out of their resonance zone. By taking into account the convection of the waves perpendicular to the density gradient, we show that the finite laser diameter can typically (see sec. V D) force an early saturation with the eigenmodes never appearing. This may explain the lack of experimental evidence (see Ref. sec. H) for the Raman side-scatter instability as opposed to its clear observation (see Ref. sec. L) in computer simulations with periodic boundary conditions (i. e., effectively an infinitely wide laser diameter).

2. Uniform Unbounded Plasma, Infinite Extent Pump

The earliest work (Ref. sec. E) on the Raman instability assumed a uniform unbounded plasma, a pump wave of infinite extent, and typically only one-dimensional variations (i. e., back- or forward-scattering). The electromagnetic pump wave (frequency ω_o, wavefector $\underline{k}_o$) is propagating along z with linear polarization $\hat{e}_o$ along x. Above a certain threshold intensity, the pump wave (ω_o, $\underline{k}_o$) is unstable (stimulated, not spontaneous) with respect to decay into a scattered electromagnetic wave (ω_1,$\underline{k}_1$) and a Langmuir plasma wave ($\Omega \equiv \omega_2 \equiv \omega_o - \omega_1$, $\underline{K} \equiv \underline{k}_2 \equiv \underline{k}_o - \underline{k}_1$). This process is illustrated in Fig. I.2 for a backscattered electromagnetic wave with polarization along x (the configuration with the largest growth rate). The group velocities of the two scattered waves are $\underline{V}_1 = \underline{k}_1(c^2/\omega_1)$ and $\underline{V}_2 = 3K\, v_{th}^2/\Omega = 3\underline{K}(c^2/\Omega)(T_e/mc^2)$ where v_{th} is the thermal velocity of the electron distribution with temperature T_e.

We remove the fast time and space dependence of the scattered waves $\underline{E}_j(\underline{x},t) = \underline{E}_j\, a_j(\underline{x},t) \exp(i\underline{k}_j \cdot \underline{x} - i\omega_j t) + c.c.$ in favor of slowly varying amplitudes $a_j(\underline{x},t)$ (dimensionless and appropriately normalized). The evolution of these amplitudes (subscript "2" always denotes the Langmuir wave while "1" denotes the scattered electromagnetic wave) can be obtained from the coupled equations

$$\left[\frac{\partial}{\partial t} + \nu_2 + i\Delta_2 + \underline{V}_2 \cdot \underline{\nabla}\right] a_2 = \gamma_o a_1^* \qquad \text{(I.1a)}$$

$$\left[\frac{\partial}{\partial t} + \nu_1 + i\Delta_1 + \underline{V}_1 \cdot \underline{\nabla}\right] a_1 = \gamma_o a_2^* \qquad \text{(I.1b)}$$

where ν_1 and $\nu_2 \equiv \nu_p$ are phenomenological damping rates, $\Delta_1 \equiv$ $\equiv (\omega_p^2 + c^2k_1^2 - \omega_1^2)/2\omega_1$ and $\Delta_2 \equiv \Delta_p \equiv (\omega_p^2 + 3v_{th}^2 K^2 - \Omega^2)/2\Omega$ are frequency mismatches of the scattered waves with respect to the appropriate unpumped normal modes. See Refs. F VII, XI, and G XII for equivalent forms of Eq. (I.1). For Raman scattering, the coupling coefficient is

$$\gamma_o = (Kv_o/2)(\omega_p/\omega_1)^{1/2} \cos\theta \qquad \text{(I.2)}$$

where θ is the angle between the polarization of the two electromagnetic waves and $v_o \equiv eE_o/m\omega_o$ is the oscillation velocity of an electron in the pump electric field. A third coupled equation giving the reaction of a_1 and a_2 back on the pump is ignored here, and γ_o is treated as a constant.

Finite frequency mismatch Δ_1 or Δ_2 will reduce the growth rate of the instability, but a noise excitation with a broad spectrum in ω and k (such as a delta-function in time and space) will lead to an asymptotic response which picks out the particular $(\omega_1, \underline{k}_1)$ wave-packets having $\Delta_1 = \Delta_2 = 0$ (see Fig. I.3 for $\omega_1, \underline{k}_1$ diagram) and the largest growth rates. We therefore consider only this resonant case with $\Delta_1 = \Delta_2 = 0$.

Bers, Chambers, and Hawryluk (Ref. E VIII), Bers (Ref. E IX), and Chambers (Ref. G XII) have found that the time-asymptotic response to a delta-function source $(\delta(x)\delta(t))$ consist of pulses with different $(\omega_1, \underline{k}_1)$ (but all having $\Delta_1 = \Delta_2 = 0$), each being localized along the straight line connecting the pulse edges $\underline{x}_1 = \underline{V}_1 t$ and $\underline{x}_2 = \underline{V}_2 t$ (see Fig. I.4). Therefore, the instability is generally convective (no temporally growing response at fixed position). Their results indicate that, for fixed $(\omega_1, \underline{k}_1)$, an observer moving with velocity $\underline{V} = \underline{V}_1 + \alpha(\underline{V}_2 - \underline{V}_1)$, $0 \leq \alpha \leq 1$, and positioned on the above line will see a temporally growing response with growth rate

$$\gamma(\underline{V}) = \frac{2\gamma_0 (U_1 U_2)^{1/2} - (\nu_1 U_2 + \nu_2 U_1)}{U_1 + U_2} \qquad \text{(I.3)}$$

where $U_1 \equiv |\underline{V}_1 - \underline{V}| = \alpha|\underline{V}_2 - \underline{V}_1|$ and $U_2 \equiv |\underline{V}_2 - \underline{V}| = (1-\alpha)|\underline{V}_2 - \underline{V}_1|$. For given observer velocity $\underline{V}$, temporal growth is then found only when the coupling coefficient (related to pump strength) γ_o is greater than a threshold value $\gamma_c(\underline{V})$ where

$$\gamma_c(\underline{V}) \equiv \frac{(\nu_1 U_2 + \nu_2 U_1)}{2(U_1 U_2)^{1/2}} \quad . \tag{I.4}$$

This threshold is minimized for a particular observer velocity such that $U_1/U_2 = \alpha/(1-\alpha) = \nu_1/\nu_2$ which gives $\left[\gamma_c(\underline{V})\right]_{min} \equiv \gamma_c = (\nu_1\nu_2)^{\frac{1}{2}}$. Far above this convective threshold ($\gamma_o >> \gamma_c$), the growth rate $\gamma(\underline{V})$ in the moving reference frame is maximized for a different observer velocity such that $U_1/U_2 = 1$ ($\alpha = 1/2$) or $\underline{V} = (\underline{V}_1 + \underline{V}_2)/2$ with $(\gamma(\underline{V}))_{max} = \gamma_o$; note that the definition of γ_o implies that the maximum growth rate over all directions of $\underline{k}_1$ and $\underline{E}_1$ occurs for backscatter (K largest) with polarization parallel to $\underline{E}_o$ (cos θ largest).

For the one-dimensional case with $\underline{V}_1 = V_1\hat{z}$ and $\underline{V}_2 = V_2\hat{z}$, the results are essentially the same; the only new feature occurs for $V_1V_2 < 0$, in which case a stationary observer ($V = 0$) will be sitting on the line of pulse localization ($-V_1t < x = 0 < V_2t$), and Eq. (I.4) predicts an absolute instability (temporal growth at fixed position) for γ_o above a threshold value γ_a where

$$\gamma_a \equiv \frac{\nu_1|V_2| + \nu_2|V_1|}{2|V_1V_2|^{1/2}} \quad . \tag{I.5}$$

The absolute growth rate is then $\gamma(V = 0) = \left[2\gamma_o|V_1V_2|^{\frac{1}{2}} - \right.$ $\left. - (\nu_1|V_2| + \nu_2|V_1|)\right]/(|V_1| + |V_2|)$ which is usually much smaller than γ_o since $|V_2| \ll |V_1|$ except for very hot underdense plasmas (T_e/Ω large) or very near quarter critical density (k_1 small).

So far we have discussed the response only in a uniform plasma. We must now consider how this response is modified by a nonuniformity in the plasma density.

3. Nonuniform Plasma

a. Backscatter

The situation is much different in a nonuniform plasma, and again early work centered on one-dimensional variations (Ref. sec. F). We now assume that the plasma density is linearly increasing along the direction of incidence (z) of the pump wave in the local region of interest (see Fig. 5a). Going back to Eq. (I.1), we see that the frequency mismatches, $\Delta_1(\omega_1, k_1, z)$ for the electromagnetic wave and $\Delta_2(\Omega, K, z)$ for the Langmuir wave, are now spatially varying. Before, in the uniform plasma, we could choose ω_1 and $\underline{k}_1$ such that $\Delta_1 = \Delta_2 = 0$ everywhere, but this is no longer possible. We can eliminate Δ_1 by using a geometrical-optics approach (sometimes called WKB because of the phase-integral $\int \underline{k}_1(z) \cdot d\underline{x}$) and defining a spatially varying $\underline{k}_1(z)$ by setting $\Delta_1(\omega_1, k_1(z), z) = 0$; for fixed ω_1 and $\underline{k}_{1\perp} = \hat{x}k_{1x} + \hat{y}k_{1y}$, this determines the spatial

variation of the component of $\underline{k}_1$ along the density gradient:

$$k_{1z}(\omega_1, k_{1\perp}, z) \equiv \left[\omega_1^2 - \omega_p^2(z) - c^2 k_{1\perp}^2\right]^{1/2}/c. \quad (I.6)$$

Note that we have included the perpendicular wave-vector $\underline{k}_{1\perp}$ in order to show how some of the quantities depend on this parameter; however, we will concentrate in this section on the specific case $\underline{k_{1\perp} = 0}$ and defer to the next section any changes due to finite $k_{1\perp}$. The pump wave also has a spatially varying wave-vector $k_o(z) = \left[\omega_o^2 - \omega_p^2(z)\right]^{\frac{1}{2}}/c$. The resulting beat wave-vector $K(z) \equiv |\underline{k}_o(z) - \underline{k}_1(z)|$ will still give a spatially varying Langmuir wave frequency mismatch $\Delta_2(\Omega, K(z), z)$ which will vanish at only one resonance density position $z_o(\omega_1, k_{1\perp})$.

As the scattered electromagnetic wave (for fixed ω_1, $\underline{k}_{1\perp}$) propagates away from z_o, the plasma wave beat disturbance $(\Omega, \underline{K})$ becomes out of resonance with the local Langmuir normal mode, and the plasma wave density perturbation grows in amplitude at a slower rate than it would for a uniform plasma. This plasma wave density perturbation, when coupled with the oscillating electron velocity in the pump electric field, leads to a transverse current perturbation at $(\omega_1, \underline{k}_1)$ radiating a growing scattered electromagnetic wave, which is slightly out of phase with the original scattered electromagnetic wave which we assumed had propagated to this position. As the wave propagation continues to positions far from

z_o, the nonresonance of the longitudinal beat disturbance and the dephasing of the scattered wave with respect to the stimulated wave it locally generates leads to a saturation of the amplitude of the growing wave (see Fig. I.5b).† We have considered this from the viewpoint of the propagating scattered electromagnetic wave, but a similar process also occurs for the propagating Langmuir waves.

In addition to this saturation of the amplitude of the convecting pulse (the center of which moves with velocity $\underline{V} = (\underline{V}_1 + \underline{V}_2)/2$), due to propagation away from the resonance position z_o, Rosenbluth (Ref. F II), and Rosenbluth, White, and Liu (Ref. F VI) have found that for backscatter ($k_{1i} = 0$), with $V_1 V_2 < 0$ and above the uniform plasma absolute instability threshold $\gamma_o > \gamma_a$, the pulse amplitude at any fixed position also saturates (see Fig. I.5b), at essentially the same level as the propagating part of the pulse. This saturation at any fixed position is due to the arrival and destructive interference of waves generated at other positions. (Excellent discussions about this effect and ways of preventing or reducing this destructive interference, by including density fluctuations or finite extent pump or plasma, have been given by Nicholson (Ref. F X) and by Chambers (Ref. G XII). Rosenbluth, White, and Liu (Ref. F VI) find

† The initial values are assumed to be $a_2(\underline{x}, t = 0) = 0$ and $a_1(\underline{x}, t = 0) = \delta(x)\delta(y)\delta(z - z_o)$. According to Nicholson (Ref. F X), immediately following the propagating δ-function is a pulse growing linearly (rather than exponentially) in time. This effect presumably disappears for a less "spiky" initial value.

a fixed position saturation amplitude of $\exp\left\{\Gamma\left[1 - (4\gamma_a/\pi\gamma_o)\right]\right\}$, provided $\Gamma >> 1$, where γ_a is given by Eq. (I.5),

$$\Gamma \equiv \pi \gamma_o^2 / (\kappa' |V_1 V_2|) , \qquad (I.7)$$

and $\kappa' \equiv (d/dz)\left\{K(z) - \left[\Omega^2 - \omega_p^2(z)\right]^{\frac{1}{2}}/\sqrt{3}\, v_{th}\right\} \approx (d/dz)\left[\Delta_2(z)/V_2\right]$ is the derivative (evaluated at $z_o(\omega_1, k_{1\perp})$, with $k_{1\perp} = 0$ here) of the wave-vector mismatch between the plasma wave beat disturbance $(\Omega, \underline{K})$ and a Langmuir wave having frequency Ω. On the other hand, the saturation amplitude (for $V_1V_2 < 0$ or $V_1V_2 > 0$) of the convecting pulse center is just approximately e^{Γ} (Ref. F VI) and could be much larger than the fixed position amplitude if $\gamma_o \lesssim \gamma_a$ (such as might happen with large damping but small group velocity for the Langmuir wave).

We have qualitatively discussed how the pulse response is modified (from the uniform plasma case) by the propagation of the waves along the density gradient; the wave amplitude saturates at a level depending on the density scale length $L_n \equiv d\left[\ln \omega_p^2(z)\right]/dz$. For the backscatter case, we have presented the quantitative saturation amplitudes, at fixed position or moving with the pulse center, found by Rosenbluth, White and Liu (Ref. F VI). We next discuss in more detail how the density gradient affects oblique- and side-scatter.

b. Oblique- and Side-scatter

A similar picture applies to moderately oblique-scatter (see Fig. I.6a) except that now no amplification occurs at a fixed position (see Fig. I.6b). The saturation amplitude e^{Γ} of the convecting pulse is given again by Eq. (I.7) with V_1 and V_2 replaced by V_{1z} and V_{2z} -- the group velocity components along the gradient (Ref. F VII). From the definitions of κ' (below Eq. (I.7)) and Δ_2 (below Eq. (I.1)), we have

$$\kappa' |V_{1z} V_{2z}| \approx \mathrm{sgn}(V_{1z} V_{2z})(V_{1z} + V_{2z}\Omega/\omega_1)\omega_p^2/2L_n\Omega \qquad (I.8)$$

where the density scale length $L_n \equiv d\left[\ln n(z)\right]/dz$. Equations (I.7-8) indicate that Γ can be much larger for very oblique-scatter ($V_{1z} \ll c$) than for back-scatter ($V_{1z} \stackrel{\sim}{>} c$).

In particular, if $V_{1z} = -V_{2z}\Omega/\omega_1$ (at z_o) we note that κ' vanishes and Γ diverges (Ref. F VII); these "side-scattered" waves (see Fig. I.7a) have not only $\Delta_2(\Omega,K,z_o) = 0$ but also $d\Delta_2/dz = 0$ at the resonance position $z_o(\omega_1, k_{1\perp}(\omega_1))$.† The divergence of Γ is a consequence of the lack of an effective linear (i. e., convective) saturation mechanism for these waves (see Fig. I.7b) if $\underline{V}_1$ and $\underline{V}_2$ are treated as z-independent in Eq. (I.1). The time required for κ' to saturate the growth is inversely proportional

† $k_{1\perp}(\omega_1)$ or $\omega_1(k_{1\perp})$ is determined by choosing a particular $k_{1z}(\omega_1, k_{1\perp}, z)$ at the resonance position $z = z_o(\omega_1, k_{1\perp})$. For instance, here we choose k_{1z} such that $V_{1z} = -V_{2z}\Omega/\omega_1$.

to κ' and diverges as κ' vanishes here (Ref. F VI). Furthermore, finite κ'' (or $d^2\Delta_2/dz^2$) only slightly reduces the growth rate at the constant density position $z = z_o$ (Ref. F VII).

The possibility that side-scattered waves could grow to a level requiring nonlinear saturation (as mentioned in Sec. I A1) prompted considerable research (Ref. sec. G). The author, along with Nicholson and Kaufman (Ref. G I), earlier proposed a local geometrical-optics ray approach, in effect using Eq. (I.1) with $\Delta_1(\omega_1, k_1(z), z) \equiv 0$, $\underline{V}_2 = 0$, and $\Delta_2(\Omega, z) \approx \omega_p(z) - \Omega$ (cold plasma approximation with $\omega_p(z_o) \equiv \Omega$); the proposed linear saturation mechanism was the convection of the side-scattered waves out of the finite diameter laser beam (the pump wave). In that work, we proceeded to calculate the spatial amplification of the scattered waves above a steady-state level of thermal noise and, using energy conservation, obtained a pump attenuation coefficient.

The main objection to that work has been that geometrical optics is not valid for a wave at its turning point (here, the side-scattered wave) and that a second derivative $\partial^2/\partial z^2$ "diffraction" term must be included in the left-hand-side of Eq. (I.1b) in order to properly treat the refraction of this wave. However, it was implicitly assumed in that paper that the laser beam diameter D (d_L in sec. V C-D) was sufficiently small that the side-scattered waves did not have time to "feel" the density gradient; the refraction of these waves was therefore ignored, and their propagation was treated as though the plasma were locally uniform ($\underline{k}_1$ treated as a

constant). The back- and moderately oblique-scattered waves (for which geometrical optics is valid) could propagate along the density gradient sufficiently to "feel" the spatially varying Langmuir frequency mismatch $\Delta_2(\Omega,z)$, but here too the slight change in $\underline{k}_1$ over the narrow resonance zone of height $h = 4\pi L_n \nu_p/\omega_p$ along the gradient (as found in Ref. G I) was ignored; the slight variation of $K(z)$ does not affect Δ_2 for a cold plasma. In summary, the local ray-trajectories of the scattered e.m. waves were treated as straight lines over the small resonance cylinder of diameter D and height h.

Galeev, Laval, O'Neil, Rosenbluth, and Sagdeev (Refs. G II, III and later reported by Sagdeev in Ref. G IV) also used the geometrical-optics approximation but implicitly assumed that the laser beam diameter was effectively infinite; their proposed linear saturation mechanism was the refraction-bending of the side-scattered electromagnetic waves out of the narrow resonance zone (see Fig. I.7b and imagine that the straight line now drawn through $\underline{V}_1 t$ is curved downward toward negative z). In one method of solution (Refs. G II, III), they integrated the local spatially dependent growth rate $\gamma(z)$ along the curved ray-trajectory of the 90° side-scattered wave until the ray exited the resonance zone and $\gamma(z)$ became negligible. For the resulting saturation amplitude e^Γ, in a cold plasma, they found

$$\Gamma = 8.8 \left(\gamma_o/\omega_p\right)^{3/2} \left(\omega_1/\omega_o\right) k_o L_n \quad , \qquad (I.9)$$

where we have taken one-half of their energy gain in Ref. G II and have included the term ω_1/ω_o which can be found from their more exact expression in Eq. (14) of Ref. G III. This exponentiation Γ is much larger, by a factor of $(\omega_p/\gamma_o)^{\frac{1}{2}}(1 - \omega_p^2/\omega_1^2)^{\frac{1}{2}}$ (if not too near quarter critical density where $k_1 \to 0$), than the exponentiation found in Eq. (I.7) for back-scatter.

In a second method of solution (Refs. G III, IV), they dropped the time derivatives and damping rates in Eq. (1) thereby leaving thermal convection as the only means of removing the plasmons from the resonance zone; the resulting exponentiation factor (Ref. G IV, and Eq. (7) and Table I of Ref. G III), although comparable to Eq. (I.9) for reasonable plasma temperatures, mathematically diverges for a cold plasma. In all of our work which follows later in this paper, thermal convection is assumed to be negligible compared with temporal growth, and therefore we will eventually use Eq. (I.9) in comparing their work with ours (cf. Eq. (V.81d)).

Whatever objections one has to using geometrical optics in analyzing side-scattering would seem to apply most strongly here, where refraction of the 90^o side-scattered wave is crucial in obtaining the desired linear saturation of the instability. However, one might expect that Eq. (I.9) would give approximately the correct answer if the resonance zone width h (along the gradient) is sufficiently large that geometrical optics is valid along most of the ray path; this requires $|dk_{1z}/dz| \ll k_{1z}^2$ at the position $z = z_o - h/2$ or

$$h/2 \gg Z \equiv \left(c^2 L_n/\omega_p^2\right)^{1/3} , \qquad \text{(I.10a)}$$

where Z is the Airy function wavelength at the turning point (and resonance position) z_o. The resonance zone width h, to be used in Eq. (I.10a), can be obtained by first using geometrical-optics to determine the time t_s needed for the side-scattered electromagnetic wave of given $\underline{k}_{1\perp}$ (i. e., $k_{1z}(\omega_1, k_{1\perp}, z) = 0$ at the resonance zone center $z = z_o(\omega_1, k_{1\perp})$) to travel from the resonance zone edge $z_o - h/2$ to the turning point at the resonance zone center z_o and then back to $z_o - h/2$ (see Fig. I.8). One finds $t_s = 4\sqrt{L_n h/2}\,\omega_1/\omega_p c$, and setting $\gamma_o t_s \tilde{\sim} \Gamma$ from Eq. (I.9) results in the following expression for h:

$$h \approx 10\, L_n\, \gamma_o/\omega_p \; ; \qquad \text{(I.10b)}$$

this is only <u>approximate</u> since the average growth rate over the resonance zone is less than ($\sim$ half) γ_o while the actual time in the resonance zone is greater than ($\sim$ twice) t_s due to the <u>reduced</u> group velocity ($\underline{V} = \underline{V}_1/2$ for a cold uniform plasma, sec. I A 2). For a Nd:glass laser (λ_o = 1.06 microns) of 10^{16} watt/cm^2, Eq. (I.10a) is satisfied for a density scale length L_n = 100 microns (laser-fusion parameters from Ref. sec. J) but not for L_n = 10 microns (present laser-fusion experiments in Ref. sec. H). Thus, for parameters of interest in explaining present experiments, the derivation of Eq. (I.9) cannot be trusted because it relies on treating refraction

by the approximation of geometrical-optics in a region (within a distance Z of the turning point) where such a treatment is never valid. (In Ref. G I, on the other hand, the growth was assumed to be convectively saturated by finite laser diameter before refraction became important).

Liu, Rosenbluth, and White (Ref. G V) abandoned the geometrical-optics approximation and included a second derivative $\partial^2/\partial z^2$ "diffraction" term in the left-hand-side of Eq. (I.1b) while Fourier transforming in the two remaining "perpendicular" directions x and y (giving $\underline{k}_1 \equiv \hat{x}k_{1x} + \hat{y}k_{1y}$). Keeping our earlier terminology, but with $\Delta_1(z) \equiv [\omega_p^2(z) + c^2k_{1\perp}^2 - \omega_1^2]/2\omega_1$ now, we modify Eq. (I.1) to give

$$\left[\frac{\partial}{\partial t} + \nu_2 + i\Delta_2(z) + V_{2z}\frac{\partial}{\partial z}\right] a_2 = \gamma_o a_1^* \qquad \text{(I.11a)}$$

$$\left[\frac{\partial}{\partial t} + \nu_1 + i\Delta_1(z) - i\frac{c^2}{2\omega_1}\frac{\partial^2}{\partial z^2}\right] a_1 = \gamma_o a_2^* \ , \qquad \text{(I.11b)}$$

which is equivalent to their Eqs. (I.3-4) if we use an appropriate transformation on a_1 and a_2 (and if we correct a sign error in their Eq. (4)). There is no k_{1z} or V_{1z} appearing in Eq. (I.11b) since this equation determines the entire z-dependence of a_1. They then dropped the time derivatives, damping rates, and the Langmuir wave frequency mismatch $\Delta_2(z)$ and proceeded to calculate the amplification e^{Γ}, at the resonance zone $z_o(\omega_1, k_{1\perp}(\omega_1))$, above a steady-state level of thermal noise; they found $\Gamma = (\pi\gamma_o^2/V_{2z})(4\omega_1 L_n/3\omega_p^2)$,

which interestingly is just 2/3 of the value one would obtain from Eqs. (I.7-8) if $V_{1z} = 0$.

The proposed saturation mechanism in that paper was the refraction of the 90° side-scattered wave out of a resonant-interaction region of width $z_{int} = (2\pi L_n c^2/3\omega_p^2\Gamma)^{1/3}$, obtained by comparing the diffraction term $(c^2/2\omega_1)d^2a_1/dz^2 \sim (c^2/2\omega_1)a_1/z_{int}^2$ with the coupling term $\gamma_o a_2^* \sim \gamma_o^2 a_1 z_{int}/V_{2z}$. However, this z_{int} is independent of L_n, contrary to the known (see sec. I A 2) infinite resonance region in a uniform ($L_n \to \infty$) plasma! They also claim that stabilizing effects from the finite radius R of the laser beam (pump wave) can be neglected provided $R \gg R_{min} \equiv k_o z_{int}^2$, which again is independent of L_n, whereas in a uniform plasma any finite radius would lead to a convective saturation of the instability before refraction could take place! It is, therefore, uncertain under what physical and mathematical conditions their approximations remain valid. Since their expression for Γ diverges in the mathematical limit of a cold plasma, we will not be able to compare our later results in this paper (where thermal convection is assumed to be negligible) with their results.

In a later paper, Liu, Rosenbluth, and White (Ref. F VII) and Liu (Ref. G XIII) again considered the same set of equations, Eq. (I.11), containing the refraction and diffraction of the side-scattered electromagnetic waves; but, here they took the limit where the thermal convection ($V_{2z}\,\partial/\partial z$) of the Langmuir waves out of the resonance zone is negligible compared with the Langmuir wave frequency mismatch $\Delta_2(z)$

and the temporal growth $(\partial/\partial t)$ of the waves. Fourier transforming in time (drop $\partial/\partial t$ in Eq. (I.11) and let ω_1 be complex), they obtained a single second-order differential equation in z, equivalent to

$$\left[\frac{d^2}{dz^2} - 2\omega_1\Delta_1(z)/c^2 + 2\omega_1\gamma_0^2/c^2\Delta_2^*(z)\right]a_1 = 0 , \quad (I.12)$$

which they proceeded to solve for complex eigenvalues $\omega'_{ln}(\underline{k}_{l\perp}) = \mathrm{Re}(\omega'_{ln}) + i\gamma'_n$, with $a_{ln}(\omega'_{ln}, \underline{k}_{l\perp}, z)$ subject to evanescence for large positive z (increasing plasma density) and outgoing wave boundary conditions for large negative z (no sources at $z \to -\infty$).

Equation (I.12) is a Helmholtz equation with a complex potential having two roots and a singularity in the complex z-plane (assuming a linear density gradient along the real z axis; additional roots and singularities can appear for more complicated density profiles). For ω_1 lying in a certain region of the complex ω_1-plane, the two roots (turning points) are close together and far from the singularity, reducing Eq. (I.12) to a harmonic oscillator equation with eigenmodes a_{ln} evanescent for large real z and eigenvalues with imaginary part (growth rate) given by

$$\gamma'_n = K v_o \frac{\omega_p}{\omega_o}\left[1 - \frac{(2n+1)(\omega_p/Kc)^{1/2}}{KL_n(2v_o/c)^{3/2}}\right] \quad (I.13)$$

where $n = 0,1,2,\ldots$ (Refs. F VII; G XIII). The condition for the validity of this result (which depends on ignoring the singularity) is that the second term in the square brackets be much smaller than one; thus, Eq. (I.13) is not valid near threshold. At threshold ($\gamma'_{n=0} = 0$), the singularity lies between the two roots and Liu, Rosenbluth, and White found (analytically and numerically)

$$\left[\left(\frac{v_o}{c}\right)^2\left(\frac{Kc}{\omega_p}\right)^{2/3}\left(KL_n\right)^{4/3}\right]_{thres.} = 0.24 \quad . \qquad (I.14)$$

For modes described by Eq. (I.13), the eigenmode width is approximately the distance between the two roots, or (see Refs. F VII; G XIII)

$$\Delta z_n \approx L_n \left(v_o/c\right)^{1/4}\left(k_o L_n\right)^{-1/2} \quad . \qquad (I.15)$$

These localized (along z) eigenmodes are, however, still generally convective along the "perpendicular" directions x and y; the eigenmodes become absolutely unstable only at the quarter critical density where $k_{1\perp} = 0$ (Refs. F VII; G X, XIII). The perpendicular convection of these modes out of a finite size plasma is the only linear saturation mechanism that was mentioned in that work. These same authors (Ref. G IX) later generalized their work to a spherical nonuniform plasma.

However, several questions immediately arise concerning their work. What, for instance, is the connection of that work with all the previous work which involved the concept of a wave-packet growing convectively until saturated by the effects of refraction

or finite laser-diameter? Is the previous work incorrect or incomplete? Liu, Rosenbluth, and White (Ref. F VII) found eigenmodes, but what happens in the limit of a uniform plasma where there are no eigenmodes? From Eq. (I.13) we see that as $L_n \to \infty$, the spacing between the eigenvalues goes to zero and $\gamma_n' \to v_o K\omega_p/\omega_o$, a finite value which is always less than or equal to the known uniform plasma growth rate, γ_o, from Eq. (I.2). Thus, as $L_n \to \infty$, the eigenvalues do not seem to disappear (the eigenvalue equation leading to Eq. (I.13) appears to remain valid) nor do they approach exactly γ_o (the agreement between γ_n' and γ_o at one particular position, the quarter critical density point, is not sufficient). For finite density scale length L_n, as the pump strength (e. g., v_o/c) decreases, one eventually approaches the threshold ($\gamma_{n=0}' = 0$) given by Eq. (I.14); however, damping was ignored in their work, and no other physical explanation was offered for this threshold behavior. In fact, in the limit of vanishing pump strength, there is no indication in their work of how one recovers the known response (see sec. III B) to an electromagnetic perturbation in a nonuniform, unpumped plasma (for which there are no eigenmodes).

In support of their work, we mention the clear observation (Ref. sec. L) of Raman side-scattering in computer simulations with periodic boundary conditions along y (infinitely wide plasma and laser-diameter); there is even some indication that the side-scattered waves are localized along z for given k_y (Ref. G XI).

But, this makes all the more puzzling the lack of conclusive experimental evidence (Ref. sec. H) for the Raman side-scatter instability; evaluating Eq. (I.14) at one-ninth critical density ($\omega_o = 3\omega_p$) and using a steep density gradient with scale length $L_n = 10\ \mu$ m., one obtains a threshold ($\gamma'_{n=0} = 0$) intensity of $I_o = 1.6 \times 10^{15}$ watt/cm^2 for a Nd:glass laser pump wave, exceeded in many laser-fusion experiments (Refs. H III-VI, VIII-XI, XIII-XV). Thus, it appears that their work and also computer simulations neglect some effect relevant to observation of the instability in an actual laser-fusion experiment.

We conclude this section by noting that the Raman side-scatter instability is potentially important even in cases where the Raman back-scatter instability is suppressed by a steep density gradient, but that all the previous attempts at understanding Raman side-scatter have led to confusing or apparently contradictory results. Our desire to resolve some of the questions we have raised in this section on side-scattering motivates our present work; to simplify our task, we restrict ourselves to the case considered by Liu, Rosenbluth, and White (Ref. F VII): a cold plasma or a large pump approximation, where the thermal convection of the Langmuir waves out of the resonance zone is negligible. This case encompasses most of the questions raised in this section.

B. Motivation for Present Work

As mentioned above, we are motivated in this paper by our desire to resolve certain questions that arise when one tries to understand and relate past work on the Raman side-scatter instability. In particular, we will address the following questions:

(1). How are wave-packets and eigenmodes related to the actual space-time response to a delta-function source, and when, if ever, is one description dominant?

(2). What form does the response take in the limits of uniform density ($L_n \to \infty$), zero pump strength ($v_o \to 0$), early time, or some combination of these limits?

(3). In the absence of damping, what is the physical explanation for the threshold behavior of the eigenmodes?

(4). How does a finite radius for the laser pump wave affect the response?

(5). Why has the Raman side-scatter instability been clearly observed in computer simulations, yet not at all in actual laser-fusion experiments?

To answer these questions, we first reduce the problem to the simplest physical model (e. g., linear density profile matched onto uniform or vacuum region, fixed ions, either a cold plasma or a large growth rate to make the plasma wave convection negligible, delta-function electromagnetic noise) that contains the most essential features (refraction, diffraction, space-time evolution, non-negative density profile). The model is discussed in more detail in the

next section. The need to include refraction and diffraction was discussed in the previous section; refraction in the nonuniform plasma can bend the side-scattered electromagnetic wave (for any given $\underline{k}_{l\perp} = \hat{x}k_{lx} + \hat{y}k_{ly}$) along z and out of the resonance zone, and diffraction must generally be included since the side-scattered wave is at its turning point. A linear density profile for all z would lead to nonphysical results, as implied in sec. I D 2. For our simple model, the describing equations can be reduced (Ref. F VII; G XIII) to a single Helmholtz (or Schrödinger) second-order differential equation in z for the $(\omega_l, \underline{k}_{l\perp})$ component of the electric field $E_l(z, \omega_l, \underline{k}_{l\perp})$† of the scattered electomagnetic wave; the derivation of this differential equation is given in sec. II.

Since the Raman instability is a three-wave stimulated scatter (of the electromagnetic pump wave, off a Langmuir wave, and into a lower frequency electromagnetic wave), at least one of the two product waves (the Langmuir wave or the scattered electromagnetic wave) must be present as noise at $t = 0$ in order to initiate the process. To give answers to the above list of questions, it is sufficient (since our problem is linear in E_l) to confine the initiating noise to $t = 0$ and to a single position z_s along the gradient (noise $\sim \delta(t)\delta(z - z_s)$). The Langmuir wave is nonpropagating in the cold plasma assumed here, so our attention is primarily directed toward the scattered electromagnetic

† See sec. I C for reduction of the vector problem to a scalar problem.

wave, which is taken to be initiated by the noise source (described in more detail in the next section). Thus, there is still a finite and reasonably well-known electromagnetic response even in the limit of $v_o \to 0$ (where the Langmuir wave becomes uncoupled from the electromagnetic wave, and has vanishing amplitude). This limiting form for the response (to the delta-function source) must be contained in our results for the Raman side-scatter instability in order to answer question (2); this is accomplished by using a well-known general mathematical procedure (see Ref. sec. P), outlined in sec. I D, to obtain the Green's function solution $G_1(z,z_s;\omega_1,\underline{k}_{1\perp})$ for $E_1(z,\omega_1,\underline{k}_{1\perp})$ with the delta-function source located at $z = z_s$ as mentioned earlier.

The space-time response is then obtained by inverting the Fourier transform $\underline{G}_1(z,z_s;\omega_1,\underline{k}_{1\perp})$[†] with an integration along the Bromwich contour in the complex ω_1-plane; the result is the Green's function $\underline{G}_1(z,z_s;t,\underline{k}_{1\perp})$ representing the electromagnetic response to the $\underline{k}_{1\perp}$ component of the electromagnetic noise (bremsstrahlung; see Ref. sec. M) which is present at $t = 0$ and at position $z = z_s$, all of this occuring in a nonuniform plasma pumped by an electromagnetic wave $(\omega_o,\underline{k}_o = \hat{z}\,k_o)$. Since we are considering only the linear (in E_1) problem, we ignore the noise components present at other times and positions; in principle, the full solution could

---

[†] See sec. I C for discussion of the vector nature of $\underline{G}_1$.

be obtained by integrating $\underline{G}_1(z,z_s';t,t_s';\underline{k}_{1\perp})$ over some distribution of noise $S(z_s',t_s',\underline{k}_{1\perp})$ in space z_s' and time t_s' (Ref. sec. P). The integration in k_{1x} and k_{1y} will be discussed later. Rather than consider this complicated linear superposition, we just initiate the instability in the simplest way (the delta-function source $\delta(t)\delta(z - z_s)$) and follow the space-time evolution of the response.

In the absence of the pump, the response slowly decays like an inverse fractional power of time as the electromagnetic wave-packets propagate and refract away from the source position z_s (see Fig. I.9 and sec. III B). Wave-packets of all frequencies are produced due to the delta-function in time.

In the presence of the pump wave, some of these wave-packets will encounter their resonance zone before they propagate out of the nonuniform plasma or before they meet their turning point (see Fig. I.10); these wave-packets will grow while they are in their resonance zone. Since all frequencies are present, we can simultaneously look at back-, oblique-, and side-scatter and compare their saturation amplitudes with previous estimates discussed in sec. I A 3. Since we have a differential equation with boundary conditions, we can also expect the eigenmodes found by Liu, Rosenbluth, and White (Ref. F VII). A mathematical procedure essentially identical to ours was applied by Sedlacek (Ref. P III) to the problem of electrostatic oscillations in a cold plasma; it is clear from his work (or other references, such as Refs. P I-II, on solving differential equations and initial-value problems) that the eigenmodes are

connected with the poles of $G_1(z,z_s;\omega_1,\underline{k}_{1\perp})$ in the complex ω_1-plane, while the wave-packets are associated with the branch-points (and the branch-cuts) of $G_1(z,z_s;\omega_1,\underline{k}_{1\perp})$ in the complex ω_1-plane. This immediately answers the first part of question (1) and shows that the actual space-time response consists simultaneously of both wave-packets and eigenmodes; the more detailed question of when one particular description dominates over the other is the subject of much of the rest of this paper.

One can, however, predict qualitatively many features of the space-time response by applying crude physical arguments. At early times, before the side-scattered wave-packet (for given $\underline{k}_{1\perp}$) has been able to refract out of its resonance zone (similar to the case of Ref. G I, as discussed in sec. I A 3b), the effect of nonuniformity on side-scattering should be negligible (for back- or oblique-scattering, nonuniformity gives the saturation discussed in sec. I A 3a); thus, the side-scattered eigenmodes (which have the largest growth rate in Ref. F VII) should be negligible on this time scale (no eigenmodes in the effective absence of nonuniformity). This requires that the numerical coefficients multiplying the temporally growing exponentials in the eigenmodes must be small; in fact, these coefficients must vanish in the limit of a uniform plasma (while the growth rate approaches a positive constant according to Ref. F VII, as discussed in sec. I A 3b). Thus, one must wait some length of time before the temporal growth of the eigenmodes can overcome these small coefficients and lead to dominance over the transient wave-packets (which eventually

refract out of the plasma as shown in Fig. I.10).

To estimate this length of time, we first note that the maximally growing side-scattered eigenmode must be localized within a resonance zone width of the turning point position for the side-scattered wave-packet; the wave cannot propagate past the turning point to higher densities, and if it escaped out of the resonance zone it would become uncoupled from the Langmuir wave and propagate out of the plasma without further growth. The eigenmodes must therefore represent the result of a certain amount of reflection on the lower-density side of the resonance zone; this leads to the temporally growing wave pattern represented by the eigenfunctions. The fact that the pump wave introduces a second turning point (in the complex z-plane) was first pointed out by Drake and Lee (Ref. F III) for Raman back-scatter ($\underline{k}_{\perp} = 0$) at the quarter-critical position ($k_{1z} \tilde{>} 0$), and was later extended to side-scatter ($|\underline{k}_{\perp}| >> k_{1z}$) by Liu, Rosenbluth, and White (Ref. F VII). Thus, the eigenmodes should be expected to establish themselves as the dominant response after their component waves have undergone several "bounces" between the two turning points and "communicated" the necessary knowledge about the nonuniformity and the boundary conditions; that is, provided the pump strength $v_o = e E_o/m \omega_o$ is not so small that the waves lose more energy (through damping or transmission through the lower turning point) than they gain by traveling through the resonance zone. The dominance of the eigenmodes should, therefore, be expected to begin a short time (depending on v_o and L_n) <u>after</u> the side-scattered wave-packet has refracted

out of its resonance zone (i. e., after the time $t_s(z_s,k_{1\perp})$ shown in Fig. I.10; this is minimized for the source at the resonance zone edge in Fig. I.8).

Since we have Fourier transformed in the "perpendicular" directions x and y, all of the waves (wave-packets and eigenmodes with given $\underline{k}_{1\perp}$) are periodic and of infinite extent in the x-y plane; but, each of these standing waves in the x-y plane can be viewed as a superposition of two traveling waves propagating parallel and anti-parallel to $\underline{k}_{1\perp} = \hat{x}k_{1x} + \hat{y}k_{1y}$. If the noise source were also localized in x and y (e. g., noise $\sim\delta(x)\delta(y)\delta(z - z_s)\delta(t)$), an integration of $\underline{G}_1(z,z_s;t,\underline{k}_{1\perp})\exp(i\underline{k}_{1\perp}\cdot\underline{x})$ over k_{1x} and k_{1y} would be required to obtain the full three-dimensional Green's function response $\underline{G}_1(z,z_s;t,x,y)$. It is not necessary, however, to actually perform this integration in order to see qualitatively that the effect will be to superpose traveling waves with nearly the same $\underline{k}_{1\perp}$ and ω_1 and form propagating wave-packets in the x-y plane (Ref. F VII). That is, the previously discussed wave-packets in the z-t response (for given $\underline{k}_{1\perp}$) will now form three-dimensional wave-packets moving along well-defined trajectories in x-y-z-t space labelled by wave-packet frequency ω_{1A} (see Eq. (III.16) for ω_{1A}) and perpendicular wave-vector $(\underline{k}_{1\perp})_A$; for a given wave-packet, propagation along z will change its local k_{1z}, while at a fixed z-position there will be no wave-packets with $(k_{1\perp})_A > \left[\omega_{1A}^2 - \omega_p^2(z)\right]^{\frac{1}{2}}/c$ (they would be evanescent). The localized eigenmodes (Ref. F VII) in the z-t response (for given $\underline{k}_{1\perp}$) will now

form localized (along z) two-dimensional wave-packets moving along straight-line trajectories in x-y-t space labelled by wave-packet perpendicular wave-vector $(\underline{k}_{1\perp})_A$ and eigenmode number n (see sec. I A 3b); the eigenfrequency $\omega'_{1n}(\underline{k}_{1\perp})$ is then determined for each of these wave-packets.

The main point to be extracted from the qualitative arguments in the preceding paragraph is that, although we will mainly discuss and calculate the response in z-t space for fixed $\underline{k}_{1\perp}$, the wave-packets and eigenmodes should nevertheless be viewed as convecting simultaneously along x and y with a group velocity $\underline{V}_{g\perp}(\underline{k}_{1\perp},\omega_1)$ (ω_1 replaced by $\omega'_{1n}(\underline{k}_{1\perp})$ for the eigenmodes). If we calculate in z-t space a certain behavior for the wave-packets or for the eigenmodes (fixed $\underline{k}_{1\perp}$) during a time interval (0,t), then this behavior also occurs in the x-y plane within the spatial interval $(0,\underline{V}_{g\perp}t)$. In particular, if the eigenmodes are found to dominate the response only after the time t_s (at which refraction saturates the growth of the side-scattered wave-packet), then the eigenmodes can dominate the response also only after the side-scattered wave-packet has convected a distance $\ell_s \equiv V_{g\perp}t_s$ perpendicular to the direction of incidence of the pump wave.

The pump wave is typically a focused laser with small focal diameter d_L ($\lesssim$ 30 microns; see Ref. sec. H), so it is conceivable that $d_L < \ell_s$. In this case the waves would convect across and out of the laser beam and, thereby, lead to an early saturation of the side-scattered wave-packets and, more importantly, an end to the

growth of the eigenmodes. At this early time (t_s) the eigenmodes are still negligible relative to the wave-packets, and with no further growth the eigenmodes would remain negligible for all time.

The situation is somewhat analogous to that considered by Goedbloed and Sakanaka (Ref. Q I), who pointed out that one may not be so much interested in whether a certain plasma configuration is strictly MHD stable as in whether the temporal growth rate is small enough to lead to only negligible growth over the finite containment time-scales necessary for fusion. Similarly, we may not be so much interested in the temporal growth of eigenmodes of an infinitely wide system in x and y (such as in past computer simulations with periodicity along x and y) as we are in knowing the linear (convection) saturation amplitudes of waves propagating unstably only across a narrow focused laser beam.

An estimate of t_s based on Eqs. (I.9-10b), including the reduced group velocity, indicates that

$$t_s \approx 12 \left(\frac{\omega_i}{\omega_p}\right)^{3/4} \left(\frac{K V_o}{\omega_p}\right)^{1/2} \frac{L_n}{c} \quad , \qquad (I.16)$$

and using the reduced group velocity in the resonance zone (from sec. I A 2, $V = \underline{V}_1/2$ in a cold plasma) we have

$$l_s \approx c\, t_s/2 \qquad (I.17)$$

if not too near the quarter critical position where $\underline{V}_{1\perp} \propto \underline{k}_{1\perp} \to 0$. Using typical laser-fusion experiment parameters from Ref. sec. H (Nd:glass laser of 10^{16} watt/cm.^{2} and a density scale length L_n = 10 microns) and choosing $\omega_o/\omega_p = 3$, Eqs. (I.17, 9) give $\ell_s \gtrsim 30$ microns with a side-scattered wave packet saturation exponentiation of $\Gamma = 4$. Since for such high intensity lasers the focal diameter $d_L \lesssim 30$ microns (Ref. sec. H), one might expect an early saturation of the side-scattered wave-packets (at a level below the above value of $\Gamma = 4$) and, more importantly, an early end to the temporal growth of the infinite medium (along x and y) eigenmodes (at a level even below that of the wave-packets).

It should be emphasized that this conclusion cannot apply too near the quarter critical position since $V_{g\perp}$ and ℓ_s vanish at that position. However, for density profiles n(z) with a scale length $L_n(z)$ increasing slower than $n^{1/4}(z)$ (e. g., exponential with L_n = constant, or $n \propto r^{-3}$ with $L_n \propto n^{-1/3}$), the eigenmode instability threshold is highest in the high-density region near quarter critical (Rev. F VII).

In the rest of this paper, we describe in more detail the model, mathematical procedure, approximations, examples and calculations we have used to verify the qualitative picture we have assembled in this section.

C. Model and Physical Mechanism for the Instability

The density (see Fig. I.11 for profile) is taken to be constant for $z < 0$, but it can linearly increase for $z > 0$. This is the simplest (see secs. III B; V) non-negative nonuniform density profile, and it allows our results to reduce easily to known results (in terms of Airy functions) in the limit of zero pump strength. The plasma is assumed to be unmagnetized (i. e., no static magnetic field).

The electromagnetic pump wave,

$$\underline{E}_o(\underline{x},t) = \hat{x}\, E_o \exp\left\{i\int k_o(z)dz - i\omega_o t\right\} + \text{c.c.} \quad , \qquad (I.18)$$

is incident along $\hat{z}$ and linearly polarized along $\hat{x}$ (see Figs. I.11, 12), where $k_o(z) = \left[\omega_o^2 - \omega_p^2(z)\right]^{\frac{1}{2}}/c$. We are far from the turning point of the pump (the Raman instability only occurs at densities below quarter-critical, as shown in Fig. I.1), so k_o and E_o are slowly varying along $\hat{z}$; we will usually be interested only in the local values of k_o and E_o at the resonance zone center $z_o(\omega_1, \underline{k}_{1\perp})$ (see Figs. I.10, 12). In Fig. I.12 we illustrate the spatial orientation of the side-scattered electromagnetic wave $(\omega_1, \underline{k}_1)$ (shown at its turning point inside the resonance zone) and the Langmuir wave $(\Omega = \omega_o - \omega_1^*,\ \underline{K} = \underline{k}_o - \underline{k}_1)$ which are coupled together by the pump wave $(\omega_o, \underline{k}_o)$.

The Langmuir wave is coupled with the two electromagnetic waves through the two "nonlinear" forces $\underline{v}_o \times \underline{B}_1$ and $\underline{v}_1 \times \underline{B}_o$ in the Lorentz force equation

$$\dot{\underline{v}} = \frac{\partial \underline{v}}{\partial t} + \underline{v}\cdot\underline{\nabla}\,\underline{v} = -\frac{e}{m}\left(\underline{E} + \underline{v}\times\underline{B}/c\right) , \qquad (I.19)$$

where $\underline{v}$ is the velocity of a cold electron fluid element, and $\underline{v}_o \equiv e\underline{E}_o/m\omega_o$ and $\underline{v}_1 \equiv e\underline{E}_1/m\omega_1$ are essentially the oscillation velocities of electrons in the electric field of each of the two electromagnetic waves. Including only the lowest order nonlinearity in the total electric field $\underline{E}$, Eq. (I.19) gives (see sec. II)

$$\frac{\partial \underline{v}}{\partial t} = -\frac{e}{m}\underline{E} - \frac{e^2}{2m^2}\underline{\nabla}\left(\int \underline{E}\,dt'\right)^2 + \cdots . \qquad (I.20)$$

The second term above (the gradient of the ponderomotive potential) represents a longitudinal nonlinear force which has a component at frequency $\Omega = \omega_o - \omega_1^*$ giving rise to the longitudinal nonlinear current $\underline{J}_L(\Omega)$ and (through the continuity equation and Poisson's equation) the density perturbation $\delta n(\Omega)$ shown in Fig. I.12; this process resonantly drives up the Langmuir wave if $\Omega \approx \omega_p(z)$.

We assume fixed ions throughout this paper since they do not effectively respond at the high frequencies and short time-scales of interest here. Inclusion of mobile ions would allow one to study filamentation, self-focusing, and Brillouin scattering, as mentioned in sec. I A 1.

We also assume a cold plasma, since a finite temperature is not required by, but only complicates, the Raman instability; a finite temperature mathematically leads to a higher order differential equation that must be solved, and physically leads to thermal convection of the Langmuir wave out of the resonance zone. However, if the pump strength is large enough, the temporal growth will (as pointed out in Refs. F VII; G IX) dominate this convection (i. e., if $\gamma_o h/V_{gz} >> 1$ the Langmuir wave will grow substantially before it propagates out of the resonance zone of width h given by Eq. (I.10b)).

The scattered electromagnetic wave is coupled with the Langmuir wave and the pump wave through the transverse nonlinear current $\underline{J}_T(\omega_1)$ (see Fig. I.12), given essentially by the product of the density perturbation $\delta n(\Omega)$ at frequency Ω with the electron velocity $\underline{v}_o$ at frequency ω_o. This current resonantly radiates electromagnetic waves at frequency $\omega_1 = \omega_o - \Omega^*$ and wavevector $\underline{k}_1 = \underline{k}_o - \underline{K}$ (if $\underline{K}$ is such that $\omega_1^2 = \omega_p^2(z) + c^2k_1^2$), as described by the wave equation

$$\frac{\partial^2 \underline{E}}{\partial t^2} - c^2 \nabla^2 \underline{E} = -4\pi \frac{\partial \underline{J}}{\partial t} - 4\pi c^2 \underline{\nabla} \rho \quad . \qquad (I.21)$$

The charge density ρ (at frequency ω_1 and wavevector $\underline{k}_1$) is nonzero only if $\underline{\nabla} \cdot \underline{J}(\omega_1) \neq 0$ which occurs only if $k_{1x} = -K_x \neq 0$. This term, $\underline{\nabla}\rho(\omega_1)$, acts to cancel the longitudinal part of the current $\underline{J}(\omega_1)$ and leaves a transverse driving current $\underline{J}_T(\omega_1)$

acting along the direction of $(\hat{x} - k_{1x}\underline{k}_1/k_1^2)$, where $k_1^2(z) \equiv$ $\equiv \left[\omega_1^2 - \omega_p^2(z)\right]/c^2$.

The $\underline{\nabla}\rho(\omega_1)$ also introduces an additional longitudinal term proportional to $(\underline{k}_1 \underline{E}_1(\omega_1) \cdot \underline{\nabla} n_o(z))/k_1^2$ (i. e., an electromagnetic wave with a polarization component along a density gradient is not a purely transverse wave). Physically, this longitudinal term allows the electromagnetic wave $(\omega_1, \underline{k}_{1\perp})$, as it reaches its turning point $z_t(\omega_1, k_{1\perp})$ where $k_{1z}(z) = 0$, to linearly drive a Langmuir wave at the critical density position $z_t(\omega_1, k_{1\perp} = 0)$ where $\omega_p(z) =$ $= \omega_1$ and $k_1(z) = 0$ (Ref. R II).

For the Raman instability problem, this "resonance absorption" of the scattered electromagnetic waves should be a small effect (centered near $\omega_p(z) \approx \omega_o/2$) because the transverse current $\underline{J}_T(\omega_1)$ (giving the instability) leads to scattered electromagnetic waves, with polarization

$$\hat{e}_1(z, \omega_1, \underline{k}_{1\perp}) = \frac{\left(\hat{x} - k_{1x}\underline{k}_1/k_1^2\right)}{\left(1 - k_{1x}^2/k_1^2\right)^{1/2}} \quad , \qquad (I.22)$$

which have vanishing $\hat{z}$-component as $k_{1z}(z) \to 0$. The "resonance absorption" longitudinal term also introduces a shift in the turning point position $z_t(\omega_1, k_{1\perp})$ (Ref. R II); this shift is much smaller than $Z \equiv (c^2 L_n/\omega_p^2)^{1/3}$ (see also Eq. (I.10a)) if we restrict $k_{1\perp} Z \gg 1$ (i. e., $\omega_p(z)$ not too near $\omega_o/2$). Hence, we drop this longitudinal term in Eq. (I.21).

We have so far discussed the process whereby the presence of an electromagnetic wave of frequency $\omega_1 \approx \omega_o - \omega_p(z)$ can stimulate the emission of another such wave and a Langmuir wave of frequency $\Omega \approx \omega_p(z)$ (from a decay of the pump wave); that the phase relationship is such as to lead to a growth of these scattered waves (rather than a decay or a frequency shift) must be determined from the detailed derivation in sec. II. We must now decide how to initiate this electromagnetic wave in order to start the stimulated process.

The vector differential equation, Eq. (I.21), for $\underline{E}_1(z,\omega_1,\underline{k}_{1\perp})$ can be written as

$$\left[\frac{d^2}{dz^2} + k_{1z}^2\right]\underline{E}_1 \approx -\frac{4\pi e}{mc^2}\frac{\omega_1}{\omega_o}\rho^*(\Omega)E_o\left(1-\frac{k_{1x}^2}{k_1^2}\right)^{1/2}\hat{e}_1 + \underline{S}\ ; \qquad \text{(I.23)}$$

the first term on the right comes from $\underline{J}_T(\omega_1)$ ($e > 0$ here), $\underline{S}(z,\omega_1,\underline{k}_{1\perp})$ represents the $(\omega_1,\underline{k}_{1\perp})$ component of a transverse current noise source $\underline{S} = (4\pi/c^2)(\partial/\partial t)\underline{J}^T_{noise}$, and the term $k_{1z}^2(z,\omega_1,k_{1\perp}) \equiv \left[\omega_1^2 - \omega_p^2(z) - c^2k_{1\perp}^2\right]/c^2$ can also be written as $-2\omega_1\Delta_1(z)/c^2$ to compare with Eqs. (I.11, 12). The equation for the Langmuir wave charge density $\rho(z,\Omega,\underline{K} = \underline{k}_o - \underline{k}_1)$ can be written as

$$\Delta_p(z,\Omega)\rho(\Omega) \approx \frac{\omega_p^2 e K^2 E_o}{8\pi m\omega_o\omega_1^*\Omega}\underline{E}_1^*(\omega_1)\cdot\hat{x} \qquad \text{(I.24)}$$

where $\Delta_p \equiv \left[\omega_p^2(z) - \Omega^2\right]/2\Omega$ is the frequency mismatch in a cold plasma and the term on the right comes from $\underline{J}_I(\Omega)$. As discussed in sec. I B, we have ignored on the right of Eq. (I.24) any effects of a longitudinal current noise source (i. e., longitudinal Cerenkov as in Ref. N I, or bremsstrahlung as in Ref. N II).

As seen from Eqs. (I.23, 24), the induced scattered electromagnetic waves are polarized along $\hat{e}_1$, given by Eq. (I.22), provided $\underline{S}$ has a finite component along $\hat{e}_1$. The other orthogonal component of $\underline{S}$ (perpendicular to both $\hat{e}_1$ and $\underline{k}_1$) is in the direction of $(-k_{1y}\,\hat{z} + k_{1z}\,\hat{y})/(k_{1y}^2 + k_{1z}^2)^{\frac{1}{2}}$ and drives a component of $\underline{E}_1(\omega_1)$ perpendicular to $\hat{x}$; for this component, $\rho(\Omega) = 0$ and no growth occurs. Hence, we take only the $\hat{e}_1$ component of Eq. (I.23) and define $E_1(z,\omega_1,\underline{k}_{1\perp}) \equiv \hat{e}_1 \cdot \underline{E}_1(z,\omega_1,\underline{k}_{1\perp})$ and $S(z,\omega_1,\underline{k}_{1\perp}) \equiv \hat{e}_1 \cdot \underline{S}(z,\omega_1,\underline{k}_{1\perp})$. Using $\rho(\Omega)$ from Eq. (I.24), we have

$$\left[\frac{d^2}{dz^2} + Q(z,\omega_1,\underline{k}_{1\perp})\right] E_1(z,\omega_1,\underline{k}_{1\perp}) = S(z,\omega_1,\underline{k}_{1\perp}) \qquad \text{(I.25a)}$$

$$Q(z,\omega_1,\underline{k}_{1\perp}) \approx k_{1z}^2(z,\omega_1,k_{1\perp}) + \frac{D^2/c^2}{\omega_p^2(z) - (\omega_o - \omega_1)^2} \qquad \text{(I.25b)}$$

where the pump-strength parameter is

$$D(\omega_1,\underline{k}_{1\perp}) \equiv K v_o \omega_p \left(1 - \frac{k_{1x}^2}{k_1^2}\right)^{1/2} . \qquad \text{(I.25c)}$$

We ignore the weak z-dependence of D and just evaluate it at the resonance zone center $z_o(\omega_1, k_{1\perp})$. The above expression for Q is valid for Re $(\omega_1) \geq 0$; the full expression for Q (see sec. II) is symmetric about the Im(ω_1)-axis.

Finally, for our model we choose $S(z,\omega_1,\underline{k}_{1\perp}) = \delta(z - z_s)$, as motivated in sec. IB, and rename $E_1(z,\omega_1,\underline{k}_{1\perp})$ the Green's function $G_1(z,z_s;\omega_1,\underline{k}_{1\perp})$. In z-t space, this corresponds to the source $S(z,t,\underline{k}_{1\perp}) = \delta(t)\delta(z - z_s)$. The weak ω_1-dependence of $\hat{e}_1(z,\omega_1,\underline{k}_{1\perp})$ can be included in determining $\underline{G}_1(z,z_s;t,\underline{k}_{1\perp})$, from an ω_1-integration of $\hat{e}_1 G_1(z,z_s;\omega_1,\underline{k}_{1\perp})$, by evaluating $\hat{e}_1$ at the saddle-point frequencies and poles of $G_1(z,z_s;\omega_1,\underline{k}_{1\perp})$ exp $(-i\omega_1 t)$.

In this section we have described the assumed model and physical instability-mechanism leading to Eq. (I.25), with $S = \delta(z - z_s)$, for $G_1(z,z_s;\omega_1,\underline{k}_{1\perp})$. In the next section we describe the general procedure for solving this equation and obtaining $\underline{G}_1(z,z_s;t,\underline{k}_{1\perp})$, our final goal.

D. General Mathematical Procedure

In the previous section we briefly described how the Raman instability problem (in a cold, nonuniform, unmagnetized plasma) can be reduced to the mathematical problem of finding the Green's function solution, $G_1(z,z_s;\omega_1,\underline{k}_{1\perp})$, to Eq. (I.25) with the source $S = \delta(z - z_s)$. The standard solution is (Ref. sec. P)

$$G_1(z_g,z_\ell;\omega_1,\underline{k}_{1\perp}) = \frac{\Psi_1(z_\ell,\omega_1,\underline{k}_{1\perp})\,\Psi_2(z_g,\omega_1,\underline{k}_{1\perp})}{W(\omega_1,\underline{k}_{1\perp})} \qquad \text{(I.26)}$$

where the Wronskian (or conjunct in Ref. P III) is defined as $W \equiv \Psi_1 d\Psi_2/dz - \Psi_2 d\Psi_1/dz$ and (z_g, z_ℓ) are defined respectively as the greater (g) or lesser (ℓ) of the two positions (z, z_s). The functions Ψ_1 and Ψ_2 are solutions of the homogeneous Eq. (I.25) (with S = 0) subject to the separate boundary conditions

Ψ_1 { is outgoing for $z \to -\infty$ (I.27a)

or

matches onto outgoing solution at $z = 0$ (I.27b)

Ψ_2 { is outgoing for $z \to +\infty$ (I.28a)

or

evanescent for $z \to +\infty$. (I.28b)

Assuming for the moment that we know $G_1(z_g, z_\ell; \omega_1, \underline{k}_{1\perp})$, we obtain the z-t response by inverting the ω_1-transform (Laplace) by integrating in the complex ω_1-plane along the Bromwich contour (B) above all singularities and branch-points of the integrand (see Ref. P III):

$$\underline{G}_1(z_g, z_\ell; t, \underline{k}_{1\perp}) = \int_B \frac{d\omega_1}{2\pi} e^{-i\omega_1 t} \hat{e}_1 G_1(z_g, z_\ell; \omega_1, \underline{k}_{1\perp}) \qquad (I.29)$$

where the polarization vector $\hat{e}_1(z, \omega_1, \underline{k}_{1\perp})$ is given by Eq. (I.22). The problem now is to determine Ψ_1 and Ψ_2, and to answer this we consider first a uniform plasma (sec. I D 1) and then a non-uniform plasma (sec. I D 2).

1. *Uniform Plasma*

Assuming $\exp(-i\omega_1 t)$ time dependence as in Eq. (I.29), the boundary conditions Eqs. (I.27a, 28a) and the homogeneous Helmholtz equation Eq. (I.25) are satisfied by

$$\Psi_1 = \exp\left\{-i\left[Q(\omega_1, \underline{k}_{1\perp})\right]^{1/2} z_\ell\right\} \qquad \text{(I.30a)}$$

$$\Psi_2 = \exp\left\{+i\left[Q(\omega_1, \underline{k}_{1\perp})\right]^{1/2} z_g\right\} \qquad \text{(I.30b)}$$

$$W = 2i\left[Q(\omega_1, \underline{k}_{1\perp})\right]^{1/2} \qquad \text{(I.30c)}$$

provided we choose the branch-cuts (emanating from the branch-points where $Q = 0$ or ∞) such that $\mathrm{Re}\,(\sqrt{Q}) > 0$ for $\mathrm{Re}\,(\omega_1) > 0$ and $\mathrm{Re}(\sqrt{Q}) < 0$ for $\mathrm{Re}\,(\omega_1) < 0$ along the Bromwich contour <u>above</u> the branch-points. In evaluating $\underline{G}_1(z_g, z_\ell; t, \underline{k}_{1\perp})$ from Eq. (I.29), the Bromwich countour (B) can be "depressed" (using Cauchy's theorem; see Ref. S I) into a contour (B') only around the branch-cuts (there are no poles of W^{-1}) plus a negligible contour of infinite radius (see Fig. I.13). For the uniform unpumped plasma (sec. III A), $Q(\omega_1, \underline{k}_{1\perp})$ is sufficiently simple that the ω_1-integration can be performed exactly. For the uniform pumped plasma (sec. III C), the saddle-point frequencies (Ref. sec. U) and time-asymptotic ($t\left[\omega_p^2(z_s) + c^2 k_{1\perp}^2\right]^{\frac{1}{2}} \gg 1$) response can be obtained.

2. Nonuniform Plasma

It is now generally desirable to transform variables from z to a dimensionless variable $\rho(z,\omega_1,\underline{k}_{1\perp})$ in terms of which Q has a simple form (e. g., for the nonuniform unpumped plasma in sec. III B we choose $\rho = -Z^2 k_{1z}^2(z,\omega_1,\underline{k}_{1\perp})$ with $d\rho/dz = Z^{-1}$, where $Z \equiv (c^2 L_n/\omega_p^2)^{1/3}$). If we somehow know two linearly independent solutions A and B of the homogeneous transformed version of Eq. (I.25), then Ψ_1 and Ψ_2 can be written as appropriate linear combinations of A and B. Assuming that solution A already satisfies boundary condition Eq. (I.28b), we write

$$\Psi_1 = a(\omega_1,\underline{k}_{1\perp})\,A(\rho_\ell,\omega_1,\underline{k}_{1\perp}) - i\,B(\rho_\ell,\omega_1,\underline{k}_{1\perp}) \qquad \text{(I.31a)}$$

$$\Psi_2 = A(\rho_g,\omega_1,\underline{k}_{1\perp}) \qquad \text{(I.31b)}$$

$$W(\omega_1,\underline{k}_{1\perp}) = -i\,(BA' - AB')\,\frac{d\rho}{dz} \qquad \text{(I.31c)}$$

where $\rho_\ell \equiv \rho(z_\ell,\omega_1,\underline{k}_{1\perp})$, $\rho_g \equiv \rho(z_g,\omega_1,\underline{k}_{1\perp})$, $A' = dA/d\rho$, and $B' = dB/d\rho$.

The coefficient $a(\omega_1,\underline{k}_{1\perp})$ is determined by the requirement that Ψ_1 satisfy boundary condition Eq. (I.27b): i. e., Ψ_1 from Eq. (I.31) must have the same value and first z-derivative as Ψ_1 from Eq. (I.30) at the boundary position $z = 0$ between the uniform and nonuniform plasma regions shown in Fig. I.11. We find

$$a(\omega_1,\underline{k}_{1\perp}) = i\,\frac{\left\{B(\rho_o,\omega_1,\underline{k}_{1\perp}) - i\,\dfrac{B'(\rho_o,\omega_1,\underline{k}_{1\perp})\,d\rho/dz}{[Q(z=0,\omega_1,\underline{k}_{1\perp})]^{1/2}}\right\}}{\left\{A(\rho_o,\omega_1,\underline{k}_{1\perp}) - i\,\dfrac{A'(\rho_o,\omega_1,\underline{k}_{1\perp})\,d\rho/dz}{[Q(z=0,\omega_1,\underline{k}_{1\perp})]^{1/2}}\right\}} \qquad (I.32)$$

where $\rho_o \equiv \rho(z = 0,\omega_1,\underline{k}_{1\perp})$ and $d\rho/dz$ is evaluated at $z = 0$. The coefficient $a(\omega_1,\underline{k}_{1\perp})$ has branch-points where $Q(z = 0,\omega_1,\underline{k}_{1\perp}) = 0$ or ∞ (the solutions A and B introduce no additional branch-points). The complicated form of $a(\omega_1,\underline{k}_{1\perp})$ in Eq. (I.32) is required in order for $a(\omega_1,\underline{k}_{1\perp})$ to approach, far from its branch-points, certain limiting forms (necessary if Ψ_1 in Eq. (I.31) is to be essentially outgoing near $z = 0$ for waves with turning point positions $z_t(\omega_1,k_{1\perp}) >> Z \equiv (c^2L_n/\omega_p^2)^{1/3} > 0$) and yet remain continuous across the $\mathrm{Im}\,(\omega_1)$-axis.

We have now specified Ψ_1 and Ψ_2 in terms of two linearly independent (and still somewhat arbitrary) solutions A and B (with A assumed evanescent as $z \to +\infty$) of the homogeneous transformed version of Eq. (I.25). For the nonuniform unpumped plasma (see sec. III B), exact solutions are available in terms of the two Airy functions, and we choose $A(\rho,\omega_1,\underline{k}_{1\perp}) = \mathrm{Ai}(\rho)$ and $B(\rho,\omega_1,\underline{k}_{1\perp}) = \mathrm{Bi}(\rho)$. For the nonuniform pumped plasma (see sec. V), exact solutions are not currently available, and we instead use phase-integral (or WKBJ) techniques (see sec. IV and Ref. sec. T) in the complex ρ-plane to obtain approximate solutions $A(\rho,\omega_1,\underline{k}_{1\perp})$ and $B(\rho,\omega_1,\underline{k}_{1\perp})$.

Although these approximate solutions are not valid too near the transition points where $Q(z,\omega_1,\underline{k}_{1\perp}) = 0$ or ∞, they are valid in regions completely encircling these points. Thus, although we cannot use these approximate solutions to look at the side-scattered wave right at its turning point, we can look at the side-scattered wave slightly before and after it encounters its turning point (and resonance zone) and, thereby, obtain the side-scatter exponentiation factor Γ (see sec. I A 3b), the saturation time t_s (see sec. I B), and the resonance zone width h (see sec. I A 3b). In principle, if one desired more detailed information about the turning point (and resonance zone) region, a Langer's transformation (Ref. sec. T) or a series expansion (illustrated in sec. III B for a non-uniform unpumped plasma) could be used to obtain approximations for A and B valid at the turning point; such calculations are not carried out in this paper.

II. DERIVATION OF BASIC EQUATIONS

In describing the physical mechanism for the Raman instability and displaying the form of the equation (i. e., Eq. (I.25a)) that is to be solved later in secs. III and V, we have already outlined in sec. I C the derivation of the basic equations. We do not wish to repeat ourselves here but, rather, will concentrate on a few of the more important intermediate steps and complexities that may not be obvious from just reading sec. I C.

First of all, in going from Eq. (I.19) to Eq. (I.20), we approximate $\underline{v} = -(e/m)\int^t \underline{E}\, dt'$ to first order in the total electric field and use this in Eq. (I.19) to get an equation for $\partial\underline{v}/\partial t$ valid to second order in $\underline{E}$. Using $\underline{\nabla} \times \int^t \underline{E}\, dt' = -(1/c)\int^t \partial\underline{B}/\partial t\, dt' = -\underline{B}/c$, one term from $\underline{v} \cdot \underline{\nabla}\, \underline{v}$ cancels with $-(e/mc)\underline{v} \times \underline{B}$ while the remaining term gives $(e^2/2m^2)\underline{\nabla}\left[\int^t \underline{E}\, dt' \cdot \int^t \underline{E}\, dt''\right]$ resulting in Eq. (I.20). The validity of this expansion requires $(v_o/c) \equiv (e\, E_o/m\, \omega_o c) \ll 1$.

From Eq. (I.20), we can compute the current $\underline{J} = -en\underline{v}$, $n = n_o + \delta n$, which in turn gives the charge density $\rho = -e\delta n$ from the continuity equation $\partial^2\rho/\partial t^2 = -\underline{\nabla} \cdot \partial\underline{J}/\partial t = e\underline{\nabla} \cdot (n_o \partial\underline{v}/\partial t) - \underline{\nabla} \cdot \partial(\rho\underline{v})/\partial t$ or, using Eq. (I.20) and Poisson's equation,

$$\left[\frac{\partial^2}{\partial t^2} + \omega_p^2(z)\right]\rho \approx -\frac{e\omega_p^2}{8\pi m}\nabla^2\left(\int \underline{E}\, dt'\right)^2 - \underline{\nabla}\cdot\frac{\partial}{\partial t}(\rho\underline{v}) \quad . \tag{II.1}$$

We have made two approximations here: first, we dropped a term $-(e^3/2m^2)\underline{\nabla}(\int \underline{E}\, dt')^2 \cdot \underline{\nabla} n_o$ which is valid provided $k_o L_n \gg 1$; second, we dropped a term $-(e^2/m)\underline{E} \cdot \underline{\nabla} n_o$ which (when computing $\rho(\Omega)$) requires $(\gamma + \nu_p)/\omega_p \gg k_o/2K^2 L_n$ or essentially $k_o h \gg 1$ (γ = growth rate, ν_p = plasmon damping, and h = resonance zone width) and which (when computing $\rho(\omega_1)$ and $\underline{E}_1(\omega_1)$) requires $(\gamma + \nu_1)/\omega_p \gg 2\pi(\omega_p/\omega_1)(\hat{e}_1 \cdot \hat{z})/k_1(z)L_n$ (ν_1 = damping of scattered electromagnetic wave with polarization $\hat{e}_1$ and effective wavenumber $k_1(z) \equiv (\omega_1^2 - \omega_p^2(z))^{\frac{1}{2}}/c$). Since we later find $\hat{e}_1 = (\hat{x} - k_{1x}\underline{k}_1/k_1^2)/(1 - k_{1x}^2/k_1^2)^{\frac{1}{2}}$ or $\hat{e}_1 \cdot \hat{z} = (k_{1x}/k_1)k_{1z}/(k_{1z}^2 + k_{1y}^2)$, the above requirement will be no more difficult to satisfy than our earlier requirement on γ provided $k_{1y}/k_o \gtrsim 8\pi(\omega_p/\omega_1)k_{1x}k_{1z}(z)/k_{1y}^2$ (assuming $k_{1x}/k_{1y} \ll 1$ and $k_{1z}/k_{1y} \ll 1$); although the right-hand-side of this inequality vanishes at the turning point, for fixed ratios k_{1x}/k_{1y} and k_{1z}/k_{1y} this sets a lower bound on k_{1y} and thus on how close we can be to the "quarter critical" position ($\omega_p \to \omega_1 \to \omega_o/2$) and still use our equations.

We next Fourier transform Eq. (II.1) in order to obtain $\rho(\Omega)$ and $\rho(\omega_1)$. For $\rho(\Omega)$, we also drop the term $-\underline{\nabla} \cdot \partial\left[\rho^*(\omega_1)\underline{v}_o\right]/\partial t$ since it turns out to be negligible provided $(\gamma + \nu_p)/\omega_p \gg (v_o/c)^2(\omega_1/\omega_p)k_{1x}^2/k_1^2(z)$ while, from Eq. (I.2), $\gamma_o/\omega_p \approx (v_o/c)\omega_o/(\omega_p\omega_1)^{\frac{1}{2}}$. The result is

$$\underline{E}(\Omega) = i\frac{e\omega_p^2}{m\omega_o}\frac{\underline{K}}{\left[(\Omega+i\nu_p)^2-\omega_p^2(z)\right]}\times$$

$$\times\left[\frac{\underline{E}_o\cdot\underline{E}^*(\omega_o-\Omega^*)}{\omega_o-\Omega}+\frac{\underline{E}_o^*\cdot\underline{E}(\omega_o+\Omega)}{\omega_o+\Omega}\right] \qquad \text{(II.2)}$$

where we have used $\underline{E}(\Omega) = -i4\pi\rho(\Omega)\underline{K}/K^2$ (assuming an exponential variation $\exp\left(i\int\underline{K}\cdot d\underline{x}\right)$ and $k_o h \gg 1$) and also $\underline{E}^*(-\omega^*) = \underline{E}(\omega)$ from the reality condition on $\underline{E}(t) = \int \exp(-i\omega t)\underline{E}(\omega)d\omega$. For $\rho(\omega_1)$, keeping both terms in Eq. (II.1),

$$\rho(\omega_1) = \frac{e\omega_p^2}{4\pi m\omega_o c^2 k_1^2}\nabla^2\left[\underline{E}_o\cdot\frac{\underline{E}^*(\omega_o-\omega_1^*)}{\omega_o-\omega_1}+\underline{E}_o^*\cdot\frac{\underline{E}(\omega_o+\omega_1)}{\omega_o+\omega_1}\right]-$$

$$-\frac{e\omega_1}{m\omega_o c^2 k_1^2}\nabla\cdot\left[\underline{E}_o\rho^*(\omega_o-\omega_1^*)-\underline{E}_o^*\rho(\omega_o+\omega_1)\right]. \qquad \text{(II.3)}$$

Equation (II.2) is appropriate for $\underline{E}(\Omega)$ or $\rho(\Omega)$ whenever $|\Omega| \lesssim \omega_p$, representing a longitudinal plasma wave; Eq. (II.3) is the more general equation for $\rho(\omega)$ and is valid even when $|\omega_1| \gtrsim \omega_p$, representing an approximately transverse electromagnitic wave (the transverse component of the electric field, $\underline{E}_1(\omega_1)$, is determined from Eq. (I.21)).

Finally, we Fourier transform Eq. (I.21) and use Eq. (II.3) to obtain (defining $\overleftrightarrow{I}$ to be the unit tensor):

$$\left[k_1^2(z)+\nabla^2\right]\underline{E}_1(\omega_1)=\frac{-4\pi e\omega_1}{mc^2\omega_o}\left[\overleftrightarrow{I}+k_1^{-2}(z)\underline{\nabla}\underline{\nabla}\right]\cdot$$

$$\cdot\left[\underline{E}_o\rho^*(\omega_o-\omega_1^*)-\underline{E}_o^*\rho(\omega_o+\omega_1)\right]. \qquad \text{(II.4)}$$

We have dropped a term on the right of Eq. (II.4) that is proportional to $\left[k_1^2+\nabla^2\right]\underline{\nabla}\left[\underline{E}_o\cdot\underline{E}^*(\omega_o-\omega_1^*)/(\omega_o-\omega_1)+\underline{E}_o^*\cdot\right.$ $\left.\cdot\underline{E}(\omega_o+\omega_1)/(\omega_o+\omega_1)\right]$. Using Eq. (II.2) to get $E^*(\omega_o-\omega_1^*)=E^*(\Omega)$ and using Eq. (II.4) to get $\left[k_1^2+\nabla^2\right]\underline{E}_1(\omega_1)$, this term effectively only alters Eq. (II.4) by changing $k_1^{-2}(z)\underline{\nabla}\,\underline{\nabla}$ to $(1+\alpha)k_1^{-2}(z)\,\underline{\nabla}\,\underline{\nabla}$ where $|\alpha|\lesssim(v_o/c)^2\omega_p^2/2\omega_1(\gamma+\nu_p)\lesssim$ $(v_o/c)(\omega_p/\omega_o)(\omega_p/\omega_1)^{\frac{1}{2}}\ll 1$ (using Eq. (I.2) for γ_o). If ω_1 is replaced by $-\omega_1^*$ everywhere in Eq. (II.4), we get back the complex conjugate of Eq. (II.4), for the quantity $\underline{E}_1(-\omega_1^*)$. Since the complex conjugate of Eq. (II.4) for $\underline{E}_1^*(\omega_1)$ is also a solution, this gives $\underline{E}_1(-\omega_1^*)=\underline{E}_1^*(\omega_1)$ as required for reality. We therefore consider for now only $\mathrm{Re}(\omega_1)\geq 0$, and look at the terms $\rho^*(\omega_o-\omega_1^*)$ and $\rho(\omega_o+\omega_1)$.

If we take $\omega_o-\omega_1^*=\Omega\approx\omega_p$, $\omega_o+\omega_1\approx 2\omega_o-\omega_p\geq 3\omega_p$ ($\omega_o\geq 2\omega_p$ for the Raman instability), and $\rho(\omega_o+\omega_1)$ is non-resonant with a local Langmuir wave and is therefore negligible. For $\rho^*(\Omega)$ we use Eq. (II.2) which has two terms: the first term involves $\underline{E}_1^*(\omega_1)$ which we are trying to calculate in Eq. (II.4); the second term involves $\underline{E}(\omega_o+\Omega)=\underline{E}(2\omega_o-\omega_1^*)$ which corresponds

to the four-wave process where two photons $(\omega_o, \underline{k}_o)$ are incident on a Langmuir wave $(\Omega = \omega_o - \omega_1^*, \ \underline{K} = \underline{k}_o - \underline{k}_1)$ and scatter into two new waves $(\omega_1, \underline{k}_1)$, which we are looking at in Eq. (II.4), and $(2\omega_o - \omega_1^*, \ 2\underline{k}_o - \underline{k}_1)$. If we assume that $\underline{E}_1(\omega_1)$ is a resonant normal mode (i. e., an electromagnetic wave satisfying Eq. (II.4)) with $c^2k_1^2(z) = \omega_1^2 - \omega_p^2(z)$, and $c^2k_o^2(z) = \omega_o^2 - \omega_p^2(z)$, then in order for $\underline{E}(2\omega_o - \omega_1^*)$ to be a resonant electromagnetic wave with $c^2|2\underline{k}_o - \underline{k}_1|^2 = (2\omega_o - \omega_1)^2 - \omega_p^2(z)$ requires $\underline{k}_o \cdot \underline{k}_1 = \left[\omega_o\omega_1 - \omega_p^2(z)\right]/c^2$. This is impossible to satisfy except for forward scattering $(\hat{k}_o \cdot \hat{k}_1 = 1)$ at zero density (i. e., no scattering at all of incident photons), so we drop the nonresonant term $\underline{E}(\omega_o + \Omega)$ in Eq. (II.2).

The last step is to substitute our expression for $\rho^*(\Omega)$ into Eq. (II.4) and simplyfy. Assuming an exponential variation $\exp i\int \underline{k}_1 \cdot d\underline{x}$, we replace $\underline{\nabla}$ by $i\underline{k}_1(z)$ on the right of Eq. (II.4) (ignoring variations of the resonant denominator in $\rho^*(\Omega)$, valid for $k_o h \gg 1$). Since $\underline{E}_o = E_o \hat{x}$, the vector dependence of the right side of Eq. (II.4) is given by $(\hat{x} - \underline{k}_1 k_{1x}/k_1^2)$ which results in the polarization $\hat{e}_1$ given in Eq. (I.22). The vector $\underline{k}_1$ is obtained by Fourier transforming Eq. (II.4) in the x and y directions and calculating $\underline{E}_1(\omega_1)$ for each value of $\underline{k}_{1\perp} = k_{1x}\hat{x} + k_{1y}\hat{y}$. Whenever $\underline{k}_1$ is used on the right side of Eq. (II.4) (e. g., in $\hat{e}_1$), we use $k_{1z}(z) \equiv \left[\omega_1^2 - \omega_p^2(z) - c^2k_{1\perp}^2\right]^{\frac{1}{2}}/c$ from geometrical optics; on the left side of Eq. (II.4), we keep the full second

derivative d^2/dz^2 in order to determine accurately the z variations, so that we replace $k_1^2(z) + \nabla^2$ by $k_{1z}^2(z) + d^2/dz^2$. The use of this $k_{1z}(z)$ in $\hat{e}_1$ is only meant as a rough approximation and is not meant to be taken too seriously when $k_{1z}(z) \lesssim Z^{-1} \equiv$ $\equiv (c^2 L_n/\omega_p^2)^{-1/3}$, where Z is an effective minimum wavelength from the Airy function. After factoring $\hat{e}_1$ from both sides of Eq. (II.4), $\hat{e}_1$ will seldom be mentioned again. Our final equation for $E_1(z,\omega_1,\underline{k}_{1\perp})$ is then

$$\left[k_{1z}^2(z) + \frac{d^2}{dz^2}\right] E_1 = \omega_p^2 \left(\frac{v_o}{c}\right)^2 \left(1 - \frac{k_{1x}^2}{k_1^2}\right) \times \tag{II.5}$$

$$\times \left[\frac{|\underline{k}_o - \underline{k}_1|^2}{(\omega_o - \omega_1 - i\nu_p)^2 - \omega_p^2(z)} + \frac{|\underline{k}_o + \underline{k}_1|^2}{(\omega_o + \omega_1 + i\nu_p)^2 - \omega_p^2(z)}\right] E_1$$

where the second term on the right here is from the second term on the right in Eq. (II.4) (i. e., the $\rho(\omega_o + \omega_1)$ term) and is necessary when $\mathrm{Re}(\omega_1) \leq 0$ in order to have $E_1^*(z,\omega_1,\underline{k}_{1\perp}) =$ $= E(z,-\omega_1^*,-\underline{k}_{1\perp})$ from the reality condition. For $\mathrm{Re}(\omega_1) \geq 0$, this gives Eq. (I.25) which is the basic equation we will be working with in later sections.

III. APPLICATION OF MATHEMATICAL PROCEDURE TO SIMPLER CASES

Before applying the mathematical procedure outlined in sec. I D to our main problem of interest (i. e., the nonuniform pumped case in sec. V), we first "test" it on three simpler limiting cases where either the pump vanishes, or the density scale-length becomes infinitely large, or both. For these three cases, the results are generally considered to be "well-known" (at least qualitatively) and will serve as checks on our procedure and on the results we obtain later in sec. V.

A. Uniform Plasma, No Pump

For this case, $Q(z,\omega_1,\underline{k}_{1\perp})$ in Eq. (I.25) becomes just

$$Q(\omega_1,k_{1\perp}) = k_{1z}^2(\omega_1,k_{1\perp}) \equiv \frac{(\omega_1+i\nu_1)^2-\omega^2}{c^2} \qquad \text{(III.1)}$$

where $\omega^2 \equiv \omega_p^2 + c^2k_{1\perp}^2$, and using Eq. (I.30) in Eq. (I.26),

$$G_1(z_g,z_\ell;\omega_1,k_{1\perp}) = -i\frac{c}{2}\,\frac{\exp\left\{i\left[(\omega_1+i\nu_1)^2-\omega^2\right]^{1/2}\frac{z_g-z_\ell}{c}\right\}}{\left[(\omega_1+i\nu_1)^2-\omega^2\right]^{1/2}} \qquad \text{(III.2)}$$

where the branch-cuts (emanating from the branch-points) are chosen as in Fig. I.13. For this simple case, the ω_1-integration in Eq. (I.29) can be performed exactly except for the $\hat{\epsilon}_1(\omega_1,\underline{k}_{1\perp})$ which we evaluate at the saddle-point frequency ω_A found below. The

result is $\underline{G}_1(z_g, z_\ell; t, \underline{k}_{1\perp}) = \hat{e}_1(\omega_A, \underline{k}_{1\perp}) \exp(-\nu_1 t) G_1(\Psi)$ where

$$G_1(\Psi) = -\frac{c}{2} J_o(\Psi) \qquad \text{(III.3a)}$$

$$\Psi \equiv \omega \left[t^2 - \frac{(z_g - z_\ell)^2}{c^2} \right]^{1/2} \qquad \text{(III.3b)}$$

if $(z_g - z_\ell) < ct$ and $G_1 = 0$ if $ct < (z_g - z_\ell)$ (this is just the "light cone"), where J_o is the Bessel function of order zero. Since $(z_g - z_\ell)^2 = (z - z_s)^2$, Ψ and G_1 are symmetric about the source position z_s (as expected for a uniform plasma). For large phase $\Psi >> 1$, $J_o(\Psi)$ can be expanded giving

$$G_1(\Psi) \approx -c(2\pi\Psi)^{-1/2} \sin\left(\Psi + \frac{\pi}{4}\right) \qquad \text{(III.4)}$$

which can also be obtained by using the saddle-point approximation (Ref. sec. U) on Eqs. (III.2 and I.29).

Our basic procedure from sec. I D 1 was to depress the original Bromwich ω_1-integration contour into a contour only around our arbitrarily positioned branch-cuts; for the saddle-point approximation of this integral (Eq. (I.29)), however, we must deform this "branch-cut" contour into a new contour which follows the path of steepest descent (see Ref. sec. U) for the integrand in Eq. (I.29). Using Eq. (III.2), one can easily show that a saddle-point (for the integrand) can only exist above the branch-cut in

Fig. I.13. This is further discussed in sec. III C (in the paragraph preceding Eq. (III.36)) and illustrated in Fig. III.6 which shows lines of constant real and imaginary part of the phase of the integrand (here, the phase Ψ is given by Eq. (III.24b)).

The saddle-point frequency $\omega_1 = \omega_A$ obtained this way, or by just using $\omega_A \equiv \partial\Psi/\partial t$ with Ψ given by Eq. (III.3b), is

$$\omega_A(\eta) = \omega/(1-\eta^2)^{1/2} \qquad \text{(III.5a)}$$

$$\eta \equiv (z-z_s)/ct \ , \qquad \text{(III.5b)}$$

so that trajectories of wave-packets of constant frequency ω_A are straight lines in t-z space. The wave-packet wavenumber along z is just $k_z \equiv -\partial\Psi/\partial z$ or

$$k_z(\eta) = \frac{\omega_A \eta}{c} = \frac{(\omega_A^2-\omega^2)^{1/2}}{c} \qquad \text{(III.6)}$$

as expected. The lines of constant phase Ψ in t-z space are hyperbola with the light cone giving the asymptotes. The lines of constant ω_A and Ψ are shown in Fig. III.1, while $(2/c)G_1 = -J_o(\Psi)$ is plotted (but reduced by a factor of 0.0075) in Fig. III.4a as described in sec. III B.

Finally, a brief comment may be in order concerning the choice of Eq. (I.22) for $\hat{e}_1$ since we have no pumped instability here to give a preferred polarization direction. Nevertheless, for any wave with given ω_1 and $\underline{k}_{1\perp}$, at any location Eq. (I.21) will pick from the noise current $\underline{J}_{noise}$ only the transverse component (of proper ω_1 and $\underline{k}_{1\perp}$) which is perpendicular to $\underline{k}_1$ (where k_{1z} is determined from Eq. (I.21)). Among all the polarizations in the plane perpendicular to $\underline{k}_1$, we limit ourselves to $\hat{e}_1$ in order to compare our later pumped results in sec. III C and sec. V with the known unpumped results of secs. III A, B.

B. Nonuniform Plasma, No Pump

For this case, Eq. (I.25b) gives

$$Q(z,\omega_1,k_{1\perp}) = k_{1z}^2(z,\omega_1,k_{1\perp}) = -\frac{\rho}{Z^2} \qquad \text{(III.7)}$$

where $\rho \equiv -Z^2 k_{1z}^2$, $k_{1z}^2 \equiv \left[(\omega_1 + i\nu_1)^2 - \omega^2(z)\right]/c^2$, $\omega^2(z) \equiv$ $\equiv \omega_p^2(z) + c^2 k_{1\perp}^2$, and $Z \equiv (c^2 L_n/\omega_p^2)^{1/3}$. In terms of this new dimensionless variable ρ, the homogeneous transformed version of Eq. (I.25a) now reads

$$\left[\frac{d^2}{d\rho^2} - \rho\right] f_1(\rho) = 0 \qquad \text{(III.8)}$$

which has the two solutions (Airy functions)

$$A(\rho) = Ai(\rho) \qquad \text{(III.9a)}$$

$$B(\rho) = Bi(\rho) \qquad \text{(III.9b)}$$

as discussed in sec. I D 2. Using Eq. (I.31), with $W = i/\pi Z$, Eq. (I.26) becomes (III.10)

$$G_1(z_g, z_\ell; \omega_1, k_{1\perp}) = -i\pi Z\left\{\left[aAi(\rho_\ell) - iBi(\rho_\ell)\right]Ai(\rho_g)\right\}$$

where the branch-cuts and branch-points of $a(\omega_1, k_{1\perp})$ (at $\pm\omega(z = 0)$ now) are shown in Fig. I.13, $\rho_\ell \equiv \rho(z_\ell)$, $\rho_g \equiv \rho(z_g)$, and $a(\omega_1, k_{1\perp})$ is given by Eq. (I.32).

To perform the ω_1-integration in Eq. (I.29), we depress the Bromwich contour and change to an integration around each branch-cut (as discussed in sec. I D 1 and shown in Fig. I.13). Since $Ai(\rho)$ and $Bi(\rho)$ are entire analytic functions, they do not change across the branch-cuts of $a(\omega_1, k_{1\perp})$ and, therefore, the term $Bi(\rho_\ell)\, Ai(\rho_g)$ does not contribute to the integral. From the form of $a(\omega_1, k_{1\perp})$ given in Eq. (I.32), we find that in going from a point ω_1 to the corresponding point $\omega_1' = \omega_1^*$ around and on the other side of a branch-cut gives $a(\omega_1' = \omega_1^*, k_{1\perp}) = -a^*(\omega_1, k_{1\perp})$;

but, since the direction of integration is then reversed, $a d\omega_1$ at ω_1' equals the complex conjugate of $a d\omega_1$ at ω_1. Thus, we can reduce our ω_1-integration to an integral along one side of each branch-cut with $a(\omega_1, k_{1\perp})$ replaced by $2\mathrm{Re}(a)$; with $\mathrm{Re}(a)$ the same but $d\omega_1$ in opposing directions on these two branch-cut sides, and $\exp(-i\omega_1 t) - \exp(i\omega t) = -2i \sin \omega_1 t$, Eq. (I.29) reduces to $\underline{G}_1(z_g, z_\ell; t, \underline{k}_{1\perp}) = \hat{e}_1(\omega_{1s}, \underline{k}_{1\perp}) \exp(-\nu_1 t) G_1(\rho_g, \rho_\ell; t, k_{1\perp})$ where

$$G_1 = -2Z \int_{\omega(z=0)}^{\infty} d\omega_1 \, \mathrm{Re}(a) \sin(\omega_1 t) \, Ai(\rho_\ell) Ai(\rho_g). \qquad \text{(III.11)}$$

In the above, we have evaluated $\hat{e}_1$ at the saddle-point frequency ω_{1s} that will be found below, and all the effects of ν_1 are incorporated in the single term $\exp(-\nu_1 t)$ by transforming to a new $\omega_1 = (\omega_1)_{\mathrm{old}} + i\nu_1$. The integration in Eq. (III.11) is now along the real axis (above the branch-cut in Fig. I.13) with ρ_ℓ and ρ_g real (the ν_1 now removed from the definitions of k_{1z}^2 and ρ).

The term $Ai(\rho_g)$ will be exponentially small unless $\rho_g \leq 0$ or $\omega_1 \geq \omega_g \equiv \omega(z_g)$ and, since $\omega_g \geq \omega_s \equiv \omega(z_s)$ ($z_g \geq z_s$ by definition), ω_s provides an absolute lower bound on frequencies of interest here. It is easy to show from Eq. (I.32) that, for $\rho(z = 0) \ll -1$ (or $\omega_1^2 - \omega^2(z = 0) \gg c^2/Z^2$), $\mathrm{Re}(a) \approx 1$ above the cut (where our integration lies). In order to use this here requires $\omega_s^2 - \omega^2(0) \gg c^2/Z^2$ or $z_s \gg Z$ (i. e., the distance from the boundary at $z = 0$ to the source at z_s must greatly

exceed the effective minimum wavelength along z). As mentioned in sec. I D 2, this ($\mathrm{Re}(a) \gtrsim 1$ and $z_s \gg Z$) makes $\Psi_1(\rho) = a\,\mathrm{Ai}(\rho) - iB\mathrm{i}(\rho)$ essentially an outgoing (i. e., left-going) wave for $z > 0$ and eliminates waves reflected from the discontinuity in density gradient at $z = 0$ (see Fig. I.11).

We evaluate Eq. (III.11) asymptotically and take $\xi \equiv L_n\omega_s^3/c\omega_p^2 = (Z\omega_s/c)^3 \gg 1$ as our large parameter. It is then convenient to define new dimensionless variables $\tilde{z} \equiv \omega^2(z)/\omega_s^2 = 1 + (\omega_s/c)(z - z_s)/\xi$, $\tilde{t} \equiv \omega_s t/\xi$, and $\tilde{\omega}_1 = \omega_1/\omega_s$. It is also convenient to divide $\tilde{t} - \tilde{z}$ space into eight regions, as shown in Fig. III.2, even though G_1 sometimes takes on the same form in two different regions. In regions 1,3,4, and 6, $\rho_\ell \lesssim -1$ and $\rho_g \lesssim -1$ so we use the appropriate asymptotic (or WKB) form for $\mathrm{Ai}(\rho)$:

$$\mathrm{Ai}(\rho) \approx \pi^{-1/2}(-\rho)^{-1/4}\sin\left[\frac{2}{3}(-\rho)^{3/2} + \frac{\pi}{4}\right]. \qquad \text{(III.12)}$$

In regions 2 and 5, $\rho_\ell \lesssim -1$ but $-1 \lesssim \rho_g \leq 0$ so we write $\mathrm{Ai}(\rho_g) = \exp\left\{\ln\left[\mathrm{Ai}(\rho_g)\right]\right\}$ in Eq. (III.11) and use the series expansion

$$\mathrm{Ai}(\rho_g) = \mathrm{Ai}(0)\left(1 + \rho_g^3/6 + \cdots\right) + \mathrm{Ai}'(0)\left(\rho_g + \rho_g^4/12 + \cdots\right) \qquad \text{(III.13)}$$

where $Ai(0) = 0.3550$ and $A'i(0) = -0.2588$. For $\tilde{t} \ll 1$ and $|1 - \tilde{z}| \ll 1$, our eventual solutions for G_1 in regions 1 and 6 become just Eq. (III.4) while our solutions for G_1 in regions 2 - 5 approach in magnitude Eq. (III.4) for $\tilde{t} \sim 2/\xi^{1/3} \ll 1$, so in regions 0 and 7 we use Eq. (III.3) for G_1. The boundaries for the various regions will be discussed below; the boundary at $z = 0$, however, is now at $\tilde{z}(z = 0)$ which is constrained to lie in the range $0 \leq \tilde{z}(z = 0) < 1$ with $1 - \tilde{z}(z = 0) \gg 1/\xi^{2/3}$ in terms of our new variables.

In regions 1 and 6, the saddle-point equation for Eq. (III.11) is

$$\tilde{t} + 2\tilde{\omega}_1\left(\tilde{\omega}_1^2 - \tilde{z}_g\right)^{1/2} = 2\tilde{\omega}_1\left(\tilde{\omega}_1^2 - \tilde{z}_\ell\right)^{1/2} \qquad \text{(III.14a)}$$

which for solution requires the condition

$$\tilde{t} \leq 2\left(\tilde{z}_g\right)^{1/2}\left(\tilde{z}_g - \tilde{z}_\ell\right)^{1/2} \qquad \text{(III.14b)}$$

since $\tilde{\omega}_1 \geq \tilde{\omega}_g = (\tilde{z}_g)^{\frac{1}{2}}$. In region 1, $\tilde{z}_g = 1$ and $\tilde{z}_\ell = \tilde{z}$ so that Eq. (III.14b) with the equal sign gives the equation for the solid line (Fig. III.2) in the center of region 2. Region 1 cannot extend all the way up to this solid line, however, because along this solid line $\omega_1 = \omega_g = \omega_s$ $(\tilde{\omega}_1 = \tilde{\omega}_g = 1)$ and $\rho_g = 0$ invalidating the use of Eq. (III.12) for $Ai(\rho_g)$ and thus invalidating Eq. (III.14a). In region 6, $\tilde{z}_g = \tilde{z}$ and $\tilde{z}_\ell = 1$ so that Eq. (III.14b)

with the equal sign now gives the equation for the solid line (Fig. III.2) in the center of region 5. Along this line $\omega_1 = \omega_g = \omega(z)$ ($\tilde{\omega}_1 = \tilde{\omega}_g = (\tilde{z})^{\frac{1}{2}}$), and $\rho_g = 0$ again. In regions 3 and 4, the saddle-point equation for Eq. (III.11) is

$$\tilde{t} - 2\tilde{\omega}_1\left(\tilde{\omega}_1^2 - \tilde{z}_g\right)^{1/2} = 2\tilde{\omega}_1\left(\tilde{\omega}_1^2 - \tilde{z}_\ell\right)^{1/2} \qquad \text{(III.15a)}$$

which for solution requires the condition

$$\tilde{t} \geq 2\left(\tilde{z}_g\right)^{1/2}\left(\tilde{z}_g - \tilde{z}_\ell\right)^{1/2}, \qquad \text{(III.15b)}$$

just the opposite of Eq. (III.14b). In region 3, $\tilde{z}_g = 1$ and $\tilde{z}_\ell = \tilde{z}$, while in region 4, $\tilde{z}_g = \tilde{z}$ and $\tilde{z}_\ell = 1$. Although Eqs. (III.14a and 15a) give different wave-packet (constant $\tilde{\omega}_1$) trajectories, they both give the same formal solution for the saddle-point (wave-packet) frequency $\tilde{\omega}_1 = \tilde{\omega}_A$:

$$\tilde{\omega}_A^2 = \frac{1 + \tilde{z} + \left(4\tilde{z} + \tilde{t}^2\right)^{1/2}}{4\left[1 - (1-\tilde{z})^2/\tilde{t}^2\right]} \quad . \qquad \text{(III.16)}$$

(Subscript distinguishes this solution from $\tilde{\omega}_B$, used in regions 2 and 5). For future reference, we note here that a saddle-point for Eq. (I.29), using Eq. (III.10), exists only <u>above</u> the branch-cuts as chosen in Fig. I.13. This can be easily seen by using Eq. (III.12) and looking at the phase of the integrand of Eq. (I.29) (e. g., the

phase Ψ must vanish on the "light cone" boundary; also $\partial\Psi/\partial\omega_1 = 0$ for a saddle-point).

In regions 2 and 5, the saddle-point equation for Eq. (III.11) is

$$\tilde{t} - i2\tilde{\omega}_1 \xi^{-1/3} \frac{Ai'(\rho_g)}{Ai(\rho_g)} = 2\tilde{\omega}_1 (\tilde{\omega}_1^2 - \tilde{z}_\ell)^{1/2} \qquad \text{(III.17a)}$$

where Eq. (III.13) is now used for $Ai(\rho_g)$. In terms of our new variables, we have $\rho = \xi^{2/3}(\tilde{z} - \tilde{\omega}_1^2)$ and $\rho_g = \xi^{2/3}(\tilde{z}_g - \tilde{\omega}_1^2)$ and, since Eq. (III.13) is valid only for $-1 \lesssim \rho_g \leq 0$ here, we set the boundaries of regions 2 and 5 by requiring $-1 \lesssim \rho_g \leq 0$. If we write $\tilde{\omega}_1 = \tilde{\omega}_g + \delta\tilde{\omega}$, $|\delta\tilde{\omega}| \ll \tilde{\omega}_g = (\tilde{z}_g)^{1/2}$, $-1 \lesssim \rho_g \leq 0$ gives $0 \leq \delta\tilde{\omega} \lesssim 1/2\tilde{\omega}_g\xi^{2/3}$; using Eq. (III.14a or 15a), although not strictly valid here, we can relate $\delta\tilde{\omega}$ to the $\tilde{t} - \tilde{z}$ plane and obtain $\delta\tilde{\omega} \approx [\tilde{t} - 2\tilde{\omega}_g(\tilde{z}_g - \tilde{z}_\ell)^{1/2}]^2/(2\tilde{\omega}_g)^3$ provided $\tilde{z}_g - \tilde{z}_\ell \gtrsim 1/\xi^{2/3}$ which is also the required condition for $\rho_\ell \lesssim -1$ since we used Eq. (III.12) for $Ai(\rho_\ell)$ in arriving at Eq. (III.17a). Substituting this $\delta\tilde{\omega}$ into the above inequality for $\delta\tilde{\omega}$ results in

$$\left|\tilde{t} - 2(\tilde{z}_g)^{1/2}(\tilde{z}_g - \tilde{z}_\ell)^{1/2}\right| \lesssim 2\frac{(\tilde{z}_g)^{1/2}}{\xi^{1/3}} \qquad \text{(III.17b)}$$

giving the approximate boundaries for regions 2 and 5 (i. e., the pairs of dashed lines about regions 2 and 5 in Fig. III.2). Using Eq. (III.13), we find that the solution to Eq. (III.17a),

provided Eq. (III.17b) is satisfied, is the saddle-point frequency $\tilde{\omega}_1 = \tilde{\omega}_B + i\tilde{\gamma}_B$ (valid for both regions 2 and 5):

$$\tilde{\omega}_B^2 = \tilde{z}_g + 2.361\,\xi^{-2/3}\left[1.470\,\mathrm{Re}(C) - 1\right] \qquad \text{(III.18a)}$$

$$\tilde{\gamma}_B = 1.736\,\xi^{-2/3}\,\mathrm{Im}(C)/\tilde{z}_g \qquad \text{(III.18b)}$$

$$C \equiv \left\{1 - i\,(0.3686)\,\xi^{1/3}(\tilde{z}_g)^{-1/2} \times \left[\tilde{t} - 2(\tilde{z}_g)^{1/2}(\tilde{z}_g - \tilde{z}_\ell)^{1/2}\right]\right\}^{1/2} \qquad \text{(III.18c)}$$

where the branch-cut is chosen such that $\mathrm{Re}(C) > 0$. Interestingly, on the center lines (where $C = 1$) of regions 2 and 5, Eq. (III.18a) gives $\rho_g = -1.11$ which already is pushing the limits $-1 \lesssim \rho_g \leq 0$ we used in obtaining the approximate boundaries given by Eq. (III.17b)! However, even on the boundary lines given by Eq. (III.17b), $\mathrm{Re}(C)$ is increased to only 1.059 and ρ_g increased to only 1.31, so we continue to use Eqs. (III.13, 17a, and 18) within the $\tilde{t} - \tilde{z}$ space boundaries given by Eq. (III.17b).

Since we required $\tilde{z}_g - \tilde{z}_\ell \gtrsim 1/\xi^{2/3}$ above, we must terminate regions 2 and 5 when the upper dashed lines fail this condition and this occurs when $\tilde{t} \approx 4/\xi^{1/3}$; at this time, the lower dashed lines have reached the position $\tilde{z}_g - \tilde{z}_\ell = 1 - 9/\xi^{2/3}$ and, for convenience, we place a horizontal boundary here for regions 2 and 5 separating them from regions 0 and 7 (see Fig. III.2). Each of

the dashed boundary lines pertaining to regions 2 and 5 really should be viewed as a zone (of finite thickness) where the exact Airy function, rather than Eqs. (III.12 or 13), should be used. In particular, the above mention horizontal dashed line at $\tilde{t} = 4/\xi^{1/3}$ was motivated as a limit to regions 2 and 5 and not as the beginning of a region (0 and 7) where Eq. (III.3) could be used for G_1. Our use of Eq. (III.3) up to $\tilde{t} = 4/\xi^{1/3}$ is motivated primarily by the agreement of our eventual solutions for regions 1 and 6 with Eq. (III.4) for $\tilde{t} \ll 1$ and $|1 - \tilde{z}| \ll 1$ and, hence, requires $\xi^{1/3}/4 \gg 1$ (this also assures $9/\xi^{2/3} \ll 1$).

Using the above saddle-point frequencies, for large phase $\Psi \gg 1$, we find asymptotically for Eq. (III.11) in regions 1, 3, 4, and 6:

$$G_1 \approx \frac{-(c/2)(\pi\xi)^{-1/2}\sin(\Psi + \pi/4)}{\left[(2\tilde{\omega}_A^2 - \tilde{z}_g)(\tilde{\omega}_A^2 - \tilde{z}_\ell)^{1/2} + S(2\tilde{\omega}_A^2 - \tilde{z}_\ell)(\tilde{\omega}_A^2 - \tilde{z}_g)^{1/2}\right]^{1/2}} \tag{III.19a}$$

where

$$\Psi = \xi\left\{\tilde{\omega}_A\tilde{t} - \frac{2}{3}\left[(\tilde{\omega}_A^2 - \tilde{z}_\ell)^{3/2} + S(\tilde{\omega}_A^2 - \tilde{z}_g)^{3/2}\right]\right\} \tag{III.19b}$$

and

$$S \equiv \operatorname{sgn}\left[\tilde{t} - 2(\tilde{z}_g)^{1/2}(\tilde{z}_g - \tilde{z}_\ell)^{1/2}\right] . \tag{III.19c}$$

The quantity S equals +1 in regions 3 and 4 and -1 in regions 1 and 6 In regions 2 and 5 we find

$$G_1 \approx -0.97\, c\left(\xi \tilde{z}_g\right)^{-1/2}\left(\tilde{\omega}_B^2-\tilde{z}_g\right)^{-1/4}\exp\left(-1.063\,\xi^{4/3}\tilde{\gamma}_B^2\right)\times$$
$$\times Ai\left[\xi^{2/3}\left(\tilde{z}_g-\tilde{\omega}_B^2\right)\right]\sin\left(\Psi+\frac{\pi}{4}\right) \qquad \text{(III.20a)}$$

where

$$\Psi=\xi\left\{\tilde{\omega}_B\tilde{t}-\frac{2}{3}\left(\tilde{\omega}_B^2-\tilde{z}_\ell\right)^{3/2}\right\}. \qquad \text{(III.20b)}$$

Finally, in regions 0 and 7 we just use Eq. (III.3) or

$$G_1 \approx -\frac{c}{2}\,J_o(\Psi) \qquad \text{(III.21a)}$$

with

$$\Psi=\xi\left[\tilde{t}^2-(1-\tilde{z})^2\right]^{1/2}, \qquad \text{(III.21b)}$$

where this becomes exact as $\tilde{t} \to 0$ and $\tilde{z} \to 1$ (but staying above the "light cone" boundaries).

Qualitatively, Eqs. (III.14a, 15a, 16, 19b, and 21b) give the results indicated in Fig. III.3 where we show wave-packet (constant $\tilde{\omega}_A$) trajectories (the solid lines starting at $\tilde{t} = 0$ and $\tilde{z} = 1$) and lines of constant phase Ψ (the roughly hyperbolic

solid lines). The wave-packet trajectory labeled $\tilde{\omega}_A = 1$ (given by the equal sign in Eq. (III.14b) with $\tilde{z}_g = 1$ and $\tilde{z}_\ell = \tilde{z}$) corresponds to the trajectory labeled $\omega_A = \omega$ in Fig. III.1. The dashed line (given by the equal sign in Eq. (III.14b) but with $\tilde{z}_g = \tilde{z}$ and $\tilde{z}_\ell = 1$ now) is the line of turning points ($\rho_g = 0$) for waves with different frequencies $\tilde{\omega}_A$; on this line $\partial\Psi/\partial z = 0$ since $k_z \equiv -\partial\Psi/\partial z$ must vanish at the turning point.

Quantitatively, we turn to Fig. (III.4) where we plot $(2/c)G_1$, according to Eqs. (III.19, 20, and 21), on the vertical axis (same as $\tilde{t}$) at various fixed times $\tilde{t}$ as a function of position $\tilde{z}$. By using a small interval $\Delta\tilde{t} \ll 1/\tilde{\omega}_A\xi$ between each plotting time, and reducing $(2/c)G_1$ by some overall multiplicative factor (0.0075 in Fig. III.4a and 0.02 in Figs. III.4b-d) to eliminate overlap between the plots at different $\tilde{t}$, the lines of constant phase and the position of the line of turning points (where $k_z = 0$) can be clearly seen. We have purposely left blank various time intervals (of duration $\Delta\tilde{t} = 0.1$) in order to periodically allow (i. e., at the edges of these blank intervals) an entire trace of G_1 versus $\tilde{z}$ (at fixed $\tilde{t}$) to be clearly discernable from all the other traces. These traces show that in regions of small $\tilde{t}$ or near the "light cone" boundaries (where $\tilde{\omega}_A \to \infty$), where the *uniform* plasma solution might be expected to be valid, $|(2/c)G_1|$ rapidly increases in magnitude in agreement with Eqs. (III.3 or 21) as $\Psi \to 0$. In Fig. III.4, we chose $\xi = 300$ giving $\xi^{1/3} = 6.69$ and

$4/\xi^{1/3} = 0.60$. Thus, Fig. III.4a contains all of regions 0 and 7 and part of regions 1 and 6 for $\tilde{t} \geq 0.2$. The agreement between Eqs. (III.21a and 19a) is excellent for $\tilde{t} \lesssim 10/3\xi^{1/3} = 0.5$, but only good to fair for $0.5 < \tilde{t} \lesssim 0.6$ and clearly would be nonexistent (at least for $\tilde{z} > 1$) for $\tilde{t} > 4/\xi^{1/3} = 0.6$. In Fig. III.4b, we deliberately lower the boundary between regions 2, 3, 4, and 5 and regions 0 and 7 down to $\tilde{t} = 10/3\xi^{1/3}$ just for the sake of comparison: the matching at the various boundaries is not much better than before (e. g., regions 3 and 4 are out of phase with regions 2 and 5). The phase matching of regions 3 and 4 with regions 2 and 5 does not become satisfactory until $\tilde{t} \gtrsim 1$ (roughly $7/\xi^{1/3}$). The boundary lines can still be seen faintly (sometimes only as gentle changes in shading, as in region 2) at $\tilde{t} \sim 2$; the sharp change in shading near the right-hand "light cone" boundary in Figs. III.4b-d is ficticious and due to a sudden change in the density of plotting points used in the computer generated figure.

C. Uniform Plasma, Pumped

For this case, $Q(z,\omega_1,\underline{k}_{1\perp})$ in Eq. (I.25) becomes, for $\mathrm{Re}(\omega_1) \geq 0$, just

$$Q(\omega_1,\underline{k}_{1\perp}) \approx k_{1z}^2(\omega_1,k_{1\perp}) + \frac{D^2/c^2}{\omega_p^2-(\omega_0-\omega_1-i\nu_p)^2} \qquad \text{(III.22)}$$

where again $k_{1z}^2 \equiv \left[(\omega_1 + i\nu_1)^2 - \omega^2\right]/c^2$, $\omega^2 \equiv \omega_p^2 + c^2 k_{1\perp}^2$, and $D(\omega_1, \underline{k}_{1\perp})$ is defined by Eq. (I.25c). Note that the full expression for Q is symmetric about the $\mathrm{Im}(\omega_1)$-axis, as discussed in secs. I C and II. Using Eq. (I.30) in Eq. (I.26) gives

(III.23)

$$G_1(z_g, z_\ell; \omega_1, \underline{k}_{1\perp}) = -\frac{i}{2f} \exp\left[if(\omega_1, \underline{k}_{1\perp})(z_g - z_\ell)\right]$$

where $f \equiv \sqrt{Q}$ (an effective k_{1z}) has the branch-cuts and branch-points $\left\{\omega_b\right\} \equiv \left\{\omega_I^o, \omega_{II}^o, \omega_{III}^o, \omega_{II}^\infty, \omega_{III}^\infty\right\}$ indicated in any one of Figs. V.6a-d. The superscript "o" indicates a root of Q while "∞" indicates a singularity of Q. The branch-point $\omega_I^o \approx \omega$ corresponds to the branch-point found in sec. III A and shown in Fig. I.13.

As in the previous examples, to perform the ω_1-integration in Eq. (I.29) we first depress the Bromwich contour and change to an integration around each (of the six) branch-cuts now indicated in Fig. V.6. Since the resulting integral cannot be performed exactly (unlike the case in sec. III A), we use the saddle-point approximation (Ref. sec. U). This requires that the above "branch-cut" contours be again deformed until they follow the paths of steepest descent through the saddle-point frequencies (if more than one is found for our case here). As is clear from Fig. III.6, even if a saddle-point lies on one edge (or side) of a branch-cut (the position of which is chosen arbitrarily), the

corresponding path of steepest descent does not generally follow the edges of the branch-cut.

If B_+ denotes the "branch-cut" contours (or their deformation into paths of steepest descent) with $Re(\omega_1) \geq 0$, then Eq. (I.29) becomes

$$\underline{G}_1(z_g, z_\ell; t, \underline{k}_{1\perp}) = \hat{e}_1(\omega_{1s}, \underline{k}_{1\perp}) \exp(-\nu_1 t)\, G_1(z_g, z_\ell; t, \underline{k}_{1\perp})$$

where

$$G_1 = -\frac{i}{4\pi}\int_{B_+} d\omega_1 \frac{\exp(-i\Psi)}{f} + c.c. \qquad \text{(III.24a)}$$

$$\Psi \equiv t(\omega_1 - cf\eta) \qquad \text{(III.24b)}$$

$$\eta \equiv \frac{z_g - z_\ell}{ct} \quad . \qquad \text{(III.24c)}$$

We have evaluated $\hat{e}_1$ at the saddle-point frequency $\omega_1 = \omega_{1s}$ (if more than one saddle-point is found, an appropriate summation is needed here). As in previous examples, we have extracted an $\exp(-\nu_1 t)$ term by transforming to a new $\omega_1 = (\omega_1)_{old} + i\nu_1$ which eliminates ν_1 from k_{1z}^2 but not from the resonance denominator $\omega_p^2 - [\omega_o - \omega_1 - i(\nu_p - \nu_1)]^2$ which appears in Q. The saddle-point equation is $\partial\Psi/\partial\omega_1 = 0$, or

$$\frac{df(\omega_1)}{d\omega_1} = \frac{1}{c\eta} \quad , \qquad \text{(III.25)}$$

from which we wish to obtain the saddle-point frequency $\omega_{1s} = \omega_1(\eta)$ (the $\underline{k}_{1\perp}$-dependence will be suppressed in the interest of simpler notation).

Rather than use $f(\omega_1)$ in Eq. (III.25), we find it simpler to invert this function to get $\omega_1(f)$ and replace Eq. (III.25) by the equivalent equation

$$\frac{d\omega_1(f)}{df} = c\eta \qquad \text{(III.26)}$$

(essentially saying group velocity along z is $c\eta$) and solve for $f(\eta)$. Equation (III.22) gives (III.27)

$$\left[\omega_1^2-(\omega^2+c^2f^2)\right]\left\{\omega_p^2-\left[\omega_o-\omega_1-i(\nu_p-\nu_1)\right]^2\right\}+D^2=0$$

which has three solutions with $\mathrm{Re}(\omega_1) \geq 0$: a solution near $\omega_1 \approx \approx (\omega^2 + c^2f^2)^{\frac{1}{2}}$, a solution near $\omega_1 \approx \omega_o - \omega_p - i(\nu_p - \nu_1)$, and one near $\omega_1 \approx \omega_o + \omega_p - i(\nu_p - \nu_1)$. Since $\omega \equiv (\omega_p^2 + c^2k_{1\perp}^2)^{\frac{1}{2}}$, and $f \equiv \sqrt{Q}$ is an effective k_{1z}, the first solution is a modified version of the usual electromagnetic wave normal mode: using it in Eq. (III.26), with the pump strength parameter D set equal to zero in the definition of f, would give the saddle-point frequency ω_A in Eq. (III.5a). The second and third solutions result from the "beat" of the plasma wave (density perturbation δn) with the pump

wave (velocity perturbation v_o) which gives a contribution to the transverse current in the electromagnetic wave equation (see sec. I C). We can solve Eq. (III.27) approximately if we assume we are near at most two of these frequencies but far from the third. Since the last solution has $\omega_1 > \omega_o$, it is not of much interest here and will be ignored for now.

Assuming $0 \leq \mathrm{Re}(\omega_1) \ll \omega_o$, Eq. (III.27) gives $\omega_1(f) = \omega_1[Y(f)]$ where

$$\omega_1(Y) \approx \omega_R - i(\nu_p - \nu_1) + i\gamma_o Y + i\gamma_o(1+Y^2)^{1/2} \qquad \text{(III.28a)}$$

$$Y(f) \equiv -\frac{i}{2\gamma_o}\left[(\omega^2 + c^2f^2)^{1/2} - \omega_R + i(\nu_p - \nu_1)\right] \qquad \text{(III.28b)}$$

with $\omega_R \equiv \omega_o - \omega_p$ and γ_o the uniform plasma growth rate given by Eq. (I.2). From Eq. (III.28),

$$d\omega_1(f)/df = c^2 f F(Y)/(\omega^2 + c^2f^2)^{1/2} \qquad \text{(III.29a)}$$

$$F(Y) \equiv \left[Y + (1+Y^2)^{1/2}\right]/2(1+Y^2)^{1/2} \qquad \text{(III.29b)}$$

and using this in Eq. (III.26) gives

$$f(Y,\eta) = \frac{\eta\omega}{cF(Y)\left[1 - \eta^2/F^2(Y)\right]^{1/2}} \qquad \text{(III.29c)}$$

as the saddle-point equation. Equation (III.29c) can now be used in Eq. (III.28b) to give (III.30)

$$Y(\eta) = -\frac{i}{2\gamma_o}\left\{\frac{\omega}{\left[1-\eta^2/F^2(Y)\right]^{1/2}} - \omega_R + i(\nu_p - \nu_1)\right\} .$$

After solving this equation for $Y(\eta)$, we obtain $\omega_1(\eta)$ and $f(\eta)$ from Eqs. (III.28a and 29c) for use in Eq. (III.24).

Note that the approximation under which Eq. (III.28a) was obtained from Eq. (III.27) requires $|\omega_1 - \omega_R + i(\nu_p - \nu_1)| >>$ $>> D^2/2\omega_p\omega_1^2 = \gamma_o^2/\omega_1$ or equivalently

$$\left|Y + (1+Y^2)^{1/2}\right| >> \gamma_o/\omega_1 , \qquad \text{(III.31)}$$

and any solution $Y(\eta)$ to Eq. (III.30) which violates this condition must be discarded. All solutions satisfying Eq. (III.31) also satisfy $\mathrm{Re}\left[(\omega^2 + c^2f^2)^{\frac{1}{2}}\right] = \omega\mathrm{Re}\left[(1 - \eta^2/F^2)^{-\frac{1}{2}}\right] \geq 0$, which we assumed in solving Eq. (III.27) for $\mathrm{Re}(\omega_1) \geq 0$, so this introduces no branch-cuts.

Now we must put in the branch-points (at $Y = \pm i$) and branch-cuts in the complex Y-plane for the function $(1 + Y^2)^{\frac{1}{2}}$. If we put in the branch-cut vertically from $-i$ to $+i$, this defines two independent Riemann sheets: we denote by $\boxed{1}$ the sheet on which $(1 + Y^2)^{\frac{1}{2}} \approx +Y$ for $|Y| >> 1$, and we denote by $\boxed{2}$ the other sheet on which $(1 + Y^2)^{\frac{1}{2}} \approx -Y$ for $|Y| >> 1$. It is also convenient to

consider two other Riemann sheets composed of parts of the first two sheets: sheet $[3]$ consists of the right half-plane of $[1]$ and the left half-plane of $[2]$, and $(1 + Y^2)^{\frac{1}{2}} \approx +1$ for $|Y| \ll 1$; sheet $[4]$ consists of the right half-plane of $[2]$ and the left half-plane of $[1]$, and $(1 + Y^2)^{\frac{1}{2}} \approx -1$ for $|Y| \ll 1$. The branch-cuts on sheets $[3]$ and $[4]$ run vertically from $+i$ to $+i\infty$ and from $-i$ to $-i\infty$.

On sheet $[1]$ for $|Y| \gg 1$, $1/F = 1 + 1/4\ Y^2 + \ldots$, $1/F^2 = 1 + 1/2\ Y^2 + \ldots$, and

$$\omega_1(Y) = \omega_R - i(\nu_p - \nu_1) + 2i\gamma_o Y + i(1 - 1/4Y^2 + \cdots)\gamma_o/2Y \qquad \text{(III.32a)}$$

$$f(Y) = \left[\eta\omega/c(1-\eta^2)^{1/2}\right]\left[1 + 1/4Y^2(1-\eta^2) + \cdots\right] \qquad \text{(III.32b)}$$

$$Y(\eta) = -\frac{i}{2\gamma_o}\left[\frac{\omega}{(1-\eta^2)^{1/2}} - \omega_R + i(\nu_p - \nu_1) + \frac{\eta^2\omega}{4Y^2(1-\eta^2)^{3/2}} + \cdots\right]. \qquad \text{(III.32c)}$$

On sheet $[2]$ for $|Y| \gg 1$, $1/F = 4Y^2 + 3 + \ldots$, $1/F^2 = 16Y^4 + 24Y^2 + \ldots$, and

$$\omega_1(Y) = \omega_R - i(\nu_p - \nu_1) - i(1 - 1/4Y^2 + \cdots)\gamma_o/2Y \qquad \text{(III.33a)}$$

$$f(Y) = \left[4\eta\omega Y^2/c(1-16\eta^2Y^4)^{1/2}\right]\left[1 + 3/4Y^2(1-16\eta^2Y^4) + \cdots\right] \qquad \text{(III.33b)}$$

$$Y(\eta) = -\frac{i}{2\gamma_o}\left[\frac{\omega}{(1-16\eta^2Y^4)^{1/2}} - \omega_R + i(\nu_p - \nu_1) + \right. \qquad \text{(III.33c)}$$

$$\left. + \frac{12\eta^2Y^2\omega}{(1-16\eta^2Y^4)^{3/2}} + \cdots\right].$$

On sheet [3] for $|Y| \ll 1$, $1/F = 2(1 - Y + \cdots)$, $1/F^2 = 4(1 - 2Y + \cdots)$, and

$$\omega_1(Y) = \omega_R - i(\nu_p - \nu_1) + i\gamma_0(1 + Y + \cdots) \qquad \text{(III.34a)}$$

$$f(Y) = \left[2\eta\omega/c(1-4\eta^2)^{1/2}\right]\left[1 - Y/(1-4\eta^2) + \cdots\right] \qquad \text{(III.34b)}$$

$$Y(\eta) = -\frac{i}{2\gamma_0}\left\{\frac{\omega}{(1-4\eta^2)^{1/2}} - \omega_R + i(\nu_p - \nu_1) - \right.$$

$$\left. - \frac{4\eta^2 Y\omega}{(1-4\eta^2)^{3/2}} + \cdots\right\}. \qquad \text{(III.34c)}$$

Finally, on sheet [4] for $|Y| \ll 1$, $1/F = 2(1 + Y + \cdots)$, $1/F^2 = 4(1 + 2Y + \cdots)$, and

$$\omega_1(Y) = \omega_R - i(\nu_p - \nu_1) - i\gamma_0(1 - Y + \cdots) \qquad \text{(III.35a)}$$

$$f(Y) = \left[2\eta\omega/c(1-4\eta^2)^{1/2}\right]\left[1 + Y/(1-4\eta^2) + \cdots\right] \qquad \text{(III.35b)}$$

$$Y(\eta) = -\frac{i}{2\gamma_0}\left\{\frac{\omega}{(1-4\eta^2)^{1/2}} - \omega_R + i(\nu_p - \nu_1) + \right.$$

$$\left. + \frac{4\eta^2 Y\omega}{(1-4\eta^2)^{3/2}} + \cdots\right\}. \qquad \text{(III.35c)}$$

Using Eqs. (III.32c, 33c, 34c, 35c, 31), one can find five solutions $Y_N(\eta)$: three on sheet $\lfloor 3 \rfloor$ and two on sheet $\lfloor 4 \rfloor$ as shown in Figs. III.5a,b, respectively. We use sheets $\lfloor 3 \rfloor$ and $\lfloor 4 \rfloor$ because two of the solutions (II and V), as η varies from 0 to 1, thread their way between the branch-points at $\pm i$. It is not too difficult to verify that these are the only valid solutions to Eq. (III.30). By rearranging the terms in Eq. (III.30), and squaring twice, one can remove all square-roots and obtain a twelfth-order polynomial equation (and, hence, twelve solutions) for the quantity $Y(\eta)$. By comparing these solutions back to Eq. (III.30), one finds three extraneous solutions (due to squaring the correct equation) on sheet $\lfloor 1 \rfloor$ and four solutions which violate Eq. (III.31) on sheet $\lfloor 4 \rfloor$; this leaves only five valid solutions . However, we are only interested in those solutions for which $\mathrm{Im}(\Psi) \geq 0$ in Eq. (III.24), and this eliminates solutions III-V from further consideration.

As a final comment here on the general properties of the solutions $Y_N(\eta)$, we note that if Eqs. (III.32-35) are used to plot the saddle-point frequencies, $\omega_1(Y_N(\eta))$, they all (even solutions III-V) turn out to lie either above the branch-cut from the turning point ω_I^o (e. g., see Fig. V.6a or b for the branch-cuts) or on the continuation of this Riemann sheet reached by crossing (i. e., traveling under) this branch-cut from above. This

is in agreement with the location of the saddle-point frequency $\omega_A(\eta)$ in the uniform umpumped case (sec. III A), as shown in Fig. III.6 where the saddle-point lies on the sheet composed of the upper-half-plane (e. g., regions a and c) of Fig. III.6a and the lower half-plane (e. g., regions a' and c') of Fig. III.6b. In Fig. III.6, the solid lines are contours of constant Re (Ψ) (with Ψ given by Eq. (III.24b)) and the dashed lines are contours of constant Im(Ψ) (becoming increasingly negative as $\gamma = \mathrm{Im}(\omega_1) \to -\infty$). In the steepest descent saddle-point approximation (as opposed to the stationary phase method), the contour of ω_1-integration is depressed until it lies in the "valley" region along the curve marked with arrows. In the uniform pumped case discussed in this section, we have just found similar behavior but with five saddle-points rather than one. Solutions III-V all lie roughly below or to the side of the branch-point $\omega_{II}^{\infty} \equiv \omega_R - i(\nu_p - \nu_1)$ and on dashed lines for which $\mathrm{Im}(\Psi) < 0$ for all η. Solution I starts approximately at $\omega_A = \omega/(1 - \eta^2)^{\frac{1}{2}}$ for small η and lies on or slightly below the real ω_1-axis for $\eta > 0$. As $\eta \to 1$, $\omega_1(\gamma_I(\eta)) \to \omega_R - i(\nu_p - \nu_1) - \gamma_o$ (ignoring terms much smaller than γ_o) and this solution ends. Solution II starts approximately at $\omega_R - i(\nu_p - \nu_1)$ for $\eta = 0$, rapidly gains an imaginary part $\gamma \gtrsim \gamma_o$ as η increases, and then approaches $\omega_A = \omega/(1 - \eta^2)^{\frac{1}{2}}$ as $\eta \to 1$. Thus, the pump has essentially split the umpumped saddle-point ω_A into two saddle points,

$\omega_1(Y_I(\eta))$ and $\omega_1(Y_{II}(\eta))$, and created an additional "valley" for the ω_1-integration contour to follow as it is depressed down to $\gamma \to -\infty$.

Having obtained the saddle-points (examples given below), we return to Eq. (III.24), deform the contours B_+ into contours following the paths of steepest descent, and obtain $G_1(\eta;t,\underline{k}_{1\perp})$ where

$$G_1 = \frac{-c}{(2\pi)^{1/2}} \sum_s \frac{\exp\left[\mathrm{Im}(\Psi_s)\right] \sin\left[\mathrm{Re}(\Psi_s) + \theta_s + \frac{\pi}{4}\right]}{\left[(t/\eta^2)\left|f_s^2 d^2\omega_1(f)/df^2\right|\right]^{1/2}} \qquad \text{(III.36)}$$

with the subscript "s" denoting evaluation at one of the saddle-points (I or II), and $f_s^2 d^2\omega_1(f)/df^2 = \left|f_s^2 d^2\omega_1/df^2\right| \exp(i2\theta_s)$. We next obtain the quantities appearing in Eq. (III.36), for the saddle-points I and II, for ranges of η which give relatively simple results.

For ω_1 far from the resonance frequency ω_R, we have $|Y_N(\eta)| >> 1$ and we consider here situations (η sufficiently small or large) where we can drop the fourth term on the right side of Eq. (III.32c) giving

$$Y(\eta) \approx -\frac{i}{2\gamma_o}\left[\omega_A(\eta) - \omega_R + i(\nu_p - \nu_1)\right] \qquad \text{(III.37)}$$

where $\omega_A(\eta) = \omega/(1 - \eta^2)^{\frac{1}{2}}$ as in Eq. (III.5a). If we define $\eta_o \equiv \left[1 - (\omega/\omega_R)^2\right]^{\frac{1}{2}}$ by setting $\omega_A(\eta_o) \equiv \omega_R$, then Eq. (III.37) is

valid only if $|Y(\eta)| \gg (\eta^2\omega/8\gamma_o)^{1/3}/(1-\eta^2)^{\frac{1}{2}}$ which requires $0 \leq \eta \ll \eta_o$ for solution I and $\eta_o \ll \eta \leq 1$ for solution II. In the remainder of this section, we will assume $\omega_R > \omega$ and $(\omega_R - \omega)/2\gamma_o \tilde{\sim} 2(\eta_o^2\omega/8\gamma_o) \gg 1$, but $\eta_o \ll 1$ still, in order to have a well-defined range of η values over which solutions I and II are valid. Using Eqs. (III.32a, b, and 37) we find

$$\mathrm{Re}(\Psi_s) \approx \omega t(1-\eta^2)^{1/2} - t[\omega_A(\eta)-\omega_R]/4|Y(\eta)|^2 \qquad \text{(III.38a)}$$

$$\mathrm{Im}(\Psi_s) \approx (\nu_p-\nu_1)t/4|Y(\eta)|^2 \qquad \text{(III.38b)}$$

$$(f_s^2/\eta^2)d^2\omega_1/df^2 \approx \omega(1-\eta^2)^{1/2}\{1 - [1+\eta^2\omega/\gamma_o Y(1-\eta^2)^{1/2}]/4Y^2(1-\eta^2)\} \qquad \text{(III.38c)}$$

where "s" denotes saddle-point I for $0 \leq \eta \ll \eta_o$ and saddle-point II for $\eta_o \ll \eta \leq 1$. Note that Eq. (III.36), using Eqs. (III.38a-c), represents only a slight modification of the uniform unpumped results of Eq. (III.4) with the agreement becoming exact as $\gamma_o \to 0$.

For ω_1 near the resonance frequency ω_R, we have $|Y_{II}(\eta)| \ll 1$; the other two limiting cases, $Y_I(\eta) \tilde{\to} +i$ (as $\eta \to 1$) and $|Y_{II}(\eta)| \gg 1$ (on sheet $[2]$ as $\eta \to 0$), both give a damped response(with a damping rate of $(\nu_p - \nu_1)$) and must, therefore, be ignored in the presence of growing (or at least undamped) waves when determining the asymptotic response. All the terms shown in Eq.(III.34c)

must be kept now and give (for $|Y| \ll 1$)

$$Y_{II}(\eta) \approx \frac{\omega/(1-4\eta^2)^{1/2} - \omega_R + i(\nu_p - \nu_i)}{\left[4\eta^2\omega/(1-4\eta^2)^{3/2} + 2i\gamma_o\right]} \quad . \qquad \text{(III.39)}$$

Note that in the denominator of Eq. (III.39), the last term, $2i\gamma_o$, is much smaller than the first term by virtue of the assumption made in the previous paragraph. If we now set $\omega/(1 - 4\eta_R^2)^{\frac{1}{2}} \equiv \omega_R$, we obtain $\underline{\eta_R = \eta_o/2}$; i. e., the actual trajectory of the resonant maximally growing wave-packet has a group velocity along z of only one-half the value that might have been predicted from Eqs. (III.37 , 38b) or from Fig. III.1 by setting $\omega_A(\eta) = \omega_R$ for the frequency matching condition. This agrees with the results obtained by other authors (see sec. I A 2). Using Eqs. (III.34a, b, and 39), we find

$$Re(\Psi_s) \approx \frac{t}{2}\left[\omega_R + \omega(1-4\eta^2)^{1/2}\right] + \\ + t\left\{\frac{\eta^2\omega\, Re\left[Y_s^2(\eta)\right]}{(1-4\eta^2)^{5/2}} - \frac{\gamma_o}{2}\, Im\left[Y_s^2(\eta)\right]\right\} \qquad \text{(III.40a)}$$

$$Im(\Psi_s) \approx t\left\{\gamma_o - \frac{\nu_p - \nu_i}{2} + \right. \\ \left. + \frac{\eta^2\omega\, Im\left[Y_s^2(\eta)\right]}{(1-4\eta^2)^{5/2}} + \frac{\gamma_o}{2} Re\left[Y_s^2(\eta)\right]\right\} \qquad \text{(III.40b)}$$

$$\frac{f_s^2}{\eta^2}\frac{d^2\omega_1}{df^2} \approx 2\omega(1-4\eta^2)^{1/2}\left\{-\frac{i2\eta^2\omega}{\gamma_o(1-4\eta^2)^{3/2}} + \right.$$

$$\left. + \left[1 - Y_s\,\frac{1-8\eta^2}{1-4\eta^2}\right]\right\} \qquad \text{(III.40c)}$$

where the subscript "s" now denotes saddle-point solution II. Equations (III.39, 40) are valid only for $|\eta - \eta_R| \ll \eta_R$.

In Eq. (III.40b), the third and fourth terms can be combined and simplified to reduce Eq. (III.40b) to the form

(III.41)

$$Im(\Psi_s) \approx t\gamma_o\left[1 - \frac{(\eta-\eta_R)^2}{2\eta_R^2}\right] - \frac{t(\nu_p-\nu_1)}{2}\left[1 - \frac{\eta-\eta_R}{\eta_R}\right]$$

where we have used $\omega/(1-4\eta^2)^{\frac{1}{2}} - \omega_R \approx 4\eta_R\omega(\eta-\eta_R)/(1-4\eta_R^2)^{3/2}$ and then replaced $1 - 4\eta_R^2 \approx 1$ everywhere since $4\eta_R^2 = \eta_o^2 \ll 1$ by assumption. Equation (III.41) shows that $Im(\Psi_s)$ is maximized at $\eta = \eta_M$ where

$$\eta_M = \eta_R\left(1 + \frac{\nu_p-\nu_1}{2\gamma_o}\right) \qquad \text{(III.42a)}$$

and

$$Im\left[\Psi_s(\eta_M)\right] \approx t\left(\gamma_o - \frac{\nu_p-\nu_1}{2}\right) \qquad \text{(III.42b)}$$

and that $\mathrm{Im}(\Psi_s)$ falls below zero for $|\eta - \eta_M| > \left[2 - (\nu_p - \nu_1)/\gamma_o\right]^{\frac{1}{2}}$; since this latter inequality cannot generally be satisfied and still remain within the range of validity ($|\eta - \eta_R| \ll \eta_R$) of Eqs. (III.39-41), it is more useful to use the second derivative at η_M, $\left[d^2\mathrm{Im}(\Psi_s)/d\eta^2\right]_M = -\gamma_o/\eta_R^2$, when determining the width (in η) of the growing wave-packets. Clearly, by expanding Eq. (III.36) about the maximum growth trajectory η_M, one obtains a growing and expanding wave-packet traveling along $\pm z$ at half the group velocity that a wave of this frequency ($\omega_1 \approx \omega_R = \omega_o - \omega_p$) would normally have in a uniform unpumped plasma - in agreement with sec. I A 2.

Thus, we find general agreement with sec. III A in regions of $t - z$ space where one would not expect, from frequency matching considerations, strong growth to occur. For $\eta \sim \eta_R = \left[1 - (\omega/\omega_R)^2\right]^{\frac{1}{2}}/2$, however, we find strongly growing wave-packets (over a range of η) with properties in agreement with those discussed in sec. I A 2.

In concluding sec. III, we note that in these simple cases we have been able to use the mathematical procedure outlined in sec. I D to obtain known or physically reasonable results. Although nothing particularly new was discovered in this section, we have developed sufficient confidence to move on to the somewhat more complicated case of a nonuniform pumped plasma (sec. V). First, however, we quickly review the phase-integral (or WKBJ) method in sec. IV and also obtain there some results that will be needed later (in sec. V).

IV. THE PHASE-INTEGRAL (WKBJ) METHOD

We recall from sec. I D 2 that our basic mathematical procedure (for solving the Raman instability problem) calls for obtaining two linearly independent solutions (A and B) to Eq. (I.25) with $S = 0$. We have already studied, in sec. III, three simple limiting cases where this equation can be solved exactly; in general (i. e., in sec. V), however, exact solutions are not currently available. We therefore turn to an approximate method of solution, the phase-integral (or WKBJ) method, which is described and summarized (with an example included in sec. IV C) in this section. This approximation method is capable of yielding accurate solutions everywhere in the complex plane (of the position variable in Eq. (I.25)) except near certain "transition" points where $Q(z) = 0$ or ∞. This is sufficient for dealing with the questions we wish to answer (see sec. I B) because we are primarily interested here in the large-scale effects (e. g., growth and saturation of growth) induced by these "transition" regions rather than on the precise details of how these effects were actually accomplished. In this section (IV), we investigate the rules for tracing the phase-integral (WKBJ) solutions around (but not too near) the above-mentioned transition points(in Eq. (I.25), Q has one simple pole and two simple zeros). In sec. IV C, we consider the special case where the

pole and one of the zeros are "nearby" since this turns out to be important in sec. V.

A. Introduction

The phase-integral (or WKBJ) method has been treated extensively in the literature (Ref. sec. T). We particularly recommend Heading (Ref. T I) as an introduction to the subject and Fröman and Fröman (Ref. T IV), a more rigorous treatment, to answer questions the reader is likely to have after reading Heading. Skorupski (Ref. T V) generalizes the work of Fröman and Fröman to the complex plane, as required for our problem here. Finally, we mention Berry and Mount (Ref. T VI) as a more recent survey of the literature. In this section we will only briefly describe the method and those concepts needed for applying the rules that are given in sec. IV B. Sections (A and B) represent our attempt at summarizing, in "cookbook" style, the essential results actually needed to apply the method; we give here no derivations, details, or complete error estimates, but instead refer the reader to references (T I, IV, V) for such complicated and time-consuming matters .

Given an equation of the form

$$\left[\frac{d^2}{d\rho^2} + \lambda^2 q(\rho)\right] f = 0 , \qquad \text{(IV.1)}$$

in the phase-integral method we look for solutions of the form (completely general)

$$f(\rho) = a_1(\rho) f_1(\rho) + a_2(\rho) f_2(\rho) \qquad \text{(IV.2a)}$$

where

$$f_1(\rho) \equiv (\rho, c) \equiv q^{-1/4}(\rho) \exp\left[i \Psi(\rho, c)\right] \qquad \text{(IV.2b)}$$

$$f_2(\rho) \equiv (c, \rho) \equiv q^{-1/4}(\rho) \exp\left[-i \Psi(\rho, c)\right] \qquad \text{(IV.2c)}$$

$$\Psi(\rho, c) \equiv \lambda \int_c^{\rho} q^{1/2}(\rho')\, d\rho' \quad . \qquad \text{(IV.2d)}$$

We have used Heading's notation in Eqs. (IV.2b,c) (in sec. V , we multiply these functions by a convenient constant), where c is the "phase reference level" and is typically chosen to equal one of the transition points T where $q(T) \to 0$ or ∞ (thus, T also is a branch-point of $q^{1/4}$ and $q^{\frac{1}{2}}$). The phase-integral Ψ gives the method its name, and the determination of the coefficients $a_1(\rho)$ and $a_2(\rho)$ for all ρ, given their presumed known value at some point or in some limit (e. g., $\rho \to \infty$), is the goal of the method.

Although the coefficients $a_1(\rho)$ and $a_2(\rho)$ are often nearly constant over large regions of the complex ρ-plane, one or the other of the coefficients will occasionally change as ρ varies (the

Stokes effect; see Ref. sec. T); these changes, however, are found to occur in a predictable manner (both the region of change and the amount of change suffered on crossing this region). When discussing these changes, it is convenient to first define certain sets of lines in the complex ρ-plane: the (generalized) Stokes lines are contours of constant real phase

$$Re(\Psi) = \text{constant} , \qquad (IV.3a)$$

and the (generalized) anti-Stokes lines are contours of constant imaginary phase

$$Im(\Psi) = \text{constant} . \qquad (IV.3b)$$

The (principal) Stokes and anti-Stokes lines are the particular lines, out of the above two infinite sets, for which the above constants are set equal to zero and for which the "phase reference level" c is successively set equal to each of the transition points T. The adjectives "generalized" and "principal" are placed in parentheses above since they are our own and such distinctions are not typically made in the literature (Heading and Fröman and Fröman use only what we here call the "principal" lines, while Skorupski uses all the lines but calls them all just Stokes and

anti-Stokes lines). The Cauchy-Riemann equations (Ref. S I) can be used to show that the generalized Stokes and anti-Stokes lines are mutually orthogonal except at the branch-points (i. e., transition points T) where $q^{\frac{1}{2}}(\rho)$ ceases to be analytic. Some examples are shown in Figs. IV.1,2 and V.3-5.

Along the generalized anti-Stokes lines, the WKBJ solutions, given by Eq. (IV.2b, c), are purely oscillatory and, assuming an exponential time-dependence of $\exp(-i\omega t)$ with $\mathrm{Re}(\omega) > 0$ (for instance), we can define a direction of propagation (indicated by arrows in Fig. IV.1 and later figures) for these waves. Along the generalized Stokes lines, these WKBJ solutions are purely growing or decaying, and we can define a direction in which each solution grows (again indicated by arrows in Fig. IV.1 and later figures). At a non-branch-point intersection of a generalized Stokes and anti-Stokes line, the directions of growth and propagation are related (by the Cauchy-Riemann equations) for each of the WKBJ solutions. This relation has been called "Heading's rule", but here we choose to more pictorially call it the "right-hand SAN rule" which we state as follows: for each of the WKBJ solutions, the direction of growth (the Stokes line arrow) crossed into the direction of propagation (the anti-Stokes line arrow) is normal (up) to the complex ρ-plane. If the time-dependence had been chosen as $\exp(i\omega t)$ with $\mathrm{Re}(\omega) > 0$, we would call it a left-hand

rule. With the directions of growth now presumed known, an additional definition is typically used in the literature: a WKBJ solution is termed dominant in a given region if, in that region, its direction of growth is away from the "phase reference level" c; it is termed subdominant if its direction of growth is toward c. Note that the property of dominance or subdominance is dependent on the choice of "phase reference level": in changing this level from ρ_1 to ρ_2 (for instance), we pick up Heading's "dominancy changing factor"

$$\left[\rho_1,\rho_2\right] \equiv \exp\left[i\Psi(\rho_1,\rho_2)\right] \qquad \text{(IV.4)}$$

with the properties $(\rho,\rho_2) = (\rho,\rho_1)\left[\rho_1,\rho_2\right]$, $(\rho_2,\rho) = \left[\rho_2,\rho_1\right]\cdot(\rho_1,\rho)$, and $\left[\rho_2,\rho_1\right] = \left[\rho_1,\rho_2\right]^{-1}$. This factor could be large or small if the path between ρ_1 and ρ_2 has a sufficiently long projection along a generalized Stokes line. Finally, we note that the dominance or subdominance of a WKBJ solution reverses upon crossing the generalized anti-Stokes line that intersects the "phase reference level" c.

Having defined the generalized Stokes and anti-Stokes lines and discussed the general properties of the WKBJ solutions, Eqs. (IV.2b, c), we are now in a position to discuss the changes that occur in the coefficients $a_1(\rho)$ and $a_2(\rho)$ as ρ varies in the complex plane. Essentially, the results found (in Ref. sec. T) are

as follows: along a generalized anti-Stokes line, the relative changes in both $a_1(\rho)$ and $a_2(\rho)$ are at most on the order of a quantity called (by Skorupski) the "μ-integral",

$$\mu \equiv \lambda^{-1} \int_{\rho_1}^{\rho} \left| q^{-1/4}(\rho') \left[d^2 q^{-1/4}(\rho')/d\rho'^2 \right] d\rho' \right| , \qquad (\text{IV}.5)$$

where the integration path $\rho_1 - \rho$ (lying only in the region where one is trying to evaluate a_1 and a_2) is a part of the integration path $c - \rho$ used in Eq. (IV.2d). The validity of the phase-integral method requires $\mu \ll 1$; if one uses $q(\rho) = (\rho - T)^n$, this gives (over a semi-circle)

$$\mu = \frac{\pi \left| n(n+4) \right|}{16 \lambda \left| \rho - T \right|^{(n+2)/2}} \ll 1 , \qquad (\text{IV}.6)$$

which (for $n \geq -1$) sets a minimum distance of approach to the transition point T(Ref. T V). Setting $c = T$ in Eq. (IV.2d), Skorupski also shows that (for $n \geq -1$)

$$|\Psi| = \frac{\pi (n+4) |n|}{8 (n+2)^2 \mu} > \frac{0.2}{\mu} \gtrsim 1 , \qquad (\text{IV}.7)$$

the intuitively reasonable result (see also sec. III B) that the phase must be large in order to use the phase-integral method. This eliminates any paradoxes concerning the second major result: when moving (ρ) along any generalized anti-Stokes line (or jumping

between two principal anti-Stokes lines), if one crosses (in the counterclockwise direction) a principal Stokes line (radiating from any transition point) then the coefficient $a_s(\rho)$ of the subdominant WKBJ solution (f_s) changes according to

$$(a_s)_{new} = (a_s)_{old} + S \cdot a_d \ , \qquad (IV.8)$$

where $a_d(\rho)$ is the coefficient (unchanged) of the dominant WKBJ solution (f_d) and S is the Stokes constant; if crossing in the clockwise direction, replace S by -S. In general, S should have a subscript denoting which principal Stokes line of T is being crossed (although S is often the same for all lines).

It should be emphasized here that, when a principal Stokes line (from a transition point T) is encountered (when traveling along a generalized anti-Stokes line), one must change the "phase reference level" c to the point T since the Stokes constant S is generally tabulated relative to only a transition point as the "phase reference level"; using a different value for c would introduce different "dominancy changing factors" in each of Eqs. (IV.2b, c), relative to what f_1 and f_2 would be if c = T, and this difference would change the Stokes constants (Ref. T I). According to the first result (above Eq. (IV.5)), one can apparently ignore this principal Stokes line, but this is true only if one has no intention of ever crossing the second principal anti-Stokes line from

T that lies on the other side of this principal Stokes line. (The first principal anti-Stokes line from T can be crossed, but not the second because the direction of growth of the original dominant solution would then be reversed on this path around T; see Ref. T II, pages 226 - 227). Thus, to find solutions valid around T, one must change the "phase reference level" to T and, if the resulting "dominancy changing factor" is taken into account, then Eq. (IV.8) will give a negligible change (since $|\Psi| \ll 1$) in a_s ("subdominant" here meaning relative to T) in agreement with the first result (above Eq. (IV.5)).

The discussion in the preceding paragraph has presupposed that we know a_1 and a_2 at some point on a generalized anti-Stokes line. If instead, a_1 and a_2 are known on one principal anti-Stokes line from T and we wish to know them on the next principal anti-Stokes line (around T in the counterclockwise direction), then we find, upon moving to a generalized anti-Stokes line sufficiently far away from T as to satisfy $|\Psi| \gtrsim 1$ (and $\mu \ll 1$), that the subdominant solution f_s is exponentially small (smaller than the error in a_d multiplied by f_d) and its coefficient must be considered as unknown in the phase-integral method. In Eq. (IV.8), however, we are supposed to use on the right-hand-side the known values of a_1 and a_2 from the principal anti-Stokes line. (Equation (IV.8) was actually originally derived

(Ref. sec. T) for precisely this case, and we are merely generalizing the rule to include generalized anti-Stokes lines on which a_1 and a_2 are known for some reason). The resulting discontinuity in a_s (as evaluated on the two principal anti-Stokes lines), therefore, does not violate our first rule (above Eq. (IV.5)) because the actual coefficient a_s is not known on the generalized anti-Stokes line (which also never reaches either of the principal anti-Stokes lines, but only asymptotically approaches them with $\mathrm{Im}(\Psi) \gtrsim 1$ held fixed) and, as implied above, this discontinuity in $a_s f_s$ is smaller than the error in $a_d f_d$ evaluated on the generalized anti-Stokes line.

Finally, we return to the fact that the transition point T is also a branch-point of $q^{\frac{1}{4}}$ and $q^{\frac{1}{2}}$ and that branch-cuts must, therefore, be drawn in the complex ρ-plane. It is, therefore, necessary to know how the coefficients and WKBJ solutions differ on the two sides of a branch-cut (so that we can cross it if necessary). The general rule is that for a zero (of q) of multiplicity n, the exact solutions to Eq. (IV.1) exhibit no branch-behavior (i. e., they are entire analytic functions), so the continuity of Eq. (IV.2a) must be preserved even if we must alter its form. Examples of this will be given in the next section. For a first order pole, however, such as appears in our problem in sec. V, the exact solutions to Eq. (IV.1) do have an intrinsic branch-behavior. Examples of this will be given in the next section and again in sec. IV C.

B. Rules for Easy Application

We summarize here the procedure discussed in the previous section and present some of the more useful quantitative results (e. g., the Stokes constants) obtained from the literature (Ref. sec. T). In general, when applying the phase-integral method, one must do the following:

(a) Find the positions of all transition points, all principal Stokes and anti-Stokes lines, and a sufficient number of generalized Stokes and anti-Stokes lines (usually by inspection) to establish their trend. Place branch-cuts (from the transition points) in convenient positions (typically so as to be avoided).

(b) Apply the boundary condition that defines the first of the two independent solutions (e. g., A and B) of Eq. (IV.1) -- do this by drawing the appropriate arrows (see sec. IV A and Fig. IV.1) on the Stokes and anti-Stokes line that intersects this boundary point ρ_o (or limiting region, such as $\rho \to \infty$) and labeling these arrows with the local values of the coefficients a_1 and a_2. Relative to the first transition point T (i. e., setting the phase reference level $c = T$) that one encounters near ρ_o, this boundary solution $A(\rho_o)$ must be either subdominant

or be applied on a principal anti-Stokes line from T. Start outward from ρ_o along some arbitrary path.

(c) Continue this same solution (i. e., coefficients a_1 and a_2) to neighboring generalized Stokes and anti-Stokes lines using similar arrows with labels, but stop when encountering a principal Stokes line or branch-cut from any transition point T. If none are encountered, go to step (i).

(d) If not already done, switch the old phase reference level $(c)_{old}$ to $(c)_{new} = T$ and use new coefficients

$$(a_1)_{new} = (a_1)_{old} \cdot \left[(c)_{old}, (c)_{new}\right]$$

$$(a_2)_{new} = (a_2)_{old} \cdot \left[(c)_{new}, (c)_{old}\right]$$

to label similar arrows near T. If a principal Stokes line is encountered first, go to step (e); if a branch-cut is encountered first, skip down to step (g).

(e) From the direction of the arrows, note which WKBJ solution is subdominant and then cross the above mentioned principal Stokes line and change the subdominant coefficient from the value obtained in step (d) (now renamed "old" again) to the new value (see Eq. (IV.8))

$$(a_s)_{new} = (a_s)_{old} + S \cdot a_d \quad .$$

For an isolated transition point with $q(\rho) \propto (\rho - T)^n$ $(n \geq -1)$, use

$$S = 2i \cos\left[\pi/(n + 2)\right]$$

if going around T in the counterclockwise direction and minus this $(-S)$ if going in the clockwise direction. For non-isolated transition points, one can often treat them as merging into a single "compound" transition point as in sec. IV C where $S = T_n$ (for further examples, see Heading, Ref. T I).

(f) Having crossed the above mentioned principal Stokes line, one should again put arrows on the generalized Stokes and anti-Stokes lines for f_1 and f_2 and label these arrows with the new coefficients (a_d unchanged) obtained in step (e). Go to step (c).

(g) If one wishes to cross the encountered branch-cut in the sense of "jumping over" the cut or, equivalently, going around the transition point T to the corresponding position on the other side of the cut, then, upon crossing this branch-cut, the coefficients obtained in

step (d) (now renamed "old" again) are changed to new values. If $q(\rho) \propto (\rho - T)^n$, then for $n > 0$ and odd

$$(a_1)_{new} = i\,(-1)^{(n+1)/2} \cdot (a_2)_{old}$$

$$(a_2)_{new} = i\,(-1)^{(n+1)/2} \cdot (a_1)_{old}$$

and the directions of the arrows corresponding to f_1 and f_2 are reversed; for $n \geq 0$ and even

$$(a_1)_{new} = (-1)^{n/2}\,(a_1)_{old}$$

$$(a_2)_{new} = (-1)^{n/2}(a_2)_{old}$$

and the directions of the arrows corresponding to f_1 and f_2 are unchanged. As is apparent from the example in Figs. IV.1a, b, as far as the arrows are concerned the pattern remains exactly the same (upon crossing the cut) but with the labels multiplied by $\exp(-in\pi/2)$. The above rules assume the cut is crossed in the counter-clockwise direction; in the clockwise direction just replace i by $-i$. Note that the above rules maintain the continuity of the full solution $f = a_1 f_1 + a_2 f_2$

as required since the exact solution here has no branch-behavior. For $n = -1$, however, the exact sclution does have an intrinsic branch-behavior and, to preserve the required discontinuity, one now must have

$$(a_s)_{new} = (a_s)_{old} + 2i \cdot a_d$$

with the dominant coefficient unchanged. Again this is for counterclockwise crossing; for clockwise crossing replace i by -i. If this branch-cut (intrinsic) is crossed in the sense of going through onto the continuation of the Riemann sheet, then the continuity of the full solution $f = a_1 f_1 + a_2 f_2$ would once again have to be maintained.

(h) Having crossed the above mentioned branch-cut, one should again put arrows on the generalized Stokes and anti-Stokes lines for the WKBJ solutions f_1 and f_2 and label these arrows with the new coefficients obtained in Step (g). Go to step (c).

(i) The solution $f(\rho) = a_1(\rho)f_1(\rho) + a_2(\rho)f_2(\rho)$ is then known along the chosen path. New paths can be taken until the solution is known in every region (excluding a small region around every transition point) of the complex ρ-plane.

C. Stokes Constant for Pole-Zero Combination

We assume here that, for small ρ (e.g., $|\rho| << 2|X|$ in Eq. (V.2c)), our function $q(\rho)$ takes the special form (relevant to sec. V)

$$q(\rho) = 2X + \frac{1}{\rho} \quad , \qquad \text{(IV.9)}$$

where X is independent of ρ. Equation (IV.1) can then be solved exactly (Ref. sec R) in terms of Whittaker functions, and Heading (Ref. T III) has calculated the Stokes constants from the known asymptotic forms for the solution. The precise value of Heading's "Phase reference level", c, is somewhat obscure, however, and we prefer a more standard choice like setting $c = -1/2X$, the position of the zero of $q(\rho)$. As pointed out in sec. IV A, however, changing "phase reference levels" also changes the value of the Stokes constants, and we find that we must multiply his result (correcting a typographical error) by the factor $(k/e)^{2\,sk} \cdot \exp\left[-i2\pi sk(s-1)\right]$. Here $k \equiv -i\lambda/2(2X)^{\frac{1}{2}}$, $s \equiv (-1)^n$, and n is an integer labeling the two effective principal Stokes lines on the different Riemann sheets as shown in Fig. IV.2. Performing this multiplication results in

$$T_n = \frac{2\pi i}{sk\,\Gamma^2(sk)} \left(\frac{k}{e}\right)^{2sk} \exp\left[-i2\pi sk(n+s-1)\right] \qquad \text{(IV.10)}$$

as the Stokes constant we use here (we keep Heading's symbol T_n). This has the expected limit (in agreement with the Stokes constant for an isolated first order zero at $\rho = -1/2X$), as $|k| \to \infty$, of

$$T_{1,0} \xrightarrow[|k|\to\infty]{} +i \qquad \text{(IV.11a)}$$

on the principal Riemann sheet ($n = 0, 1$), if we use the asymptotic form for the gamma function $\Gamma(sk)$ with $\arg(sk) < \pi$ and $-\pi \leq \arg(k) \leq 0$ (this requires setting $s = \exp(i\pi n)$ with $n = 0$ or 1 only). In the opposite limit, $|k| \to 0$, we find

$$T_0 \xrightarrow[|k|\to 0]{} 2\pi i k \left(\frac{k}{e}\right)^{2k} (1 + 1.2k + \cdots) \qquad \text{(IV.11b)}$$

$$T_1 \xrightarrow[|k|\to 0]{} -2\pi i k \left(\frac{e}{k}\right)^{2k} \exp(-i2\pi k)(1 - 1.2k + \cdots). \qquad \text{(IV.11c)}$$

Although T_n has the proper limiting form in Eq. (IV.11a), considering the complexity of Eq. (IV.10) further verification is always welcome. This comes easily if one uses the rules in sec. IV B

to trace the solutions corresponding to the two cases of a wave incoming from the right or the left. The boundary condition in both cases is that the wave be outgoing on the far opposite side. In both cases the branch-cuts should be directed upward and the solutions traced across the lower-half-plane using T_o for the Stokes constant (finite wave damping would shift the pole above the real axis if $\exp(-i\omega t)$ time dependence with $Re(\omega) > 0$ is used). For the wave incident from the left and encountering the turning point (zero of q) first (Fig. IV.2a), we find for the reflection $\tilde{R}$ and transmission $\tilde{T}$ coefficients

$$\tilde{R} = \frac{-2\pi i \exp(-i\pi k)}{\Gamma(k)\,\Gamma(1+k)} \exp\left\{2k \ln\left[2\lambda (2X)^{1/2}\right]\right\} \qquad \text{(IV.12a)}$$

$$\tilde{T} = \exp(-i\pi k) \; . \qquad \text{(IV.12b)}$$

For $Re(k) = 0$, this gives

$$|\tilde{T}| = \exp\left[-\pi\,|Im(k)|\right] \qquad \text{(IV.12c)}$$

$$|\tilde{R}| = 1 - |\tilde{T}|^2 \qquad \text{(IV.12d)}$$

in exact agreement with Budden (Ref. R I). For the wave incident from the right (Fig. IV.2b) and encountering the resonance (pole of q), we find

$$\tilde{R} = 0 \qquad \text{(IV.13a)}$$

$$\tilde{T} = \exp(-i\pi k) \qquad \text{(IV.13b)}$$

so that our results are again in exact agreement with Budden for Re(k) = 0.

We mentioned earlier that a first order pole gives a solution to Eq. (IV.1) with an intrinsic branch-cut. Taking this case (or letting $X \to 0$ in Eq. (IV.9)), the two independent exact solutions are (see Ref. sec. R)

$$A(\rho) = \sqrt{\rho}\, H_1^{(1)}(2\lambda\sqrt{\rho}) \qquad \text{(IV.14a)}$$

$$B(\rho) = \sqrt{\rho}\, H_1^{(2)}(2\lambda\sqrt{\rho}) \qquad \text{(IV.14b)}$$

where $H_1^{(1)}$ and $H_1^{(2)}$ are Hankel functions. These two solutions both have intrinsic branch-behavior due to the square root. Their asymptotic forms (for $\lambda|\rho|^{\frac{1}{2}} \gg 1$) are just

$$A \to \exp(-i\tfrac{3}{4}\pi)\ f_1(\rho) \qquad \text{(IV.15a)}$$

$$B \to \exp(+i\tfrac{3}{4}\pi)\ f_2(\rho) \qquad \text{(IV.15b)}$$

where f_1 and f_2 are given by Eq. (IV.2b, c). It is interesting to note that the particular combination

$$A+B = 2\sqrt{\rho}\ J_1(2\lambda\sqrt{\rho}) \qquad \text{(IV.16)}$$

has no branch-behavior, as can be verified from Figs. IV.1c, d or by expanding the Bessel function J_1. The branch-behavior of this isolated pole will, of course, continue in the presence of other transition points such as in Eqs. (IV.9 and V.2c).

This concludes our discussion of the phase-integral method. We have outlined the basic concepts, presented a list of rules to follow when applying the method, and have investigated certain details of the solution in the neighborhood of a pole and one nearby zero of $q(\rho)$ such as we will find in part of the complex ρ-plane in sec. V. Therefore, we move on to sec. V and our main problem we are investigating — the nonuniform pumped plasma.

V. NONUNIFORM PLASMA, PUMPED

For a linear density profile ($z > 0$), we see from Eq. (I.25b) that $Q(z,\omega_1,\underline{k}_{1\perp})$ generally has two roots and one pole in the complex z-plane. We simplify the form of Eq. (I.25) by transforming to the new dimensionless position variable

$$\rho(z,\omega_1,\underline{k}_{1\perp}) \equiv \frac{\omega_p^2(z) - (\omega_0 - \omega_1 - i\nu_p)^2}{D}, \qquad (V.1)$$

where the pump strength parameter $D(\omega_1,\underline{k}_{1\perp})$ is defined by Eq. (I.25c), and ν_p is a phenomenological damping rate for the Langmuir waves. The homogeneous transformed version of Eq. (I.25a) (valid only for $\mathrm{Re}\omega_1 \geq 0$; see sec. II) now reads

$$\left[\frac{d^2}{d\rho^2} + \lambda^2 q(\rho,X)\right] f_1(\rho,X) = 0 \qquad (V.2a)$$

$$\lambda(\omega_1,\underline{k}_{1\perp}) \equiv \frac{D^{3/2}(\omega_1,\underline{k}_{1\perp})\, L_n}{\omega_p^2\, c} \qquad (V.2b)$$

$$q(\rho,X) \equiv 2X - \rho + \frac{1}{\rho} = -\frac{(\rho-\rho_+)(\rho-\rho_-)}{\rho}, \qquad (V.2c)$$

where

$$X(\omega_1, \underline{k}_{1\perp}) \equiv \frac{(\omega_1+i\nu_1)^2 - c^2 k_{1\perp}^2 - (\omega_o-\omega_1-i\nu_p)^2}{2D} \qquad (V.2d)$$

$$\rho_+(X) \equiv X + (X^2+1)^{1/2} \qquad (V.2e)$$

$$\rho_-(X) \equiv X - (X^2+1)^{1/2} , \qquad (V.2f)$$

and ν_1 is a collisional damping rate for the electromagnetic waves. We have transformed our old $Q(z,\omega_1,\underline{k}_{1\perp})$ into a dimensionless potential $q(\rho,X)$, where the roots (of Q and q) are now at ρ_+ and ρ_-, and the pole is now always at $\rho = 0$. We have replaced the two parameters ω_1 and $\underline{k}_{1\perp}$ by the single dimensionless parameter $X(\omega_1,\underline{k}_{1\perp})$, which we will treat as essentially a frequency parameter since $\underline{k}_{1\perp}$ is generally treated as fixed here (see sec. I B). Note that the positions of $\rho_+(X)$ and $\rho_-(X)$, relative to each other and to $\rho = 0$, depend on the value of the complex parameter X. The branch-cuts (in the complex X-plane) for Eqs. (V.2e,f) are chosen (see Fig. V.1) such that $|\rho_+| \geq 1$ and $|\rho_-| \leq 1$ (see Fig. V.2) on the principal Riemann sheet. If we had not chosen a linear density profile (for $z > 0$), we would have the more complicating features

that λ (and X, if a nonuniform static magnetic field $\underline{B} = \hat{x}B(z)$ were included, as mentioned in sec. I A 1) would be z-dependent and there would be an additional term $\left(\frac{df_1}{d\rho}\right)\left(\frac{d^2\rho}{dz^2}\right)\Big/\left(\frac{d\rho}{dz}\right)^2$ on the left of Eq. (V.2a).

According to the procedure outlined in sec. I D 2, we must now find two solutions $A(\rho,X)$ and $B(\rho,X)$ of Eq. (V.2) valid for arbitrary complex X (X depends on ω_1 which must be integrated over). In the absence of known exact solutions, we use phase-integral (or WKBJ) techniques (Ref. T) in the complex ρ-plane to obtain approximate solutions valid in overlapping regions of the complex X- or ω_1-plane (excluding the transition-points where $\rho = 0, \rho_+$ or ρ_-).

In applying these techniques (see sec. IV), the first step (sec. V A 1) is to obtain the generalized Stokes and anti-Stokes lines in the complex ρ-plane and determine how these lines change as X changes. The next step (sec. V A 2) is to make a convenient choice for the branch-cuts which must emerge from the three transition-points ($0, \rho_+$, and ρ_-) in the complex ρ-plane. Finally (sec. V A 3), we start in a region of the complex ρ-plane far from all transition points (where a convenient choice for the solution A or B is made) and then travel through the complex ρ-plane, adding and modifying terms (according to the rules given in sec. IV B) as we cross the Stokes and anti-Stokes lines, thereby constructing the WKBJ solutions.

A. Application of Phase-Integral Method

1. Stokes and Anti-Stokes Lines

As defined in sec. IV, a principal anti-Stokes line has $\mathrm{Im}\int_T^\rho \sqrt{q}\, d\rho = 0$ where T denotes one of the transition points ($0, \rho_+$, or ρ_- here); along such a line the WKBJ solutions are purely oscillatory (we recall that the WKBJ solutions behave essentially like $\exp(\pm i\lambda\int_T^\rho \sqrt{q}\, d\rho)$, as described in sec. IV A). A principal Stokes line has $\mathrm{Re}\int_T^\rho \sqrt{q}\, d\rho = 0$, and along such a line the WKBJ solutions are purely growing or decaying.

The potential $q(\rho,X)$, given by Eq. (V.2c), has two roots (ρ_+ and ρ_-) and one pole ($\rho = 0$), all first order. In sec. IV A we discussed the patterns of Stokes and anti-Stokes lines about isolated transition points and, in Fig. IV.2, illustrated the distortion induced in these patterns by the presence of neighboring transition points. In our case, we must determine how to connect the three localized patterns (about the three transition points ρ_+, ρ_-, and 0) if we are to later (sec. V A 3) trace the WKBJ solutions across the complex ρ-plane.

To do this, one can expand $\left[q(\rho,X)\right]^{\frac{1}{2}}$ about each transition point T ($T = \rho_+, \rho_-$, or 0) in terms of the small complex distance $\delta\rho_T = \rho - T$, evaluate the phase-integral $\int_0^{\delta\rho_T} \left[q(T + \delta\rho_T, X)\right]^{\frac{1}{2}} d\delta\rho_T$ to various orders in $\delta\rho_T$, and determine (to each order) where the

real or imaginary parts of the phase-integral vanish. To lowest order (independent of $\delta\rho_T$) one obtains the angles at which the principal Stokes and anti-Stokes lines radiate from the transition point T. The next order term gives a $\delta\rho_T$-dependence to these angles and indicates the curvature of the lines near the point T. The behavior of the lines in regions intermediate between the transition points can then usually be determined by interpolation.

Actually, for our potential given by Eq. (V.2c), the phase-integral can be evaluated exactly in terms of elliptic integrals of the first and second kind with complex amplitude and modulus. The generalized Stokes and anti-Stokes lines can then be obtained from a contour plot of the real and imaginary parts of the phase-integral.

The easiest technique to use, and one which is completely general, is to start at some arbitrary small distance $\delta\rho_T = |\delta\rho_T|e^{i\phi_T}$ from a transition point T and evaluate the phase angle ϕ_q of the complex potential $q(T + \delta\rho_T, X) = |q|e^{i\phi_q}$. We then use standard root-finding methods to obtain solutions ϕ_T to the equation

$$\phi_T + \frac{\phi_q}{2} + N\frac{\pi}{2} = 0 \qquad (V.3)$$

for fixed $|\delta\rho_T|$, where $N = 0$ or ± 2 for an anti-Stokes line and $N = \pm 1$ or ± 3 for a Stokes line (more than one solution can correspond to a given N). These solutions ϕ_T are the angles at which

the lines radiate from the point T. Starting at a position $\rho = T + |\delta\rho_T|e^{i\phi_T}$ on one of these principal Stokes or anti-Stokes lines, we repeatedly step along the line by an amount $\delta\rho_T = |\delta\rho_T|e^{i\phi_T}$ ($\rho_{new} = \rho_{old} + \delta\rho_T$), where the local value of $\phi_T(\rho_{old}, X)$ (the orientation of the line) is determined by the local value of $q(\rho_{old}, X) = |q|e^{i\phi_q}$ and Eq. (V.3).

Using this latter technique, we plot the principal Stokes (dotted) and anti-Stokes (solid) lines in Figs. V.3-5 for various values of the complex parameter $X(\omega_1, \underline{k}_{1\perp})$. The generalized lines can then be found by inspection. Note that the simple pole is always at $\rho = 0$, while the positions of the two simple roots ($|\rho_+| \geq 1$ and $|\rho_-| \leq 1$) depend on the complex parameter X. Near each of the transition points ($\rho = 0, \rho_+, \rho_-$) in Figs. V.3-5, the pattern of Stokes and anti-Stokes lines approaches that of an isolated transition point, as illustrated in Fig. IV.1. All of the transition points ($\rho = 0, \rho_+, \rho_-$) are also branch-points, and branch-cuts should be drawn from them, as discussed in the next section.

2. Branch-Cuts

In the previous section, we determined the generalized Stokes and anti-Stokes lines (lines of constant real and imaginary part of $\int^{\rho} \sqrt{q}\, d\rho$, the phase-integral) for the potential $q(\rho, X)$ given in Eq. (V.2c). Due to the square-root of q, we have branch-points wherever $q = 0$ or ∞, and these branch-points must be

connected by branch-cuts in order that the phase-integral be single-valued in the cut complex plane. In the complex ρ-plane, the transition points T and the point at infinity are the branch-points, but in Figs. V. 3-5 we did not draw in the connecting branch-cuts since their position can be chosen arbitrarily.

Preliminary to making this choice of branch-cut positions, we note that the function $\left[q(\rho,X)\right]^{\frac{1}{2}} = \left[Q(z,\omega_1,\underline{k}_{1\perp})\right]^{\frac{1}{2}} c/\sqrt{D}$ has branch-points in more than one space (e. g., in the complex ω_1-plane for given z and $\underline{k}_{1\perp}$, in the complex z-plane for given ω_1 and $\underline{k}_{1\perp}$, and in the complex ρ-plane for given X). We denote these sets of branch-points (for $\mathrm{Re}\omega_1 > 0$, and $\underline{k}_{1\perp}$ fixed) as

$$\left\{\omega_b(z)\right\} \equiv \left\{\omega_I(z), \omega_{II}^{0}(z), \omega_{III}^{0}(z), \omega_{II}^{\infty}(z), \omega_{III}^{\infty}(z)\right\} \qquad (V.4a)$$

$$\left\{z_b(\omega_1)\right\} \equiv \left\{z_+(\omega_1), z_-(\omega_1), z_\infty(\omega_1)\right\} \qquad (V.4b)$$

$$\left\{\rho_b(X)\right\} \equiv \left\{\rho_+(X), \rho_-(X), \rho_\infty(X) \equiv 0\right\} \qquad (V.4c)$$

with typical relative positions shown in Figs. V.6-7.

The branch-point $\omega_1'(z)$ corresponds in the unpumped case (sec. III B) to the root of Q obtained by setting $k_{1z}^2(z,\omega_1,k_{1\perp}) = 0$ in Eq. (I.25 b) (in the pumped case there is a slight z-dependent shift from this $\omega - i\nu_1 \equiv \left[\omega_p^2(z) + c^2k_{1\perp}^2\right]^{\frac{1}{2}} - i\nu_1$). The equivalent

branch-point in the complex z- or ρ-plane is $z_+(\omega_1)$ or $\rho_+(X)$, respectively. In the unpumped case, $\omega_p^2(z_+) = (\omega_1 + i\nu_1)^2 - c^2k_{1\perp}^2$ and $\rho_+ = 2X$ (obtained by letting $D \to 0$ or $X \to \infty$), and there is a slight ω_1- or X-dependent shift from these values in the pumped case.

The remaining branch-points in Eq. (V.4) have no correspondence in the unpumped case (i. e., a singularity and a root of Q merge as $D \to 0$). The branch-points $\omega_{II}^{\infty}(z) \equiv \omega_o - \omega_p(z) - i\nu_p$ and $\omega_{III}^{\infty}(z) \equiv \omega_o + \omega_p(z) - i\nu_p$ are singularities of Q, separated from their associated neighboring roots of Q, the branch-points $\omega_{II}^{o}(z)$ and $\omega_{III}^{o}(z)$, by a small distance proportional to D or D^2 (depending upon the value of z). In the complex z- or ρ-plane, there is only one equivalent singularity of Q (i. e., branch-point), $z_\infty(\omega_1)$ (where $\omega_p^2(z_\infty) \equiv (\omega_o - \omega_1)^2$) or $\rho_\infty(X) \equiv 0$, respectively; note that we have renamed the resonance position (z_o of sec. I A 3) to explicitly indicate a pole of Q. The branch-point $z_-(\omega_1)$ or $\rho_-(X)$ is the equivalent neighboring root of Q.

Having located the branch-points $\{\omega_b(z)\}, \{z_b(\omega_1)\}$, and $\{\rho_b(X)\}$ in the complex ω_1-, z-, and ρ-planes, we now consider the branch-cut locations in the ω_1-plane. We choose some convenient prescription (e. g., straight lines between pairs of branch-points) such that, for any fixed complex position z, the branch-cut from any one of

the branch-points $\omega_1 = \omega_b(z)$ is determined:

$$\omega' = F_b(z,\alpha) \qquad (V.5)$$

where ω', a point on the branch-cut, is determined by choosing F_b, a complex function of the parameter z and the real distance variable α $(0 \le \alpha < \infty)$ along the branch-cut. For instance, for the branch-point $\omega_I(z)$ we choose the horizontal branch-cut $\omega' = F_I(z,\alpha) = \omega_I(z) + \alpha$; between the branch-points $\omega_{II}^{o}(z)$ and $\omega_{II}^{\infty}(z)$, we choose the straight line branch-cut $\omega' = F_{II}(z,\alpha) = \omega_{II}^{o}(z)(1 - \alpha) + \omega_{II}^{\infty}(z)\alpha$ with $0 \le \alpha \le 1$; between the branch-points $\omega_{III}^{o}(z)$ and $\omega_{III}^{\infty}(z)$, we similarly choose $\omega' = F_{III}(z,\alpha) = \omega_{III}^{o}(z)(1 - \alpha) + \omega_{III}^{\infty}(z)\alpha$ with $0 \le \alpha \le 1$. These branch-cuts are shown in Fig. V.6.

We must now consider the branch-cut locations in the complex z-plane. Given our arbitrary choice of branch-cuts in the complex ω_1-plane, we have no freedom of choice left in the z-plane. This is because we are considering the branch-behavior of a single function $\left[Q(z,\omega_1,\underline{k}_{11})\right]^{\frac{1}{2}}$, which happens to have more than one variable. The function $\sqrt{Q}$ has the same value regardless of whether we choose $z = z_a$ in the complex z-plane with $\omega_1 = \omega_a$ fixed or choose $\omega_1 = \omega_a$ in the complex ω_1 - plane with $z = z_a$ fixed; if, for fixed $z = z_a$, the point $\omega_1 = \omega_a$ lies on the branch-cut in the

complex ω_1-plane, then, for fixed $\omega_1 = \omega_a$, the point $z = z_a$ must lie on the branch-cut in the complex z-plane.

From Eq. (V.5), $\omega_a(\alpha) = F_b(z_a,\alpha)$ is a point on the branch-cut emanating from the branch-point $\omega_1 = \omega_b(z_a)$ in the complex ω_1-plane, for fixed $z = z_a$. From another point of view, in the complex z-plane the equation $\omega_a = F_b(z_a,\alpha)$ determines a point $z = z_a(\alpha)$ on the branch-cut emanating from the branch-point $z = z_b(\omega_a)$, for fixed $\omega_1 = \omega_a$. If $\alpha = 0$, $\omega_a = F_b(z_a,0) = \omega_b(z_a)$ and $z_a = z_b(\omega_a)$. Formally we can write

$$z' = F_b^{-1}(\omega_1, \alpha) \qquad (V.6)$$

as the equation for a point ($z_a(\alpha)$ above) on the branch-cut from the branch-point $z = z_b(\omega_1)$ in the complex z-plane, for fixed ω_1. The branch-cuts in the complex z-plane, as determined by Eq. (V.6), are shown qualitatively in Fig. V.7, for several typical values of ω_1 that are indicated in Fig. V.6. We have also drawn in Fig. V.7 the coordinate system for the complex ρ-plane since, for fixed ω_1 (and a linear density profile), ρ and z are linearly proportional:

$$z = Z\,\lambda^{2/3}\,(\rho - \rho_o) \qquad (V.7)$$

where $\rho = \rho(z,\omega_1,\underline{k}_{1\perp})$, $\rho_o \equiv \rho(z = 0,\omega_1,\underline{k}_{1\perp})$, $Z \equiv (c^2 L_n/\omega_p^2)^{1/3}$, and λ is defined in Eq. (V.2b).

As can be seen from Fig. V.7, the branch-cuts in the complex ρ-plane (where we will map out the form of the WKBJ solutions in the next section) are relatively complicated in appearance compared with our simple choices of branch-cuts in the complex ω_1-plane. We have been forced into dealing with this complication because the WKBJ solutions change form across the branch-cuts in the complex ρ-plane, and we must determine how this translates into a change in form across the branch-cuts in the complex ω_1-plane (where we must eventually perform the integration indicated in Eq. (I.29)). Fortunately, to answer such a question, very little information about the branch-cuts is needed (e. g., if the point $\omega_1 = \omega_a$ lies on a certain side of the branch-cut in the ω_1-plane, for fixed $z = z_a$, then we need to know on which side of the corresponding branch-cut in the z-plane the point $z = z_a$ lies, for fixed $\omega_1 = \omega_a$; this is answered by Figs. V.6a, 7e, f, g).

The coefficient $a(\omega_1,\underline{k}_{1\perp})$, given by Eq. (I.32), has branch-cuts shown in part (only those due to the $\left[Q(z = 0,\omega_1,\underline{k}_{1\perp})\right]^{\frac{1}{2}}$) in Fig. V.6a with the remaining branch-cuts (not shown) due to the intrinsic branch-behavior of the functions $A(\rho,\omega_1,\underline{k}_{1\perp})$ and $B(\rho,\omega_1,\underline{k}_{1\perp})$. As discussed in sec. IV C, the functions A and B have an intrinsic branch-point at $\rho(z,\omega_1,\underline{k}_{1\perp}) = 0$ and, therefore, intrinsic branch-points at $\omega_{II}^{\infty}(z)$ and $\omega_{III}^{\infty}(z)$ in the complex

ω_1-plane. We arbitrarily choose the corresponding intrinsic branch-cuts to extend vertically downward (i. e., $\omega' = \omega''_{II}(z) - i\alpha$ and $\omega' = \omega''_{III}(z) - i\alpha$, $0 \leq \alpha < \infty$) from these points in the complex ω_1-plane, and these intrinsic branch-cuts must be superimposed on those of Fig. V.6a to completely define $a(\omega_1, \underline{k}_{\perp})$. In determining the behavior of A and B in the complex ρ-plane, we must include the corresponding intrinsic branch-cut, also extending essentially (for $Re\omega_1 < \omega_o$) vertically downward (from $\rho = 0$), in addition to those branch-cuts (across which the WKBJ form changes but the value of A and B remains continuous) already shown in Fig. V.7.

Having obtained the Stokes and anti-Stokes lines (sec. V A 1), and having decided on the positions of all the branch-cuts (sec. V A 2), we are now able to apply the rules of sec. IV B for tracing the WKBJ solutions throughout the complex ρ-plane. This will be carried out in the next section, sec. V A 3.

3. WKBJ Solutions

From the discussion at the end of the previous section, and from the form of Eqs. (I.26, 31), we see that, to perform the ω_1-integration in Eq. (I.29), we must take into account the branch-cuts (in the complex ω_1-plane) shown in Fig. V.6a as well as additional branch-cuts extending vertically downward from branch-points at $\omega''_{II}(z = 0)$, $\omega''_{III}(z = 0)$, $\omega''_{II}(z_\ell)$, $\omega''_{III}(z_\ell)$, $\omega''_{II}(z_g)$, $\omega''_{III}(z_g)$,

and similarly for $Re(\omega_1) < 0$. Our original Bromwich integration contour (see sec. I D) can be depressed, leaving an integral around all the branch-cuts plus a summation over all the residues (if there are any poles of the integrand corresponding to temporally growing eigenmodes). Thus, we are primarily interested in knowing $A(\rho,X)$ and $B(\rho,X)$ for values of ω_1 in the vicinity of the branch-cuts in the complex ω_1-plane.

It is now useful to note the similarity between the unpumped nonuniform plasma (sec. III B) and the pumped nonuniform plasma considered here. As the pump strength parameter $D(\omega_1,\underline{k}_{\perp\perp})$ goes to zero, the solutions $A(\rho,X)$ and $B(\rho,X)$ become continuous across the vertical branch-cuts (see sec. IV C), and the branch-cuts between $\omega_{II}^{\infty}(0)$ and $\omega_{II}^{o}(0)$ and between $\omega_{III}^{\infty}(0)$ and $\omega_{III}^{o}(0)$ shrink to zero; this leaves only the integral around the horizontal branch-cut extending to the right of $\omega_I(0)$, so this integral gives the wave-packets found in sec. III B. We recall that in secs. III A-C we found no time-asymptotic contribution to the integral (i. e., no saddle-points) below this branch-cut. For finite $D(\omega_1,\underline{k}_{\perp\perp})$ here, we still expect to find saddle-points only above this branch-cut or on the continuation of the Riemann sheet reached by passing through this branch-cut from above (e. g., in Fig. V.6a, passing from the point "a" down through the branch-cut onto the next sheet below). These saddle-points will again determine the wave-packets (but modified by the pump).

In Figs. V.8-10, we construct the WKBJ solutions for $A(\rho,X)$ and $B(\rho,X)$ for three representative choices of frequency (ω', ω'', and ω''') along the horizontal branch-cut from $\omega_I(z = 0)$ shown in Fig. V.6a. These frequencies can be either above ("a") or below ("b") this branch-cut in the complex ω_1-plane (Fig. V.6a), with the choice determining whether the point $z = 0$ (and hence the entire real z axis) is below or above the branch-cut in the complex ρ-plane (see Fig. V.7e, f, g). Again, by "below" we mean to include also the continuation of the Riemann sheet reached by passing through the branch-cut from below, and similarly "above" includes the sheet reached from above the branch-cut. We mention here that the intrinsic branch-cut (sec. V A 2, IV C), along the negative imaginary axis (for $\mathrm{Re}\omega_1 < \omega_o$) in the complex ρ-plane, has been deliberately left out in Figs. V.8-10 in order to not further confuse the already complicated figures. It would have to be taken into account if one tried to continue the solutions across the negative imaginary axis (the Stokes constants T_n also depend upon which sheet one is on, as discussed in sec. IV C).

The solutions $A(\rho,X)$ and $B(\rho,X)$ in Figs. V.8-10 are given in terms of the WKBJ solutions using Heading's notation (Ref. T I),

$$(\rho,\rho_+) \equiv \frac{e^{i\frac{\pi}{4}}}{2\sqrt{\pi}(q)^{1/4}} \exp\left[+i\lambda\int_{\rho_+}^{\rho} q^{1/2}(\rho',X)\,d\rho'\right] \qquad (V.8a)$$

$$(\rho_+,\rho) \equiv \frac{e^{i\frac{\pi}{4}}}{2\sqrt{\pi}(q)^{1/4}} \exp\left[-i\lambda\int_{\rho_+}^{\rho} q^{1/2}(\rho',X)\,d\rho'\right], \qquad (V.8b)$$

where $q(\rho,X)$ and λ are defined in Eq. (V.2). The particular choice for the above constant coefficient is motivated by the self-imposed requirement (in order to show agreement with sec. III B) that A and B approach the two Airy functions Ai and Bi, respectively, as the pump strength D vanishes. The relevant linear combinations of (ρ,ρ_+) and (ρ_+,ρ) (for A and B), valid in the indicated regions of the complex ρ-plane in Figs. V.8-10, are given below. In each region "n" ($n = 1,2,\cdots,9$), the total solution (A or B) is $f_n + g_n$, where

$$f_1 = (\rho,\rho_+) \qquad g_1 = i(\rho_+,\rho) \qquad (V.9a)$$

$$f_2 = i(\rho,\rho_+) \qquad g_2 = (\rho_+,\rho) \qquad (V.9b)$$

$$f_3 = \left\{i - 2[\rho_-,\rho_+]^{-2} I_1\right\}(\rho,\rho_+) \qquad g_3 = 2(\rho_+,\rho) \qquad (V.9c)$$

$$f_4 = f_1 \qquad g_4 = \{i + [\rho_-, \rho_+]^{-2} T_1\}(\rho_+, \rho) \qquad (V.9d)$$

$$f_5 = \{1 - i[\rho_-, \rho_+]^{-2} T_1\}(\rho, \rho_+) \qquad g_5 = -i(\rho_+, \rho) \qquad (V.9e)$$

$$f_6 = f_2 \qquad g_6 = \{1 - i[\rho_-, \rho_+]^{-2} T_1\}(\rho_+, \rho) \qquad (V.9f)$$

$$f_7 = f_2 \qquad g_7 = \{2 - i[\rho_-, \rho_+]^{-2} T_1\}(\rho_+, \rho) \qquad (V.9g)$$

$$f_8 = -\{i + [\rho_-, \rho_+]^{-2} T_1\}(\rho, \rho_+) \qquad g_8 = g_7 \qquad (V.9h)$$

$$f_9 = f_8 \qquad g_9 = g_2 \,. \qquad (V.9i)$$

Here ,

$$[\rho_-, \rho_+] \equiv \exp\left[+i\lambda \int_{\rho_+}^{\rho_-} q_b^{1/2}(\rho', X)\, d\rho'\right] \qquad (V.10)$$

is the "dominancy changing factor" used by Heading (Ref. T I) to change the phase reference level of a WKBJ solution (e.g., $(\rho, \rho_+) = (\rho, \rho_-)\left[\rho_-, \rho_+\right], (\rho_+, \rho) = [\rho_+, \rho_-](\rho_-, \rho)$, with $\left[\rho_+, \rho_-\right] = \left[\rho_-, \rho_+\right]^{-1}$). The constant T_1 is one of the Stokes constants T_n for the pole-zero combination, treated as a "compound" transition point, in sec. IV C.

The WKBJ solutions for A and B, given in Eq. (V.9) and Figs. V.8-10, can be easily followed if one uses the rules outlined in sec. IV B. Since (ρ, ρ_+) and (ρ_+, ρ) are purely oscillatory along the anti-Stokes lines (by definition), we can multiply these functions by $\exp(-i\omega_1 t)$ and consider them as traveling waves along these lines; the arrows on the anti-Stokes lines indicate the direction of propagation of the indicated function (f_n or g_n). Also, every region of the complex ρ-plane is intersected by Stokes lines (perpendicular to the anti-Stokes lines except at a transition point), and along these Stokes lines (ρ, ρ_+) and (ρ_+, ρ) are purely growing or decaying; we occasionally draw arrows on the Stokes lines to indicate the direction in which the indicated function (f_n or g_n) increases. If the function increases as one moves (along a Stokes line) away from a transition point, it is called dominant with respect to that transition point and is labeled with a subscript "d"; otherwise it is called subdominant and lebeled with a subscript "s". The arrows on the Stokes and anti-Stokes lines are related by the "right-hand SAN rule" of sec. IV B: the Stokes arrow crossed into the anti-Stokes arrow is normal (up) to the complex plane.

It is important to determine the dominancy or subdominancy of (ρ, ρ_+) and (ρ_+, ρ) since only the coefficient of the subdominant term is changed upon crossing a principal Stokes line (one which

is the "dominancy changing factor" used by Heading (Ref. T I) to change the phase reference level of a WKBJ solution (e. g., $(\rho,\rho_+) = (\rho,\rho_-)\left[\rho_-,\rho_+\right]$, $(\rho_+,\rho) = \left[\rho_+,\rho_-\right](\rho_-,\rho)$, with $\left[\rho_+,\rho_-\right] = \left[\rho_-,\rho_+\right]^{-1}$). The constant T_1 is one of the Stokes constants T_n for the pole-zero combination, treated as a "compound" transition point, in sec. IV C.

The WKBJ solutions for A and B, given in Eq. (V.9) and Figs. V.8-10, can be easily followed if one uses the rules outlined in sec. IV B. Since (ρ,ρ_+) and (ρ_+,ρ) are purely oscillatory along the anti-Stokes lines (by definition), we can multiply these functions by $\exp(-i\omega_1 t)$ and consider them as traveling waves along these lines; the arrows on the anti-Stokes lines indicate the direction of propagation of the indicated function (f_n or g_n) increases. If the function increases as one moves (along a Stokes line) away from a transition point, it is called dominant with respect to that transition point and is labeled with a subscript "d"; otherwise it is called subdominant and labeled with a subscript "s". The arrows on the Stokes and anti-Stokes lines are related by the "right-hand SAN rule" of sec. IV B: the Stokes arrow crossed into the anti-Stokes arrow is normal (up) to the complex plane.

It is important to determine the dominance or subdominancy of (ρ,ρ_+) and (ρ_+,ρ) since only the coefficient of the subdominant term is changed upon crossing a principal Stokes line (one which

originates at a transition point) while the amount of change depends on the coefficient of the dominant term (see sec. IV). When crossing a principal Stokes line, one must remember to first change the phase reference level to the position of the transition point from which the principal Stokes line emerged (otherwise one cannot use the standard Stokes constants for that transition point, given in sec. IV B, C); after crossing the principal Stokes line, one can switch back to whatever convenient phase reference level one started with.

Note that the pole-zero "compound" transition point (see sec. IV C) is viewed as having only <u>two</u> principal Stokes lines: one emerging from the pole ($\rho = 0$), and the other (in roughly the opposite direction) emerging from the zero (ρ_-). The remaining two Stokes lines emerging from ρ_- are not viewed as having distinct Stokes constants unless the pole and zero are treated as separate and distant transition points; the problem here is that for $|X| \gg 1$ the pole and zero (ρ_-) are not distant since $\rho_- \overset{\sim}{=} (2X)^{-1}$. In order to accurately obtain the eigenvalues and a nonzero threshold pump strength, it is necessary that one use Stokes constants (e. g., the T_n) valid for arbitrarily small separation between the pole and the zero (ρ_-).

The solution $A(\rho,X)$, shown in Figs. V.8a, 9a, and 10a, is distinguished by demanding the boundary condition (abbreviated "b.c.") that A be evanescent (subdominant) as $\rho \to +\infty$; thus, $A(\rho,X) = f_1$ as $\rho \to +\infty$. This form remains valid until one crosses

one of the principal Stokes lines from ρ_+ in a region where f_1 is dominant; then A changes form to $A(\rho,X) = f_1 \pm g_1$ depending on whether ρ is above or below the branch-cut from ρ_+. In Fig. V.10a we encounter the pole-zero "compound" transition point to the left of ρ_+, and the form of A must again change upon crossing the principal Stokes line from ρ_-; $A(\rho,X) = f_4 + g_4$ above the branch-cut from ρ_- and $A(\rho,X) = f_5 + g_5$ below. The latter solution can be obtained by using the rule in sec. IV B for crossing branch-cuts or by using the solution $A = f_1 - g_1$, valid below the branch-cut from ρ_+, and extending this solution onto the continuation of the Riemann sheet reached from below the branch-cut, going around the pole-zero combination again using the Stokes constant T_1 (never crossing the intrinsic branch-cut along the negative imaginary axis), and finally emerging across and below the branch-cut from ρ_-.

The solution $B(\rho,X)$, shown in Figs. V.8b, 9b, and 10b, is distinguished by demanding the boundary condition that, as $\rho \to -\infty$, $B = f_2 + g_2$ above the branch-cut extending to the left and $B = -f_2 + g_2$ below. In Figs. V.8b and 9b, the first transition point encountered when traveling toward the right is ρ_+, and B changes form upon crossing any of the three principal Stokes lines radiating from ρ_+; $B = f_2 + 2g_2$ above the principal Stokes line extending to the right (and curving around the pole at $\rho = 0$) and $B = -f_2 + 2g_2$ below (but not crossing the principal Stokes line from

the pole). For $\mathrm{Im}\,\rho > 0$, $B = f_2 + 2g_2$ remains valid until one crosses the other (of the two) principal Stokes line of the pole-zero "compound" transition point; then we must change to $B = f_3 + g_3$. In Fig. V.10b, we first encounter the pole-zero "compound" transition point and, for $\mathrm{Im}\,\rho > 0$, $B = f_6 + g_6$ after crossing the principal Stokes line but remaining above the branch-cut from ρ_+; $B = f_9 + g_9$ below this branch-cut, as can be determined by applying the rule of sec. IV B for crossing branch-cuts or by following the solution around ρ_+. The solution again changes form upon crossing any of the three principal Stokes lines radiating from ρ_+; $B = f_7 + g_7$ above the principal Stokes line extending to the right and $B = f_8 + g_8$ below.

Having obtained the solutions A and B, we are now in a position to evaluate the "boundary" coefficient $a(X)$, given by Eq. (I.32), and the Wronskian $W(X)$ and solutions Ψ_1 and Ψ_2, given by Eq. (I.31). We then know the Green's function $G_1(\rho_g,\rho_\ell;X) = \Psi_1(\rho_\ell,X)\Psi_2(\rho_g,X)/W(X)$, from Eq. (I.26), which is the desired integrand for Eq. (I.29). Note that $\rho_\ell = \rho(z_\ell,\omega_1,k_{1\perp})$ and $\rho_g = \rho(z_g,\omega_1,k_{1\perp})$ where z_ℓ and z_g are respectively the lesser and greater of the two positions z and z_s (the source position), and $\sqrt{Q} = \lambda\sqrt{q}\,(d\rho/dz)$.

For the case depicted in Figs. V.8-9 where $\omega_{1R}(z = 0) < \omega_{1R} \leq \omega_R''$ ($\rho_{+R} \lesssim \rho = 0$, $X_R \lesssim 0$, with subscript "R" denoting "real part of"), we find: (1) if ω_1 is below the branch-cut

from $\omega_I(z = 0)$ and, consequently, $\rho(z = 0,\omega_1,\underline{k}_{1\perp})$ is above the branch-cut from ρ_+, then for $\rho(z = 0,\omega_1,\underline{k}_{1\perp}) \leq \rho_\ell \leq \rho_g < \rho_+$ ($0 \leq z_\ell \leq z_g < z_+$; see Eq. (V.4b) for z_+ and z_-) we find $A = (\rho,\rho_+) + i(\rho_+,\rho)$ and $B = i(\rho,\rho_+) + (\rho_+,\rho)$, and (with $d(\rho,\rho_+)/d\rho = i\lambda\sqrt{q}(\rho,\rho_+)$ and $d(\rho_+,\rho)/d\rho = -i\lambda\sqrt{q}(\rho_+,\rho)$) we have

$$a(X) = -1 \qquad \text{(V.11a)}$$

$$W(X) = i\frac{\lambda}{\pi}\frac{d\rho}{dz} \qquad \text{(V.11b)}$$

$$G_1 = -2i\,W^{-1}(\rho_+,\rho_\ell)\left[(\rho_g,\rho_+) + i(\rho_+,\rho_g)\right]; \qquad \text{(V.11c)}$$

(2) if ω_1 is above the branch-cut from $\omega_I(z = 0)$ and, consequently, $\rho(z = 0,\omega_1,\underline{k}_{1\perp})$ is below the branch-cut from ρ_+, then for $\rho(z = 0,\omega_1,\underline{k}_{1\perp}) \leq \rho_\ell \leq \rho_g < \rho_+$ we find $A = (\rho,\rho_+) - i(\rho_+,\rho)$ and $B = -i(\rho,\rho_+) + (\rho_+,\rho)$, and we have

$$a(X) = +1 \qquad \text{(V.12a)}$$

$$W(X) = i\frac{\lambda}{\pi}\frac{d\rho}{dz} \qquad \text{(V.12b)}$$

$$G_1 = -2i\,W^{-1}(\rho_+,\rho_\ell)\left[(\rho_g,\rho_+) - i(\rho_+,\rho_g)\right]. \qquad \text{(V.12c)}$$

There are no eigenvalues (i. e., no poles of G_1) for either case.

For the case depicted in Fig. V.10 where $\omega_R'' < \omega_{1R} < \omega_o$ ($\rho_{+R} > \rho = 0, X_R > 0$) and $\rho(z = 0, \omega_1, \underline{k}_{1\perp})$ is to the left of the principal Stokes line from ρ_-, we find: (1) if ω_1 is below the branch-cut from $\omega_I(z = 0)$ and, consequently, $\rho(z = 0, \omega_1, \underline{k}_{1\perp})$ is above the branch-cut from ρ_-, then for $\rho(z = 0, \omega_1, \underline{k}_{1\perp}) \leq \rho < \rho_- < 0$ ($0 \leq z < z_- < z_\infty$) we find $A = (\rho, \rho_+) + \{i + [\rho_-, \rho_+]^{-2} T_1\} \cdot (\rho_+, \rho)$ and $B = i(\rho, \rho_+) + (\rho_+, \rho)$, while for $\rho_- \lesssim \rho < \rho_+$ ($z_- \lesssim z < z_+$) we find $A = (\rho, \rho_+) + i(\rho_+, \rho)$ and $B = i(\rho, \rho_+) + \{1 - i[\rho_-, \rho_+]^{-2} T_1\}(\rho_+, \rho)$, and we have

$$a(X) = -1 \qquad \text{(V.13a)}$$

$$W(X) = i \frac{\lambda}{\pi} \frac{d\rho}{dz} \left\{ 1 - \frac{i}{2} [\rho_-, \rho_+]^{-2} T_1 \right\} \qquad \text{(V.13b)}$$

$$G_1 = \frac{-2i(\rho_+, \rho_\ell)}{i \frac{\lambda}{\pi} \frac{d\rho}{dz}} \left[(\rho_g, \rho_+) + \left\{ i + [\rho_-, \rho_+]^{-2} T_1 \right\} (\rho_+, \rho_g) \right] \qquad \text{(V.13c)}$$

valid for $\rho(z = 0, \omega_1, \underline{k}_{1\perp}) \leq \rho_\ell \leq \rho_g < \rho_-$ ($0 \leq z_\ell \leq z_g < z_-$), and

$$G_1 = \frac{-2i(\rho_+, \rho_\ell)}{i \frac{\lambda}{\pi} \frac{d\rho}{dz}} \left[(\rho_g, \rho_+) + i(\rho_+, \rho_g) \right] \qquad \text{(V.13d)}$$

valid for $\rho_- \lesssim \rho_g < \rho_+$ and $\rho(z = 0, \omega_1, \underline{k}_{1\perp}) \leq \rho_\ell \leq \rho_g$ ($z_- \lesssim z_g$ and $0 \leq z_\ell \leq z_g$); (2) if ω_1 is above the branch-cut from $\omega_I(z = 0)$ and, consequently, $\rho(z = 0, \omega_1, \underline{k}_{1\perp})$ is below the branch-cut from ρ_-, then for $\rho(z = 0, \omega_1, \underline{k}_{1\perp}) \leq \rho < \rho_- < 0$ ($0 \leq z < z_- < z_\infty$) we find $A = \{1 - i[\rho_-, \rho_+]^{-2} T_1\}(\rho, \rho_+) - i(\rho_+, \rho)$ and $B = -i(\rho, \rho_+) + (\rho_+, \rho)$,

while for $\rho_- \lesssim \rho < \rho_+$ $(z_- \lesssim z < z_+)$ we find $A = (\rho,\rho_+) - i(\rho_+,\rho)$ and $B = -\{i + [\rho_-,\rho_+]^{-2}T_1\}(\rho,\rho_+) + (\rho_+,\rho)$, and we have

$$a(X) = +1/\{1 - i[\rho_-,\rho_+]^{-2}T_1\} \qquad (V.14a)$$

$$W(X) = i\frac{\lambda}{\pi}\frac{d\rho}{dz}\left\{1 - \frac{i}{2}[\rho_-,\rho_+]^{-2}T_1\right\} \qquad (V.14b)$$

$$G_1 = \frac{-2i(\rho_+,\rho_\ell)\left[\{1 - i[\rho_-,\rho_+]^{-2}T_1\}(\rho_g,\rho_+) - i(\rho_+,\rho_g)\right]}{i\frac{\lambda}{\pi}\frac{d\rho}{dz}\left\{1 - i[\rho_-,\rho_+]^{-2}T_1\right\}} \qquad (V.14c)$$

valid for $\rho(z = 0,\omega_1,\underline{k}_{1\perp}) \leq \rho_\ell \leq \rho_g < \rho_-$ $(0 \leq z_\ell \leq z_g < z_-)$,

$$G_1 = \frac{-2i(\rho_+,\rho_\ell)\left[(\rho_g,\rho_+) - i(\rho_+,\rho_g)\right]}{i\frac{\lambda}{\pi}\frac{d\rho}{dz}\left\{1 - i[\rho_-,\rho_+]^{-2}T_1\right\}} \qquad (V.14d)$$

valid for $\rho(z = 0,\omega_1,\underline{k}_{1\perp}) \leq \rho_\ell < \rho_- \lesssim \rho_g < \rho_+$

$(0 \leq z_\ell < z_- \lesssim z_g < z_+)$, and (V.14e)

$$G_1 = \frac{-2i\left[(\rho_+,\rho_\ell) - [\rho_-,\rho_+]^{-2}T_1(\rho_\ell,\rho_+)\right]\left[(\rho_g,\rho_+) - i(\rho_+,\rho_g)\right]}{i\frac{\lambda}{\pi}\frac{d\rho}{dz}\left\{1 - i[\rho_-,\rho_+]^{-2}T_1\right\}}$$

valid for $\rho_- \lesssim \rho_\ell \leq \rho_g < \rho_+$ $(z_- \lesssim z_\ell \leq z_g < z_+)$. There are no eigenvalues (i. e., poles of G_1) for case (1); there are eigenvalues for case (2) when $\{1 - i[\rho_-,\rho_+]^{-2}T_1\} = 0$, and this will be further discussed in sec. V B.

For the case similar to Fig. V.10 but with ω_1 sufficiently large ($\omega_{1R} \gtrsim \omega_o$) that $\rho(z = 0,\omega_1,\underline{k}_{1\perp})$ is to the right of the principal Stokes line from ρ_-, we find: (1) if ω_1 is below the branch-cut from $\omega_I(z = 0)$ and, consequently, $\rho(z = 0,\omega_1,\underline{k}_{1\perp})$ is above the branch-cut (now passing above $\rho = 0$ and on to $\rho \to -\infty$), from ρ_+, then for $\rho_- \lesssim \rho(z = 0,\omega_1,\underline{k}_{1\perp}) \leq \rho_\ell \leq \rho_g < \rho_+$ ($z_- \lesssim 0 \leq z_\ell \leq z_g < z_+$) we find $A = (\rho,\rho_+) + i(\rho_+,\rho)$ and $B = i(\rho,\rho_+) + \{1 - i[\rho_-,\rho_+]^{-2}T_1\}(\rho_+,\rho)$, and we have

$$a(X) = -1 \qquad (V.15a)$$

$$W(X) = i\frac{\lambda}{\pi}\frac{d\rho}{dz}\left\{1 - \frac{i}{2}[\rho_-,\rho_+]^{-2}T_1\right\} \qquad (V.15b)$$

$$G_1 = \frac{-2i(\rho_+,\rho_\ell)}{i\frac{\lambda}{\pi}\frac{d\rho}{dz}}\left[(\rho_g,\rho_+) + i(\rho_+,\rho_g)\right]; \qquad (V.15c)$$

(2) if ω_1 is above the branch-cut from $\omega_I(z = 0)$ and, consequently, $\rho(z = 0,\omega_1,\underline{k}_{1\perp})$ is below the branch-cut from ρ_+, then for $\rho_- \lesssim \rho(z = 0,\omega_1,\underline{k}_{1\perp}) \leq \rho_\ell \leq \rho_g < \rho_+$ we find $A = (\rho,\rho_+) - i(\rho_+,\rho)$ and $B = -\{i + [\rho_-,\rho_+]^{-2}T_1\}(\rho,\rho_+) + (\rho_+,\rho)$, and we have

$$a(X) = +\left\{1 - i[\rho_-,\rho_+]^{-2}T_1\right\} \qquad (V.16a)$$

$$W(X) = i\frac{\lambda}{\pi}\frac{d\rho}{dz}\left\{1 - \frac{i}{2}[\rho_-,\rho_+]^{-2}T_1\right\} \qquad (V.16b)$$

$$G_1 = \frac{-2i(\rho_+,\rho_\ell)}{i\frac{\lambda}{\pi}\frac{d\rho}{dz}}\left[(\rho_g,\rho_+)-i(\rho_+,\rho_g)\right]. \qquad (V.16c)$$

Note that G_1 is identical in Eqs. (V.11c and V.15c) and also in Eqs. (V.12c and V.16c); again there are no eigenvalues for either case.

In sec. V C we will integrate G_1 over ω_1, as indicated in Eq. (I.29); the forms for G_1 found above, although valid only in limited regions of the complex ω_1- and z-planes, are sufficient for our purposes (as outlined in sec. I B). First, however, we will investigate in more detail the eigenvalues due to the poles of G_1.

B. Eigenvalues

1. Threshold

In the previous section, we found poles of G_1 (i. e., eigenvalues) when

$$\left\{1-i\left[\rho_-,\rho_+\right]^{-2}T_1\right\}=0. \qquad (V.17)$$

For the special case where $|k| \gg 1$, $k = -i\lambda/2(2X)^{\frac{1}{2}}$, we showed in sec. IV C that

$$T_1(k) \underset{|k|\to\infty}{\longrightarrow} +i \quad , \qquad (V.18)$$

exactly what one would expect since, for fixed X and $\lambda \to \infty$, the two transition points $\rho_\infty = 0$ and ρ_- can then be treated as "distant" and the Stokes constant for an isolated first order root (e. g., ρ_-) is $+i$. Thus, Eq. (V.17) reduces to

$$[\rho_-, \rho_+] = \pm i = \exp\left[i\frac{\pi}{2}(2N+1)\right] \qquad (V.19)$$

where $N = 0,1,2,\cdots$, and we see that the transition points ρ_- and ρ_+ are connected by an anti-Stokes line (see Figs. V.3a-b, 4b-c, 4d-e, 5e, 5g) the length of which increases as N increases. For $(2N+1)/\lambda \ll 1$, the transition points ρ_- and ρ_+ are centered about $\rho = +i$ with a separation

$$\Delta\rho \equiv \rho_+ - \rho_- \approx 2e^{i\frac{\pi}{8}}\left(\frac{2N+1}{\lambda}\right)^{1/2}, \qquad (V.20)$$

and the eigenvalues, expressed in terms of $X(\omega_\perp, \underline{k}_{\perp\perp})$ (see Eq. (V.2d)), are

$$X_N \approx +i\left[1 - \sqrt{1}\left(\frac{N+\frac{1}{2}}{\lambda}\right)\right]; \qquad (V.21)$$

the eigenmodes fall off exponentially outside this narrow region between ρ_- and ρ_+, so the eigenmode localization width (in the real z space) is

$$(\Delta z)_{real} = \left(\frac{d\rho}{dz}\right)^{-1} (\Delta\rho)_{real} \approx 2Z(2N+1)^{1/2}\lambda^{1/6} \qquad (V.22)$$

using Eq. (V.7). These results (cf. Eqs. (I.13-15)) were first obtained by Liu, Rosenbluth, and White (Ref. F VII; note that our definition of λ, Eq. (V.2b), differs from theirs).

At threshold, Im $\omega_1 \equiv \gamma = 0$ for the fastest growing mode and, from Eq. (V.2d), Im $X = 2\left[\omega_1\nu_1 + (\omega_o - \omega_1)\nu_p\right]$; thus, in the absence of damping we take X to be real and positive (see discussion at beginning of paragraph containing Eq. (V.14)). For $\lambda >> 1$, the eigenvalues X_N start out at $X_o \approx +i$ and come down at a 45^o angle toward the positive X-axis as N increases (see Eq. (V.21)); for $N \gtrsim \lambda$, Eq. (V.21) is invalid, but a numerical evaluation of Eq. (V.17) in sec. V B 2 (as well as an analytic calculation carried out below) indicates that the eigenvalue chain X_N eventually crosses the real axis at some large positive value of X. As λ decreases, X_o comes down from +i and the value of X at crossing (the real axis) decreases. For both of these cases $|X_N| \gtrsim 1$ for all N. Finally, for some $\lambda_o \lesssim 1$, X_o comes all

the way down to the axis, and one might guess $X_o \gtrsim 1$; λ_o is the desired threshold value of the pump strength parameter.

To determine λ_o, we cannot use Eq. (V.19) because for Im X = 0 (see Figs. V.3a, 4a, 5a) $|[\rho_-,\rho_+]| = [\rho_-,0] < 1$; in fact, for $X \gtrsim 1$ we find from sec. IV C that $[\rho_-,0] = e^{-i\pi k} = \exp[-\pi\lambda/2(2X)^{\frac{1}{2}}]$ which is equal to one only if $k = 0$, in violation of the assumption used in obtaining Eqs. (V.18, 19). In order to obtain the value of X at crossing (the real axis) as a function of λ, and in particular to obtain the threshold value of λ and X_o, it is therefore essential to use a Stokes constant T_1 that is valid even when ρ_- and $\rho = 0$ are "near" in the WKBJ sense (either because of large X or small λ); thus, we use T_1 as determined in sec. IV C, and we next consider its value in the limit $|k| \ll 1$.

For the special case where $|k| \ll 1$, we showed in sec. IV C that

(V.23)

$$T_1(k) = -2\pi i k\, e^{2k(1-i\pi)}\, k^{-2k}\,(1-1.2k+\cdots)$$

so that $|T_1| = 2\pi|k| < 1$ (if $|k| \ll 1$) as required if we want $|[\rho_-,\rho_+]^{-2}T_1| = 1$. We must next evaluate $[\rho_-,\rho_+]^{-2}$, but fortunately the phase integral can be evaluated exactly in terms of complete elliptic integrals of the first and second kind, F and E, giving

$$\int_{\rho_-}^{\rho_+} q_b^{1/2}(\rho', X)\, d\rho' = \frac{2}{3}(\rho_+ - \rho_-)^{1/2}\left\{ i\left[(\rho_+ + \rho_-)\, E(\tilde{q}) - \rho_+ F(\tilde{q})\right] + \right.$$

$$\left. + \left[(\rho_+ + \rho_-) E(\tilde{p}) - \rho_- F(\tilde{p})\right]\right\} \qquad \text{(V.24)}$$

where $\tilde{q} \equiv \left[-\rho_-/(\rho_+ - \rho_-)\right]^{\frac{1}{2}}$ and $\tilde{p} \equiv \left[\rho_+/(\rho_+ - \rho_-)\right]^{\frac{1}{2}}$. Expanding the complete elliptic integrals, assuming $X \gtrsim 1$, we find

$$\left[\rho_-, \rho_+\right]^{-2} = \exp\left\{ i\frac{4}{3}\lambda(2X)^{3/2}\left[1 + \right.\right. \qquad \text{(V.25)}$$

$$\left.\left. + \left(\frac{3}{2}\ln(8X) + 1 - \frac{3}{4}\pi i\right)/4X^2 + \cdots\right]\right\}.$$

Using Eqs. (V.23, 25), Eq. (V.17) reduces to

$$1 - 2\left[\frac{\pi\lambda}{2(2X)^{1/2}}\right]\exp\left\{\left[\frac{\pi\lambda}{2(2X)^{1/2}}\right] + i\theta\right\} = 0 \qquad \text{(V.26a)}$$

where

$$\theta = -\frac{\pi}{2} + \frac{4}{3}\lambda(2X)^{3/2} + \qquad \text{(V.26b)}$$

$$+ \frac{1}{3}\frac{\lambda}{(2X)^{1/2}}\left[1 + 6\ln(8X)\right] + \cdots .$$

For Im X = 0, θ is real and the solution to Eq. (V.26) is

$$\frac{\pi\lambda}{2(2X)^{1/2}} = 0.352 \qquad \text{(V.27a)}$$

$$\theta = 2\pi N \ , \qquad \text{(V.27b)}$$

which together determine the value of λ and X_N as each eigenvalue crosses the real X-axis. For N = 0, we find the threshold values

$$X_o \approx 0.8 \qquad \text{(V.28a)}$$

$$\lambda_o \approx 0.3 \ . \qquad \text{(V.28b)}$$

These values are only approximate since Eq. (V.25) is accurate only if $X \gg 1$; nevertheless, they do compare favorably with the results ($X_o = 0.92$, $\lambda_o = 0.32$) obtained in sec. V B 2 by numerically evaluating Eq. (V.17) and with the result (Eq. (I.14) is equivalent to $\lambda_o = 0.34$) obtained by Liu, Rosenbluth, and White (Ref. F VII). Equation (V.27a) gives $X = 9.97\,\lambda^2 \gg 1$ if $\lambda \gtrsim 1$, and using this in Eqs. (V.27b, 26b) results in

$$N \approx 19\,\lambda^4 \qquad (V.29)$$

as the approximate number of eigenmodes with $\mathrm{Im}\, X_N > 0$ ($\mathrm{Im}\, \omega_{1N} = \gamma_N > 0$ in absence of damping) for any λ.

In the next section, we will present the results of the numerical analysis of the eigenvalue equation. In sec. V B 3, we will offer a physical explanation for the threshold behavior of the eigenmodes and for various constraints that must be placed on the eigenvalue equation.

2. Numerical Evaluation

In the previous section, we investigated the eigenvalue equation, Eq. (V.17), analytically under approximations of $|k| \ll 1$ and $|k| \gg 1$ where $k \equiv -i\lambda/2\sqrt{2X}$. In this section, we make no restriction on $|k|$, but rather use the full expression for T_1 (found in sec. IV C) and write Eq. (V.17) as

$$1 + \frac{2\pi}{\alpha\,\Gamma^2(\alpha)}\left(\frac{\alpha}{e}\right)^{2\alpha} e^{\tilde{f}} = 0 \qquad (V.30)$$

where $\tilde{f}(X) \equiv 2i\lambda \int_{\rho_-}^{\rho_+} \left[q(\rho', X)\right]^{\frac{1}{2}} d\rho'$ is determined from Eq. (V.24), $\alpha \equiv -k$, and $\Gamma(\alpha)$ is the gamma function. The solutions, $X_N(\lambda)$, of Eq. (V.30) are obtained numerically and plotted in Fig. V.11 for several values of the pump strength parameter λ.

From Fig. V.11 several interesting results can be obtained. For $\lambda \gtrsim 1$, the solutions X_N for small N (i.e., $2N + 1 \lesssim \lambda$) have $|X_N| \lesssim 1$ and approach the solutions given by Eq. (V.21); this is better illustrated in Fig. V.12a where $X_o(\lambda)$ is plotted for several values of λ. In Fig. V.12a, $X_o(\lambda)$ lies on a line 45^o from horizontal for $\lambda \gtrsim 1$ (as predicted from Eq. (V.21)) and approaches a line 60^o from horizontal for $\lambda \ll 1$ (as can be predicted from Eq. (V.26a, b) with X complex now). The solution $X_o(\lambda)$ crosses the real axis (the threshold condition) at

$$X_o(\lambda_o) = 0.92 \qquad \text{(V.31a)}$$

$$\lambda_o = 0.32 \qquad \text{(V.31b)}$$

as determined from Fig. V.12a, b. Finally, we note from Fig. V.11 that the number of eigenmodes with $\text{Im } X_N > 0$ ($\text{Im } \omega_{1N} = \gamma_N > 0$ in absence of damping) rapidly increases, approximately as $N \approx 19\lambda^4$, as λ increases (for $\lambda \gtrsim 1$), in agreement with Eq. (V.29).

In the previous section and here, we investigated analytically and numerically the eigenvalue equation, Eq. (V.17 or 30), but we found in sec. V A 3 (see paragraph containing Eq. (V.14)) that the eigenvalue equation (and therefore any eigenvalue obtained here) is only valid in a particular region of the complex ω_1-plane: namely for ω_1 satisfying

$$\omega_R'' \equiv \frac{1}{2}\left(\omega_o + \frac{c^2 k_{1\perp}^2}{\omega_o}\right) < \omega_{1R} < \omega_o \qquad (V.32)$$

above the branch-cut from $\omega_I(z = 0)$ in Fig. V.6a. In the next section, we will offer a physical interpretation for the above constraints on ω_1 for the eigenvalues.

3. Physical Meaning of Constraints

In secs. V A 3, B 1, 2, we have found the eigenvalues $X_N(\omega_1, k_{1\perp})$ subject to the constraints on ω_1 given by Eq. (V.32). These constraints have a simple physical interpretation in terms of the relative positions of $z = 0$, z_-, z_∞, and z_+; as indicated in the paragraph containing Eq. (V.14), the constraints are equivalent to

$$0 < (z_-)_R < (z_\infty)_R < (z_+)_R \qquad (V.33)$$

where the subscript "R" denotes "real part of" (sometimes omitted if meaning is clear).

For a frequency $\omega_{1R} > \omega_R'' \equiv (\omega_o + c^2 k_{1\perp}^2/\omega_o)/2$, $0 < z_-(\omega_1) < z_\infty(\omega_1) < z_+(\omega_1)$ and the wave is trapped between the two turning points z_- and z_+ and near the resonance position z_∞ (remember $z_\infty = z_o$ of sec. I A 3), precisely what one would expect

for growing eigenmodes. The turning point z_+ can be identified as the reflection point present even in an unpumped *nonuniform* plasma (sec. III B); if $z_+(\omega_1)$ were less than $z_\infty(\omega_1)$, the wave (of frequency $\omega_{1R} < \omega_R''$ for this case) would reflect before reaching its resonance position and, hence, before growing. For an ω_{1R} slightly greater than ω_R'', the wave is closely trapped about the resonance position and has the largest growth rate. Of course, there must be a constructive interference between the waves reflected from z_- and z_+, and this gives the discreteness of the eigenmodes (see Eq. (V.19)). As ω_{1R} increases (for fixed λ), the spacing between the turning points increases (see Eq. (V.22) where N is increasing) and the wave spends less time at the resonance position, thereby decreasing the growth rate (see Eq. (V.21)).

We are now able to offer a physical interpretation for the threshold behavior of the eignemodes, as we promised to do in sec. I B (question number 3). We fix our attention on the fastest growing eigenmode (N = 0) and note that, as λ decreases, the separation Δz between the two turning points (z_- and z_+) decreases at a rate slightly faster than given by Eq. (V.22) until $\Delta z \approx Z$ at threshold ($\lambda_o \approx 0.32$); and, the eigenmode growth rate $\gamma'_{N=0}$ (see Eq. (I.13) or Eqs. (V.21, 35b)) decreases faster than the uniform plasma growth rate γ_o (defined in Eq. (I.2)) until $\gamma'_{N=0} = 0$ at

threshold (while γ_o is still finite). We conclude that, as the turning points come together for decreasing pump strength λ, the lower turning point becomes less effective in reflecting the waves back toward the resonance position z_∞; also, the separation Δz approaches (or becomes less than) the minimum effective wavelength $Z \equiv \left(\frac{c^2 L_n}{\omega_p^2}\right)^{1/3}$ (from the Airy function) which is insufficient to give the required constructive interference necessary for eigenmodes.

As ω_{1R} increases from ω_R'' (for fixed λ again), the boundary position $\rho_o \equiv \rho(z = 0, \omega_\perp, \underline{k}_{\perp\perp})$ becomes less negative (see Figs. V.7-10) and, for $\omega_{1R} \lesssim \omega_o - \omega_p(Z = 0) \lesssim \omega_o$, ρ_o crosses the principal Stokes line from ρ_-; as pointed out in the paragraph containing Eqs. (V.15,16), for an ω_{1R} equal to or greater than this value there are no eigenvalues. This corresponds essentially to $z_- < 0$ and the lower turning point (derived assuming a strictly linear density gradient) wants to be at a lower density than the uniform region $z < 0$; that is, the turning point z_- and typically even the resonance position z_∞) no longer exists in our system (see Figs. I.9-11 and remember $z_\infty = z_o$), and there is nothing to prevent a wave with $\omega_{1R} \gtrsim \omega_o - \omega_p(z = 0)$ from escaping the resonance region (if indeed it even exists) by refracting out to the uniform region.

Some confusion may arise now because, for $\omega_{1R} \gtrsim \omega_o + \omega_p(z = 0)$, the boundary position ρ_o again crosses one

of the two principal Stokes lines from ρ_-, and $0 < z_- < z_\infty$; however, there are still no eigenvalues. To understand this mathematically we note that, for $\omega_{1R} = \omega_o$, ρ_o is positive real and the intrinsic branch-cut (see secs. IV C, V A 2, 3) from the pole (of $q(\rho,X)$) now lies along the negative ρ-axis. As ω_{1R} increases, ρ_o curves around $\rho = 0$ in a clockwise direction and the intrinsic branch-cut from $\rho = 0$ also rotates in a clockwise direction until it lies along the positive imaginary ρ - axis. For $\omega_{1R} \gtrsim \omega_o + \omega_p(z = 0)$, ρ_o is to the left of the Stokes line extending downward from ρ_- (similar to Fig. V.10 but with the real z-axis below $\rho = 0$), but now the WKBJ solutions must be traced below $\rho = 0$ (rather than above, as in sec. V A 3) using the Stokes constant T_o when crossing the principal Stokes line (see sec. IV C); Eq. (V.17) is not valid for this situation and there are, in fact, no eigenvalues for $\omega_{1R} \lesssim \omega_o - \omega_p(z = 0)$. Physically, we would not expect eigenvalues here since the resonance (that again exists in the plasma for $\omega_{1R} > \omega_o + \omega_p(z = 0)$) now corresponds to $\omega_{1R} \approx \omega_o + \omega_p(z_\infty)$.

To be completely accurate, there is an additional constraint on the eigenvalues which was not explicitly pointed out in the earlier sections. Eq. (V.32) gives the constraint on the real part of a frequency ω_1 lying above the branch-cut from $\omega_I(z = 0)$ in Fig. V.6a; there is also a constraint on the imaginary part of ω_1, in particular an upper and lower bound.

The lower bound can be seen from Fig. V.10 and the definition of $\rho(z = 0, \omega_1, \underline{k}_{1\perp})$ using Eq. (V.1). For $\omega_{1R} \stackrel{<}{\sim} \omega_o - \omega_p(z = 0)$ and $\gamma = \mathrm{Im}\,\omega_1 < -\nu_p$, the boundary position $\rho(z = 0, \omega_1, \underline{k}_{1\perp})$ is below the real ρ-axis and to the left of the principal Stokes line extending downward from ρ_-. Most importantly, the real z-axis passes below $\rho = 0$ and through the intrinsic branch-cut (extending vertically downward from $\rho = 0$, as discussed in secs. IV C, V A 2, 3) onto the continuation of the Riemann sheet reached from the left. After applying the boundary conditions along the real z-axis, we must then trace the WKBJ solutions across the lower-half ρ-plane using ths Stokes constant T_2 (see sec. IV C). Equation (V.17) is not valid for this situation and, in fact, there is no possibility of eigenvalues here. This constraint requires all eigenmodes to grow in time or at least damp no faster than the effectively non-propagating plasma wave (in sec. I C we required $\gamma_o h/V_{gz} \gg 1$; that is, growth dominates convection of the plasma wave out of the resonance zone of width h).

The upper bound can be determined from Green's theorem

$$\int_0^\infty \left[E_1 \frac{d^2}{dz^2} E_1^* - E_1^* \frac{d^2}{dz^2} E_1\right] dz = \left[E_1 \frac{d}{dz} E_1^* - E_1^* \frac{d}{dz} E_1\right]_0^\infty,$$

Eq. (I.25) for $E_1(z, \omega_1, \underline{k}_{1\perp})$, and the boundary conditions in Eqs. (I.27b, 28b) both of which must be satisfied by an eigenmode E_1; together these imply

$$\int_0^\infty |E_1|^2 \, \mathrm{Im}\, Q(z, \omega_1, \underline{k}_{1\perp}) \, dz = -|E_1|^2 \, \mathrm{Re}\sqrt{Q}\Big|_{z=0} < 0. \qquad \text{(V.34)}$$

Far from resonance, $\mathrm{Im}\, Q \to 2\omega_{1R}(\gamma + \nu_1)/c^2$ which is positive if $\gamma > -\nu_1$. Thus, at resonance (where Im Q has a minimum) $\mathrm{Im}\, Q = 2\omega_{1R}(\gamma + \nu_1)/c^2 - D^2/2\omega_p(z = z_\infty)(\gamma + \nu_p)$ must be negative in order to satisfy Eq. (V.34), and this is only possible if $\gamma < \gamma_o$, the uniform plasma growth rate given by Eq. (I.2). Physically, we would expect $\gamma < \gamma_o$ because the wave in a nonuniform plasma does not remain at the point of exact resonance but rather is localized between the two turning points z_- and z_+. The eigenvalues given by Eq. (V.21 or I.13) satisfy this condition since $\gamma'_{N=0}/\gamma_o < 2(\omega_1\omega_p)^{\frac{1}{2}}/\omega_o \leq 1$.

We summarize and conclude our analysis of the eigenvalues by showing, in Fig. V.13, a typical plot of the eigenvalues ω'_{1N} in the complex ω_1-plane (symmetric about the imaginary axis) along with the boundaries representing the constraints discussed in this section. The real and imaginary parts of ω'_{1N} and X_N are related through Eq. (V.2d), which gives (for $\mathrm{Re}(\omega_1) \geq 0$)

$$(\omega'_{1N})_R \approx \frac{\omega_o}{2} + \frac{[2(X_N)_R D + c^2 k_{1\perp}^2]}{2\omega_o} \qquad \text{(V.35a)}$$

$$\gamma'_N \approx -\nu_p + \frac{\left[(X_N)_I D + (\omega'_{1N})_R (\nu_p - \nu_1)\right]}{\omega_o} , \quad \text{(V.35b)}$$

where $D \equiv K v_o \omega_p(z_\infty)(1 - k_{1x}^2/k_1^2)^{\frac{1}{2}}$ (from Eq. (I.25c)) has a slight ω_1-dependence through $\omega_p(z_\infty) \equiv \omega_o - \omega_1$ and $k_1^2(\omega_1) \equiv \equiv \left[\omega_1^2 - \omega_p^2(z_\infty)\right]/c^2$.

In the next section, we will evaluate the Green's function $\underline{G}_1(z_g, z_\ell; t, \underline{k}_{1\perp})$ by performing the integration over ω_1, indicated in Eq. (I.29). As a result, we will be able to determine the amplification experienced by the transient wave-packets and the time at which the eigenmodes first dominate over the wave-packets. We will then be able to answer more clearly and quantitatively the questions raised in sec. I B.

C. Green's Function

We finally come to the calculation that we have been pointing toward since sec. I D: the calculation of the Green's function $\underline{G}_1(z_g, z_\ell; t, \underline{k}_{1\perp})$ from Eq. (I.29). We use the expressions obtained in sec. V A 3 for the integrand $G_1(z_g, z_\ell, \omega_1, \underline{k}_{1\perp})$ and divide the calculation into three parts: (1) a saddle-point evaluation of the integration around the branch-cuts of G_1 in the complex ω_1-plane (see Fig. V.6a and the discussion at the beginning of sec. V A 3); (2) the contribution from the poles of G_1 in the complex ω_1-plane (see Fig. V.13 and sec. V B);

(3) a comparison of the magnitude of these two contributions (wave-packets and eigenmodes) to the asymptotic space-time response.

1. Contribution from Saddle-points

Including the exponential factor $\exp(-i\omega_1 t)$, the integrand in Eq. (I.29) is a rapidly varying function of ω_1 similar to the situation in sec. III. Thus, we again look for saddle-points and, as expected early in sec. V A 3, find them only for ω_1 above the branch-cut extending horizontally from $\omega_1(z = 0)$ in Fig. 6a (or on the continuation below the branch-cut of the Riemann sheet reached from above). Using Eqs. (V.12c, 14c, 14d, 14e, and 16c), we can write the branch-cut contribution to Eq. (I.29) as

$$\underline{G}_{cut} = -\frac{e^{-\nu_1 t}}{2}\int_{cut}\frac{d\omega'}{2\pi}\frac{\underline{I}(z_g, z_\ell, \omega', t)\,\hat{e}_1}{\left[f(z_\ell,\omega')\,f(z_g,\omega')\right]^{1/2}} + c.c. \qquad (V.36)$$

where $\omega' \equiv \omega_1 + i\nu_1$, $\hat{e}_1$ is the polarization from Eq. (I.22) evaluated at the observation position z, $f(z,\omega') \equiv \left[Q(z,\omega' - i\nu_1)\right]^{\frac{1}{2}}$ is an effective wavenumber k_z with $\mathrm{Re}(f) > 0$ above the cut (as indicated in Fig. V.6a), and the phase integrand $\underline{I}$ takes on one of four possible forms:

$$a = \exp\left(i\frac{\pi}{2} + \theta_1\right) \qquad (V.37a)$$

$$b = \exp(\theta_2) \qquad (V.37b)$$

$$a' = \frac{a}{\left\{1 - i\left[\rho_-, \rho_+\right]^{-2} T_1\right\}} \qquad (V.37a')$$

$$b' = \frac{b}{\left\{1 - i\left[\rho_-, \rho_+\right]^{-2} T_1\right\}} \qquad (V.37b')$$

where

$$\theta_1 \equiv -i\omega' t + i\int_{z_\ell}^{z_g} f(z,\omega')\,dz \qquad (V.38a)$$

$$\theta_2 \equiv \theta_1 + 2i\int_{z_g}^{z_+} f(z,\omega')\,dz\,. \qquad (V.38b)$$

We have simplified the phase integrand I by dropping terms that have no saddle-points. The rules, for choosing one of the four possible forms of I, are summarized in the space-time plot drawn in Fig. V.14.

The similarity between Fig. V.14 and the figures in sec. III B is not surprising since early in sec. V A 3 we expected the pump to only modify the saddle-point result obtained in the nonuniform umpumped case. In fact, other than the pump modification in the function $f = \sqrt{Q}$, the only modification (due to the pump) in the form of the result is in the "eigenvalue" denominator that

appears in the "primed" functions a' and b' of Eq. (V.37a', b'). We note from Fig. V.14 that the phase integrand I takes on the form a' or b' only in space-time regions where the corresponding response wave-packets have either traveled through or will travel through their resonance zones (see also Fig. I.10) before exiting the nonuniform plasma region $z \geq 0$. In the remaining regions, where I equals a or b, the corresponding wave-packets have not or will never travel through their resonance zones; the space-time response here (except for possible eigenmodes, as in sec. V C 2) is essentially identical to that found in sec. III B for a nonuniform unpumped plasma and will not be further discussed here. In the remainder of this section, we will determine the saddle-points of the phase integrand I in the regions where I equals a' or b'.

We first evaluate the phase function θ_1 by expanding $f = \sqrt{Q}$ (using Eq.(I.25b)) in powers of the pump strength and keeping only the terms up to order D^2 (we will check the validity of this later in this section):

(V.39)

$$f \approx \left\{1 + \frac{D^2}{2\left[\omega'^2 - \omega^2(z)\right]\left[\omega^2(z) - \omega^2(z_\infty)\right]}\right\} \frac{\left[\omega'^2 - \omega^2(z)\right]^{1/2}}{c},$$

where $\omega^2(z) \equiv \omega_p^2(z) + c^2k_{1\perp}^2$ and $\omega^2(z_\infty) \equiv \left[\omega_o - \omega' - i(\nu_p - \nu_l)\right]^2 + c^2k_{1\perp}^2$. Upon integrating, we find

$$\theta_1 \approx -i\omega' t + \frac{i}{c}\frac{2}{3}\left(\frac{L_n}{\omega_p^2}\right)\left[\left(\omega'^2-\omega_\ell^2\right)^{3/2} - \left(\omega'^2-\omega_g^2\right)^{3/2}\right] + \\ + \frac{i}{2c}\frac{D^2\left(L_n/\omega_p^2\right)}{\left[\omega'^2-\omega^2(z_\infty)\right]^{1/2}} \ln\left[\frac{\tilde{\alpha}(z_g)}{\tilde{\alpha}(z_\ell)}\right] \qquad (V.40a)$$

where

$$\tilde{\alpha}(z) \equiv \frac{\left[\omega'^2-\omega^2(z)\right]^{1/2} - \left[\omega'^2-\omega^2(z_\infty)\right]^{1/2}}{\left[\omega'^2-\omega^2(z)\right]^{1/2} + \left[\omega'^2-\omega^2(z_\infty)\right]^{1/2}}, \qquad (V.40b)$$

$\omega_g^2 \equiv \omega^2(z_g)$, and $\omega_\ell^2 = \omega^2(z_\ell)$. Next, the saddle-point frequency is written as $\omega' = \omega_A + \delta\omega$, where $\delta\omega$ is the modification due to the pump and ω_A is the saddle-point frequency found previously for the nonuniform unpumped plasma (sec. III B). Using this and viewing θ_1 as a function of ω' and D^2, Eq. (V.40) can be put in the convenient form

$$\theta_1(\omega', D^2) \approx \theta_1(\omega_A, 0) + \frac{1}{2}\frac{d^2\theta_1}{d\omega'^2}(\omega_A, 0)(\delta\omega)^2 + \\ + \frac{d\theta_1}{d(D^2)}(\omega', 0)\, D^2 \,, \qquad (V.41a)$$

where

$$\theta_1(\omega_A, 0) = -i\omega_A t + \frac{i}{c}\frac{2}{3}\left(\frac{L_n}{\omega_p^2}\right)\left[(\omega_A^2 - \omega_\ell^2)^{3/2} - \right. \\ \left. -(\omega_A^2 - \omega_g^2)^{3/2}\right] \,, \qquad (V.41b)$$

same as for the nonuniform unpumped plasma (sec. III B),

$$\frac{d^2\theta_1}{d\omega'^2}(\omega_A, 0) = 2\frac{i}{c}\frac{L_n}{\omega_p^2} M_1 \,, \qquad (V.41c)$$

$$\frac{d\theta_1}{d(D^2)}(\omega', 0) = \frac{i}{2c}\left(\frac{L_n}{\omega_p^2}\right)\frac{\ell n\left[\tilde{\alpha}(z_g)/\tilde{\alpha}(z_\ell)\right]}{\left[\omega'^2 - \omega^2(z_\infty)\right]^{1/2}} \,, \qquad (V.41d)$$

$$M_1 \equiv \frac{2\omega_A^2 - \omega_\ell^2}{(\omega_A^2 - \omega_\ell^2)^{1/2}} - \frac{2\omega_A^2 - \omega_g^2}{(\omega_A^2 - \omega_g^2)^{1/2}} \,, \qquad (V.41e)$$

and the coefficient $\frac{d\theta_1}{d\omega}(\omega_A, 0)$, which would appear in the term linear in $\delta\omega$, vanishes by the definition of the saddle-point ω_A (see sec. III B). The form given by Eq. (V.41a) is only valid if $|\omega_A^2 - \omega_g^2| \gg 2\omega_A|\delta\omega|$, a condition also required for the validity of Eq. (V.39); however, this is not too restrictive since the WKBJ

solutions of sec. V A 3 are also invalid near the turning point (see sec. III B, where $\omega_A = \omega_g$ gives the equation of the "line of turning points", also shown in Fig. V.14 as the line $\omega' = \omega_g$).

The saddle-point frequency (for θ_1) is defined (see Ref. sec. U) as the solution to the equation $d\theta_1(\omega', D^2)/d\omega' = 0$, which gives, from Eq. (V.41),

(V.42a)

$$\delta\omega \approx -D^2 \frac{d^2\theta_1}{d\omega' d(D^2)}(\omega', 0) \Big/ \frac{d^2\theta_1}{d\omega'^2}(\omega_A, 0)$$

where

(V.42b)

$$\frac{d^2\theta_1}{d\omega' d(D^2)} = -\frac{i}{c}\left[\omega_o - i(\nu_p - \nu_i)\right]\left(\frac{L_n}{\omega_p^2}\right)\frac{\ln\left[\tilde{\alpha}(z_g)/\tilde{\alpha}(z_\ell)\right]}{2\left[\omega'^2 - \omega^2(z_\infty)\right]^{3/2}} +$$

$$+\frac{i}{c}\frac{\omega'(L_n/\omega_p^2)}{\left[\omega'^2 - \omega^2(z_\infty)\right]}\left[\frac{1}{(\omega'^2 - \omega_\ell^2)^{1/2}} - \frac{1}{(\omega'^2 - \omega_g^2)^{1/2}}\right] +$$

$$+\frac{i}{c}\frac{\left[\omega_o - \omega' - i(\nu_p - \nu_i)\right]}{\left[\omega'^2 - \omega^2(z_\infty)\right]}\left(\frac{L_n}{\omega_p^2}\right)\left\{\frac{(\omega'^2 - \omega_g^2)^{1/2}}{\left[\omega_g^2 - \omega^2(z_\infty)\right]} - \frac{(\omega'^2 - \omega_\ell^2)^{1/2}}{\left[\omega_\ell^2 - \omega^2(z_\infty)\right]}\right\}.$$

This same equation can also be obtained from Eq. (V.38a) by differentiating with respect to ω' and performing the integral of $\frac{df}{d\omega'}$ over z. For $\omega_g^2 < \omega^2(z_\infty)$ or $\omega_\ell^2 > \omega^2(z_\infty)$, Eq. (V.42) gives $\delta\omega$ pure real (if ignore damping) and Eq. (V.41) gives θ_1 pure imaginary; that is, no growth. This is as expected since, for $z_g < z_\infty$ or $z_\ell > z_\infty$, the wave-packet has not yet reached its

resonance zone; and, if $\omega'^2 < \omega^2(z_\infty)$ (essentially same as $z_+ < z_\infty$) the wave-packet will never reach its resonance zone before it refracts out of the plasma. We will therefore concentrate, in the remainder of this section, on the case where interesting growth has occured; in the region a' of Fig. V.14 (where we are dealing with the function θ_1), this requires $\omega_\ell < \omega(z_\infty) < \omega_g < \omega'$.

We will first assume $|\omega^2(z_\infty) - \omega_g^2| \ll |\omega'^2 - \omega_g^2|$ (i. e., z_g is much closer to the resonance position $z_\infty(\omega')$ than to the turning point $z_+(\omega')$) and also $|\omega^2(z_\infty) - \omega_g^2| \ll |\omega^2(z_\infty) - \omega_\ell^2|$ (i. e., $|z_\infty - z_g| \ll |z_\infty - z_\ell|$) so that we can approximate Eq. (V.42b) by keeping only the term proportional to $\ell n\left[\tilde{\alpha}(z_g)/\tilde{\alpha}(z_\ell)\right]$ and the term proportional to $\left[\omega_g^2 - \omega^2(z_\infty)\right]^{-1}$. We also separate out the $\delta\omega$-dependence of $\left[\omega_g^2 - \omega^2(z_\infty)\right]$ by writing $\left[\omega_g^2 - \omega^2(z_\infty)\right] \approx 2(\omega_o - \omega_A)\delta\omega + \omega_g^2 - \omega^2(z_\infty(\omega_A))$, valid for $|\delta\omega| \ll (\omega_o - \omega_A)$, where $z_\infty(\omega_A)$ is the resonance position obtained using the "unpumped" saddle-point frequency ω_A. Eq. (V.42a) can then be written as

$$(\delta\omega+\alpha)(\delta\omega+\beta) \approx \Delta^2 , \qquad (V.43a)$$

where

$$\alpha(\delta\omega) \equiv \frac{(D^2/4)\left[\omega_o - i(\nu_p - \nu_i)\right]\ell n\left[\tilde{\alpha}(z_g)/\tilde{\alpha}(z_\ell)\right]}{\left[\omega_A^2 - \omega^2(z_\infty(\omega_A))\right]^{3/2}(-M_1)} , \qquad (V.43b)$$

$$\beta \equiv \frac{\omega_g^2 - \omega^2(z_\infty(\omega_A))}{2(\omega_o - \omega_A)} \quad , \qquad (V.43c)$$

$$\Delta^2 \equiv \frac{(D^2/4)}{(-M_1)\left[\omega_A^2 - \omega^2(z_\infty(\omega_A))\right]^{1/2}} \quad , \qquad (V.43d)$$

and M_1 is given by Eq. (V.41e). Under the stated assumptions here, $\tilde{\alpha}(z_g)/\tilde{\alpha}(z_\ell) \approx -\left[\omega_g^2 - \omega^2(z_\infty)\right]/4(\omega_A^2 - \omega_g^2)$ and $|\alpha(\delta\omega + \beta)| \ll \Delta^2$.

Of the two solutions to Eq. (V.43), only one satisfies our requirement for growth, $\omega_g > \omega(z_\infty)$ with $z_\infty(\omega')$ evaluated at $\omega' = \omega_A + \delta\omega$. This solution takes three forms: (1) for $z_g < z_\infty(\omega_A)$ and $|\beta| \gg 2\Delta$,

$$\delta\omega = -\beta - \frac{\Delta^2}{\beta} + \cdots \approx -\beta \quad ; \qquad (V.44a)$$

(2) for $|\beta| \ll 2\Delta$ ($z_g \approx z_\infty(\omega_A)$),

$$\delta\omega = \Delta - \frac{\alpha+\beta}{2} + \cdots \approx \Delta \quad ; \qquad (V.44b)$$

(3) for $z_g > z_\infty(\omega_A)$ and $|\beta| \gg 2\Delta$,

$$\delta\omega = \frac{\Delta^2}{\beta} - \alpha + \cdots \approx \frac{\Delta^2}{\beta} \quad . \qquad (V.44c)$$

In all three cases, $\mathrm{Re}(\delta\omega + \beta) > 0$ and $\mathrm{Re}(\delta\omega) > 0$. Using $\beta \approx \omega_p(z_g) - (\omega_o - \omega_A)$, in case (1) $\delta\omega$ increases the saddle-point frequency to $\omega' \approx \omega_o - \omega_p(z_g)$, the frequency of the wave whose resonance position $z_\infty(\omega')$ coincides with z_g. For cases (2) and (3), $\delta\omega$ is small and $\omega' \approx \omega_A$. Before interpreting these results, we will go on to determine the remaining saddle-points connected with θ_1.

Now assuming $|\omega^2(z_\infty) - \omega_\ell^2| \ll |\omega'^2 - \omega_\ell^2|$ and $|\omega^2(z_\infty) - \omega_\ell^2| \ll |\omega^2(z_\infty) - \omega_g^2|$, Eq. (V.42b) can be approximated by keeping only the term proportional to $\ln\left[\tilde{\alpha}(z_g)/\tilde{\alpha}(z_\ell)\right]$ and the term proportional to $\left[\omega^2(z_\infty) - \omega_\ell^2\right]^{-1}$. Writing $\left[\omega_\ell^2 - \omega^2(z_\infty)\right] \approx 2(\omega_o - \omega_A)\delta\omega + \omega_\ell^2 - \omega^2(z_\infty(\omega_A))$, Eq. (V.42a) takes the form

$$(\delta\omega + \alpha)(\delta\omega + \beta') \approx -\Delta^2, \qquad \text{(V.45)}$$

where β' is similar to β but with ω_g^2 replaced by ω_ℓ^2, α and Δ^2 have the same form as in Eq. (V.43), and now $\tilde{\alpha}(z_g)/\tilde{\alpha}(z_\ell) \approx 4(\omega_A^2 - \omega_\ell^2)/\left[\omega_\ell^2 - \omega^2(z_\infty)\right]$ and $|\alpha(\delta\omega + \beta')| \ll \Delta^2$.

Only one solution to Eq. (V.45) can satisfy our requirement for growth, $\omega_\ell < \omega(z_\infty)$ with $z_\infty(\omega')$ evaluated at $\omega' = \omega_A + \delta\omega$, and then only if $z_\ell < z_\infty(\omega_A)$ (i. e., $\mathrm{Re}(\beta') < 0$). The solution takes the forms: (1) for $|\beta'| \gg 2\Delta$,

$$\delta\omega = -\frac{\Delta^2}{\beta'} - \alpha + \cdots \approx -\frac{\Delta^2}{\beta'} \quad ; \qquad (V.46a)$$

(2) for $|\beta'| \ll 2\Delta$ $(z_\ell \approx z_\infty(\omega_A))$,

$$\delta\omega = i\Delta - \frac{\alpha+\beta'}{2} + \cdots \quad . \qquad (V.46b)$$

In both cases, $\mathrm{Re}(\delta\omega + \beta') < 0$ and $\mathrm{Re}(\delta\omega) > 0$ since $z_\ell < z_\infty(\omega_A)$; also, $\delta\omega$ is small so $\omega' \approx \omega_A$.

To interpret the above results (concerning the function θ_1), we look at Figs. (I.10, V.14) and consider a fixed position $z = z_g > z_s = z_\ell$ (recall that z_s is the source position) with time increasing. After passing the light-cone, the saddle-point frequency $\omega' \approx \omega_A$ of the wave-packets decreases until ω' is sufficiently small that the resonance position $z_\infty(\omega')$ has moved in from the left to coincide with z_s (assuming $z_\infty(\omega_s) > z_s$, $\omega_s \equiv \omega(z_s)$). Until now, there has been no growth and the response is essentially identical to that in sec. III B for a nonuniform unpumped plasma. For $z_\infty(\omega') > z_s$, however, the waves from the source have passed through their resonance zones at $z_\infty(\omega')$ and grown (exponentiation factor calculated later in this section) before reaching z_g. For ($|\beta'|$ or $|\beta|$) $\gg 2\Delta$, these wave-packets correspond to $\delta\omega$ given by Eq. (V.46a or 44c) (depending upon

whether z_∞ is closer to z_s or z_g), and $\omega' \approx \omega_A$ still. This is the only solution (corresponding to growth) found in the region $z_\ell = z_s < z_\infty(\omega_A) < z_g$, and it ceases to be valid outside this region. Provided $z_\infty(\omega_s) > z_g$, we eventually reach a time when $z_\infty(\omega_A) = z_g$; for all later times, $z_\infty(\omega_A) > z_g$ (corresponding to crossing the line $z_\infty(\omega') = z_g$ in Fig. V.14) and wave-packets with $\omega' \gtrsim \omega_A$, traveling from the source (at z_s) to the position $z_g > z_s$, cannot pass through their resonance zones at $z_\infty(\omega_A)$ and grow. Equation (V.44c) then ceases to be valid, and we look for a new saddle-point.

As discussed above Eq. (I.3) and in sec. III C and shown in Fig. I.4, for a uniform pumped plasma the resonant ($\omega' = \omega_o - \omega_p$) response is localized in z between the trajectory of the ω' wave-packet in an unpumped plasma and the trajectory of the Langmuir wave (which remains at a fixed position here since we have assumed a cold plasma). Thus, in a nonuniform pumped plasma we expect a Langmuir wave disturbance to remain at the resonance position $z_\infty(\omega') = z_g$ where $\omega' = \omega_o - \omega_p(z_g)$ and to continue stimulating electromagnetic waves of this frequency (observed here at $z_g > z_s$) even at later times such that $\omega_A(z_g, t) < \omega' = \omega_o - \omega_p(z_g)$ and $z_\infty(\omega_A) > z_g$. This corresponds to the $\delta\omega$ given by Eq. (V.44a). Since $z_\infty(\omega') < z_g$ for this saddle-point, provided $z_\infty(\omega_A) > z_g$ ($\mathrm{Re}(\beta) < 0$), we never cross the line

$z_\infty(\omega') = z_g$ indicated in Fig. (V.14); also, we never cross the line $\omega' = \omega_g$ (line of turning points) since $\omega' = \omega_o - \omega_p(z_g)$ is fixed for all time (provided $z_\infty(\omega_A) > z_g$) and we earlier (below Eq. (V.41)) restricted ourselves to $\omega' > \omega_g$ (i. e., not too close to the turning point for waves with frequency ω'). Thus, for this saddle-point (given by Eq. (V.44a)) the lines drawn in Fig. V.14 are not accurately placed (they were drawn assuming $\omega' \gtrsim \omega_A$, as in Eqs. (V.44c or 46a)); instead, the line segment $z_\infty(\omega') = z_g$ should essentially be moved vertically upward to infinity with our above saddle-point (and region a') valid for all times above the line $z_\infty(\omega_A) = z_g$.

We now shift to the other side of the source and consider a fixed position $z = z_\ell < z_s = z_g$, again with time increasing. After passing the light-cone, the saddle-point frequency $\omega' \gtrsim \omega_A$ of the wave-packets decreases until ω' is sufficiently small that the resonance position $z_\infty(\omega')$ has moved in from the left to coincide with z_ℓ (assuming $z_\infty(\omega_s) > z_\ell$). For $z_\infty(\omega') < z_\ell$, the response is the same as found in sec. III B for a nonuniform unpumped plasma; for $z_\infty(\omega') > z_\ell$, the waves from the source have passed through their resonance zone at $z_\infty(\omega')$ and grown before reaching z_ℓ. For ($|\beta'|$ or $|\beta|$) $\gg 2\Delta$, these wave-packets correspond to $\delta\omega$ given by Eq. (V.46a or 44c) (depending upon whether z_∞ is closer to z_ℓ or z_s), and $\omega' \gtrsim \omega_A$ still.

This is the only solution (corresponding to growth) found in the region $z_\ell < z_\infty(\omega_A) < z_s = z_g$ (and it ceases to be valid outside this region). Finally, at still later times ω_A decreases until $z_\infty(\omega_A) > z_s = z_g$ (assuming $z_\infty(\omega_s) > z_s$) prohibiting wave-packets of this frequency (or lower) from growing as they travel from z_s to z_ℓ, and the saddle-point given by Eq. (V.44c) ceases to be valid. However, the saddle-point given by $\omega' \approx \omega_o - \omega_p(z_g)$, from Eq. (V.44a), now becomes valid. This is similar to our results for $z_\ell = z_s < z_g$.

For all of the saddle-points we have found in connection with θ_1, $(\delta\omega)^2$ is either negligibly small or real so that the exponentiation factor $\Gamma_1 \equiv \mathrm{Re}(\theta_1)$ is given only by the real part of the last term in Eq. (V.41a). Since in all cases where growth has occurred, $z_\ell < z_\infty(\omega') < z_g$ and $\tilde{\alpha}(z_g)/\tilde{\alpha}(z_\ell)$ is essentially real and negative (in general, the complex argument of $\tilde{\alpha}(z_g)/\tilde{\alpha}(z_\ell)$ changes from 0 to $-\pi$ as the wave-packet crosses the resonance zone), we have $\mathrm{Im}\,\ell n\left[\tilde{\alpha}(z_g)/\tilde{\alpha}(z_\ell)\right] = -\pi$ and from Eq. (V.41)

$$\Gamma_1 = \frac{\pi}{2}\left(\frac{L_n}{\omega_p^2}\right)\left(\frac{D^2}{c}\right)\Big/\left[\omega'^2 - \omega^2(z_\infty)\right]^{1/2} . \qquad (V.47)$$

At the resonance position $z_\infty(\omega')$, ω' is the actual wave-packet frequency while $\omega(z_\infty)$ is the frequency of a wave whose turning point (essentially $z_+(\omega')$) lies at $z_\infty(\omega')$; thus,

$\left[\omega'^2 - \omega^2(z_\infty)\right]^{\frac{1}{2}} = c\, k_z(z_\infty)$, the effective z-wavevector measured at z_∞. Therefore, Eq. (V.47) gives exactly the same exponentiation factor as given by Eqs. (I.7,8) with $V_{2z} = 0$ (the result obtained by Rosenbluth, White, and Liu in Ref. F VI) and as given by one-half the energy exponentiation factor Γ_B of Ref. G I. Equation (V.47) is valid only for back- or oblique-scattered waves since our approximations break down near the turning point where $k_z \to 0$.

All of the above results, starting with Eq. (V.40), were based on the approximation given by Eq. (V.39) which breaks down if $\omega'^2 - \omega^2(z) \to 0$ (i. e., essentially if z approaches the turning point $z_+(\omega')$) or $\omega^2(z_\infty) - \omega^2(z) \to 0$ (i. e., essentially if z approaches the resonance position $z_\infty(\omega')$). Provided $|\omega_A^2 - \omega_g^2| \gg 2\omega_A|\delta\omega|$, the saddle-points given by Eqs. (V.44b, c or 46a,b) (depending upon whether z_∞ is closer to z_g or z_ℓ, respectively) satisfy Eq. (V.39). For the saddle-point given by Eq. (V.44a), the term proportional to D^2 in Eq. (V.39) remains a small correction only if $|z_\infty(\omega_A) - z_g| \ll |z_+(\omega_A) - z_g|$.

However, it is not necessary to impose the approximation of Eq. (V.39) since the phase integral function θ_1 (and also θ_2) can be written exactly in terms of elliptic integrals. We find

$$\theta_1 = -i\omega' t + i\frac{2}{3}\lambda(\rho_+ - \rho_-)^{1/2}(\rho_+ + \rho_-)\times$$

$$\times\left\{\left[E(\Psi_\ell,\tilde{p}) - E(\varphi_g,\tilde{p})\right] - \frac{\rho_-}{\rho_+ + \rho_-}\left[F(\Psi_\ell,\tilde{p}) - F(\varphi_g,\tilde{p})\right] + \right.$$

$$\left. + i\left[E(\tilde{q}) - \frac{\rho_+}{\rho_+ + \rho_-}F(\tilde{q})\right]\right\} + \qquad \text{(V.48a)}$$

$$+ i\frac{2}{3}\lambda^{2/3}Z(\rho_+ + \rho_-)\left[\eta_\ell f(z_\ell) - \sigma_g f(z_g)\right]$$

where

$$\eta_\ell \equiv \frac{\rho_+ + \rho_- - \rho_\ell}{\rho_+ + \rho_-} - \frac{\rho_+}{\rho_+ - \rho_\ell}\,, \qquad \text{(V.48b)}$$

$$\sigma_g \equiv \frac{(\rho_+ + 2\rho_- - \rho_g)\,\rho_g}{(\rho_+ + \rho_-)(\rho_g - \rho_-)} - \frac{\rho_g}{\rho_g - \rho_-}\,, \qquad \text{(V.48c)}$$

$$\Psi_\ell \equiv \arcsin\left(\frac{\rho_+ - \rho_-}{\rho_+ - \rho_\ell}\right)^{1/2}, \qquad \text{(V.48d)}$$

$$\varphi_g \equiv \arcsin\left(\frac{\rho_+ - \rho_g}{\rho_+}\right)^{1/2}, \qquad \text{(V.48e)}$$

$$\tilde{p} \equiv \left(\frac{\rho_+}{\rho_+ - \rho_-}\right)^{1/2}, \qquad (V.48f)$$

$$\tilde{q} \equiv \left(\frac{-\rho_-}{\rho_+ - \rho_-}\right)^{1/2}, \qquad (V.48g)$$

F and E are elliptic integrals of the first and second kind, respectively, and $F(\tilde{q}) \equiv F(\pi/2, \tilde{q})$ and $E(\tilde{q}) \equiv E(\pi/2, \tilde{q})$ are the corresponding complete elliptic integrals. We have previously defined the quantities λ (see Eq. (V.2b)), Z (see Eq. (I.10a)), $f(z) = \sqrt{Q}$ (see above Eqs. (V.37 and 39)), the turning points ρ_+ and ρ_- (see Eqs. (V.2e, f)), and $\rho_g \equiv \rho(z_g)$ and $\rho_\ell \equiv \rho(z_\ell)$ (from Eq. (V.1)). Equation (V.48) can be put in many forms using the various elliptic integral transformations, but the form shown is convenient for expanding in powers of the pump strength parameter D^2 (similar to what was done in Eq. (V.39), but now after the integration in Eq. (V.38a) rather than before).

Viewing the pump as modifying the saddle-point of the unpumped nonuniform plasma (sec. III B), we expand the elliptic integrals and the other terms (except for $f(z_\ell)$ and $f(z_g)$) in Eq. (V.48) in the limit of $|\tilde{q}| \ll 1$ and $|\rho_-| \ll 1$ (equivalent to small D^2 and $|X| \gg 1$ in Eq. (V.2d)) and find

$$\theta_1 \approx -i\omega' t + \frac{i}{c}\frac{2}{3}\left(\frac{L_n}{\omega_p^2}\right)\left[c^3 f(z_\ell) - c^3 f(z_g)\right] +$$

$$+ \frac{i}{c} D^2 \left(\frac{L_n}{\omega_p^2}\right)\left\{ \frac{c f(z_g)}{\left[\omega_g^2 - \omega^2(z_\infty)\right]} - \frac{c f(z_\ell)}{\left[\omega_\ell^2 - \omega^2(z_\infty)\right]} \right\} +$$

$$+ \frac{i}{c} D^2 \left(\frac{L_n}{\omega_p^2}\right) \frac{\ell n(\tilde{a})}{\left[\omega'^2 - \omega^2(z_\infty)\right]^{1/2}} + \Gamma_1 , \qquad \text{(V.49a)}$$

where

(V.49b)

$$\tilde{a} \equiv \frac{\left[\omega'^2 - \omega^2(z_\infty)\right]^{1/2} + \left[\omega'^2 - \omega_\ell^2\right]^{1/2}}{\left[\omega'^2 - \omega^2(z_\infty)\right]^{1/2} + \left[\omega'^2 - \omega_g^2\right]^{1/2}} \cdot \frac{\left[\omega_g^2 - \omega^2(z_\infty)\right]^{1/2}}{\left[\omega^2(z_\infty) - \omega_\ell^2\right]^{1/2}} ,$$

and Γ_1 is given by Eq. (V.47). In writing down Eq. (V.49), we have assumed $z_\ell \leq z_\infty(\omega') \leq z_g \leq z_+(\omega')$, which explains the appearance of the exponentiation factor Γ_1. Equation (V.49) agrees very well with Eq. (V.40), if $f(z)$ is approximated by Eq. (V.39), and is valid even when Eq. (V.39) cannot be used; this further justifies our earlier results of Eqs. (V.40 - 47), but, more importantly, Eq. (V.49) can be used in an essential part of our

next (and most interesting) calculation: the phase function θ_2 and the side-scatter exponentiation factor.

We now concentrate on the region b' of Fig. V.14, where the wave-packets have already reached their turning point $z_+(\omega')$ and are in the process of refracting toward lower densities. We assume $z_\ell \leq z_g < z_\infty(\omega') \leq z_+(\omega')$ so that the wave-packets have once again (and for the final time) traveled through their resonance zone at $z_\infty(\omega')$ and grown (see Fig. I.10, but with $z_\infty(\omega') > z_s$). From the definition of θ_2, by Eq. (V.38b), we see that we must evaluate the integral $\int f(z,\omega')dz$ between the end-points z_g and $z_+(\omega')$, where $f(z_+,\omega') = 0$; therefore, the approximation given by Eq. (V.39) cannot be used for this integral. However, we can use Eq. (V.49) (without the $-i\omega' t$ term) if we replace z_ℓ by z_g and z_g by z_+ in that equation. For θ_2, we also need the integral $\int f(z,\omega')dz$ between the end-points z_ℓ and z_g, and for this we can use Eq. (V.40), with $z_\ell \leq z_g < z_\infty(\omega') \leq \leq z_+(\omega')$, and expand assuming $|z_+ - z_\infty| \ll |z_+ - z_g|$ (i. e., $|\omega'^2 - \omega^2(z_\infty)| \ll |\omega'^2 - \omega_g^2| \leq |\omega'^2 - \omega_\ell^2|$). Adding the two integrals together gives

$$\theta_2 \approx -i\omega' t + \frac{i}{c}\frac{2}{3}\left(\frac{L_n}{\omega_p^2}\right)\left[\left(\omega'^2-\omega_\ell^2\right)^{3/2}+\left(\omega'^2-\omega_g^2\right)^{3/2}\right]+$$

$$+\frac{i}{c}D^2\left(\frac{L_n}{\omega_p^2}\right)\frac{1}{\left[\omega^2(z_\infty)-\omega_g^2\right]^{1/2}}+2\Gamma_1\,, \qquad (V.50)$$

where $\Gamma_1(\omega')$ is given by Eq. (V.47). Note that this reduces to the correct unpumped nonuniform plasma result (sec. III B) in the limit $D^2 \to 0$.

Writing the saddle-point as $\omega' = \omega_A + \delta\omega$ ($|\omega_A^2 - \omega_g^2| >> 2\omega_A|\delta\omega|$), as we did earlier in this section, θ_2 can be put in a form similar to what was done in Eq. (V.41) for θ_1, and the saddle-point (from $d\theta_2(\omega', D^2)/d\omega' = 0$) can be put in a form analogous to Eq. (V.42). We are mainly interested in the exponentiation factor $\Gamma_2 \equiv \mathrm{Re}\,(\theta_2)$, and we find

$$\Gamma_2 = \mathrm{Re}\left[2\Gamma_1 + \frac{i}{c}\left(\frac{L_n}{\omega_p^2}\right)M_2\,(\delta\omega)^2\right] \qquad (V.51a)$$

$$M_2 \equiv \frac{2\omega_A^2-\omega_\ell^2}{\left(\omega_A^2-\omega_\ell^2\right)^{1/2}} + \frac{2\omega_A^2-\omega_g^2}{\left(\omega_A^2-\omega_g^2\right)^{1/2}}\,, \qquad (V.51b)$$

with the complex saddle-point frequency $\omega' = \omega_A + \delta\omega$ determined from the equation

$$\delta\omega \approx -i\frac{\pi}{2}\frac{\omega_o}{M_2}\frac{D^2}{\left[\omega'^2-\omega^2(z_\infty)\right]^{3/2}}\,, \qquad (V.52)$$

where $\omega'^2 - \omega^2(z_\infty) \approx 2\omega_o\,\delta\omega + \omega_A^2 - \omega^2(z_\infty(\omega_A))$.

There are five solutions to Eq. (V.52), three of which (with $\mathrm{Re}(\delta\omega) < 0$) have $\mathrm{Re}\left[\omega'^2 - \omega^2(z_\infty)\right] < 0$ (i. e., essentially $z_\infty > z_+$), contrary to our assumption used in obtaining Eq. (V.50). Of the remaining two solutions (with $\mathrm{Re}(\delta\omega) > 0$), one solution (with $\mathrm{Im}(\delta\omega) > 0$) has $\Gamma_2 < 0$ and corresponds to an exponentially small contribution to Eq. (V.36). The remaining solution (with $\mathrm{Re}(\delta\omega) > 0$ and $\mathrm{Im}(\delta\omega) < 0$) has $\Gamma_2 > 0$, and we have two simple limiting forms: (1) for $\omega_A^2 - \omega^2(z_\infty(\omega_A)) >> 2\omega_0|\delta\omega|$, $\delta\omega$ is given by Eq. (V.52) with $\omega'^2 - \omega^2(z_\infty)$ replaced by $\omega_A^2 - \omega^2(z_\infty(\omega_A))$ on the right-hand-side, and $\Gamma_2 = 2\Gamma_1$ (a straight-forward extension of our previous back-and oblique-scatter results); (2) for $\omega_A^2 - \omega^2(z_\infty(\omega_A)) << 2\omega_0|\delta\omega|$, $\delta\omega$ increases to the value

$$\delta\omega \approx e^{-i\frac{\pi}{5}} D^{\frac{4}{5}} \left(\frac{\pi}{4}\right)^{\frac{2}{5}} (2\omega_0)^{-\frac{1}{5}} M_2^{-\frac{2}{5}}, \qquad (V.53a)$$

where M_2 is defined in Eq. (V.51b), and Γ_2 increases to the value

$$\Gamma_2 = \frac{5}{4}\pi^{\frac{4}{5}} \cos\left(\frac{\pi}{10}\right) M_2^{\frac{1}{5}} \left(\frac{L_n}{\omega_p^2}\right) \frac{D^{\frac{8}{5}}}{c\omega_0^{\frac{3}{5}}} . \qquad (V.53b)$$

Case (2), where $z_\infty(\omega') \approx z_+(\omega')$ and $\omega' \approx \omega_A$, corresponds to side-scatter since the resonance zone and turning point coincide, and Eq. (V.53b) gives the side-scatter exponentiation factor. In

sec. V C 3, we will return to a discussion of Eq. (V.53b), which depends weakly on the observation position $z = z_g$ through the function M_2.

Having found the phase integrand I and the saddle-point $\omega' = \omega_A + \delta\omega$ in the regions a' and b' of Fig. V.14, we approximate $\underline{G}_{cut}$ from Eq. (V.36) by expanding I about the saddle-point and evaluating $\hat{e}_1$, $f(z_\ell,\omega')$, $f(z_g,\omega')$, and $\{1 - i[\rho_-,\rho_+]^{-2}T_1\}$ at the saddle-point. This gives (see Ref. sec. U), for region a',

$$\underline{G}_{cut} \approx -\frac{\hat{e}_1}{2}\left[f(z_\ell,\omega')f(z_g,\omega')\right]^{-1/2} \times$$

$$\times\left[-2\pi\frac{d^2\theta_1}{d\omega'^2}(\omega',D^2)\right]^{-1/2}\left\{1-i[\rho_-,\rho_+]^{-2}T_1\right\}^{-1} \times$$

$$\times \exp\left(i\frac{\pi}{2} + \theta_1 - \nu_1 t\right) + c.c. \qquad (V.54)$$

and, for region b', a similar form but with θ_1 replaced by θ_2 everywhere and the term $i\pi/2$ dropped from the exponent.

The term $d^2\theta_1/d\omega'^2$ can be replaced by its unpumped ($D^2 \to 0$) value, given by Eq. (V.41c), for the saddle-point given by Eqs. (V.44c or 46a). However, as the observation position approaches the resonance position, $z_\infty(\omega_A)$, and the saddle-point takes on the form given by Eqs. (V.44b or 46b), $d^2\theta_1/d\omega'^2$ becomes <u>twice</u> its unpumped value; this corresponds to the group velocity

decreasing to half its unpumped value when the wave-packet is traveling through its resonance zone (as discussed below Eq. (I.4) and in sec. III c and shown in Fig. I.4, with $\underline{V}_2 = 0$ here). For the saddle-point given by Eq. (V.44a), $d^2\theta_1/d\omega'^2$ increases to β^2/Δ^2 times its unpumped value, thereby decreasing the contribution of this saddle-point to Eq. (V.54).

The term $d^2\theta_2/d\omega'^2$, used in Eq. (V.54) when we are considering region b' of Fig. V.14, can be replaced by its unpumped value

$$\frac{d^2\theta_2}{d\omega'^2}(\omega_A,0) = 2\frac{i}{c}\left(\frac{L_n}{\omega_p^2}\right)M_2 \qquad (V.55)$$

when the saddle-point is given by the limiting form (1), valid for $\omega_A^2 - \omega^2(z_\infty(\omega_A)) \gg 2\omega_o|\delta\omega|$ and discussed above Eq. (V.53a). However, as the resonance position $z_\infty(\omega_A)$ approaches the turning point $z_+(\omega_A)$, and the saddle-point takes on form (2) given by Eq. (V.53a), $d^2\theta_2/d\omega'^2$ becomes 5/2 times its unpumped value. The factor 5/2 has no apparent significance and does not seem to correspond to any change in the wave-packet group velocity since Eq. (V.53a) is valid along the entire z-t trajectory (for $t \gtrsim t_s$) defined by ω_A = constant and $z_\infty(\omega_A) = z_+(\omega_A)$ and shown as line "a" in Fig. I.10; along this trajectory, the group velocity must be the same as in the unpumped case.

In the next section, we will determine the contribution of the poles (i. e., eigenmodes) to Eq. (I.29). Finally, in sec. V C 3 we will compare the magnitude of our two contributions to $\underline{G}_1$.

2. Contribution from Poles

We remind the reader that we are in the process of calculating the Green's function $\underline{G}_1(z_g, z_\ell; t, \underline{k}_{1\perp})$, from Eq. (I.29), using the integrand $G_1(z_g, z_\ell, \omega_1, \underline{k}_{1\perp})$ obtained in sec. V A 3. In the previous section, we determined the contribution from the branch-cuts of G_1. In this section, we will calculate the contribution from the poles of G_1 in the complex ω_1-plane (see Fig. V.13, sec. V B, and Eq. (V.32) for the position of the eigenvalues ω'_{1N}).

This contribution, $\underline{G}_{poles}$, can be written in the same form as Eq. (V.36), where the integration is now around the poles of $I(z_g, z_\ell, \omega', t) = \tilde{I}/\{1 - i[\rho_-, \rho_+]^{-2} T_1\}$ with $\tilde{I}$ given by one of three possible forms: (1) for $z_\ell \leq z_g \lesssim z_-(\omega') < z_+(\omega')$,

$$\tilde{I} = \exp(\theta_2) \quad ; \qquad \text{(V.56a)}$$

(2) for $z_\ell \lesssim z_-(\omega') \lesssim z_g < z_+(\omega')$,

$$\tilde{I} = \exp\left(i\frac{\pi}{2} + \theta_1\right) + \exp(\theta_2) \quad ; \qquad \text{(V.56b)}$$

(3) for $z_-(\omega') \lesssim z_\ell \leq z_g < z_+(\omega')$,

$$\tilde{I} = \exp\left(i\frac{\pi}{2} + \theta_1\right) + \exp(\theta_2) + \\ + \exp\left(i\frac{\pi}{2} + \theta_3\right) - \exp(\theta_4) . \qquad (V.56c)$$

The functions θ_1 and θ_2 are defined in Eqs. (V.38 a, b), while θ_3 and θ_4 are similarly defined by

$$\theta_3 \equiv -i\omega' t - i\int_{z_\ell}^{z_g} f(z,\omega')\,dz \qquad (V.57a)$$

$$\theta_4 \equiv \theta_3 - 2i\int_{z_g}^{z_+} f(z,\omega')\,dz \ . \qquad (V.57b)$$

From the residue at the poles, we obtain (V.58a)

$$G_{\text{poles}} = \frac{i}{2} e^{-\nu_1 t} \sum_N \frac{\hat{e}_1(\omega'_{1N})}{Y_N} \frac{\tilde{I}(z_g, z_\ell, \omega'_{1N}, t)}{\left[f(z_\ell,\omega'_{1N}) f(z_g,\omega'_{1N})\right]^{1/2}} + \text{c.c.}$$

$$Y_N \equiv \frac{d}{d\omega'}\left\{1 - i\left[\rho_-,\rho_+\right]^{-2} T_1\right\}\Big|_{\omega'_{1N}} , \qquad (V.58b)$$

where the summation is over all the eigenvalues ω'_{1N}. We will next determine the derivative term Y_N that appears in Eq. (V.58).

We obtain an approximate form for Y_N by ignoring the slow ω'-dependence of the Stokes constant T_1 and writing

$$Y_N \approx -2i \int_{z_-}^{z_+} \frac{df}{d\omega'} dz \ , \qquad (V.59)$$

where we have used the eigenvalue equation, Eq. (V.17), and $f(z_-,\omega') = 0$ and $f(z_+,\omega') = 0$. The phase integral in Eq. (V.59) can be evaluated exactly in terms of elliptic integrals, similar to Eq. (V.24), giving

$$Y_N \approx -4i\lambda \frac{dX}{d\omega'} (\rho_+ - \rho_-)^{1/2} \times \qquad (V.60)$$

$$\times \left\{ i\left[E(\tilde{q}) - \tilde{p}^2 F(\tilde{q})\right] + \left[E(\tilde{p}) - \tilde{q}^2 F(\tilde{p})\right] \right\} ,$$

where $\tilde{q}$ and $\tilde{p}$ are defined in Eqs. (V.24 and 48), and λ and X are defined in Eq. (V.2). In the limit of $|\tilde{q}| \ll 1$ and $|\rho_-| \ll 1$ (equivalent to small pump strength parameter D^2, and $|X| \gg 1$ in Eq. (V.2d)), Eq. (V.60) reduces to

$$Y_N \approx -4i (2X)^{1/2} \left(\frac{Z}{c}\right)^2 \lambda^{1/3} \left[\omega_o - i(\nu_p - \nu_1)\right] \qquad (V.61)$$

with $Z \equiv (c^2 L_n/\omega_p^2)^{1/3}$; in the opposite limit of $\rho_- \approx \rho_+ \approx X \approx +i$ and $\lambda \gtrsim 1$ (i. e., far above the threshold found in sec. V B 1),

we find the same form as Eq. (V.61) but with the replacements $X \to +i$ and $4\sqrt{2} \to 2\pi$. This latter result is most easily obtained by using $\rho \approx \rho_- \approx \rho_+ \approx +i$ to simplify $f = \lambda\sqrt{q}$ (see Eq. (V.2c)) and taking the ω'-derivative of the approximation

$$-2i\int_{z_-}^{z_+} f\,dz \approx -\sqrt{i}\,\pi\lambda\,(1+X^2)\,.$$

The physical interpretation of the three forms of $\tilde{I}$ is as follows: form (1), Eq. (V.60a), consists of a single left-going (toward decreasing density) wave for all $z \lesssim z_-(\omega'_{1N})$ since the source is to the left of the resonance region, $z_s \lesssim z_-(\omega'_{1N})$, while all growing waves must come from the region $z_-(\omega'_{1N}) \lesssim z < z_+(\omega'_{1N})$ and be outgoing to the left of the lower turning-point z_- (the left-and right-going waves, corresponding to θ_1 and emitted directly from z_s, are ignored here since they will never or have not yet reached the resonance region and grown); form (2), Eq. (V.56b), consists of a right-going wave (θ_1) reflected from the turning-point z_- and a left-going wave (θ_2) reflected from the turning-point z_+, for the case $z_s \lesssim z_- \lesssim z < z_+$ (i. e., the waves from the source have entered the resonance region and are at least partially trapped between the two turning points), and it consists of two left-going waves (θ_1 directly from the source z_s and θ_2 reflected from z_+), for the case

$z \lesssim z_- \lesssim z_s < z_+$ (i. e., all waves which escape past the turning point z_- must be out-going in the region $z \lesssim z_-$); form (3), Eq. (V.56c), consists of left- and right-going waves (θ_1) emitted from z_s, a left-going wave (θ_2) corresponding to the reflection of θ_1 at the turning-point z_+, a right-going wave (θ_4) corresponding to the reflection of θ_1 at the turning-point z_-, and right- and left-going waves (θ_3) corresponding to the reflection of θ_2 and θ_4 at z_- and z_+, respectively. Note that all of the above waves, observed at a fixed position z, grow exponentially in time at the rate γ_N' of Eq. (V.35b) (including the above waves directly emitted from the source position z_s, provided z_s lies within the resonance region $z_- \lesssim z_s < z_+$ where the responding density perturbation is also exponentially growing).

3. Comparison

In comparing the magnitudes of Eqs. (V.54 and 58a), we first consider the coefficients in front of the exponentials. Using Eqs. (V.41 c, e or 55 and 51b) and Eq. (V.39) with $D^2 \to 0$ (valid since we required $|\omega_A^2 - \omega_g^2| >> 2\omega_A|\delta\omega| \approx c^2\lambda^{2/3}/z^2 = D$ in obtaining Eq. (V.53a); see also discussion after Eq. (V.41)), the coefficient in front of the exponential in Eq. (V.54), for region b', becomes approximately

$$\left|G_{cut}\right| \Big/ \left|\exp(\theta_2 - \nu_1 t)\right| \approx \frac{c}{2}(\pi\xi)^{-1/2}\left[\frac{\omega(z_s)}{c f_{max}}\right]^{1/2}, \qquad (V.62)$$

where we have ignored the term $\{1 - i\rho_-,\rho_+|^{-2}T_1\}$, $f_{max} \equiv \max\left[f(z_g,\omega'_{1N}),\ f(z_\ell,\omega'_{1N})\right]$, and $\xi \equiv (L_n/\omega_p^2)\omega^3(z_s)/c \gg 1$ is the large parameter required in a nonuniform plasma in order to use the geometrical optics description of the wave-packets far from their turning points (see sec. III B). Using Eq. (V.61), the coefficient in front of the exponential in Eq. (V.58a) becomes approximately

$$\left|G_{poles}\right| \Big/ \left|\tilde{I}\exp(-\nu_1 t)\right| \approx \frac{c}{2\pi\xi}\left|X_N\right|^{-1/2}\left[\frac{\omega(z_s)}{\omega_o}\right] \times$$

$$\times\left[\frac{\omega(z_s)}{\sqrt{D}}\right]\left|\frac{\omega^2(z_s)}{c^2 f(z_\ell,\omega'_{1N}) f(z_g,\omega'_{1N})}\right|^{1/2}. \qquad (V.63)$$

In order to use the WKB (or phase integral) approximation, however, the phase integral must satisfy $\left|\lambda \int_\rho^T \sqrt{q}\, d\rho\right| \gtrsim 1$ where $T = \rho_+$ or ρ_-. Otherwise, we must write the solution to Eq. (V.2a) near the turning points in terms of the two Airy functions (cf. sec. III B). For the wave-packets, where ρ_+ and ρ_- are not exceptionally close, the above condition gives $|T - \rho| \gtrsim \lambda^{-2/3}$.

Using $f \equiv \sqrt{Q} = \sqrt{q}\,\lambda^{1/3}/Z$, $Z \equiv (c^2 L_n/\omega_p^2)^{1/3}$, and Eq. (V.2c), this gives a lower bound on f for the wave-packets,

$$|f| \gtrsim Z^{-1} \qquad (V.64)$$

and, hence, Eq. (V.62) gives the maximum value of

$$\left|\underline{G}_{cut}\right|_{max} \Big/ \left|\exp(\theta_2 - \nu_1 t)\right| \approx \frac{c}{2\sqrt{\pi}}\,\xi^{-1/3} \qquad (V.65a)$$

in the region where the WKB approximation is valid. We have already shown in sec. III B that, for an unpumped nonuniform plasma, $|\underline{G}_{cut}|$ attains the above value at the very early time $\tilde{t} \equiv \omega(z_s)t/\xi \gtrsim 2\xi^{-1/3}$ for $z \gtrsim z_s$ and that $|\underline{G}_{cut}|$ continues to increase as time decreases until

$$\left|\underline{G}_{cut}\right|_{max} = \frac{c}{2} \qquad (V.65b)$$

at $t = 0$ and $z = z_s$. For this early time range $0 \leq \tilde{t} \lesssim 2\xi^{-1/3}$ and $z \gtrsim z_s$, we showed in secs. III B, C that we can apply the uniform plasma results for which there are no eigenmodes (i. e., they have negligible amplitude compared to the wave-packets at early times); for $\tilde{t} \gtrsim 2\xi^{-1/3}$, however, nonuniformity of the

plasma is important and our present analysis (including this nonuniformity) does give eigenmodes. Next, we will calculate $|f|_{min}$ and $|\underline{G}_{poles}|_{max}$, assuming we are in a space-time region where nonuniformity is important (giving the eigenmodes).

Assuming $\lambda \gtrsim 1$, so that ρ_+ and ρ_- are close together for the eigenmodes, the above condition for the validity of the WKB approximation becomes $|T - \rho| \gtrsim (2N+1)^{-\frac{1}{2}} \lambda^{-\frac{1}{2}}$ ($T = \rho_+$ or ρ_-) while, from Eq. (V.20), $|T - i| \lesssim (2N+1)^{\frac{1}{2}} \lambda^{-\frac{1}{2}}$. Thus, for the lower N eigenmodes, the WKB approximation is just barely valid. Setting $\rho = +i$ for the closest approach to both ρ_+ and ρ_-, and using Eq. (V.2c) and $f \equiv \sqrt{Q} = \sqrt{q}\,\lambda^{1/3}/Z$, the minimum value of f then becomes

$$\left|\frac{cf}{\omega(z_s)}\right|_{min} \approx \left[\frac{(2N+1)}{\xi}\frac{\omega(z_s)}{\sqrt{D}}\right]^{\frac{1}{2}}, \qquad (V.66)$$

and Eq. (V.63) gives

$$\left|\underline{G}_{poles}\right|_{max} \Big/ \left|\tilde{I}\exp(-\nu_1 t)\right| \approx \frac{c}{2\pi}\,\xi^{-\frac{1}{3}}\lambda^{-\frac{1}{6}}\frac{\omega(z_s)}{\omega_o} \qquad (V.67a)$$

which is $\pi^{-\frac{1}{2}}\lambda^{-1/6}\omega(z_s)/\omega_o$ smaller than Eq. (V.65a). However, $\rho = +i$ is only possible at "quarter-critical" density (where $\omega_p = \omega_1$) since, from Eq. (V.1 and 35b), $\mathrm{Im}\rho = 2\omega_p/\omega_o$; at lower densities ($\omega_p \lesssim \omega_1/2$) it is more typical to take $|q| \sim 1$,

and then $|cf/\omega(z_s)|_{min} \sim \sqrt{D}/\omega(z_s)$ which is $\sqrt{\lambda}$ larger than Eq. (V.66), thereby further decreasing Eq. (V.67a) by an additional factor of $\lambda^{-\frac{1}{2}}$. Thus, in the limit of a uniform plasma, $\lambda \to \infty$ from Eq. (V.2b) and $\underline{G}_{poles}$ vanishes.

In the opposite limit $\lambda \ll 1$, the condition $\lambda \int_{\rho}^{\rho_+} \sqrt{q}\, d\rho \gtrsim 1$ gives $|\rho_+ - \rho| \gtrsim \lambda^{-2/3}$ and $|f|_{min} \gtrsim Z^{-1}$, as in Eq. (V.64). From Eqs. (V.26a, b) with X complex, $|\rho_+| \gtrsim |2X| \gg \lambda^{-2/3}$ (leaving plenty of room to use our WKB results). Then Eq. (V.63) gives

(V.67b)

$$\left|\underline{G}_{poles}\right| \Big/ \left|\tilde{I} \exp(-\nu_1 t)\right| \ll \frac{c}{\pi\sqrt{2}}\, \xi^{-\frac{1}{3}}\, \frac{\omega(z_s)}{\omega_o},$$

which is much smaller than Eq. (V.65a). Of course for $\lambda < \lambda_o = 0.32$ from Eq. (V.31 b), the eigenmodes are decaying exponentially in time and are therefore negligible.

The conclusion thus far in this section, considering only the coefficients in front of the exponentials, is that the wave-packets are intrinsically much larger than the eigenmodes (cf. Eqs. (V.62 and 63) with $cf/\omega(z_s) \sim 1$). This remains true (although only *marginally*) even at early times with $f \to 0$ for both z_ℓ and z_g (cf. Eqs. (V.65a and 67a or b)). Thus, the eigenmodes will remain negligible until their exponential term sufficiently dominates the exponential term of the wave-packets so as to overcome this intrinsic weakness of the eigenmode coefficient.

We will next consider in detail these exponential terms in Eqs. (V.54 and 58a). We rewrite the functions θ_1 through θ_4, given in Eqs. (V.38 a, b, and 57 a, b), as

$$\theta_1 = -i\omega' t + g_1 - g_2 \qquad (V.68a)$$

$$\theta_2 = -i\omega' t + g_1 + g_2 + g_3 \qquad (V.68b)$$

$$\theta_3 = -i\omega' t - g_1 + g_2 \qquad (V.68c)$$

$$\theta_4 = -i\omega' t - g_1 - g_2 - g_3 \,, \qquad (V.68d)$$

where

$$g_1 \equiv i\lambda \int_{\rho_\ell}^{\rho_-} \sqrt{q_b}\, d\rho \qquad (V.68e)$$

$$g_2 \equiv i\lambda \int_{\rho_g}^{\rho_-} \sqrt{q_b}\, d\rho \qquad (V.68f)$$

$$g_3 \equiv i2\lambda \int_{\rho_-}^{\rho_+} \sqrt{q_b}\, d\rho \,. \qquad (V.68g)$$

In the discussion below Eq. (V.34) (see also Eqs. (V.35b and I.2)), we showed that the eigenmode growth rate γ_N' is always less than the uniform plasma growth rate γ_o but that the ratio approaches its limiting maximum value $2(\omega_p\omega_1)^{\frac{1}{2}}/\omega_o \leq 1$ for $N = 0$ and $\lambda \to \infty$. We therefore evaluate g_1 and g_2 only for $\lambda \gtrsim 1$ and $N = 0$, since for $\lambda << 1$ or $N >> 1$ the eigenmodes remain negligible (compared with the wave-packets) for a longer time (we are interested here in determining the minimum time necessary for the eigenmodes to dominate). For $\lambda \gtrsim 1$, we showed in Eq. (V.19) that an anti-Stokes line connects the transition points ρ_- and ρ_+ (for N not too large) so that g_3 is pure imaginary and does not contribute to the magnitude of Eq. (V.58a).

We calculate g_2 assuming $\lambda \gtrsim 1$, $\rho_- \lesssim \rho_g < \rho_+$, and for now $|\rho_g - 1| << 1$. Using $q \approx (\rho_+ - \rho)(\rho - \rho_-)/i$ and setting $\mathrm{Re}(\rho_g) = 0$ (i. e., $z_g = \mathrm{Re}\, z_\infty$), we find $\mathrm{Re}(g_2) \approx$ $\approx (1 - 2\omega_p/\omega_o)^2/2\sqrt{2} << \lambda$ valid only for $|\mathrm{Im}\, \rho_g - 1| =$ $= |1 - 2\omega_p/\omega_o| << 1$. For the eigenmodes, an anti-Stokes line connects ρ_- and ρ_+, and another anti-Stokes line starts at $\rho = 0$ and curves off toward the right, while one Stokes line from each of ρ_- and ρ_+ curves down and around the right-hand-side of $\rho = 0$ (see Figs. V.3a-b, 4b-c, 4d-e, 5e, 5g). Thus, $\mathrm{Re}(g_2) = 0$ everywhere along the anti-Stokes line connecting ρ_- and ρ_+ and monotonically increases as we approach the anti-Stokes line from

$\rho = 0$: the maximum value (assuming $\mathrm{Im}\rho \geq 0$ or $\omega_p \geq 0$) of $\mathrm{Re}\,(g_2)$ can then be obtained at $\rho_g = 0$. Writing g_2 in terms of elliptic integrals of the first and second kind and expanding in inverse powers of $\lambda \gtrsim 1$ results in $g_2 \tilde{\simeq} (2N+1)2\pi/3 + \mathcal{O}(1) + \mathcal{O}(\lambda)^{-\frac{1}{2}}$ at $\rho_g = 0$. Thus, for $\rho_- \lesssim \rho_g < \rho_+$, $|\mathrm{Re}\, g_2| \lesssim 1$ and can be ignored in evaluating the magnitude of the exponential term $\tilde{I}$ in Eq. (V.58a); of course, the same holds for g_1 when $\rho_- \lesssim \rho_\ell < \rho_+$.

We next calculate g_1, assuming $\lambda \gtrsim 1$ and $\rho_\ell \lesssim \rho_-$. For $1 \lesssim |\rho_- - \rho_\ell| \lesssim |\rho_+ - \rho_-| \tilde{\simeq} 2(2N+1)^{\frac{1}{2}}/\sqrt{\lambda}$, we obtain

$$\mathrm{Re}(g_1) \approx -\frac{\lambda}{2\sqrt{2}} |\rho_- - \rho_\ell|^2 , \qquad (V.69)$$

similar to our result in the above paragraph for g_2 except for the sign (we are now on the left-hand-side of the anti-Stokes line that comes down from ρ_- and curves around $\rho = 0$ and off to the right in Figs. V.3a-b, 4b-c, 4d-e, 5e, 5g). For $|\rho_- - \rho_\ell| >> 1 >> |\rho_+ - \rho_-|$, we can write g_1 in terms of elliptic integrals of the first and second kind and, expanding this assuming $|\rho_\ell| >> 1$ and $\lambda >> 1$, we find

$$\mathrm{Re}(g_1) \approx -2\lambda \frac{(\omega'_{1N})_R}{\omega_0} \left[-\mathrm{Re}(\rho_\ell)\right]^{\frac{1}{2}} + \\ + \mathcal{O}(1) + \mathcal{O}\left[-\mathrm{Re}(\rho_\ell)\right]^{-\frac{1}{2}} , \qquad (V.70)$$

where $(\omega'_{1N})_R$ is given by Eq. (V.35a). The same results apply to g_2 when $\rho_g \lesssim \rho_-$.

We will compare the exponential terms in Eqs. (V.54 and 58a) for $z_s = z_\ell \lesssim \mathrm{Re}(z_-) < z_g = \mathrm{Re}(z_+)$ and at a time corresponding to the line of turning points in Figs. III.3 and V.14 : i. e., $\omega' = \omega_g$ or $\tilde{t} \approx 2(\tilde{z}_g^{\,2} - \tilde{z})^{\frac{1}{2}}$ (from sec. III B), which reduces to

$$t \approx 2\left[Z^3 \omega_s^2 c^{-4} \delta z\right]^{1/2} \qquad (V.71)$$

for the case here with $\delta z \equiv z_g - z_\ell = \mathrm{Re}(z_+) - z_s$ and $Z \equiv (c^2 L_n/\omega_p^2)^{1/3}$. If we had chosen $z_g \lesssim \mathrm{Re}(z_-)$, the eigenmodes would have been exponentially smaller since $\mathrm{Re}(g_2) \lesssim -1$ (as well as for g_1) in θ_2. If we had chosen $\mathrm{Re}(z_-) \lesssim z_\ell = z_s \lesssim \mathrm{Re}(z_+)$, both g_1 and g_2 would have been negligible, but the small value of $\delta z \lesssim \mathrm{Re}(z_+ - z_-) = 2(2N+1)^{\frac{1}{2}} \lambda^{1/6} Z$ and $t \lesssim 2\sqrt{2}(2N+1)^{\frac{1}{2}} \cdot \lambda^{1/12} \xi^{2/3}/\omega_s$ (i. e., $\tilde{t} \equiv \omega_s t/\xi \lesssim 3\xi^{-1/3}$) would give essentially uniform plasma behavior over this small space-time region and, since the ratio of the uniform plasma wave-packet growth rate γ_o to the growth rate $\gamma'_{N=0}$ of the fastest growing eigenmode is always greater than $\omega_o/2(\omega_p\omega_1)^{\frac{1}{2}} \geq 1$, the term $\mathrm{Re}(-i\omega' t) = \gamma'_{N=0} t$ in Eq. (V.68) cannot overcome the corresponding term $\gamma_o t$ of the wave-packets (see sec. III C). In view of the intrinsic weakness of the eigenmode coefficient (shown earlier in this

section), the eigenmodes would still be negligible compared to the wave-packets for this choice of z_ℓ and z_g with t given by Eq. (V.71). However, if we choose $z_s = z_\ell \lesssim \mathrm{Re}(z_-) < z_g = \mathrm{Re}(z_+)$, with t still given by Eq. (V.71), the side-scattered wave-packet resonance position $z = \mathrm{Re}(z_\infty)$ (which lies between z_- and z_+) is now to the right of the source position z_g. Hence, the side-scattered wave-packet must travel for some distance and time (see Eq. (V.71)) before it can reach the resonance zone where it can start growing, while the particular term $\mathrm{Re}(-i\omega' t) = \gamma'_{N=0} t$ in Eq. (V.68) for the eigenmode (with $N = 0$) starts growing at $t = 0$. The only remaining question is whether the large negative value of $\mathrm{Re}(g_1)$ (g_2 negligible here) can overcome this apparent initial temporal growth advantage of the eigenmodes, and this will be considered next.

Writing Eqs. (V.69, 70) in terms of $\delta\rho \equiv \delta z/Z\lambda^{2/3}$ with $\delta z = \mathrm{Re}(z_+) - z_s = z_g - z_\ell$, we have for $1 \lesssim \delta\rho \lesssim 2(2N+1)^{\frac{1}{2}}\lambda^{-\frac{1}{2}}$

$$\mathrm{Re}(g_1) \approx -\frac{\lambda}{2\sqrt{2}}(\delta\rho)^2 , \qquad \text{(V.72a)}$$

and for $\delta\rho \gg 1$

$$\mathrm{Re}(g_1) \approx -2\lambda \frac{(\omega'_{1N})_R}{\omega_o}(\delta\rho)^{1/2} + O(1), \qquad \text{(V.72b)}$$

where we have assumed $\lambda >> 1$. For $\lambda >> 1$, we also have $\gamma'_{N=0} \approx$ $\approx 2\gamma_o(\omega_p\omega_1)^{\frac{1}{2}}/\omega_o = \lambda^{2/3}c^2/Z^2\omega_o$, and using $t = 2\lambda^{1/3}(\delta\rho)^{1/2}\omega_s Z^2/c^2$ from Eq. (V.71) gives

$$\mathrm{Re}(-i\omega' t) = \gamma'_{N=0} t = 2\lambda \frac{\omega_s}{\omega_o}(\delta\rho)^{1/2} . \quad \text{(V.73)}$$

In comparing Eqs. (V.72b and 73), note that $(\omega'_{1N})_R \approx$ $\approx (\omega_o + c^2k_{1\perp}^2/\omega_o)/2 = \omega(z_o) \equiv \{[\omega_o - \omega(z_o)]^2 + c^2k_{1\perp}^2\}^{\frac{1}{2}}$ is just the frequency of the side-scattered wave and, by assumption, is greater than or equal to ω_s ($z_o = \mathrm{Re}(z_\infty)$) since waves of lower frequency than ω_s are evanescent (see sec. III B). Thus, for $\delta\rho >> 1$, the large negative value of $\mathrm{Re}(g_1)$ is more than sufficient to overpower the term $\mathrm{Re}(-i\omega' t)$, for t given by Eq. (V.71), and we conclude $\mathrm{Re}(\theta_1) \approx \mathrm{Re}(\theta_2) \lesssim 0$.

On the other hand, the total side-scatter exponentiation factor Γ_2 (including growth both before and after the wave-packet encounters its turning point at z_+) was earlier given in Eq. (V.53b). The term M_2 defined in Eq. (V.51b) is z-dependent (as mentioned below Eq. (V.53b)) but is not valid right at the turning point z_+ (where we would like to compare the wave-packets with the eigenmodes, as decided above Eq. (V.71)) since we required above Eq. (V.51a) that $|\omega_A^2 - \omega_g^2| >> 2\omega_A|\delta\omega|$ (recall that $\omega_g = \omega_A$ at $z_g = z_+$). We will return to this point below, but for now we

just set $z_\ell = z_g = z_s$, assume $\omega_A \approx \omega_s = \omega_\ell = \omega_g$, and obtain $M_2 \approx 2\omega_A^2/\left[\omega_A^2 - \omega_s^2\right]^{\frac{1}{2}} = 2\omega_A^2/(\delta\rho D)^{\frac{1}{2}}$ for use in Eq. (V.53b). We then take one-half of Γ_2 since we are really only interested for now in the growth accumulated up to the time the wave-packet encounters its turning-point at $z_g = z_+$, and find (V.74)

$$\frac{\Gamma_2}{2} = \frac{5}{4}\left(\frac{\pi}{2}\right)^{4/5}\cos\left(\frac{\pi}{10}\right)\lambda\left(\frac{\omega_A}{\omega_o}\right)^{2/5}(\delta\rho)^{-1/10}$$

where, for the side-scattered wave-packet, $\omega_A = \omega(z_o) = (\omega_o + c^2k_{1\perp}^2/\omega_o)/2$.

We can use Eq. (V.74) for $\mathrm{Re}(\theta_2)$, to go along with Eq. (V.62) in determining $|G_{cut}|$, provided $|\omega_A^2 - \omega_s^2| = \delta\rho D >> 2\omega_A|\delta\omega|$. Using $\delta\omega$ from Eq. (V.53a) and M_2 found above, this inequality becomes

$$\delta\rho >> \left(\frac{\pi}{2}\right)^{1/2}\left(\frac{\omega_A}{\omega_o}\right)^{1/4} \approx 1. \qquad (V.75)$$

This is essentially a requirement, for the use of Eq. (V.74), that the source be outside the resonance zone; i. e., $z_s << z_o - h/2$ in Figs. I.8,10 (for the side-scattered wave, the resonance position $z_o = \mathrm{Re}(z_\infty)$ coincides with the turning point $\mathrm{Re}(z_+)$). For smaller values of $\delta\rho$, so that $z_o - h/2 \lesssim z_s \leq z_o$, the side-scattered wave-packet does not travel the full width $(h/2)$ of

its growing region before it reaches its turning point at $Re(z_+) = z_o$ and, therefore, $Re(\theta_2)$ is smaller than $\Gamma_2/2$. We can estimate the proper value of $Re(\theta_2)$ by noting that, for $\delta\rho \lesssim 1$, the wave-packet temporal growth rate remains at nearly the uniform plasma value $\gamma_o = \lambda^{2/3}c^2/Z^2[2(\omega_A\omega_p)]^{\frac{1}{2}}$, $\omega_p = \omega_o - \omega_A$, over most of the wave-packet trajectory so that $Re(\theta_2) \approx \gamma_o t$. Using Eq. (V.71), this gives

$$Re(\theta_2) \approx \lambda \frac{\omega_s}{(\omega_A\omega_p)^{1/2}} (\delta\rho)^{1/2}, \qquad (V.76)$$

valid for $\delta\rho \lesssim 1$. Setting Eq. (V.76) equal to $\Gamma_2/2$ for $\lambda^{2/3}Z\ \delta\rho = \delta z = h/2$, and using $\omega_s \approx \omega_A$ here ($z_s \approx z_+$), results in

$$h \approx \lambda^{2/3} Z\, 2\left(\frac{\pi}{2}\right)^{4/3}\left[\frac{5}{4}\cos\left(\frac{\pi}{10}\right)\right]^{5/3}\left(\frac{\omega_A}{\omega_o}\right)^{2/3}\left(\frac{\omega_p}{\omega_A}\right)^{5/6} \qquad (V.77)$$

as an estimate of the resonance zone size. As explained in a similar discussion concerning Eq. (I.10b), this simple calculation can give only an approximate form for h since the average growth rate over the entire resonance zone is less than (~ half) γ_o while the time spent in the resonance zone is greater than (~ twice) that given by Eq. (V.71) due to the reduced group velocity there (secs. I A 2 and III C give $\underline{V}_g = (\underline{V}_1 + \underline{V}_2)/2 \approx \underline{V}_1/2$).

Roughly canceling these two effects again gives Eq. (V.77) for h. This corresponds to a value of $\delta\rho = h/2\,\lambda^{2/3}Z \lesssim 1$, as expected, and roughly agrees with our earlier estimate $h \gtrsim \lambda^{2/3}Z\,5(\omega_p/\omega_A)^{\frac{1}{2}}$ from Eq. (I.10b).

We summarize our results concerning the exponential terms (in Eqs. (V.54 and 58a)) in Fig. V.15. The top curve is $\mathrm{Re}(\theta_2)$ vs. $\delta\rho$ for the side-scattered wave-packet where we use Eq. (V.76), for $\delta\rho \lesssim 1$, and Eq. (V.74), for $\delta\rho \gg 1$. The bottom curve is $\mathrm{Re}(\theta_2)$ vs. $\delta\rho$ for the N = 0 eigenmode where we use Eqs. (V.72a and 73), for $2\lambda^{-\frac{1}{2}} \lesssim \delta\rho \lesssim 1$, and Eqs. (V.72b and 73), for $\delta\rho \gg 1$, in evaluating Eqs. (V.68a, b and 56 b) (g_2 and g_3 negligible here). These two curves of the exponentiation factor $\mathrm{Re}(\theta_2)$ are evaluated at the turning point time, given by Eq. (V.71), as a function of the distance $\delta z \equiv \mathrm{Re}(z_+) - z_s$ between the source z_s and the turning point z_+ ($\delta\rho = \delta z/\lambda^{2/3}Z$). We previously showed in this section that the side-scattered wave-packet is intrinsically dominant (considering only the coefficients in front of the exponentials) over the eigenmodes, and Fig. V.15 shows that it remains dominant (including the exponential terms) over the eigenmodes even up to and past the time the waves reach the turning point z_+ regardless of the distance between z_+ and the source z_s. Since the side-scattered wave-packet continues to grow while it is in its resonance zone, and its growth rate here is greater

than that of the eigenmodes, it also remains dominant at the "side-scatter saturation time" t_s when it exists its resonance zone (as shown in Fig. I.10). As shown in Fig. I.8, the minimum value of t_s occurs for the source located at the resonance zone edge and, assuming no pump modification in the group velocity, would be given by twice Eq. (V.71) with $\delta z = h/2$. However, the reduced group velocity in the resonance zone (sec. I A 2 and III C) increases t_s by an additional factor of 2 for a given value of h, i. e., Eq. (V.77). The minimum value of t_s is thus approximately

$$t_s \approx 8\left(\frac{\pi}{2}\right)^{2/3}\left[\frac{5}{4}\cos\left(\frac{\pi}{10}\right)\right]^{5/6} \times \times\left(\frac{\omega_A}{\omega_o}\right)^{1/3}\left(\frac{\omega_p}{\omega_A}\right)^{5/12}\lambda^{1/3}\,\frac{\omega_s Z^2}{c^2} \qquad (V.78)$$

The temporally growing eigenmodes will begin to dominate over the saturated side-scattered wave-packet shortly thereafter, or at a time on the order of $2\,t_s$.

We have so far discussed the response only at a given $\underline{k}_{1\perp}$, as indicated in Eq. (I.29). This would be sufficient if the plasma and pump wave were of infinite extent and the source periodic along x and y, but if our source delta-function in Eq. (I.25a)

had also been proportional to $\delta(y)$, for example, an integration over k_{1y} would also be necessary in Eq. (I.29). As discussed earlier in the middle of sec. I B, such an integration converts the periodic behavior in y into a "wave-packet" behavior in y with all the waves (both the old wave-packets from Eq. (V.54) and the eigenmodes from Eq. (V.58a)) now moving with a group velocity V_{gy} along t-y trajectories labeled by a saddle-point (i. e., wave-packet) k_{1y}. Usually, $V_{gy} = k_{1y} c^2/\omega_1$ as in an unpumped plasma; however, in the resonance zone the pumped uniform plasma theory (secs. I A 2 and III C) predicts a reduced group velocity $\underline{V}_g = (\underline{V}_1 + \underline{V}_2)/2$ or $V_{gy} = (c^2/\omega_1 - 3v_{th}^2/\Omega)k_{1y}/2 \approx k_{1y}c^2/2\omega_1$. Thus, by time t_s all of the waves will have convected along y a distance

$$y_s \approx \frac{t_s k_{1y} c^2}{2\omega_1} \quad . \qquad \text{(V.79)}$$

We have so far ignored variations along y in our system (plasma and pump wave intensity), but if, for instance, the pump wave (e. g., a laser) has a finite diameter d_L, we have a new effect: all waves stop growing when they have convected along y a distance greater than d_L! Since we have already concluded that at time t_s the eigenmodes are negligible compared with the

side-scattered wave-packet, provided some nonlinear process has not earlier saturated the wave-packet growth (i. e., $\Gamma_2 \lesssim \ell n(n\lambda_D^3)$ the "Coulomb logarithm" as mentioned in Ref. G III), the eigenmodes will <u>forever remain</u> negligible if

$$\gamma_s \gtrsim d_L \ . \qquad (V.80)$$

The conditions necessary for experimentally observing the eigenmodes are, therefore, as follows: for dominance over the side-scattered wave-packet we must have an observation time or pump wave (i. e., laser pulse) duration

$$t_L \gtrsim 2t_s \qquad (V.81a)$$

and a pump wave (laser focal) diameter

$$d_L \gtrsim 2\gamma_s \ ; \qquad (V.81b)$$

for observation above thermal noise we must have a sufficiently large exponentiation

$$\Gamma_2 \geq \Gamma_2' >> 1 \ , \qquad (V.81c)$$

where Γ_2' (typically set equal to 10 here) is some arbitrarily set lower bound of growth below which we consider the waves to be negligible. We obtain Γ_2 from Eq. (V.74) evaluated at $\delta\rho = h/2\ \lambda^{2/3}Z$ using Eq. (V.77); this gives a side-scattered wave-packet exponentiation factor

$$\Gamma_2 \approx 2\left(\frac{\pi}{2}\right)^{2/3}\left[\frac{5}{4}\cos\left(\frac{\pi}{10}\right)\right]^{5/6}\left(\frac{\omega_A}{\omega_o}\right)^{1/3}\left(\frac{\omega_A}{\omega_p}\right)^{1/12}\lambda \qquad (V.81d)$$

or equivalently

$$\Gamma_2 \approx 0.96\left(\frac{\omega_A}{\omega_o}\right)^{5/12}\left(\frac{\omega_p}{\omega_o}\right)^{11/12}\left(\frac{Kc}{\omega_p}\right)^{3/2}\left[\lambda_o(\mu m)\right]^{1/2} \times$$

$$\times L_n(\mu m)\left[I_o(10^{17}\ \text{watts/cm}^2)\right]^{3/4} \qquad (V.81e)$$

Note that Eq. (V.81d) is equal to Eq. (I.9) multiplied by the small factor $(\omega_p\omega_A/\omega_o^2)^{1/6}$, so the agreement between the two exponentiation factors is very good. Equation (V.81a) is shown in the next section to be easily satisfied; however, Eq. (V.81b) is much more restrictive.

The lower bound on d_L (for eigenmode observation) given by Eq. (V.81b) depends on both pump wave intensity

$I_o \equiv (v_o/c)^2 m^2 \omega_o^2 c^3/2\pi e^2$ and density scale length L_n, but we can approximately eliminate either one of these variables (see Eqs. (V.82 a, b, e, f) below) by using Eq. (V.81c). Equation (V.81b) then takes on one of two forms: (1) if for given L_n the intensity satisfies

$$\left(\frac{v_o}{c}\right)^2 \gtrsim 2^{-4/3}\left(\frac{\pi}{2}\right)^{-8/9}\left[\frac{5}{4}\cos\left(\frac{\pi}{10}\right)\right]^{-10/9}\left(\Gamma_2'\right)^{4/3} \times$$

$$\times\left(\frac{\omega_o}{\omega_A}\right)^{4/9}\left(\frac{\omega_p}{\omega_A}\right)^{1/9}\left(\frac{Kc}{\omega_p}\right)^{-2/3}\left(KL_n\right)^{-4/3} \qquad (V.82a)$$

or equivalently

$$I_o\left(10^{17}\,\text{watts/cm}^2\right) \gtrsim 23\left(\frac{\Gamma_2'}{10}\right)^{4/3}\left(\frac{\omega_o}{\omega_A}\right)^{5/9}\left(\frac{\omega_o}{\omega_p}\right)^{11/9} \times$$

$$\times\left(\frac{Kc}{\omega_p}\right)^{-2}\left[L_n(\mu m)\right]^{-4/3}\left[\lambda_o(\mu m)\right]^{-2/3}, \qquad (V.82b)$$

then (for eigenmode observation) d_L must satisfy

$$d_L \gtrsim 2^{8/3}\left(\frac{\pi}{2}\right)^{4/9}\left[\frac{5}{4}\cos\left(\frac{\pi}{10}\right)\right]^{5/9}\left(\Gamma_2'\right)^{1/3} \times$$

$$\times\left(\frac{\omega_A}{\omega_o}\right)^{2/9}\left(\frac{\omega_A}{\omega_p}\right)^{5/9}\left(\frac{ck_{1y}}{\omega_A}\right)\left(\frac{cL_n^2}{\omega_p}\right)^{1/3} \qquad (V.82c)$$

or equivalently

$$d_L(\mu m) \gtrsim 10\left(\frac{\Gamma_2'}{10}\right)^{1/3}\left(\frac{\omega_A}{\omega_p}\right)^{7/9}\left(\frac{\omega_o}{\omega_p}\right)^{1/9}\times \times\left(\frac{c\,k_{1y}}{\omega_A}\right)\left[L_n(\mu m)\right]^{2/3}\left[\lambda_o(\mu m)\right]^{1/3}; \qquad (V.82d)$$

(2) from another point of view, if for given I_o the density scale length satisfies

$$L_n \gtrsim \frac{1}{2}\left(\frac{\pi}{2}\right)^{-2/3}\left[\frac{5}{4}\cos\left(\frac{\pi}{10}\right)\right]^{-5/6}\Gamma_2'\times \times\left(\frac{\omega_o}{\omega_A}\right)^{1/3}\left(\frac{\omega_p}{\omega_A}\right)^{1/12}\left(\frac{v_o}{c}\right)^{-3/2}\left(\frac{Kc}{\omega_p}\right)^{-1/2}K^{-1} \qquad (V.82e)$$

or equivalently

$$L_n(\mu m) \gtrsim 10\left(\frac{\Gamma_2'}{10}\right)\left(\frac{\omega_o}{\omega_A}\right)^{5/12}\left(\frac{\omega_o}{\omega_p}\right)^{11/12}\times \times\left(\frac{Kc}{\omega_p}\right)^{-3/2}\left[\lambda_o(\mu m)\right]^{-1/2}\left[I_o(10^{17}\ \text{watts/cm}^2)\right]^{-3/4}, \qquad (V.82f)$$

then (for eigenmode observation) d_L must satisfy

$$d_L \gtrsim 4\Gamma_2' \left(\frac{\omega_A}{\omega_p}\right)^{1/2} \left(\frac{c k_{1y}}{\omega_A}\right) \left(\frac{v_o}{c}\right)^{-1} K^{-1} \qquad (V.82g)$$

or equivalently

$$d_L(\mu m) \gtrsim 48 \left(\frac{\Gamma_2'}{10}\right) \left(\frac{\omega_A}{\omega_p}\right)^{1/2} \left(\frac{\omega_o}{\omega_p}\right) \times \qquad (V.82h)$$

$$\times \left(\frac{c k_{1y}}{\omega_A}\right) \left(\frac{Kc}{\omega_p}\right)^{-1} \left[I_o(10^{17} \text{ watts/cm}^2)\right]^{-1/2} .$$

Equations (V.82c, d, g, h) agree exactly with Eq. (V.81b) only if $\Gamma_2' = \Gamma_2$, but the sense (or direction) of the inequality is still preserved if we use the smaller constant Γ_2' assuming $\Gamma_2' \lesssim \Gamma_2$. Again, Eqs. (V.82a, b, e, f) are just different ways of writing the same condition given by Eq. (V.81c). In Eqs. (V.82b, d, f, h) the pump wavelength λ_o, L_n, and d_L are all in units of microns, and I_o is in units of 10^{17} watts/cm^2. From previous definitions, we recall that $\omega_A = \omega_o - \omega_p = \omega(z_o) \equiv$ $\equiv (\omega_o + c^2 k_{1\perp}^2/\omega_o)/2$ for the side-scattered wave and $K = |\underline{k}_o - \underline{k}_{1\perp}| =$ $= (k_o^2 + k_{1\perp}^2)^{\frac{1}{2}}$.

The usefulness of Eqs.(V.82a - h) can be demonstrated as follows: if the density scale length L_n of our plasma was fixed, Eq.(V.82b) would give the minimum laser intensity I_o and Eq. (V.82d) an absolute minimum laser focal diameter d_L needed to observe the eigenmodes; if, instead, our laser had a fixed intensity I_o, then Eq. (V.82f) would give the minimum density scale length L_n that must be arranged in the plasma and Eq. (V.82h) again an absolute minimum laser focal diameter d_L needed to observe the eigenmodes. Multiplying the intensity I_o (either given by Eq. (V.82b) or fixed) by d_L^2 (using either Eq. (V.82d) or Eq. (V.82h), respectively), results in a single expression for the absolute minimum laser power $P_o \equiv I_o d_L^2$ needed for eigenmode observation:

$$\left(\frac{V_o}{c}\right)^2 d_L^2 \gtrsim 16\left(\Gamma_2'\right)^2\left(\frac{\omega_A}{\omega_p}\right)\left(\frac{c\,k_{1y}}{\omega_A}\right)^2 K^{-2} \qquad (V.83a)$$

or equivalently

$$P_o\left(10^{12}\,\text{watts}\right) \gtrsim 2.3\left(\frac{\Gamma_2'}{10}\right)^2\left(\frac{\omega_A}{\omega_p}\right)\times$$
$$\times\left(\frac{\omega_o}{\omega_p}\right)^2\left(\frac{c\,k_{1y}}{\omega_A}\right)^2\left(\frac{Kc}{\omega_p}\right)^{-2}, \qquad (V.83b)$$

with P_o expressed in units of 10^{12} watts. Again Eq. (V.83) agrees exactly with Eq. (V.81b) only if $\Gamma_2' = \Gamma_2$. We note, however,

that the condition $d_L \gtrsim 2y_s$ is required only along y (the side-scatter direction) and not along x (the polarization direction, $\underline{E}_o = E_o\hat{x}$). Since we usually set $k_{1x} = 0$ for maximum growth (see Eqs. (I.2 or 25c)), the only requirement for the validity of our results is that the plasma and pump wave be relatively uniform compared with the resonance zone width h from Eq. (V.77); if Δx_L is the focal width of the laser along x, we require $\Delta x_L >> h$ (note that $k_o h >> 1$ was assumed in sec. II). Thus, by using a noncircular focal cross-section flattened along x, we can now write the power as $P_o = I_o d_L \Delta x_L$ and reduce our power requirement from Eq. (V.83) by the factor $\Delta x_L/d_L$ (typically $<< 1$).

These expressions for the minimum necessary d_L (which do not in general agree with each other) and P_o are only approximate since we have used Γ_2' (a constant) rather than Γ_2 (a function of I_o and L_n proportional to $I_o^{3/4} L_n$) in Eqs. (V.82c, d, g, h and V.83a, b); the expressions are correct only if we replace Γ_2' by Γ_2. For instance, if $\Gamma_2' = \Gamma_2/2$ then Eq. (V.82d) (as written) is a factor of $(1/2)^{1/3}$ <u>smaller</u> and Eq. (V.82h) (as written) a factor of $1/2$ <u>smaller</u> than the correct minimum d_L, and Eq. (V.83b) is a factor of $(1/2)^2$ <u>smaller</u> than the correct minimum P_o. That is why we used the word "absolute" above, since the correct minimum (i. e., the <u>greatest</u> lower bound) is generally larger. Since the correct expressions for

the lower bounds on d_L and P_o require using Γ_2 in place of Γ_2' in Eq. (V.82 c, d, g, h and V.83 a, b), the correct minimum d_L and P_o are not independent of the exponentiation factor Γ_2 but rather increase with Γ_2. Thus, once we have reached $\Gamma_2 = \Gamma_2'$ and satisfied Eqs. (V.82d or h), a further increase in I_o or L_n will increase Γ_2 past Γ_2' and increase the necessary d_L past the forms given by Eq. (V.82d) or Eq. (V.82h), respectively, if the eigenmodes are to be observed; this makes the observation of the eigenmodes more difficult (in spite of the large Γ_2) because the condition on d_L from Eqs. (V.82d or h) (or equivalently on P_o) is generally already restrictive. The eigenmodes cannot be observed if $\Gamma_2 < \Gamma_2'$, because of insufficient growth, and generally they cannot be observed if $\Gamma_2 >> \Gamma_2'$ (unless nonlinear saturation occurs), because of the restrictive condition on d_L or P_o for the eigenmodes to dominate over the side-scattered wave-packet; the most favorable conditions for eigenmode observation thus occur at $\Gamma_2 = \Gamma_2'$ (the equality in Eqs. (V.82b or f)), provided Eqs. (V.82d or h, or V.83b) can be satisfied.

In the next three sections, we will apply these results to three situations where one might try to look for the Raman instability: a typical laboratory theta-pinch, laser-fusion experiments, and computer simulations.

D. Examples

1. Theta-Pinch Parameters

We do not wish to go into a long discussion of various theta-pinch experiments and fusion proposals (see Ref. A VI), but rather just take as typical parameters a density $n \gtrsim 10^{17}\text{cm}^{-3}$, a density scale length $L_n \gtrsim 10$ cm along the axis, and a radius $r_p \lesssim 1$ cm. Using a CO_2 laser with $\lambda_o = 10.6$ μm and $\omega_o = 2 \times 10^{14}\ \text{sec}^{-1}$, we then have the following additional relations: $\omega_o/\omega_p \gtrsim 10$, $\omega_A/\omega_p \gtrsim 9$, $K \gtrsim \sqrt{2}\, k_o$, $Kc/\omega_p \gtrsim 14$, $ck_{1y}/\omega_A \gtrsim 0.99$.

Taking $\Gamma_2' = 10$, Eq. (V.82b) then gives

$$I_o \gtrsim 9.3 \times 10^{9}\ \text{watts/cm}^2\ , \qquad \text{(V.84a)}$$

Eq. (V.82d) gives

$$d_L \gtrsim 33\ \text{cm}\ , \qquad \text{(V.84b)}$$

while Eq. (V.83b) gives ($P_o \equiv I_o d_L^2$)

$$P_o \gtrsim 1.0 \times 10^{13}\ \text{watts} \qquad \text{(V.84c)}$$

as the conditions that must be satisfied in order to observe the eigenmodes (assuming no nonlinear saturation). While Eq. (V.84a) gives an easily obtainable intensity, the required d_L is much larger than even the typical theta-pinch plasma radius! Even if L_n were decreased significantly in order to reduce the requirement on d_L (although thereby increasing the required I_o), the power requirement from Eq. (V.84c) remains unaltered and prohibitively large (equivalent to 10 kilo-joules delivered in 1 nano-second). From Eq. (V.81a), the required laser pulse duration is $t_L \gtrsim (d_L/c)/(ck_{1y}/\omega_A)$ or $t_L \gtrsim 1.1$ nano-sec. From Eqs. (V.81d, e), at an intensity of $I_o = 10^{10}$ watts/cm^2 we have $\lambda \gtrsim 3.0$ and $\Gamma_2 \gtrsim 10.9$. However, the side-scattered wave-packet requires a distance $y_s \gtrsim 16.5$ cm to saturate at the level $\Gamma_2 \gtrsim 10.9$, whereas the plasma radius is only $r_p \lesssim 1$ cm; thus, the wave-packet will saturate early at a level of only $(\Gamma_2)_{actual} \lesssim (10.9)(2r_p/y_s) \lesssim 1$ or even less if the actual laser focal diameter $d_L < 2r_p$ so that the wave-packet would exit the pumped region before leaving the plasma. For the sake of completeness, the growth rate of the wave-packet (at the center of the resonance zone) is given by Eq. (I.2) as $\gamma_o/\omega_p =$ $= 0.067(\omega_p/\omega_1)^{\frac{1}{2}}(Kc/\omega_p)\left[I_o(10^{17}\text{w/cm}^2)\right]^{\frac{1}{2}}\lambda_o(\mu\text{m}) \gtrsim 1.1 \times 10^{-3}$ at $I_o = 10^{10}$ w/cm^2 while the resonance zone width is given by

Eq. (V.77), with $Z \equiv (c^2 L_n/\omega_p^2)^{1/3} \approx 0.28$ mm, as $h \approx 4.9\, Z\, \lambda^{2/3} \cdot \cdot (\omega_A/\omega_o)^{2/3}(\omega_p/\omega_A)^{5/6} \approx 1.5\, Z \approx 0.43$ mm using $\lambda = 3$.

We conclude that the observation of the eigenmodes in a plasma with theta-pinch parameters and an axially directed laser is highly unlikely: it would require an extremely high power laser ($P_o \gtrsim 10^{13}$ watts for 1 nsec.) and a density scale length somehow reduced much below 1 cm. However, by firing the laser in perpendicular to the theta-pinch axis rather than along the axis, $L_n \ll 1$ cm can be achieved, and with $L_n = 1$ mm the requirements are $I_o \gtrsim 4.3 \times 10^{12}$ watts/cm^2 and $d_L \gtrsim 1.5$ cm; moreover, with $h \lesssim 0.090$ mm (using $\lambda = 3$) we can take $\Delta x_L = 0.5$ mm $>> h$ (as discussed below Eq. (V.83)) and reduce the power requirement to $P_o = I_o d_L \Delta x_L \gtrsim 3.3 \times 10^{11}$ watts (e. g., 15 joules delivered in $t_L \approx 50$ pico-secs) by using a noncircular focal cross-section with the polarization perpendicular to the theta-pinch axis (now the side-scatter direction). We finish this section by noting that, from Eq. (V.83b), we roughly have the required $P_o(10^{12}\text{w}) \sim 2(ck_{1y}/\omega_A)^2(\omega_A/\omega_p)$, which decreases as $\omega_p \to \omega_A \to \omega_o/2$: this motivates considering a lower frequency laser or a higher density plasma (e. g., a laser-pellet fusion experiment, as in the next section).

2. Laser-Pellet Fusion Parameters

a. Slab Plasma

In present experiments (see Ref. sec. H) using high intensity short duration laser pulses such as from a Nd:glass laser with $\lambda_o = 1.06\ \mu m$ and $\omega_o = 2 \times 10^{15}\ sec^{-1}$, typical parameters in the underdense plasma region are a density $n \lesssim 10^{20} cm^{-3}$ and a density scale length $L_n \lesssim 10 \mu m$. Since our power requirement from Eq. (V.83b) (necessary for observing eigenmodes) is minimized for $\omega_p \to \omega_A \to \omega_o/2$, we pick a value of ω_p reasonably close to $\omega_o/2$ (and yet not so close as to violate approximations made in sec. II): we take $\omega_o/\omega_p = 3$, $\omega_A/\omega_p = 2$, $K = k_o(11/8)^{\frac{1}{2}}$, $Kc/\omega_p = (11)^{\frac{1}{2}}$, and $ck_{1y}/\omega_A = \sqrt{3}/2$.

Using $\Gamma_2' = 10$, Eq. (V.82b) then gives

$$I_o \gtrsim 4.5 \times 10^{16}\ watts/cm^2, \qquad (V.85a)$$

Eq. (V.82d) gives

$$d_L \gtrsim 80\ \mu m, \qquad (V.85b)$$

while Eq. (V.83b) gives ($P_o \equiv I_o d_L^2$)

$$P_o \gtrsim 2.9 \times 10^{12} \text{ watts} \qquad (V.85c)$$

as the conditions that must be satisfied in order to observe the eig modes (assuming no nonlinear saturation). The intensity given by Eq. (V.85a) has been exceeded or approached in many experiments, but only by reducing the focal diameter d_L to 30 μm or less (see Ref. sec. H). All of the conditions listed in Eq. (V.85) will undoubtedly soon be exceeded: the power requirement of 3×10^{12} watts is equivalent to 300 joules delivered in 100 pico-seconds, and the pulse duration requirement of only $t_L \lesssim 0.31$ pico-sec is no problem. In raising the power to this level with short duration pulses, however, the density scale length may be reduced below 10 μm thereby further increasing the intensity requirement (perhaps past 10^{17} watts/cm^2), and unless the actual focal width d_L is correspondingly reduced according to Eq. (V.82d) this would increase the power requirement past that given by Eq. (V.83b). Thus, in trying to observe the eigenmodes, it may be a losing battle if one tries to attain the necessary power by compressing the pulse duration and, if the power requirement is not reached, it does no good to increase I_o by strong focusing because Eq. (V.82d) would

eventually be violated. Also, although at an intensity of $I_o \approx 5 \times 10^{16}$ watts/cm^2 we have $\lambda = 3.8$ and $\Gamma_2 \gtrsim 11$, the side-scattered wave-packet requires a distance $y_s \gtrsim 40$ μm to saturate at the level $\Gamma_2 \gtrsim 11$ and this distance may exceed the actual laser focal width d_L; if this happens, the convective saturation will occur early at a level of only $(\Gamma_2)_{actual} \gtrsim 11(d_L/y_s)$, and this may explain the lack of experimental evidence for the side-scattered wave-packet (although there are other possible explanations such as an unexpectedly small L_n, or density fluctuations $\delta n/n_o \gtrsim h/2L_n$ along y over a distance scale $y < y_s$ corresponding to an effective density scale length $L_y \lesssim 2y_s L_n/h$). For the sake of completeness, the growth rate of the wave-packet (at the center of the resonance zone) is given by Eq.(I.2) (see also sec. V D 1) as $\gamma_o/\omega_p = 0.12$ at $I_o = 5 \times 10^{16}$w/cm^2 while the resonance zone width is given by Eq. (V.77) (see also sec. V D 1), with $Z \equiv (c^2 L_n/\omega_p^2)^{1/3} =$ $= 1.3$ μm, as $h \gtrsim 5.1\, Z \gtrsim 6.4$ μm using $\lambda = 3.8$.

For a laser-pellet fusion reactor, a density scale length $L_n \gtrsim 100\,\mu$m is generally thought to be typical in the underdense plasma region (see Ref. sec. J). Equation (V.82b) then gives

$$I_o \gtrsim 2.1 \times 10^{15} \text{ watts/cm}^2 , \qquad (V.86a)$$

Eq. (V.82d) gives

$$d_L \gtrsim 370 \ \mu\text{m} , \qquad (V.86b)$$

while the power requirement ($P_o \equiv I_o d_L^2$) remains at $P_o \gtrsim$ $\gtrsim 2.9 \times 10^{12}$ watts as the conditions required for eigenmode observation (again assuming no nonlinear saturation). The intensity given by Eq. (V.86a) is exceeded in typical proposed laser-pellet reactors (Ref. sec. J) and in many present laser-fusion experiments(Ref. sec. H). However, the focal width requirement, given by Eq. (V.86b), is somewhat restrictive for a single laser beam (reactor proposals envision using multiple over-lapping laser beams to cover a spherical pellet surface, but this case will be looked at in the next section); this is especially true in present experiments where $d_L \lesssim 100$ at this power. If a density scale-length of $L_n \gtrsim 100$ μm is reached (e.g., by using a laser pre-pulse in present experiments), the resonance zone width would be $h \gtrsim 5.1\, Z \gtrsim 14$ μm using $Z \equiv (c^2 L_n/\omega_p^2)^{1/3} \gtrsim$ $\gtrsim 2.8$ μm and $\lambda = 3.8$ (equivalent to $\Gamma_2 \gtrsim 11$ and $\gamma_o/\omega_p =$ $= 2.5 \times 10^{-2}$). Thus, by using a noncircular focal cross-section,

with the width along the polarization reduced to $\Delta x_L \gtrsim 30\ \mu m >> h$ and the width along the side-scatter direction increased to $d_L \gtrsim \gtrsim 370\ \mu m$, we could satisfy Eqs. (V.86a, b) and yet reduce the power requirement to only $P_o \equiv I_o d_L \Delta x_L \gtrsim 2.3 \times 10^{11}$ watts (equivalent to 23 joules delivered in 100 pico-seconds). This is within present laser capabilities, although this type of focusing would be extremely difficult (the slit-like focal spot would have to be straight within 30 μm over the entire length of 370 μm).

In conclusion, it appears to be very difficult to arrange all the parameters (plasma and laser) in a manner satisfactory for the observation of the eigenmodes in a slab profile laser-fusion experiment. Generally, this requires a laser power $P_o \gtrsim 3 \times 10^{12}$ watts, although this power requirement can be reduced somewhat ($\sim \Delta x_L/d_L$) by using a noncircular focal cross-section; for this purpose, a density scale length $L_n \gtrsim \gtrsim 100\ \mu m$ seems best since the required d_L is then sufficiently large that one can adjust Δx_L to satisfy $d_L >> \Delta x_L \gtrsim 30\ \mu m$ (also, larger d_L allows the laser power to be delivered over a longer pulse duration before the laser ponderomotive force and local plasma heating have a chance to create density gradients

over the focal diameter d_L; at 1 keV temperature, sound waves take 3 pico-sec to travel 1 μm). Thus, this appears to be one possible explanation for the lack of experimental evidence for these eigenmodes. In the next section, we will consider the modifications introduced by a spherical pellet-plasma.

b. Spherical Plasma

The eigenmode calculation has been extended to the case of a spherical nonuniform plasma $n = n(r)$ by Liu, Rosenbluth, and White (Ref. G IX). They reduced the problem down to two dimensions by considering a cross-section of the spherical pellet containing both the incident laser $\hat{k}_o = \hat{z}$ and the scattered electromagnetic wave $\hat{k}_1 = \hat{y}$. Expanding $n = n_o\left[1 - (r - r_o)/L_n\right]$ about the resonance position (i. e., radius) r_o, and taking the center of the sphere at $(z = r_o, y = 0)$, they then used the approximation $r \approx r_o - z + y^2/2r_o$ in $n(r)$ (valid for $|z/r_o| \ll 1$ and $|y/r_o| \ll 1$). By dropping the $\partial^2/\partial y^2$ term in Eq. (I.21) (valid for $|y/r_o| \ll 1$), and factorizing $\underline{E}_1(z, y, \omega_1) = \underline{E}_1(z', \omega_1, k_{1y}) \exp\left[ik_{1y}\, y(1 + z'/r_o + y^2/6r_o^2)\right] +$ + c.c. with $z' \equiv z - y^2/2r_o$, they obtained an equation for $E_1(z', \omega_1, k_{1y})$ identical in form to Eq. (I.25a) with z replaced by z' but with the additional term $-2k_{1y}^2\, z'/r_o$ added to $Q(z', \omega_1, k_{1y})$. This in turn gives an equation

identical in form to Eq. (V.2) but in terms of a variable $\rho' \equiv a\rho(z', \omega_1, k_{1y})$, parameters $\lambda' \equiv \lambda/\sqrt{a}$ and $X' \equiv \equiv \left[X + 2ic^2k_{1y}^2(\gamma + \nu_p)L_n/\omega_p r_o D\right]/a$, and the function $q'(z', X') \equiv 2X' - \rho' + 1/\rho'$, where $\gamma \equiv \mathrm{Im}\,\omega_1$ is the growth rate and $a \equiv (1 + 2c^2k_{1y}^2L_n/\omega_p^2 r_o)^{\frac{1}{2}}$. Thus, all of our results obtained in sec. V A-C are still valid provided we substitute ρ' for ρ, λ' for λ, and X' for X everywhere. We do not wish to go into this in any more detail here but rather just point out that the spherical plasma modifications, to our previous slab plasma results, are small whenever $2(ck_{1y}/\omega_A)^2(\omega_A/\omega_p)^2L_n/r_o \lesssim 1$.

For proposed laser-pellet fusion reactors (Ref. sec. J), typically $L_n \gtrsim 100$ μm and $r_o \gtrsim 600$ μm giving $2(ck_{1y}/\omega_A)^2 \cdot (\omega_A/\omega_p)^2L_n/r_o \gtrsim 1$ for $\omega_A/\omega_p = 2$. Thus, Eqs. (V.86a, b) and $P_o \gtrsim 3 \times 10^{12}$ watts are still approximately correct in giving the necessary conditions for observing the eigenmodes. Equation (V.86b) can be checked another way by noticing that the back- and side-scatter wave-packet saturation is due to suffering a density change corresponding to a change in position of half the resonance zone width, or $h/2$, and that a corresponding density change in the spherical case with z held fixed requires a distance along y of $(r_o h)^{\frac{1}{2}}$. Thus, an effective resonance zone width along y is $h_y \gtrsim 2(r_o h)^{\frac{1}{2}}$, and the <u>maximum required</u> laser focal diameter (i. e., an upper bound on the quantity that

appears on the right in Eqs. (V.81b, 86b, etc.)) is necessarily $2h_y \stackrel{\sim}{>} 4(r_o h)^{\frac{1}{2}}$ (it is an upper bound because refraction will not allow z to remain fixed, but will cause an earlier saturation than predicted by h_y alone and, thus, an earlier appearance of the eigenmodes and a less stringent requirement on d_L for their observation). We can, therefore, believe Eqs. (V.81b and 86b) whenever they give an smaller requirement on d_L than $4(r_o h)^{\frac{1}{2}}$; otherwise, the curvature of the spherical plasma has a major effect on the side-scattered wave-packet saturation. In our present case with $h \stackrel{\sim}{>} 14$ μm, both estimates give 370 μm.

The intensity given by Eq. (V.86a) is exceeded in typical proposed laser-pellet reactors (Ref. sec. J). However, $d_L/2 \sim$ $\sim 200\,\mu$m does not very well satisfy $|y/r_o| \ll 1$ (a requirement in the extension of the eigenmodes to a spherical plasma), and this may lead to an early saturation of the eigenmodes at a level comparable to that of the side-scattered wave-packet. Also, although in a laser-pellet reactor the intensity is required to be highly uniform (multiple over-lapping laser beams), the polarization will not be uniform but rather will change on a distance scale d_{pol} comparable to the spacing of the individual laser beam focal centers. This spacing or d_{pol} may or may not exceed 370 μm, and if $d_{pol} < 370\,\mu$m the eigenmodes would saturate early before they could be observed above the side-scattered

wave-packet. For the side-scattered wave-packet, $y_s \gtrsim 185$ μm, so its convective saturation would remain at Γ_2 except for very small d_L or d_{pol}. At an intensity of $I_o = 10^{16}$ watts/cm^2, $\Gamma_2 \gtrsim 32$ and $y_s \gtrsim 270$ μm, and even if d_{pol} were reduced to 150 μm $\Gamma_2 \gtrsim 18$ would still be sufficiently large that the side-scattered wave-packet and eigenmodes would probably saturate together and at an earlier nonlinear level. Since growth sufficiently large as to require nonlinear (as opposed to linear convective) saturation is undesirable (as discussed in sec. I A 1), and an intensity as high as 10^{16} watts/cm^2 is typical, this indicates possible <u>future</u> problems (in spite of the previously discussed, and expected, lack of present experimental evidence for the Raman instability) that may be encountered as laser-fusion experiments approach the parameters typical of proposed laser-pellet fusion reactors. It should be pointed out, however, that random density fluctuations $\delta n/n_o \gtrsim h/2L_n \sim 0.1$ over a density scale $y < y_s \sim 200\,\mu$m would tend to decrease the growth rate over the refraction saturation distance y_s and thus reduce Γ_2 below our expression. Also, going to an appropriate noncircular focal cross-section (shortened perpendicular to the polarization), for each separate laser beam incident on the pellet, would reduce d_L.

3. Computer Simulation

In computer simulations (see Ref. sec. L) with periodicity typically assumed along y, there is no finite resonance region along y to convectively saturate the growing eigenmodes. The response will therefore continue to evolve until at least the eigenmodes saturate by nonlinear processes; the side-scattered wave-packet will saturate convectively (by refraction) at an exponentiation Γ_2 above noise unless Γ_2 is so large ($\gtrsim \ell n(n\,\lambda_D^2)$, the coulomb logarithm) that nonlinear processes have also caused an early saturation here too. Thus, in such simulations the response always evolves eventually (provided $\lambda > \lambda_o \gtrsim 0.3$, the eigenmode threshold from Eq. (V.31b)) to a nonlinear stage where the eigenmodes are dominant over -- or at least comparable with -- the side-scattered wave-packet; the time required for this to occur is given roughly by Eq. (V.81a). This would correspond to an experimental situation where either d_L satisfies Eq. (V.81b) and I_o exceeds the threshold given by $\lambda > \lambda_o \gtrsim 0.3$ or, although d_L may not satisfy Eq. (V.81b), Γ_2 from Eq. (V.81e) is so large that the side-scattered wave-packet -- and possibly even the eigenmodes -- have nonlinearly saturated at an exponentiation below Γ_2. In order to suppress this automatic nonlinear evolution in periodic plasma simulations,

one could simulate a pericdic array of plasma blocks separated by a distance $y \lesssim y_s$ (in an attempt to disperse the waves forming the eigenmode before they reach the next plasma block with its corresponding resonance zone). Of course, one would need only one plasma block centered on the spatial grid and surrounded on both sides by a vacuum region (width $\lesssim y_s$); the pericdic boundary conditions would then simulate automatically the other plasma blocks. Or, one could use absorbing boundaries to end the eigenmode growth and thereby simulate the effects of finite d_L.

VI. CONCLUSION

We have investigated the electromagnetic "Green's function" response to a delta-function transverse current source in a plasma which can be nonuniform and pumped by a laser driving the Raman instability. The precise meaning of these terms, the configuration used, and basic approximations and restrictions have been given in the introductory section. We have considered the four basic cases — a. Uniform, No Pump; b. Nonuniform, No Pump; c. Uniform, Pumped; d. Nonuniform, Pumped — with particular emphasis placed on mathematical similarities and differences among the four cases. By applying the same mathematical procedure to all four cases, we have been able to demonstrate that the Green's function for case (d) reduces to the appropriate Green's function for cases (a) - (c) as the pump strength goes to zero or the nonuniformity scale length goes to infinity. In particular, the eigenvalues found to occur in case (d) either vanish or require an infinitely long time to observe as one approaches cases (a) - (c).

The response in cases (a) - (c) consists of wave-packets (possibly growing) of different frequency, each traveling along a well-defined space-time (z - t) trajectory labeled by the saddle-point frequency. The response in case (d) consists of such wave-packets with the addition of localized growing eigenmodes.

These eigenmodes dominate at late times over the transient refracting wave-packets. However, for very early times case (d) reduces to case (c) and the wave-packets predominate. In fact, in the section on case (d), we have shown that the eigenmode response does not dominate until after refraction has saturated that convectively growing wave-packet whose turning point coincides with its resonance zone. This "side-scattered" wave-packet has the largest saturation amplitude of any wave-packet since it remains within its resonance zone the longest time. In applying the results obtained here to any experiment, one must first compare the temporal duration of the laser pulse with the "side-scatter wave-packet saturation time" to determine whether one is in the "transient" or "eigenmode" regime. This discussion is for the model assumed here (i. e., periodic in x and y, with the response given in the z-t plane); for a more realistic model (i. e., a source localized in y as well as in z and t, and a laser of finite extent along y), one should also compare the spatial width of the laser beam pulse with the "sidescatter wave-packet saturation distance" obtained by multiplying the above time by the wave-packet group velocity along y. Here we are assuming that the integration of our periodic Green's function over k_y merely introduces a convective behavior along y with wave-packet trajectories, extending into y-z-t space, labeled

by a saddle-point frequency and y wavevector.

For parameters typical of a theta-pinch, we found a refraction saturation time of a few nanoseconds and a refraction saturation distance of tens of centimeters — much larger than either typical laser beam diameters or theta-pinch plasma diameters. Therefore, we expect a negligible effect from the eigenmodes and that a local convectively growing wave-packet approach neglecting refraction would be more appropriate. Backscattered waves would be saturated by passing out of the resonance zone, and sidescattered waves would be saturated by passing out of the finite diameter laser beam. For parameters typical of a laser-fusion experiment, we found a refraction saturation time on the order of a picosecond — much smaller than the laser pulse duration. However, the refraction saturation distance was found to be 40 microns or more — marginally greater than typical focal spot diameters for a single intense laser beam. Our above conclusion then usually applies here also. For a laser-fusion computer simulation, however, the system is periodic along y — infinitely wide plasma and laser beam, and a discrete set of k_y values — and, after the refraction saturation time (on the order of a picosecond), the temporally growing eigenmodes will dominate. The convective nature of the eigenmodes along y is lost due to the periodicity.

ACKNOWLEDGMENTS

To my advisor, Allan N. Kaufman, I wish to express my gratitude for all the time he has spent, and patience he has demonstrated, in teaching me what a physicist should be and in preparing me to become one.

In the several years that have gone into this thesis, my wife Sherry has been an unending source of encouragement. I thank her and my two sons, Edward and Christopher, for all their understanding and support. Considerable thanks are also due to my parents for their support over all the years of my education.

I greatly appreciate the stimulating discussions I have had with fellow graduate students Bruce Cohen, Harry Mynick, Dwight Nicholson, and Gary Smith. Also deserving of recognition here, for his help with some of the computer plots, is Phillip Yau.

I have greatly benefited from enlightening conversations and useful information and references provided by Vladimir Fuchs, George Johnston, Shayne Johnston, A. Bruce Langdon, C. S. Liu, and Claire Max.

To Charles K. Birdsall and Wulf B. Kunkel, I owe my thanks for providing general guidance through my years as a graduate student.

Finally, I wish to thank Georgella Perry for her general assistance while I was a graduate student, and Dessa Bucksbaum for typing this thesis.

* This work was supported by the U. S. Energy Research and Development Administration, under the auspices of the Division of Physical Research.

FIGURE CAPTIONS

Chapter I

I.1 Density regions associated with various instabilities.

I.2 Raman instability in a uniform plasma (backscatter shown). V_1 and V_2 are group velocities of the scattered waves.

I.3 Diagram of $(\omega_1, \underline{k}_1)$ for resonance $\Delta_1 = \Delta_2 = 0$. For a cold plasma, resonance shell in $\underline{k}_1$-space is a sphere and $\omega_1(\underline{k}_1) = \omega_o - \omega_p$ is independent of $\hat{k}_1$.

I.4 Space-time response for given $(\omega_1, \underline{k}_1)$.
(a). Back-scatter; (b). Oblique-scatter.

I.5 (a). Back-scatter ($V_1 V_2 < 0$) in a density gradient.
(b). Pulse growth and saturation.

I.6 (a). Oblique-scatter in a density gradient.
(b). Pulse growth and saturation.

I.7 (a). Side-scatter in a density gradient.
(b). Pulse growth ($\underline{V}_1$ and $\underline{V}_2$ z-dependence ignored).

I.8 Refraction of side-scattered wave-packet (turning point coincides with resonance zone center at z_o) for given $\underline{k}_{1\perp}$. Growth occurs only for $0 \leq t \leq t_s$, while wave-packet is in resonance zone.

I.9 Several representative wave-packets for the space-time response with given $\underline{k}_{\perp}$ and no pump. The lowest frequency non-evanescent wave-packet is (a) which has its turning point at the source position z_s. Both wave-packets (b) have the same frequency but initially propagate in opposite directions along z. The wave-packets (c) have very high frequency, propagate with essentially the speed of light along z, and define the light-cone below which there is no response.

I.10 Representative wave-packets for the pumped space-time response with given $\underline{k}_{\perp}$. The side-scattered wave-packet (a) encounters its resonance zone at its turning point position. The temporally growing eigenmodes (with maximum growth rate) are localized within the resonance zone (a). A wave-packet of lower frequency than (a) encounters its turning point before its resonance zone and does not grow. The two oblique (or back)-scattered wave-packets (b) enounter their resonance zone (b) (at different times) in the underdense region to the left of the source position z_s. A wave-packet, of much higher frequency than (b), encounters the uniform plasma or vacuum to the left of $z = 0$ before its resonance zone (e. g., $\omega > \omega_o$) and does not grow.

I.11 Density profile showing boundary at $z = 0$ between uniform (or vacuum) and nonuniform plasma regions. The density gradient $d\omega_p^2(z)/dz \equiv \omega_p^2/L_n$ is taken to be constant. The electromagnetic pump wave is incident along the density gradient. The delta-function source $\delta(z - z_s)$, for the scattered electromagnetic waves, is located at position z_s.

I.12 Orientation of the three waves, the electromagnetic fields, and the nonlinear currents and charge densities for the special case of side-scattering with $k_{1x} = 0$. The longitudinal current $\underline{J}_L(\Omega)$ drives $\delta n(\Omega)$ (i. e., the Langmuir wave). The transverse current $\underline{J}_T(\omega_1)$ drives $\underline{E}_1$ and $\underline{B}_1$ of the side-scattered electromagnetic wave. The electron oscillation velocities $\underline{v}_o$ and $\underline{v}_1$ are used in obtaining currents and $\underline{v} \times \underline{B}$ forces.

I.13 The complex ω_1-plane showing the Bromwich contour B and the depressed contour B'. The semi-circle of radius R (dashed line) gives negligible contribution to the integral as $R \to \infty$. The branch-points and branch-cuts shown are for the uniform unpumped plasma. $\omega \equiv (\omega_p^2 + c^2k_{11}^2)^{\frac{1}{2}}$, and ν_1 represents damping.

FIGURE CAPTIONS

Chapter III

III.1 Trajectories of wave-packets of constant frequency ω_A (straight lines) and lines of constant phase Ψ (hyperbolas), for uniform unpumped plasma. The source is at position z_s, and $\omega^2 \equiv \omega_p^2 + c^2 k_{1\perp}^2$. Outside the light-cone, the response is zero.

III.2 Space-time diagram, for nonuniform unpumped plasma, showing the eight different regions used in calculating the asymptotic response G_1. The dimensionless variables are $\tilde{t} \equiv \omega_s t/\xi$ and $\tilde{z} \equiv \omega^2(z)/\omega_s^2$, where $\omega^2(z) \equiv \omega_p^2(z) + c^2 k_{1\perp}^2$, $\omega_s \equiv \equiv \omega(z_s)$, and $\xi \equiv L_n \omega_s^3/c\omega_p^2$. The source z_s is at $\tilde{z} = 1$, while the boundary $z = 0$ (between uniform and nonuniform plasma) is at $\tilde{z}(z = 0)$ and lies between $\tilde{z} = 0$ and $\tilde{z} = 1$.

III.3 Trajectories of wave-packets of constant frequency $\tilde{\omega}_A \equiv \omega_A/\omega_s$ (lines ending at the point $\tilde{z} = 1$, $\tilde{t} = 0$) and lines of constant phase Ψ (hyperbola-like lines). The dashed line is the line of turning points for wave-packets with different $\tilde{\omega}_A$. See Fig. III.2 for further definitions.

III.4 Plot of Green's function $(2/c)G_1$ on vertical axis (same as $\tilde{t}$), at various fixed times $\tilde{t}$, as a function of position $\tilde{z}$. Various time intervals (of duration $\Delta\tilde{t} = 0.1$)

have been purposely left blank. We have multiplied $(2/c)G_1$ by 0.0075 in Fig. III.4a and by 0.02 in Figs. III.4b-d, and have used $\xi = 300$. Note change of plotting scale in going from Figs. III.4a to b.

III.5 The complex Y-plane showing the branch-cuts between +i and -i and the five saddle-point solutions $Y_N(\eta)$, with $\eta \equiv |z - z_s|/ct$. This is for the uniform pumped plasma. Fig. III.5a shows the sheet labeled $\lceil 3 \rceil$ in sec. III C with the solutions I - III. Fig. III.5b shows the sheet labeled $\lceil 4 \rceil$ with solutions IV and V. $b \equiv (\omega_R - \omega)/2\gamma_o$ and $a \equiv (b/2)^{1/3}$, where γ_o is the uniform plasma growth rate given by Eq. (I.2), $\omega^2 \equiv \omega_p^2 + c^2k_{1\perp}^2$, and $\omega_R \equiv \omega_o - \omega_p$.

III.6 Contours, in the complex ω_1-plane, of constant $\mathrm{Re}(\Psi)$ (solid lines) and constant $\mathrm{Im}(\Psi)$ (dashed lines), for the uniform unpumped plasma (but discussed also in sec. III C). The saddle-point frequency $\omega_A(\eta)$, $\eta \equiv |z - z_s|/ct$, is shown as well as the contour of steepest descent, passing through ω_A, which lies partially on both of the two Riemann sheets shown in Figs. III.6a, b. The branch-cuts extend from $\pm\omega$ to infinity along the real ω_1-axis. $\omega^2 \equiv \omega_p^2 + c^2k_{1\perp}^2$.

FIGURE CAPTIONS

Chapter IV

IV.1 Generalized Stokes (dashed) and anti-Stokes (solid) lines, with arrows indicating direction of propagation (on anti-Stokes lines) and growth (on Stokes lines). The arrows are labeled (e. g., +i, -2i) according to the value of the WKBJ coefficient (a_1 or a_2) for that WKBJ solution corresponding to that arrow (if no label is present for an arrow, the coefficient is taken to equal 1). For cases (a, b), the transition point is a first order zero, and two different boundary conditions (designated b. c.) are taken: incoming wave (a) or outgoing wave (b). For cases (c,d), the transition point is a first order pole, and the boundary conditions are incoming (c) or outgoing (d).

IV.2 Generalized Stokes and anti-Stokes lines for the pole (p) - zero (z) combination. The intrinsic branch-cut is chosen to lie in the upper-half-plane. The solution (arrows and labels) is obtained by the procedure given in sec. IV B. Case (a): incoming wave from left is partially reflected, with outgoing wave on the right (boundary condition b. c.). Case (b): incoming wave is not reflected if one uses an outgoing wave on left (b. c.). Large circle indicates that the pole-zero pair can be treated as a "compound" transition

point, with Stokes constants T_n. One reaches T_2 by going through the intrinsic branch-cut in a counterclockwise direction.

FIGURE CAPTIONS

Chapter V

V.1 The complex X-plane, showing the branch-cut used in defining $\rho_+ \equiv X + (X^2 + 1)^{\frac{1}{2}}$ and $\rho_- \equiv X - (X^2 + 1)^{\frac{1}{2}}$ such that $|\rho_+| \geq 1$ and $|\rho_-| \leq 1$.

V.2 The complex ρ-plane, showing the positions of $\rho_+(X)$ and $\rho_-(X)$, for three values of $|X|$ (2, 1, 0.5), as $\theta = \arg(X)$ varies from 0 to 180 degrees. The positions are symmetric about the real ρ-axis for $\mathrm{Im}X \leq 0$ and $\mathrm{Im}X \geq 0$.

V.3 The positions of the Stokes (dotted) and anti-Stokes (solid) lines for $|X| = 4/3$ and various values of $\theta = \arg(X)$:

(a). $\theta = 0$; (b) $\theta = \pi/8$; (c) $\theta = \pi/4$; (d) $\theta = 3\pi/8$;

(e) $\theta = \pi/2$; (f) $\theta = 5\pi/8$; (g) $\theta = 3\pi/4$;

(h) $\theta = 7\pi/8$; (i) $\theta = \pi$. There are two roots of $q(\rho)$, at $\rho_+(X)$ and $\rho_-(X)$, and one pole, at $\rho = 0$.

V.4 The positions of the Stokes (dotted) and anti-Stokes (solid) lines for $|X| = 0.93$ and various values of $\theta = \arg(X)$:

(a) $\theta = 0$; (b) $\theta = \pi/8$; (c) $\theta = \pi/4$; (d) $\theta = 3\pi/8$;

(e) $\theta = \pi/2$; (f) $\theta = 5\pi/8$; (g) $\theta = 3\pi/4$; (h) $\theta = 7\pi/8$;

(i) $\theta = \pi$.

V.5 The positions of the Stokes (dotted) and anti-Stokes (solid) lines for $|X| = 0.80$ and various values of $\theta = \arg(X)$:
(a) $\theta = 0$; (b) $\theta = \pi/16$; (c) $\theta = \pi/8$;
(d) $\theta = 3\pi/16$; (e) $\theta = \pi/4$; (f) $\theta = 5\pi/16$;
(g) $\theta = 3\pi/8$; (h) $\theta = 7\pi/16$; (i) $\theta = \pi/2$.

V.6 The positions of the roots ($\omega_I(z)$, $\omega^o_{II}(z)$, and $\omega^o_{III}(z)$) and poles ($\omega^\infty_{II}(z)$ and $\omega^\infty_{III}(z)$) of $Q(z, \omega_1, \underline{k}_{1\perp}) = \lambda^2(d\rho/dz)^2 q(\rho,X)$, and the branch-cuts in the complex ω_1-plane used in defining $\sqrt{Q}$, for several typical values of z (shown in Fig. V.7) along the real z-axis:
(a) $z = 0$; (b) $z = z' > 0$; (c) $z = z'' > z'$;
(d) $z = z''' > z''$. The roots, poles, and branch-cuts are symmetric about the imaginary ω_1-axis. The solutions $A(\rho,X)$ and $B(\rho,X)$ have intrinsic branch-cuts (not shown) which we take to extend vertically downward from $\omega^\infty_{II}(z)$ and from $\omega^\infty_{III}(z)$. $\omega^2 = \omega_p^2(z) + c^2k_{1\perp}^2$.

V.7 The positions of the roots ($z_-(\omega_1)$ and $z_+(\omega_1)$) and the pole ($z_\infty(\omega_1)$) of $Q(z, \omega_1, \underline{k}_{1\perp}) = \lambda^2(d\rho/dz)^2 q(\rho,X)$, and the branch-cuts in the complex z-plane used in defining $\sqrt{Q}$, for several typical values of ω_1 (shown in Fig. V.6):
(a) $\omega_1 = \omega_I(z = 0)$; (b) $\omega_1 = \omega_I(z')$; (c) $\omega_1 = \omega_I(z'')$;
(d) $\omega_1 = \omega_I(z''')$; (e) $\omega_1 = \omega'$; (f) $\omega_1 = \omega''$;
(g) $\omega_1 = \omega'''$. Also shown is the relation between the

complex z- and ρ-planes, with the corresponding points being $(z_\infty, \rho_\infty = 0)$, (z_-, ρ_-), and (z_+, ρ_+).

V.8 The WKBJ approximation for the solutions $A(\rho,X)$ and $B(\rho,X)$ in the complex ρ-plane (compare with Fig. V.7e), for $X(\omega_1, \underline{k}_{1\perp})$ evaluated at $\omega_1 = \omega'$ shown in Fig. V.6a. The imposed boundary conditions (b. c.) are : (a) $A = f_1$ as $\rho \to +\infty$; (b) $B = f_2 \pm g_2$ above or below the branch-cut as $\rho \to -\infty$. The solutions f_n and g_n are given in Eq. (V.9). The solutions A and B have an intrinsic branch-cut (not shown) extending essentially (for Re $\omega_1 < \omega_o$) vertically downward from $\rho = 0$.

V.9 Same as Fig. V.8, but with $\omega_1 = \omega''$ shown in Fig. V.6a. See also complex ρ-plane in Fig. V.7f.

V.10 Same as Fig. V.8, but with $\omega_1 = \omega'''$ shown in Fig. V.6a. See also complex ρ-plane in Fig. V.7g.

V.11 The complex X-plane, showing the eigenvalues $X_N(\lambda)$, N = 0,1,2..., for several values of the pump strength parameter λ: (a) $\lambda = 0.30$; (b) $\lambda = 0.60$; (c) $\lambda = 0.90$; (d) $\lambda = 1.20$; (e) $\lambda = 1.50$.

V.12 (a) The complex X-plane, showing the position of the eigenvalue $X_o(\lambda)$ for the values of λ used in Fig. V.11; (b) The imaginary part of $X_o(\lambda)$ vs. λ, showing the cross-over ($\mathrm{Im}X_o = 0$) at $\lambda_o = 0.32$ corresponding to threshold (in absence of damping). From part (b), $X_o(\lambda_o) = 0.92$.

V.13 The complex ω_1-plane, showing the eigenvalues $\omega'_{1N}(\lambda)$, $N = 0,1,2,\ldots$, (corresponding to the $X_N(\lambda)$ of Fig. V.11) for $\lambda = 0.6$ and $\nu_p \approx \gamma_o/3$, where the uniform plasma growth rate γ_o (see Eq. I.2) is evaluated at $\omega_1 = \omega''_R \equiv \equiv (\omega_o + c^2k_{1\perp}^2/\omega_o)/2$. The drawing is only qualitative, with the imaginary axis expanded by a factor of two and $\gamma_o = \omega_o/20$ chosen for convenience to illustrate the detail. Also shown are the boundaries (dashed lines) representing the constraints on the eigenvalues, as discussed in sec. V B 3: $-\nu_p \leq \mathrm{Im}(\omega'_{1N}) < \gamma_o$ and $\omega''_R < \mathrm{Re}(\omega'_{1N}) \lesssim \omega_o - \omega_p(z = 0)$.

V.14 Space-time plot showing the regions where the saddle-points have different forms. The symbols a, b, a', b' correspond to the functions defined in Eq. (V.37). The boundaries between the various regions are formed by the following lines: the wave-packet trajectories (lines of essentially constant saddle-point frequency ω') where $z_+(\omega') = z_s$ and $\omega' = \omega_s \equiv \left[\omega_p^2(z_s) + c^2k_{1\perp}^2\right]^{\frac{1}{2}}$ (the minimum possible saddle-point frequency, where z_s = source position), where $\omega' \to \infty$ (the light-cone), and where the resonance position $z_\infty(\omega')$ equals zero, z_s, or the turning point position $z_+(\omega')$; the line of turning points where $z_+(\omega') = z_g$ and $\omega' = \omega_g \equiv \left[\omega_p^2(z_g) + c^2k_{1\perp}^2\right]^{\frac{1}{2}}$ (z_g equals greater of z or z_s); the line of points on the wave-packet trajectories where

$z_g = z_\infty(\omega')$ (not same as line where $z_\infty = z_+$). The boundary lines depend upon the saddle-point frequency ω' and have been drawn assuming the special case $\omega' \approx \omega_A$, the unpumped solution (sec. III B).

V.15 The exponentiation factor $\mathrm{Re}(\theta_2)$, evaluated at the turning point time given by Eq. (V.71), as a function of the distance $\delta z \equiv \mathrm{Re}(z_+) - z_s$ between the source z_s and the turning point z_+. $\delta\rho \equiv \delta z/\lambda^{2/3}Z$, and h is the resonance zone width from Eq. (V.77). Γ_2 is the side-scatter exponentiation factor given by Eq. (V.74).

REFERENCES

A. Reviews of Laser-plasma Interactions

I. R. E. Kidder, Physics of High Energy Density (Academic Press Inc., New York, 1971), p. 306.

II. F. F. Chen, Laser Interaction and Related Plasma Phenomena, edited by H. Schwarz and H. Hora (Plenum Press, New York, 1974), Vol. 3A, p. 291.

III. D. F. DuBois, Laser Interaction and Related Plasma Phenomena, edited by H. Schwarz and H. Hora (Plenum Press, New York, 1974), Vol. 3A, p. 267.

IV. W. Kruer, E. Valeo, K. Estabrook, J. Thomson, B. Langdon, and B. Lasinski, Fifth IAEA Conference on Plasma Physics and Controlled Nuclear Fusion Research, Tokyo, Japan (1974), UCRL-75537 (1974).

V. Advances in Plasma Physics, edited by A. Simon and W. Thompson (John Wiley and Sons Inc., Publishers, 1976), Vol. 6.

VI. M. Kristiansen and M. O. Hagler, Nuclear Fusion 16, 999 (1976) (Laser heating of magnetized plasmas).

See also D V; G III, VII.

B. Brillouin in Solid State Physics

I. L. Brillouin, Ann. Phys. (Paris) 17, 88 (1922).

II. N. M. Kroll, J. Appl. Phys. 36, 34 (1965).

III. Y. R. Shen and N. Bloembergen, Phys. Rev. 137, 1787 (1965).

IV. C. L. Tang, J. Appl. Phys. 37, 2945 (1966).

V. N. Bloembergen, Am. J. Phys. 35, 989 (1967).

C. Raman in Solid State Physics

I. C. V. Raman, Indian J. Phys. 2, 387 (1928).

II. C. V. Raman and U. S. Krishnan, Nature 121, 501 (1928).

III. P. A. Wolff, Proceedings 2nd International Conference on Light Scattering in Solids (Paris, 1971).

D. Brillouin in Plasmas

I. I. S. Danilkin, Sov. Phys. Tech. Phys. 10, 524 (1965).

II. V. Ts. Gurovich and V. I. Karpman, Sov. Phys. JETP 29, 1048 (1969).

III. S. E. Bodner and J. L. Eddleman, Phys. Rev. A5, 355 (1972).

IV. D. Forslund and A. Galeev, International Centre for Theoretical Physics, Trieste, Italy, Report IC/73/125 (1973).

V. M. Rosenbluth and R. Sagdeev, Comments on Plasma Physics and Controlled Fusion 1, 129 (1973).

VI. W. L. Kruer, E. J. Valeo, and K. G. Estabrook, Fifth Annual Symposium on Anomalous Absorption of Intense High Frequency Waves, UCLA (1975), UCRL-76612 (1975).

See also E I, X; F VII, IX; G VII, XIII; K III.

E. Raman Instability in Uniform Plasma

I. T. F. Volkov, Plasma Physics and the Problem of Controlled Thermonuclear Reactions (Pergamon Press, New York, 1960), Vol. 4, p. 114.

II. N. Bloembergen and Y. R. Shen, Phys. Rev. 141, 29 (1966).

III. G. G. Comisar, Phys. Rev. 141, 200 (1966).

IV. D. L. Bobroff and H. A. Haus, J. Appl. Phys. 38, 390 (1967).

V. N. E. Andreev, Zh. Eksp. Teor. Fiz. 59, 2105 (1972), Sov. Phys. JETP 32,1141 (1971).

VI. N. M. Kroll and P. L. Kelley, Phys. Rev. A4, 763 (1971).

VII. E. S. Cassedy and C. R. Evans, J. Appl. Phys. 43, 4452 (1972).

VIII. A. Bers, F. W. Chambers, and R. J. Hawryluk, Q. P. R.No. 111, R. L. E., M. I. T. (1973).

IX. Abraham Bers, Q. P. R. No. 113, R. L. E., M. I. T. (1974), PRR-752 (1975), Proceedings of the U. S. - Australian Plasma Wave Seminar AINSE, Sydney, Australia, 1975.

X. J. F. Drake, P. K. Kaw, Y. C. Lee, G. Schmidt, C. S. Liu, and Marshall N. Rosenbluth, Phys. Fluids 17, 778 (1974).

See also G XII.

F. Raman Instability in Nonuniform Plasma, Backscatter

I. A. D. Piliya, *Proceedings 10th Conference on Phenomena in Ionized Gases*, Oxford (1971).

II. M. N. Rosenbluth, Phys. Rev. Lett. 29, 565 (1972).

III. J. F. Drake and Y. C. Lee, Phys. Rev. Lett. 31, 1197 (1973).

IV. L. M. Gorbunov, Usp. Fiz. Nauk 109, 631 (1973), Sov. Phys. Uspekhi 16, 217 (1973).

V. G. Laval, R. Pellat, and D. Pesme, Phys. Lett. 46A, 281 (1973).

VI. M. N. Rosenbluth, R. B. White, and C. S. Liu, Phys. Rev. Lett. 31, 1190 (1973).

VII. C. S. Liu, M. N. Rosenbluth, and R. B. White, Phys. Fluids 17, 1211 (1974).

VIII. Bruce I. Cohen, Ph. D. Thesis, University of California, Berkeley, LBL-3291, 1975.

IX. D. W. Forslund, J. M. Kindel, and E. L. Lindman, Phys. Fluids 18, 1002 (1975).

X. Dwight R. Nicholson, Ph. D. Thesis, University of California, Berkeley, LBL-3267, 1975.

XI. Kyoji Nishikawa and C. S. Liu, Advances in Plasma Physics, edited by A. Simon and W. Thompson (John Wiley and Sons Inc., Publishers, 1976), Vol. 6, p. 3.

See also G I - III, VII, VIII, XII, XIII; K I.

G. Raman Instability in Nonuniform Plasma, Back- and Side-scatter

I. M. A. Mostrom, D. R. Nicholson, and A. N. Kaufman, Nonlinear Attenutation of an Electromagnetic Beam by Side- and Back-scattering in an Inhomogeneous Plasma, LBL-2032, May 1973 and Bull. Am. Phys. Soc. 17, 1065 (1972).

II. A. A. Galeev, G. Laval, T. M. O'Neil, M. N. Rosenbluth, and R. Z. Sagdeev, ZhETF Pis. Red. 17, 48 (1973), Sov. Phys. JETP Lett. 17, 35 (1973).

III. A. A. Galeev, G. Laval, T. O'Neil, M. N. Rosenbluth, and R. Z. Sagdeev, Zh. Eksp. Teor. Fiz. 65, 973 (1973), Sov. Phys. JETP 38, 482 (1974).

IV. R. Z. Sagdeev, Usp. Fiz. Nauk 110, 437 (1973), Sov. Phys. Usp. 16, 557 (1974).

V. C. S. Liu, M. N. Rosenbluth, and R. B. White, Phys. Rev. Lett. 31, 697 (1973).

VI. H. H. Klein, W. M. Manheimer, and E. Ott, Phys. Rev. Lett. 31, 1187 (1973).

VII. M. N. Rosenbluth and R. Z. Sagdeev, Nuclear Fusion 13, 941 (1973), Comments on Plasma Physics and Controlled Fusion, 11, No. 1, 3 (1974).

VIII. P. Kaw, R. White, D. Pesme, M. Rosenbluth, G. Laval, R. Varma, and F. Huff, International Centre for Theoretical Physics, Trieste, Italy, Report IC/73/142 (revised 1974),

Comments on Plasma Physics and Controlled Fusion, 11, No. 1, 11 (1974).

IX. C. S. Liu, M. N. Rosenbluth, and R. White, Proceedings of the Fifth Conference on Plasma Physics and Controlled Nuclear Fusion Research, Tokyo, 1974 (International Atomic Energy Agency, Vienna, 1975), Vol. II, p. 515.

X. V. P. Silin and A. N. Starodub, Zh. Eksp. Teor. Fiz. 67, 2110 (1974), Sov. Phys. JETP 40, 1047 (1975).

XI. D. Biskamp and H. Welter, Phys. Rev. Lett. 34, 312 (1975).

XII. Frank W. Chambers, Ph. D. Thesis, Massachusetts Institute of Technology, 1975.

XIII. C. S. Liu, Advances in Plasma Physics, edited by A. Simon and W. Thompson (John Wiley and Sons, Inc., Publishers, 1976), Vol. 6, p. 121.

See also F VII.

H. Laser-Fusion Experiments

I. J. W. Shearer, S. W. Mead, J. Petruzzi, F. Rainer, J. E. Swain, and C. E. Violet, Phys. Rev. A 6, 764 (1972).

II. J. L. Bobin, M. Decroisette, B. Meyer, and Y. Vitel, Phys. Rev. Lett. 30, 594 (1973).

III. M. Decroisette, B. Meyer, and Y. Vitel, Phys. Lett. 45A, 443 (1973).

IV. L. M. Goldman, J. Soures, and M. J. Lubin, Phys. Rev. Lett. 31, 1184 (1973).

V. G. H. McCall, F. Young, A. W. Ehler, J. F. Kephart, and R. P. Godwin, Phys. Rev. Lett. 30, 1116 (1973).

VI. J. Soures, L. M. Goldman, and M. Lubin, Nuclear Fusion 13, 829 (1973).

VII. V. D. Dyatlov, R. N. Medvedev, V. N. Sizov, and A. D. Starikov, ZhETF Pis. Red. 19, 124 (1974), JETP Lett. 19, 76 (1974).

VIII. Laser Interaction and Related Plasma Phenomena, edited by H. Hora and H. J. Schwartz (Plenum, New York, 1974), Vol. 3.

IX. Ping Lee, D. V. Giovanielli, R. P. Godwin, and G. H. McCall, App. Phys. Lett. 24, 406 (1974).

X. M. Lubin, E. Goldman, J. Soures, L. Goldman, W. Friedman, S. Letzring, J. Albritton, P. Koch, and B. Yaakobi, in Plasma Physics and Controlled Nuclear Fusion (International Atomic Energy Agency, Vienna, Austria, 1974), Paper F4-2.

XI. B. H. Ripin, J. M. McMahon, E. A. McLean, W. M. Manheimer, and J. A. Stamper, Phys. Rev. Lett. 33, 634 (1974).

XII. J. Soures, S. Kumpan, and J. Hoose, App. Optics 13, 2081 (1974) (for laser parameters only).

XIII. W. C. Mead, W. L. Kruer, J. D. Lindl, and H. D. Shay, UCRL-77139 (1975).

XIV. Y. L. Pan, G. B. Zimmerman. J. H. Nuckolls, UCRL-76865 (1975), submitted to Phys. Rev. Lett.

XV. R. A. Haas, W. C. Mead, W. L. Kruer, D. W. Phillion, H. N. Kornblum, J. D. Lindl, D. MacQuigg, V. C. Rupert, and K. G. Tirsell, Phys. Fluids 20, 322 (1977).

J. Laser-Fusion Parameters

I. J. Nuckolls, L. Wood, A. Thiessen, and G. Zimmerman, Nature 239, 139 (1972).

II. J. S. Clark, H. N. Fisher, and R. J. Mason, Phys. Rev. Lett. 30, 89 (1973).

III. P. Mulser, R. Siegel, and S. Witkowsky, Phys. Lett. 6c, 187 (1973).

IV. J. Nuckolls, J. Emmett, and L. Wood, Physics Today, August 1973, p. 46.

V. K. A. Brueckner and S. Jorna, Rev. Mod. Phys. 46, 325 (1974).

VI. J. L. Emmett, J. Nuckolls, and L. Wood, Sci. Amer. 230, No. 6, 24 (1974).

K. Simulations, One Dimension, Backscatter

I. D. W. Forslund, J. M. Kindel, and E. L. Lindman, Phys. Rev. Lett. 30, 739 (1973) and LA-UR-73-500 (1973).

II. W. L. Kruer, K. G. Estabrook, K. H. Sinz, Nuclear Fusion 13, 952 (1973).

III. D. W. Forslund, J. M. Kindel, and E. L. Lindman, Phys. Fluids 18, 1017 (1975).

See also G XI.

L. Simulations, Two Dimensions, Back- and Side-scatter

I. A. B. Langdon and B. Lasinski, UCRL-75935 (1974).

II. A. Bruce Langdon and Barbara F. Lasinski, UCRL-77518 (1975), Methods in Computational Physics (Academic Press, New York, 1976), Vol. 16, p. 327.

See also G VI, XI; K III.

M. Bremsstrahlung

I. T. Birmingham, J. Dawson, and C. Oberman, Phys. Fluids 8, 297 (1965).

II. G. Bekefi, Radiation Processes in Plasmas, (John Wiley and Sons, Inc., New York, 1966), Chapters 3 and 5.

N. Longitudinal Noise (Longitudinal Cerenkov and Bremsstrahlung Radiation)

I. C. Oberman and G. Auer, Phys. Fluids 17, 1980 (1974).

II. G. Auer and C. Oberman, PPL-MATT-1073 (Sept. 1974).

P. General Mathematical Procedure

I. E. L. Ince, Ordinary Differential Equations (Dover Publications, Inc., New York, 1926).

II. P. M. Morse and H. Feshbach, Methods of Theoretical Physics (McGraw-Hill, New York, 1953).

III. Z. Sedlacek, J. Plasma Physics 5, 239 (1971).

Q. σ-Stability Analogy

I. J. P. Goedbloed and P. H. Sakanaka, Phys. Fluids 17, 908 (1974).

R. Wave Propagation in Nonuniform Media

I. K. G. Budden, Radio Waves in the Ionosphere (Cambridge University Press, 1961).

II. V. L. Ginzburg, Propagation of Electromagentic Waves in Plasma (Gordon and Breach, New York, 1961).

S. Complex Analysis

I. E. T. Whittaker and G.N. Watson, A Course of Modern Analysis (Cambridge University Press, 1952).

T. Phase Integral (WKBJ) Techniques

I. J. Heading, An Introduction to Phase-Integral Methods (John Wiley and Sons, Inc., New York, 1962).

II. J. Heading, Quart. Journ. Mech. and Applied Math., Vol. XV, Pt. 2, 1962, pp. 215-244.

III. J. Heading, Journal London Math. Soc. 37 (1962), pp. 195-208.

IV. N. Fröman and P. O. Fröman, JWKB Approximation, Contributions to the Theory (John Wiley and Sons, Inc., New York, 1965).

V. A. Skorupski, WKB Approximation in the Complex Plane and Applications to Plasma Theory (International Atomic Energy Agency, 1966), International Centre for Theoretical Physics, Trieste, IC/66/45.

VI. M. V. Berry and K. E. Mount, Rep. Prog. Phys. 35 (1972), pp. 315-397.

U. Saddle-point Approximation

I. A. Erdelyi, Asymptotic Expansions (Dover Publications, New York, 1956).

II. M. A. Evgrafov, Asymptotic Estimates and Entire Functions (Gordon and Breach, New York, 1957).

LIST OF FREQUENTLY USED SYMBOLS

a =	boundary coefficient	Eq. (I.32)
A =	solution of Eqs. (I.25, 28b)	Eq. (I.31)
a_1 =	WKBJ coefficient	
a_2 =	WKBJ coefficient	
B =	solution (linearly independent of A) of Eq. (I.25)	Eq. (I.31)
$\underline{B}_o$ =	pump (laser) magnetic field	
$\underline{B}_1$ =	scattered electromagnetic wave magnetic field	
c =	speed of light; or phase reference level	Eq. (IV.2d)
$\cos\theta$ =	$\hat{e}_o \cdot \hat{e}_1$	Eq. (I.2)
$D \equiv$	$v_o K \omega_p (1 - k_{1x}^2/k_1^2)$ = a pump strength parameter	Eq. (I.25c)
d_L =	laser diameter	
e =	electronic charge (> 0)	
$\hat{e}_o$ =	$\hat{x}$ = polarization of incident laser	
$\hat{e}_1$ =	polarization of scattered wave	Eq. (I.22)
$\underline{E}_o$ =	pump (laser) electric field	
$\underline{E}_1$ =	scattered electromagnetic wave electric field	
$f \equiv$	$\sqrt{Q}$ = an effective k_{1z}	Eq. (III.23)
F		Eq. (III.29)
f_1 =	WKBJ solution in sec. IV, or a particular WKBJ term in sec. V	Eq. (IV.2)

f_2 = WKBJ solution in sec. IV, or a particular WKBJ term in sec. V — Eq. (IV.2)

$\underline{G}_1$ = Green's function for scattered electromagnetic wave

h = resonance zone width

$\underline{J}$ = current density — Eq. (I.21)

$\underline{K} \equiv \underline{k}_o - \underline{k}_1$ = beat wave-vector

$\underline{k}_o$ = wave-vector of incident laser

$\underline{k}_1$ = wave-vector of scattered electromagnetic wave

$k_1(z) \equiv \left[\omega_1^2 - \omega_p^2(z)\right]^{\frac{1}{2}}/c$ — Eq. (I.22)

$\underline{k}_{1\perp} = \hat{x}k_{1x} + \hat{y}k_{1y}$

$k_{1z} = \left[\omega_1^2 - \omega_p^2(z) - c^2k_{1\perp}^2\right]^{\frac{1}{2}}/c$ — Eq. (I.6)

$L_n \equiv d\left[\ln n(z)\right]/dz$ = density scale length — Eq. (I.8)

$\ell_s = y_s$ = refraction saturation distance — Eq. (I.17)

m = electron mass

n = electron density

N = eigenmode label — Eq. (V.19)

n_o = unperturbed plasma density

q = dimensionless Helmholtz potential (Q) — Eq. (IV.1) and Eq. (V.2)

Q = Helmholtz potential — Eq. (I.25b)

S = source — Eq. (I.25a)
or Stokes constant — Eq. (IV.8)

t = time

T = transition point

$\tilde{t} \equiv \omega_s t/\xi$ = dimensionless time — Eq. (III.14a)

T_e = electron temperature

T_n = Stokes constants (n = 0,1,2 used) — Eq. (IV.10)

t_s = refraction saturation time — Eq. (I.16)

$v_o = eE_o/m\omega_o$ — Eq. (I.2)

$\underline{V}_1 = \underline{k}_1(c^2/\omega_1)$ — Eq. (I.1)

$\underline{V}_2 = 3\underline{K}\, v_{th}^2/\Omega$ — Eq. (I.1)

v_{th} = electron thermal velocity

W = Wronskian — Eq. (I.26)

X = dimensionless frequency parameter — Eqs. (IV.9;V.2)

y = position variable perpendicular to $\hat{z}$ and $\hat{e}_o$

Y — Eq. (III.28)

z = position variable along density gradient

$Z \equiv (c^2 L_n/\omega_p^2)^{1/3}$ = effective *minimum* wavelength — Eq. (I.10a)

$\tilde{z} \equiv \omega^2(z/\omega_s^2$ = dimensionless position — Eq. (III.16)

z_g = greater of z or z_s — Eq. (I.26)

z_ℓ = lesser of z or z_s — Eq. (I.26)

z_s = source position

$z_+(\omega_1)$ = root of $Q(z,\omega_1)$ — Eq. (V.4b)

$z_-(\omega_1)$ = root of $Q(z,\omega_1)$ — Eq. (V.4b)

$z_o(\omega_1)$ = resonance position, $\omega_p(z_o) \equiv \omega_o - \omega_1$ — sec. I A 3a

$z_\infty(\omega_1) = z_o(\omega_1)$ = resonance position, pole of $Q(z,\omega_1)$ — Eq. (V.4b)

$\tilde{z}_g \equiv \omega_g^2/\omega_s^2$ — Eq. (III.14a)

$\tilde{z}_\ell \equiv \omega_\ell^2/\omega_s^2$ — Eq. (III.14a)

$\gamma \equiv \mathrm{Im}(\omega_1)$ = growth rate

Γ = exponentiation factor — Eq. (I.7)

$\gamma_o = (K v_o/2)(\omega_p/\omega_1)^{\frac{1}{2}} \cos\theta$ — Eq. (I.2)

Γ_1 = exponentiation factor (back- or oblique-scatter) — Eq. (V.47)

Γ_2 = exponentiation factor (side-scatter) — Eq. (V.51a)

γ_N' = eigenmode growth rate — Eq. (V.35b)

$\delta\omega \equiv \omega' - \omega_A$ — Eq. (V.41a)

$\Delta_1 \equiv (\omega_p^2 + c^2k_1^2 - \omega_1^2)/2\omega_1$ — Eq. (I.1)

$\Delta_2 \equiv \Delta_p \equiv (\omega_p^2 + 3v_{th}^2K^2 - \Omega^2)/2\Omega$ — Eq. (I.1)

$\eta \equiv (z - z_s)/ct$ or — Eq. (III.5)

$= (z_g - z_\ell)/ct$ — Eq. (III.24)

$\theta = \cos^{-1}(\hat{e}_o \cdot \hat{e}_1)$

θ_1 = a particular phase-integral — Eq. (V.37a)

θ_2 = a particular phase-integral — Eq. (V.37b)

θ_3 = a particular phase-integral — Eq. (V.57a)

θ_4 = a particular phase-integral — Eq. (V.57b)

λ	= WKBJ large parameter	Eq. (IV.1)
	or a dimensionless pump strength	Eq. (V.2)
λ_D	$\equiv (T_e/4\pi n\, e^2)^{\frac{1}{2}}$ = Debye length	
μ	= WKBJ "μ-integral"	Eq. (IV.5)
ν_1	= damping rate of electromagnetic waves	Eq. (I.1)
ν_2	$\equiv \nu_p$ = damping rate of Langmuir plasma waves	Eq. (I.1)
ξ	$\equiv L_n\omega_s^3/c\omega_p^2$	Eq. (III.17a)
ρ	= dimensionless position variable;	Eq (I.31;V.1)
	also used for charge density	Eq. (I.21)
ρ_ℓ	$\equiv \rho(z_\ell)$ = dimensionless position	Eq. (I.31)
ρ_g	$\equiv \rho(z_g)$ = dimensionless position	Eq. (I.31)
$\rho_+(X)$	= root (zero) of $q(\rho,X)$	Eq. (V.2e)
$\rho_-(X)$	= root (zero) of $q(\rho,X)$	Eq. (V.2f)
$\rho_\infty = 0$	dimensionless resonance position, pole of $q(\rho,X)$	Eq. (V.4c)
Ψ	= wave-packet phase	Eq. (III.3)
	or phase at arbitrary frequency	Eq. (III.24)
	or phase-integral	Eq. (IV.2)
Ψ_1	= solution of Eqs. (I.25, 27)	Eq. (I.26)
Ψ_2	= solution of Eqs. (I.25, 28)	Eq. (I.26)
ω	$\equiv \left[\omega_p^2(z) + c^2k_{1\perp}^2\right]^{\frac{1}{2}} = \omega(z)$	Eq. (III.1)
Ω	$\equiv \omega_o - \omega_1 \equiv \omega_2$ = beat frequency	

ω_A = saddle-point (wave-packet) frequency for

uniform unpumped plasma Eq. (III.5a)

or nonuniform unpumped plasma Eq. (III.16)

$\omega_g \equiv \omega(z_g)$ = frequency of wave with turning point at z_g

$\omega_\ell \equiv \omega(z_\ell)$ = frequency of wave with turning point at z_ℓ

$\omega_p \equiv (4\pi ne^2/m)^{\frac{1}{2}}$ = plasma frequency

$\omega_R \equiv \omega_o - \omega_p$ = resonance frequency Eq. (III.28)

$\omega_s \equiv \omega(z_s)$ = frequency of wave with turning point at z_s

ω_o = frequency of incident laser

ω_1 = frequency of scattered electromagnetic wave

$\omega_2 \equiv \Omega$ = beat frequency

$\omega_I(z)$ = root of $Q(z,\omega_1)$ Eq. (V.4a)

$\omega_{II}^{o}(z)$ = root of $Q(z,\omega_1)$ Eq. (V.4a)

$\omega_{III}^{o}(z)$ = root of $Q(z,\omega_1)$ Eq. (V.4a)

$\omega_{II}^{\infty}(z)$ = pole of $Q(z,\omega_1)$ Eq. (V.4a)

$\omega_{III}^{\infty}(z)$ = pole of $Q(z,\omega_1)$ Eq. (V.4a)

$\omega_{1R} \equiv \mathrm{Re}(\omega_1)$

$\omega' \equiv \omega_1 + i\nu_1$ = an integration variable, Eq. (V.36)

sometimes taken to be a saddle-point frequency

$\omega_R'' \equiv (\omega_o + c^2 k_{1\perp}^2/\omega_o)/2$ Eq. (V.32)

$(\omega_{1N}')_R$ = eigenmode frequency Eq. (V.35a)

$\tilde{\omega}_A \equiv \omega_A/\omega_s$ = dimensionless saddle-point frequency Eq. (III.16)

$\tilde{\omega}_B \equiv \omega_B/\omega_s$ = dimensionless saddle-point frequency Eq. (III.18a)

$\tilde{\omega}_g \equiv \omega_g/\omega_s$

$\tilde{\omega}_\ell \equiv \omega_\ell/\omega_s$

$\tilde{\omega}_1 \equiv \omega_1/\omega_s$ = dimensionless frequency Eq. (III.14a)

$\omega^2(z_\infty) \equiv \left[\omega_o - \omega' - i(\nu_p - \nu_1)\right]^2 + c^2 k_{1\perp}^2$ Eq. (V.39)

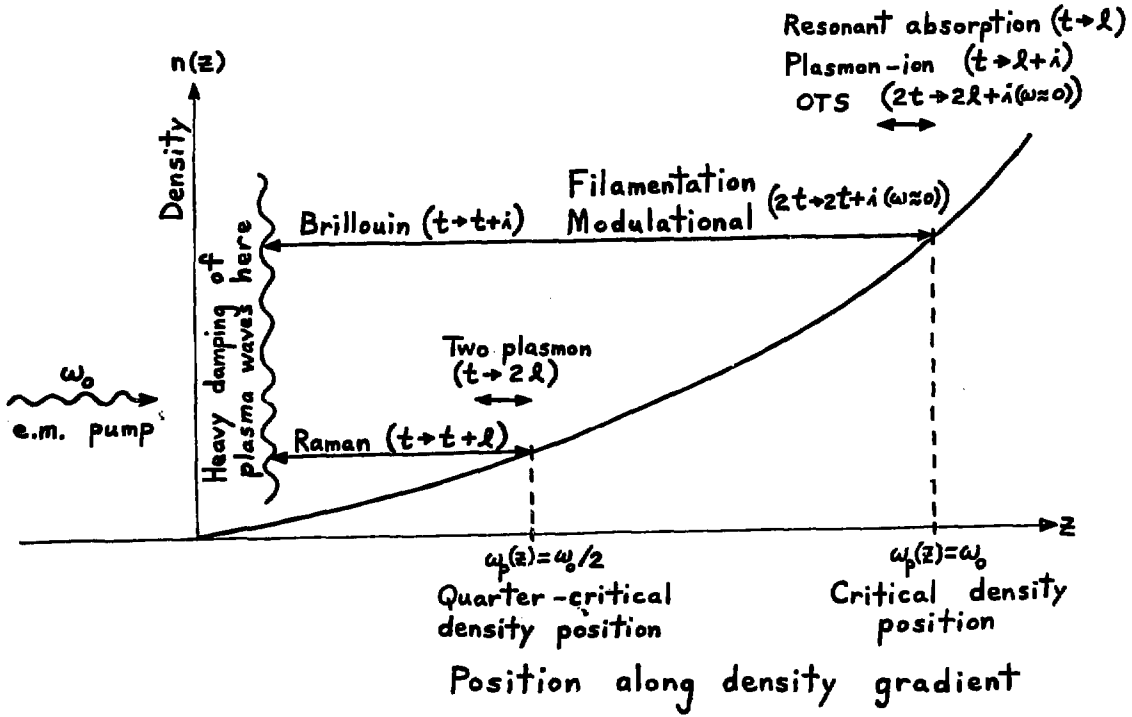

Fig. I.1

XBL 7710-6881

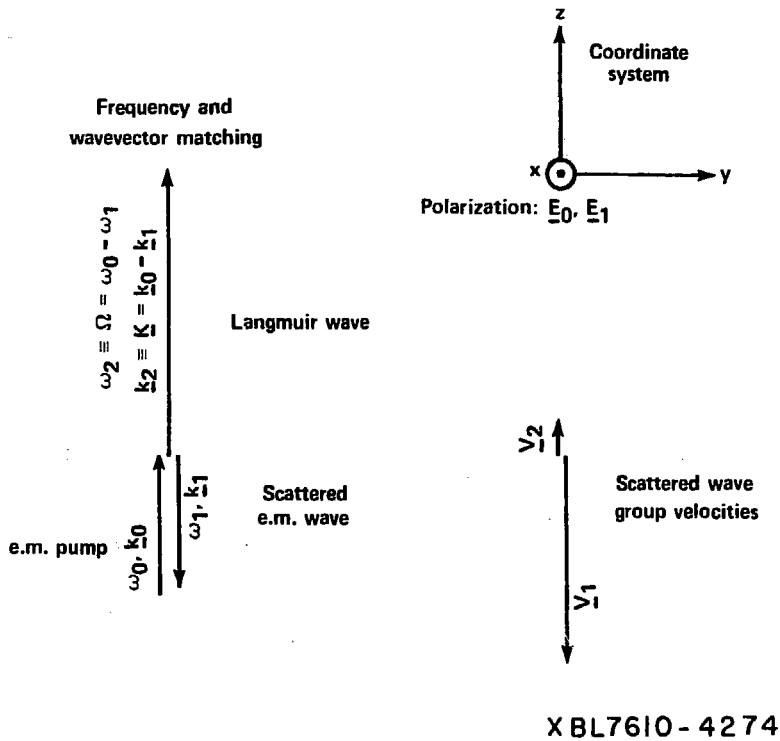
Frequency and
wavevector matching
$\omega_2 \equiv \Omega = \omega_0 - \omega_1$
$\underline{k}_2 \equiv \underline{K} = \underline{k}_0 - \underline{k}_1$
Langmuir wave
Scattered
e.m. wave
$\omega_1, \underline{k}_1$
e.m. pump
$\omega_0, \underline{k}_0$
z
Coordinate
system
x
y
Polarization: $\underline{E}_0, \underline{E}_1$
V_2
V_1
Scattered wave
group velocities
XBL7610-4274

Fig. I.2

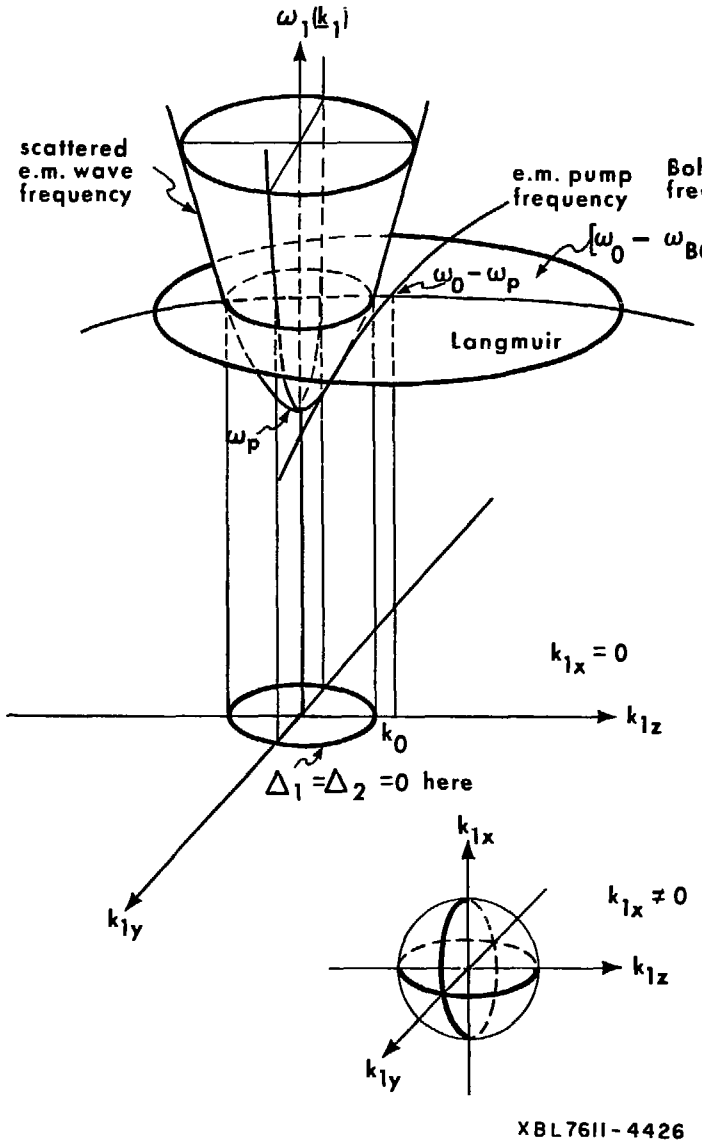
$\omega_1(\underline{k}_1)$
scattered e.m. wave frequency
e.m. pump frequency
Bohm-Gross frequency
$[\omega_0 - \omega_{BG}(K)]$
$\omega_0 - \omega_p$
Langmuir
ω_p
$k_{1x} = 0$
k_{1z}
k_0
$\Delta_1 = \Delta_2 = 0$ here
k_{1y}
k_{1x}
$k_{1x} \neq 0$
k_{1z}
k_{1y}
XBL7611-4426

Fig. I.3

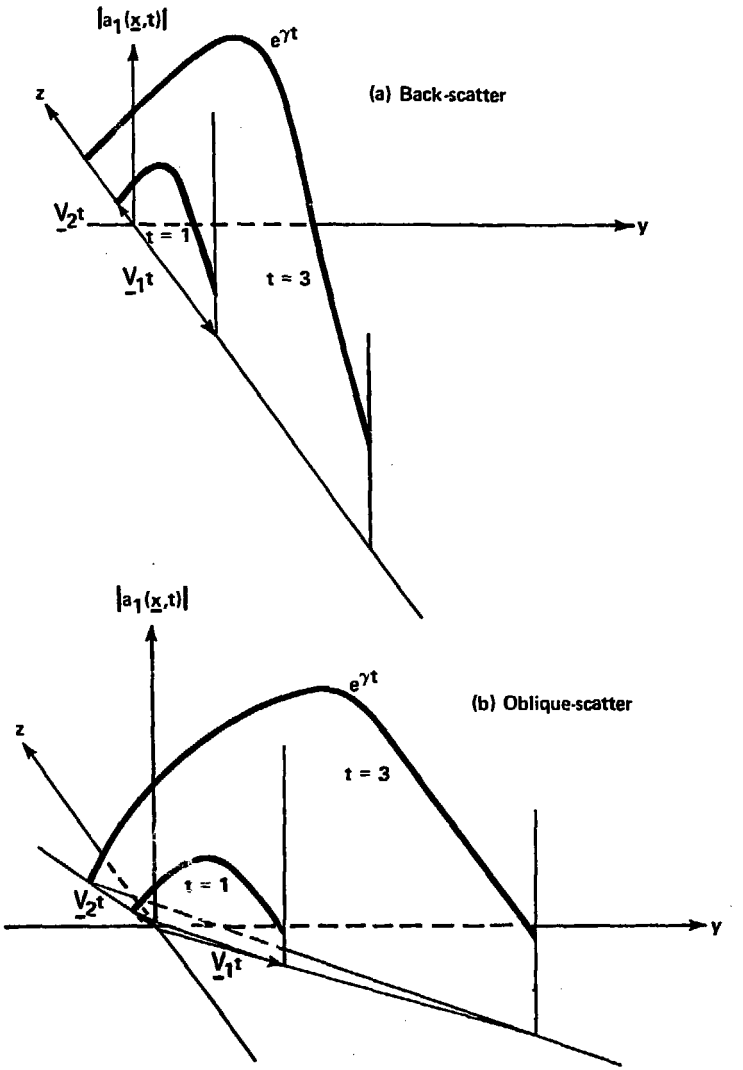

XBL 7610 – 4284

Fig. I.4

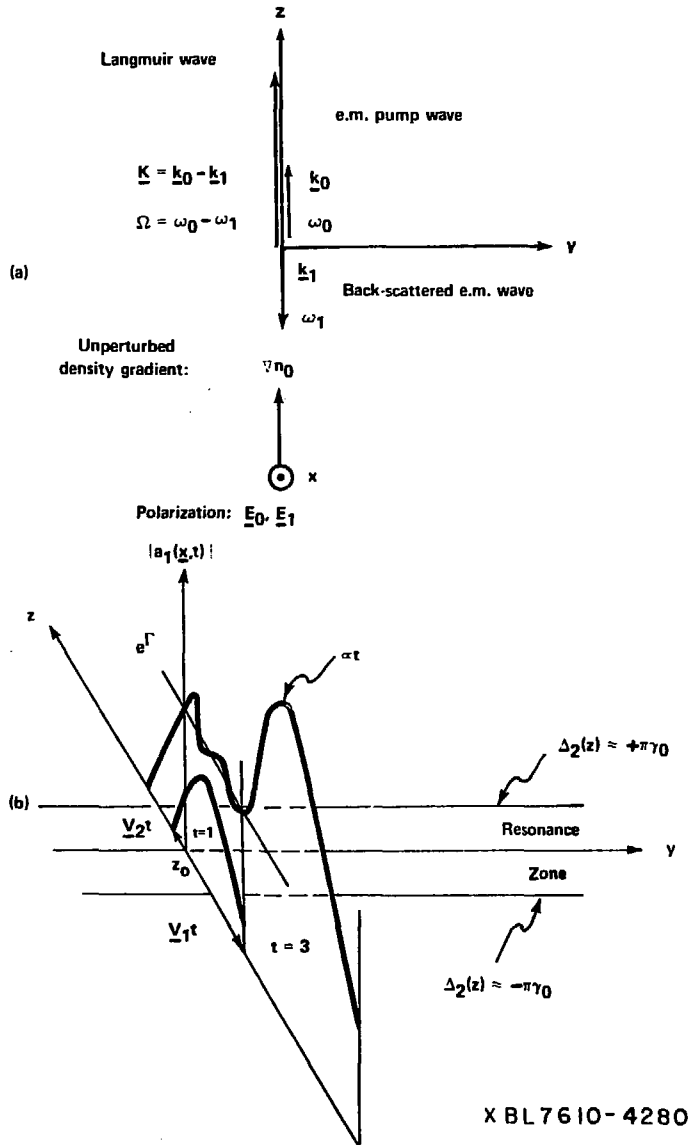
z
Langmuir wave
e.m. pump wave
$\underline{K} = \underline{k}_0 - \underline{k}_1$
$\Omega = \omega_0 - \omega_1$
$\underline{k}_0$
ω_0
y
(a)
$\underline{k}_1$
Back-scattered e.m. wave
ω_1
Unperturbed density gradient:
∇n_0
x
Polarization: $\underline{E}_0, \underline{E}_1$
$|a_1(\underline{x},t)|$
z
e^{Γ}
$\propto t$
$\Delta_2(z) \approx +\pi\gamma_0$
(b)
$\underline{V}_2 t$
t=1
Resonance
y
z_0
Zone
$\underline{V}_1 t$
t = 3
$\Delta_2(z) \approx -\pi\gamma_0$
XBL7610-4280

Fig. I.5

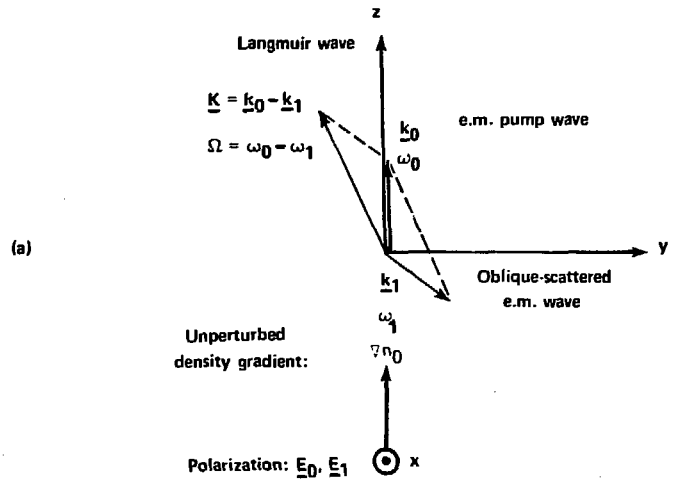
(a)
z
Langmuir wave
$\underline{K} = \underline{k}_0 - \underline{k}_1$
$\Omega = \omega_0 - \omega_1$
$\underline{k}_0$
ω_0
e.m. pump wave
y
$\underline{k}_1$
Oblique-scattered
e.m. wave
ω_1
Unperturbed
density gradient:
∇n_0
Polarization: $\underline{E}_0$, $\underline{E}_1$
x

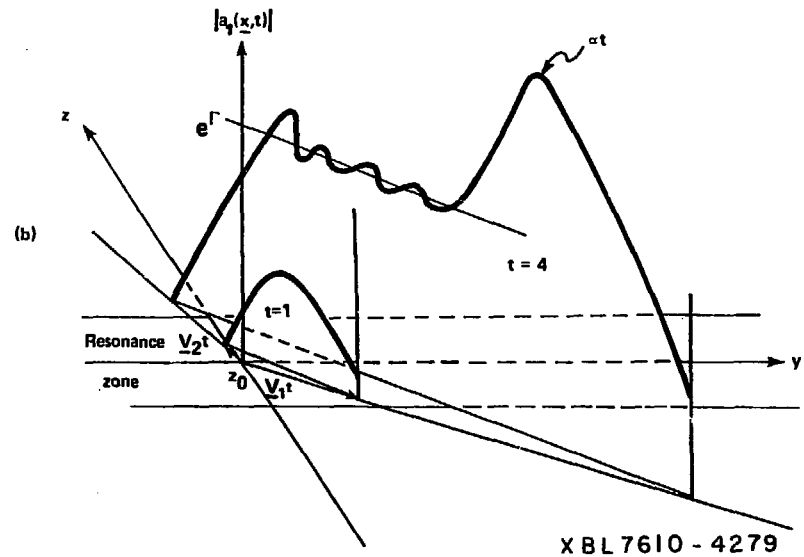
(b)
$|a_1(\underline{x},t)|$
αt
z
e^{Γ}
t = 4
t=1
Resonance
zone
$\underline{V}_2 t$
z_0
$\underline{V}_1 t$
y
XBL7610-4279

Fig. I.6

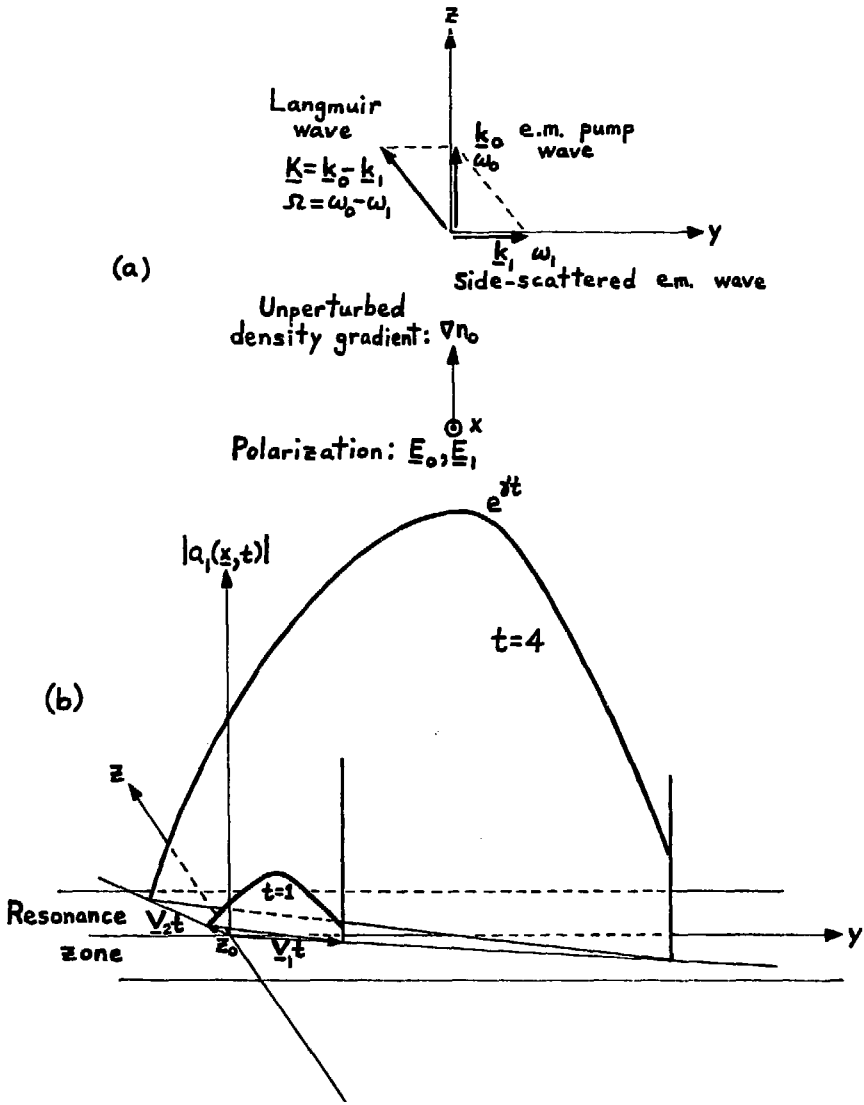

XBL 7710-6885

Fig. I.7

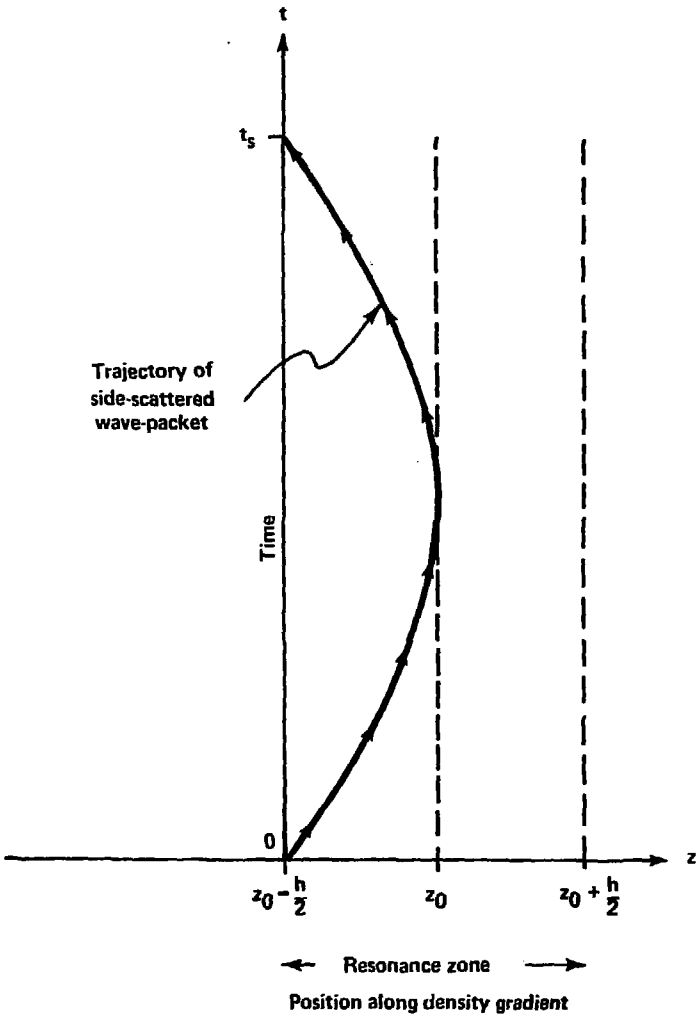

XBL7610-4276

Fig. I.8

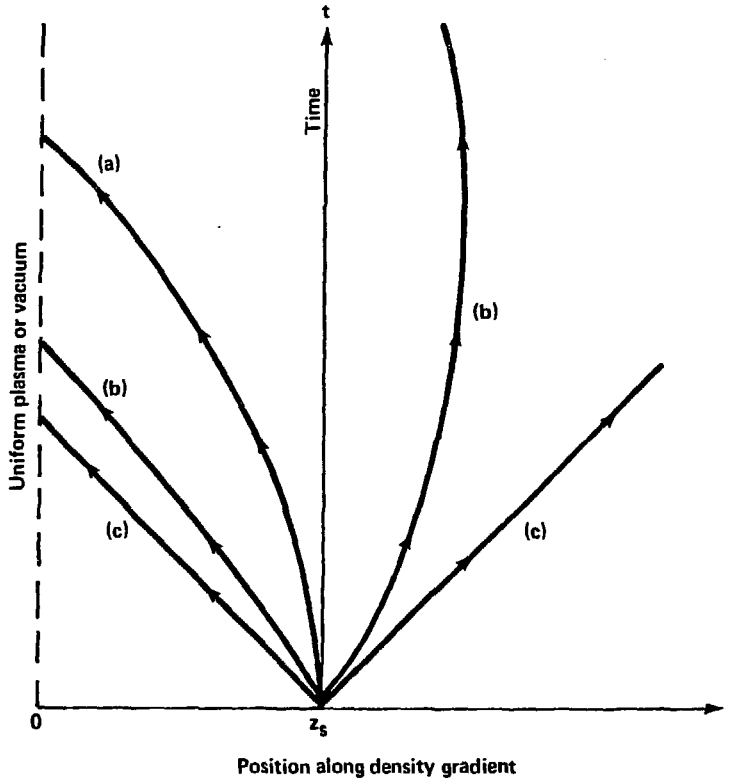

XBL7610-4277

Fig. I.9

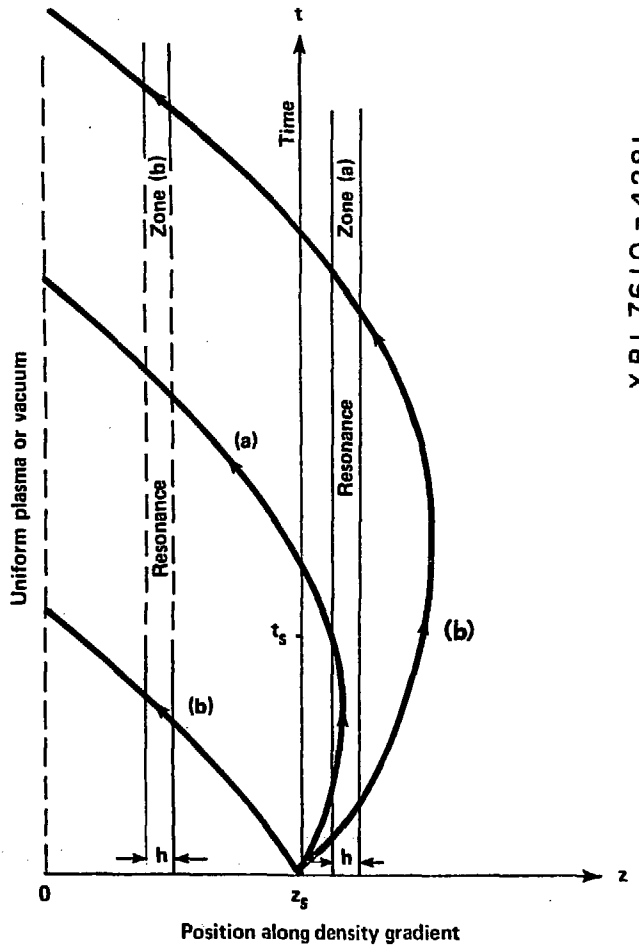

XBL7610-4281

Fig. I.10

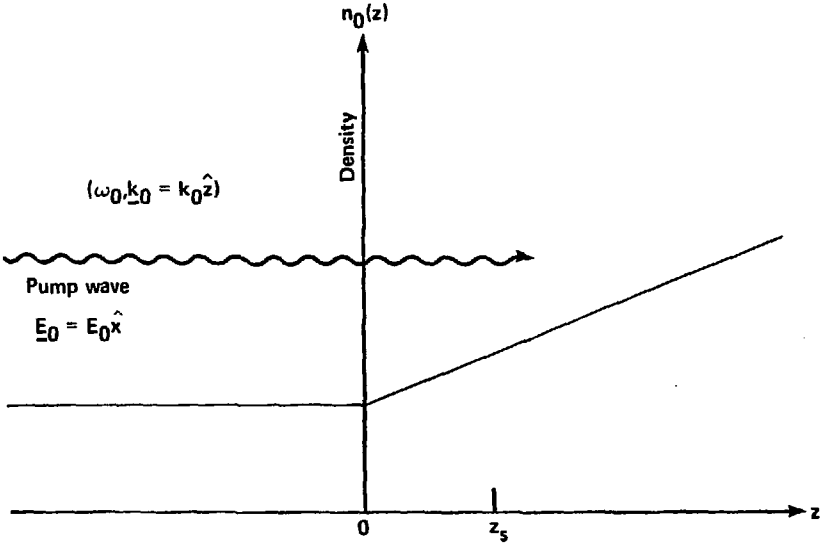

Position along the density gradient

XBL7610-4275

Fig. I.11

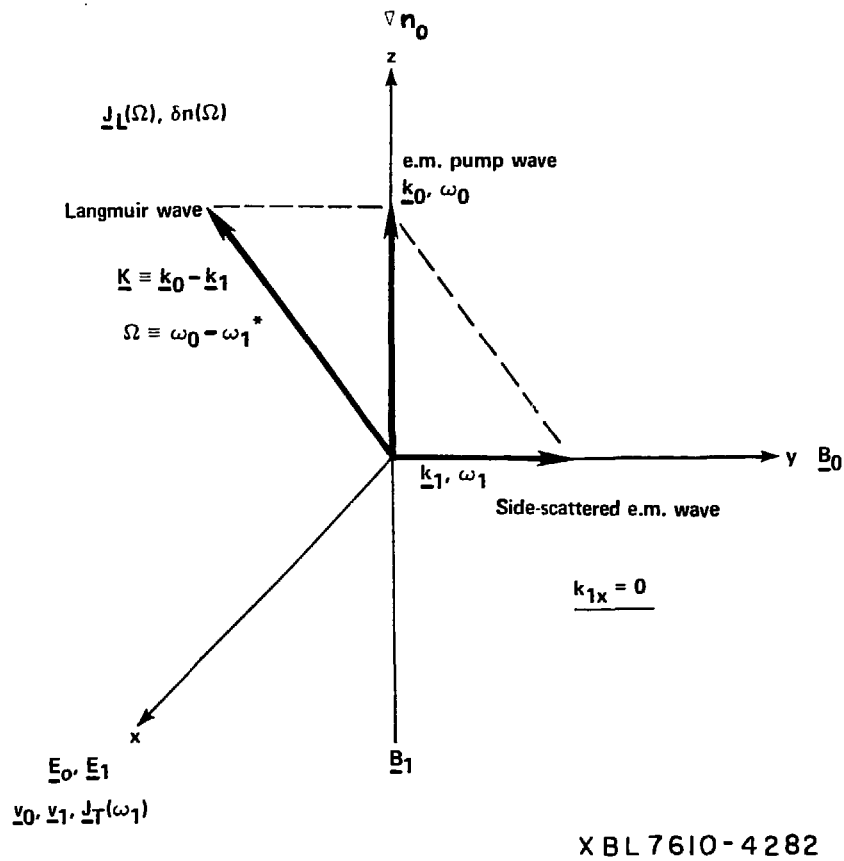
∇n_0
z
$\underline{J}_L(\Omega)$, $\delta n(\Omega)$
e.m. pump wave
$\underline{k}_0$, ω_0
Langmuir wave
$\underline{K} \equiv \underline{k}_0 - \underline{k}_1$
$\Omega \equiv \omega_0 - \omega_1^*$
y $\underline{B}_0$
$\underline{k}_1$, ω_1
Side-scattered e.m. wave
$k_{1x} = 0$
x
$\underline{E}_0$, $\underline{E}_1$
$\underline{v}_0$, $\underline{v}_1$, $\underline{J}_T(\omega_1)$
$\underline{B}_1$
XBL 7610-4282

Fig. I.12

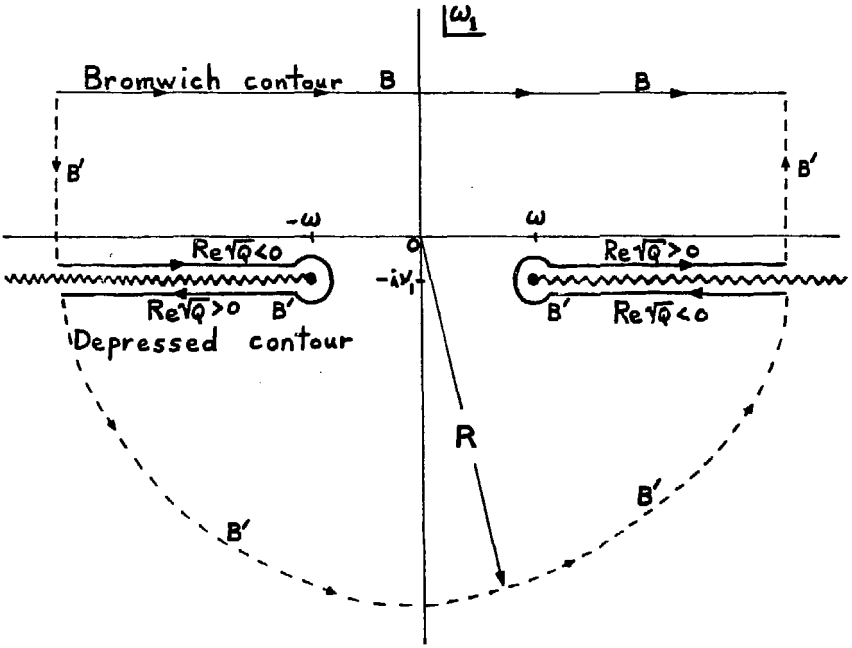

XBL 7710-6884

Fig. I.13

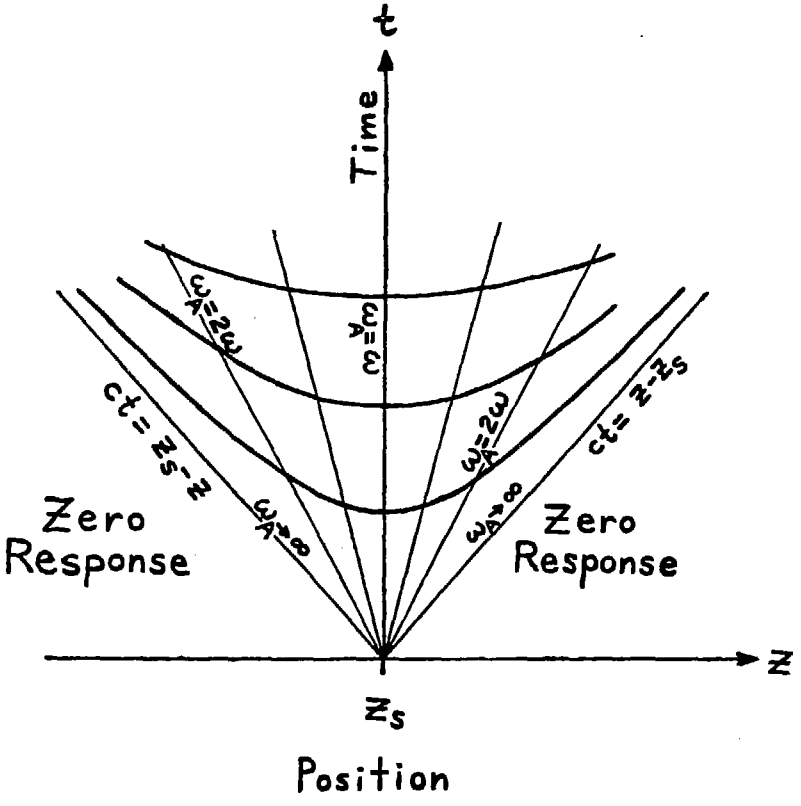

XBL 7710-6871

Fig. III.1

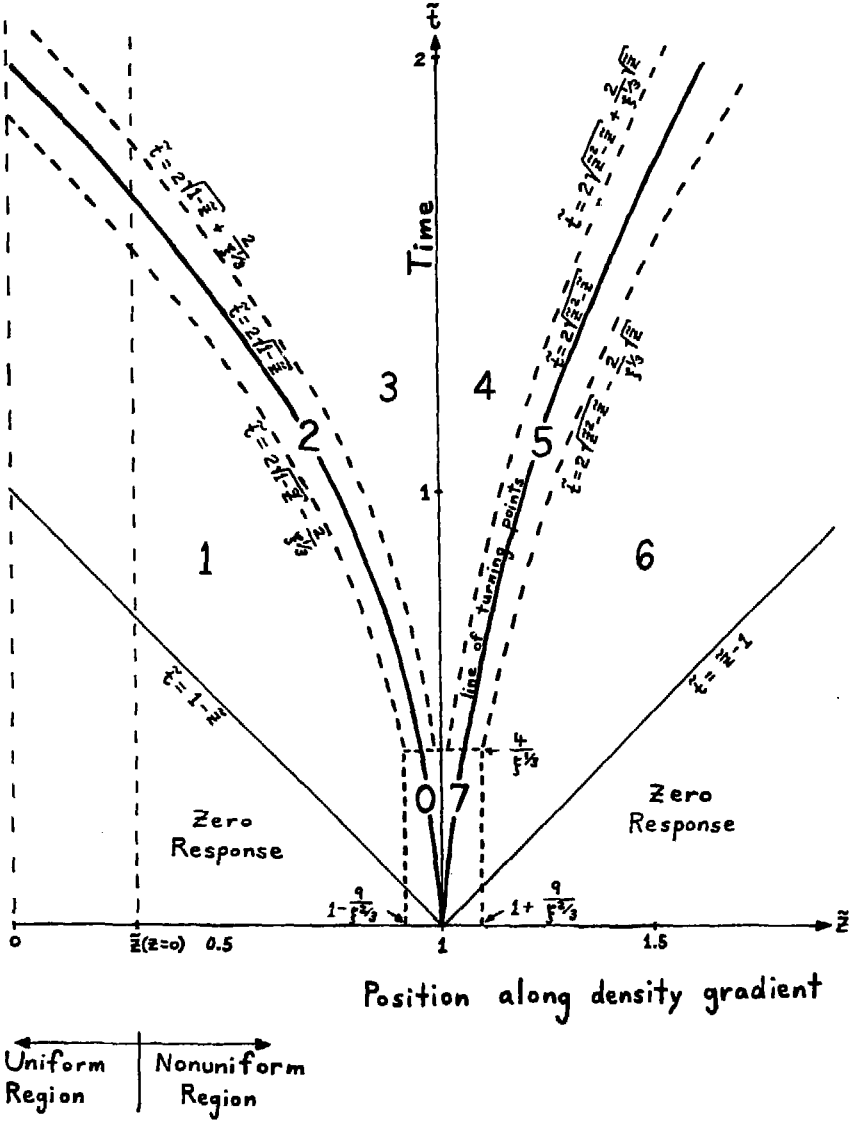
Time
Zero Response
Zero Response
line of turning points
Position along density gradient
Uniform Region
Nonuniform Region
XBL 7710-6866

Fig. III.2

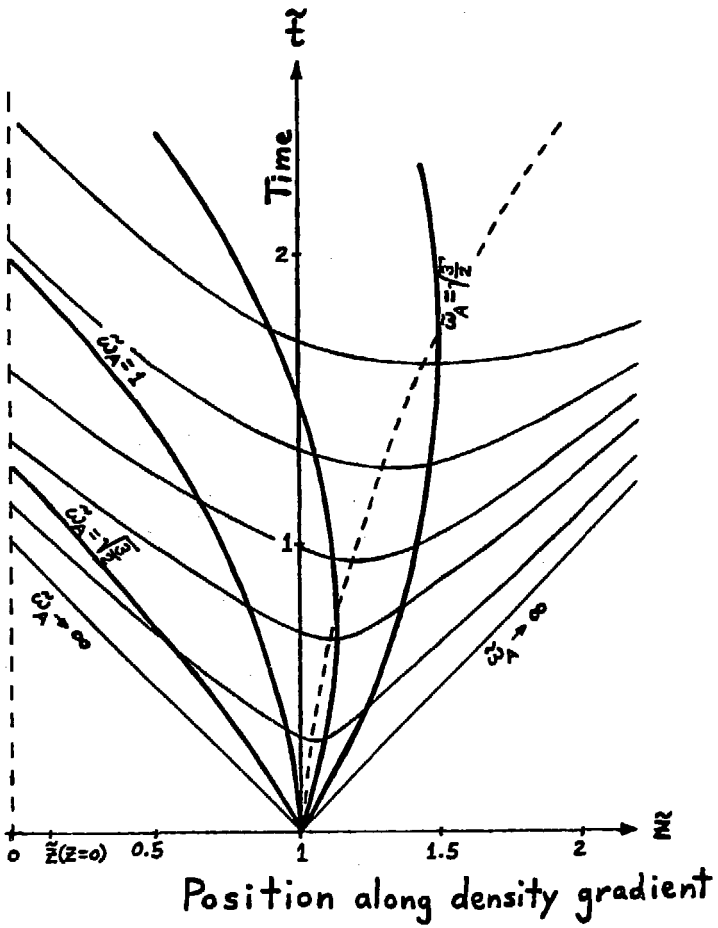

Fig. III.3

XBL 7710-6872

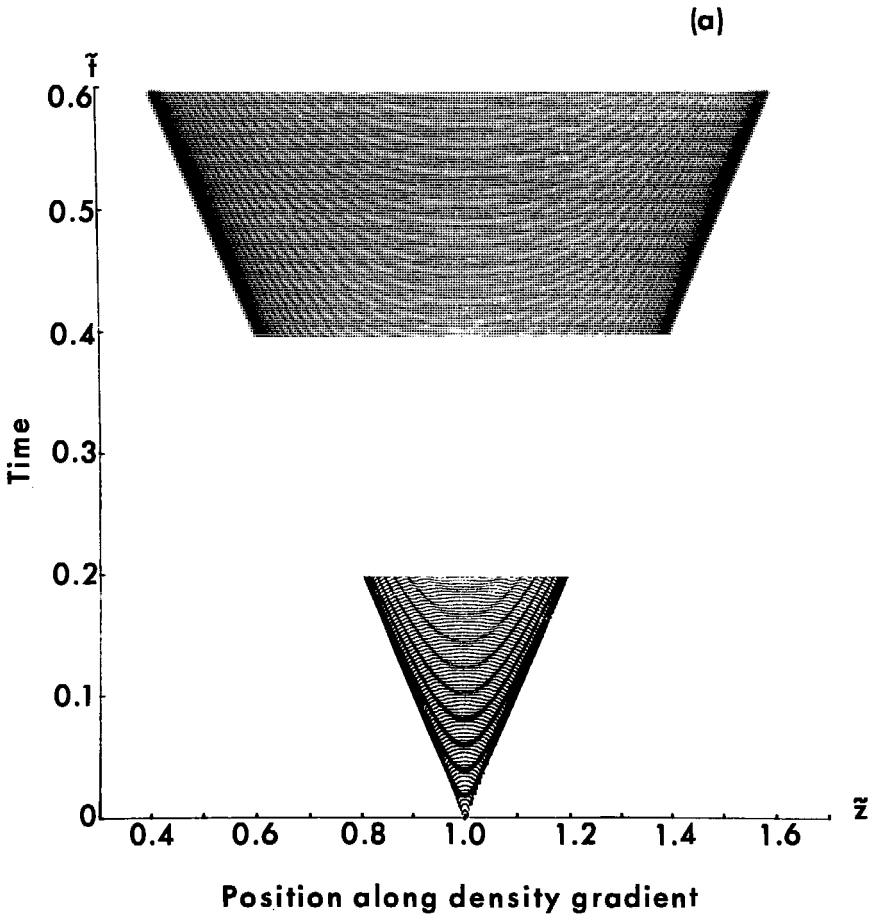

XBB 7710-9951

Fig. III.4a

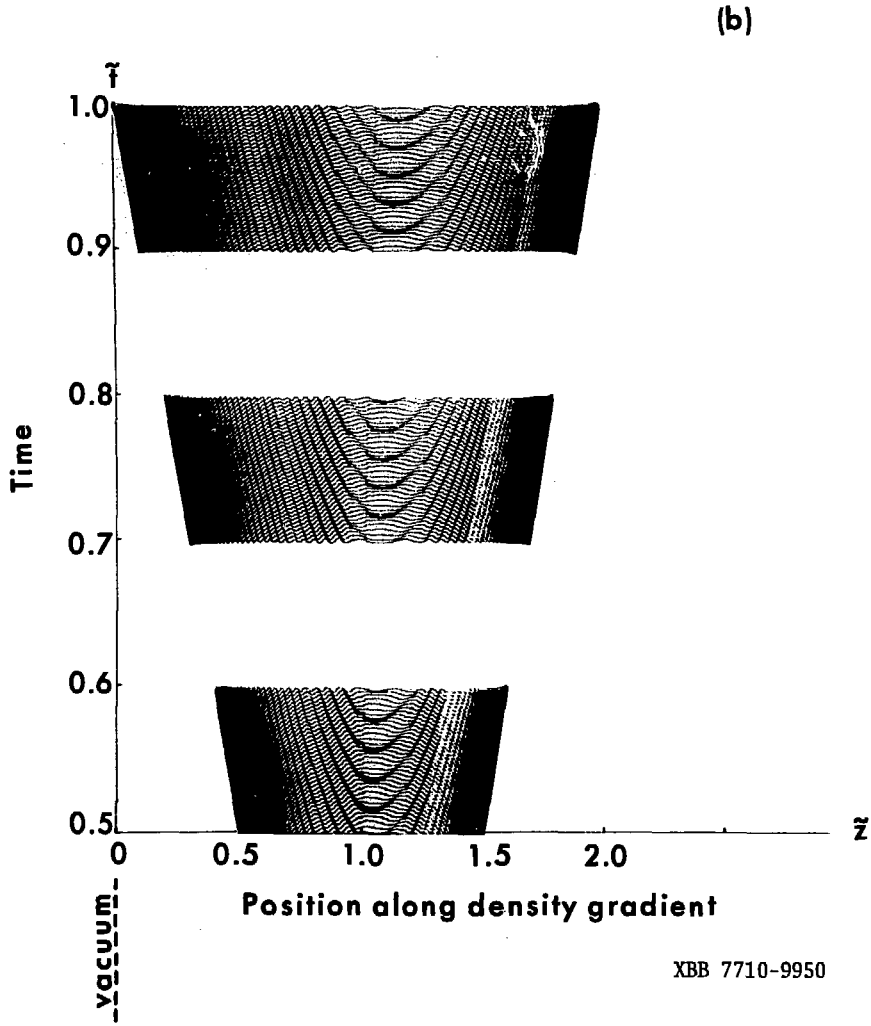
(b)
t̃
1.0
0.9
0.8
0.7
0.6
0.5
Time
0
0.5
1.0
1.5
2.0
z̃
Position along density gradient
vacuum
XBB 7710-9950

Fig. III.4b

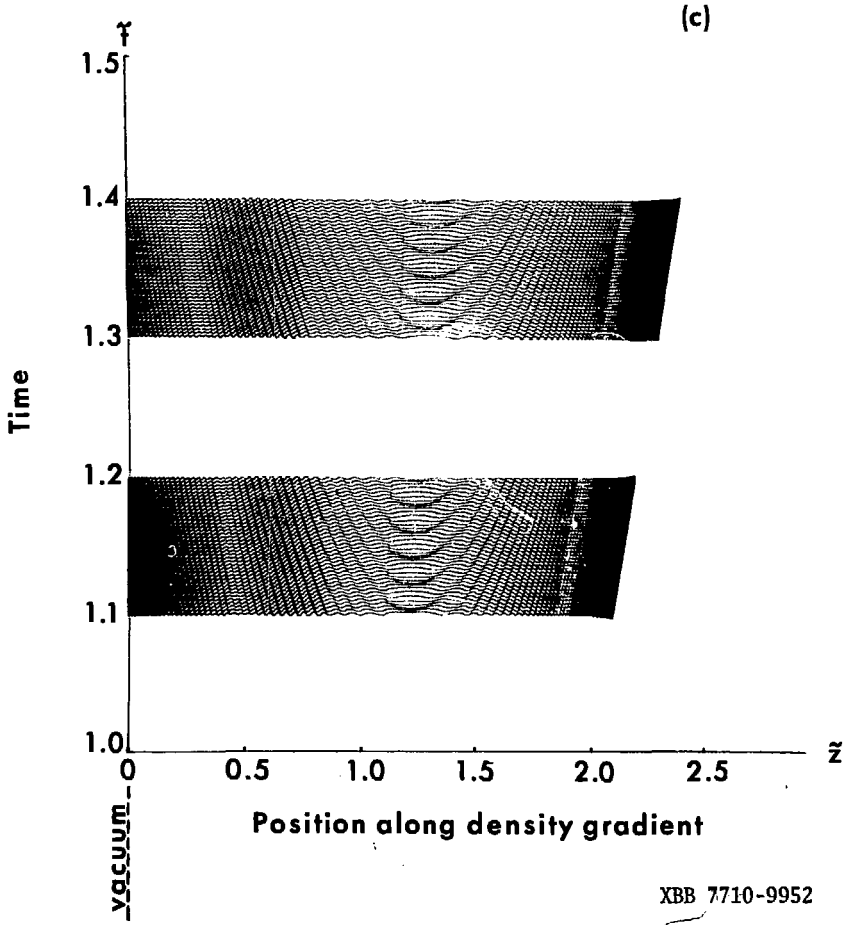
(c)
τ̃
1.5
1.4
1.3
1.2
1.1
1.0
Time
0
0.5
1.0
1.5
2.0
2.5
z̃
vacuum
Position along density gradient
XBB 7710-9952

Fig. III.4c

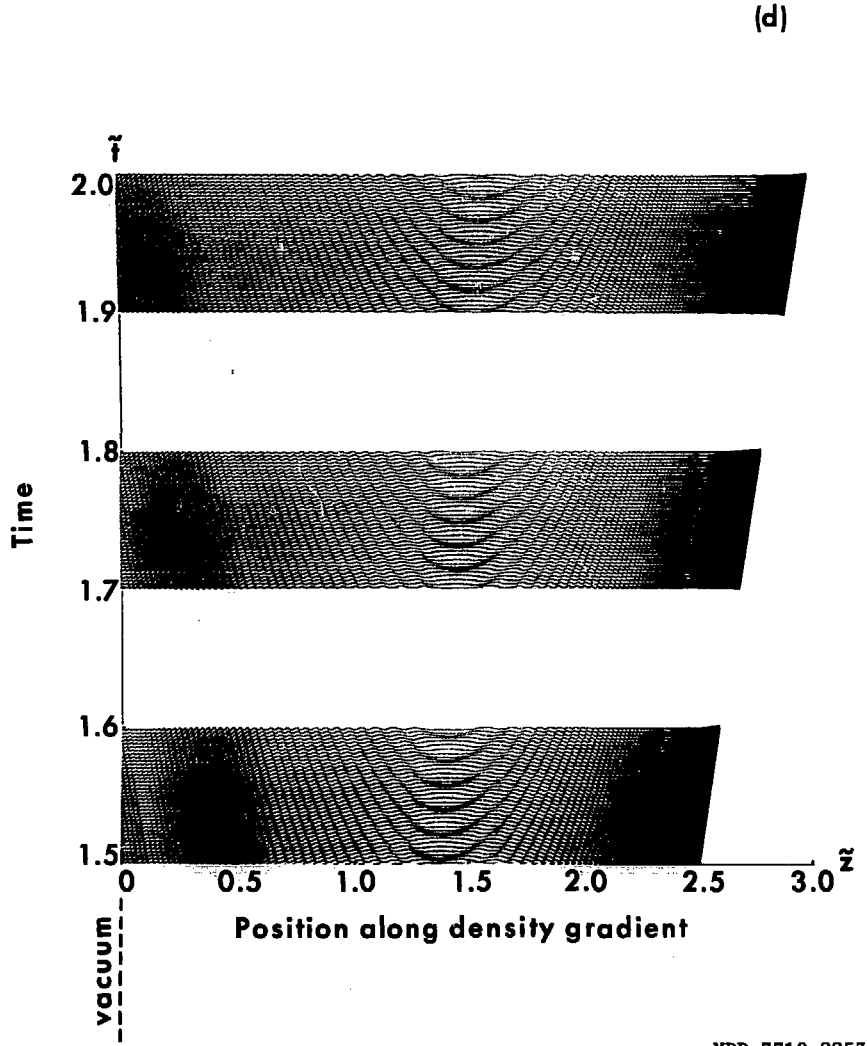
(d)
t̃
2.0
1.9
1.8
1.7
1.6
1.5
Time
0
0.5
1.0
1.5
2.0
2.5
3.0
z̃
Position along density gradient
vacuum
XBB 7710-9953

Fig. III.4d

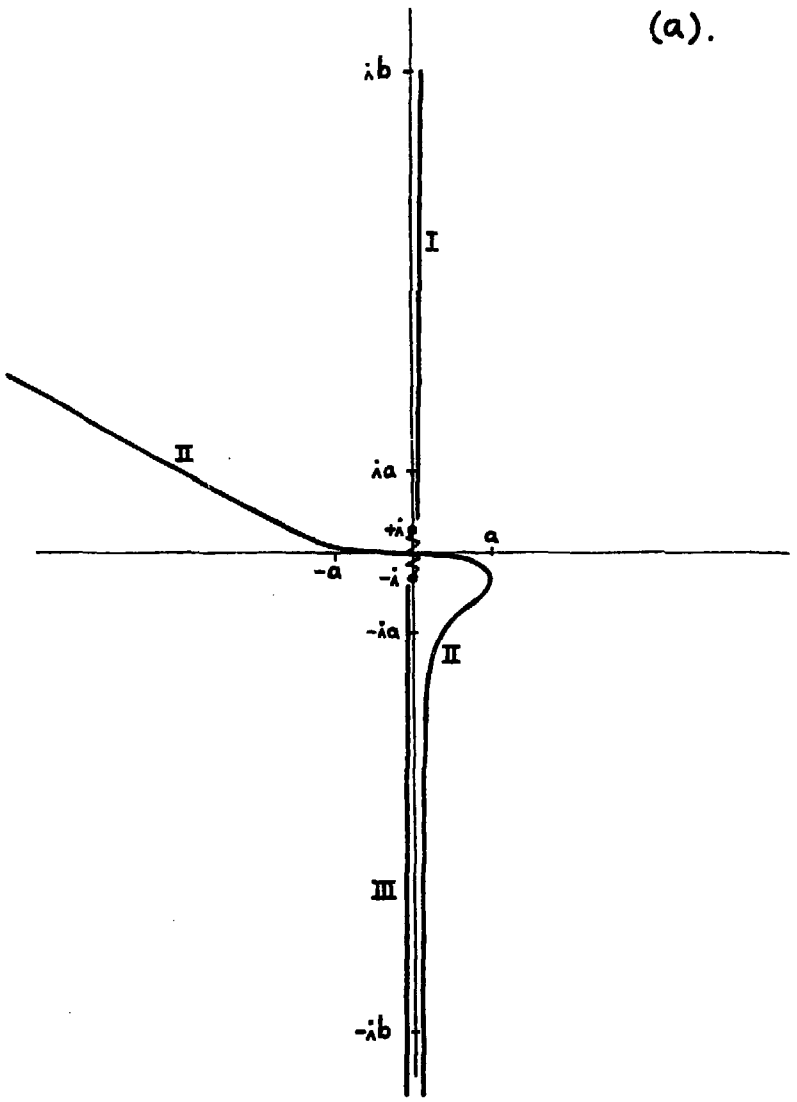

XBL 7710-6873

Fig. III.5a

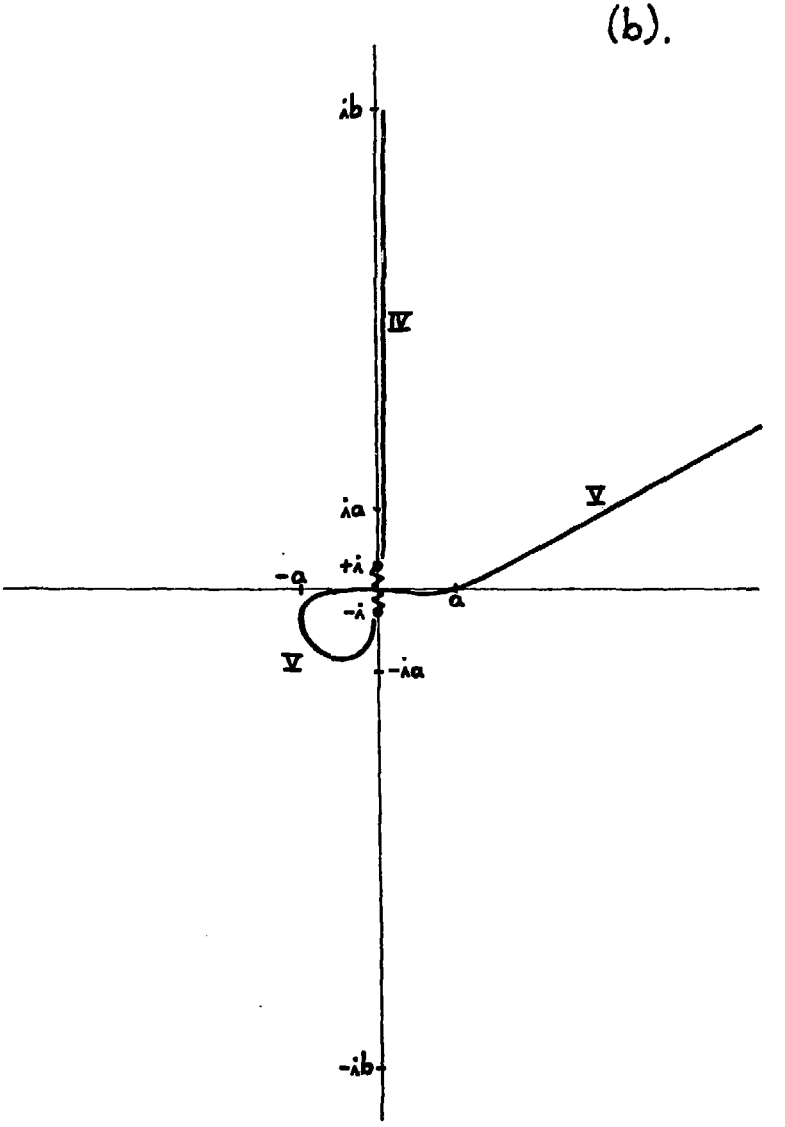

XBL 7710-6874

Fig. III.5b

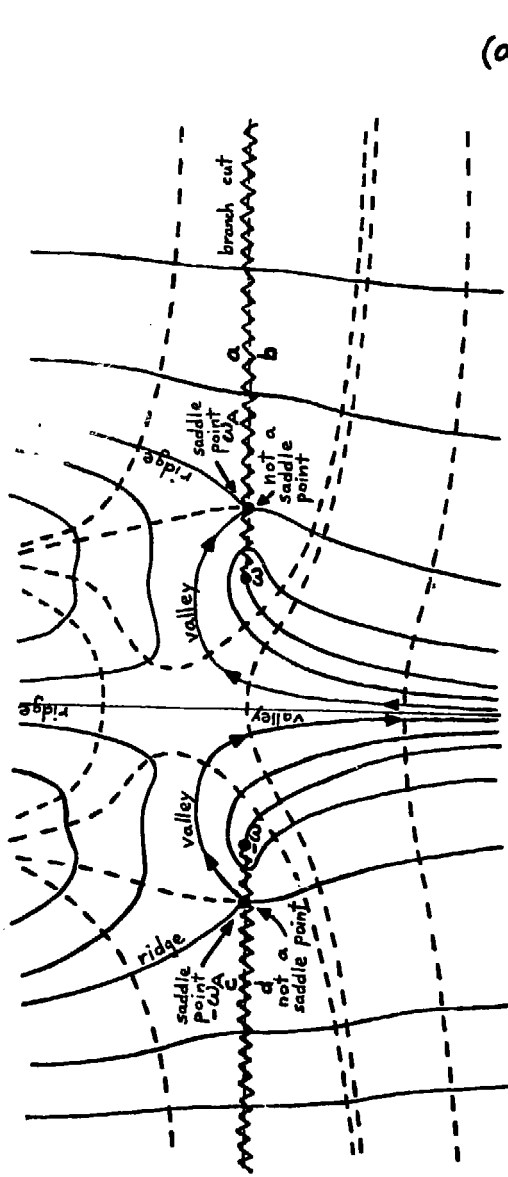

XBL 7710-6875

Fig. III.6a

(b)

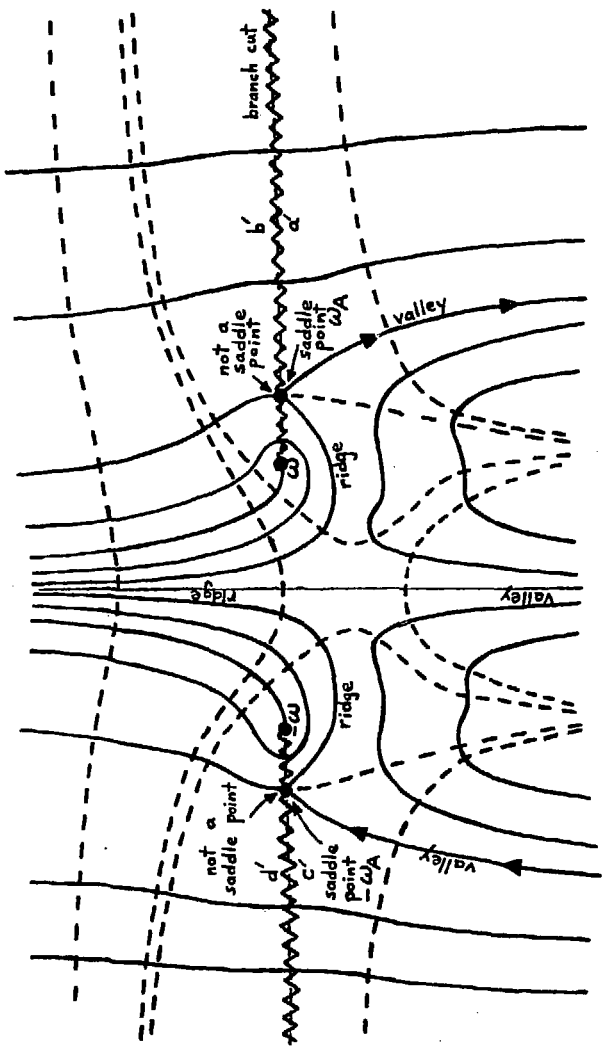

XBL 7710-6877

Fig. III.6b

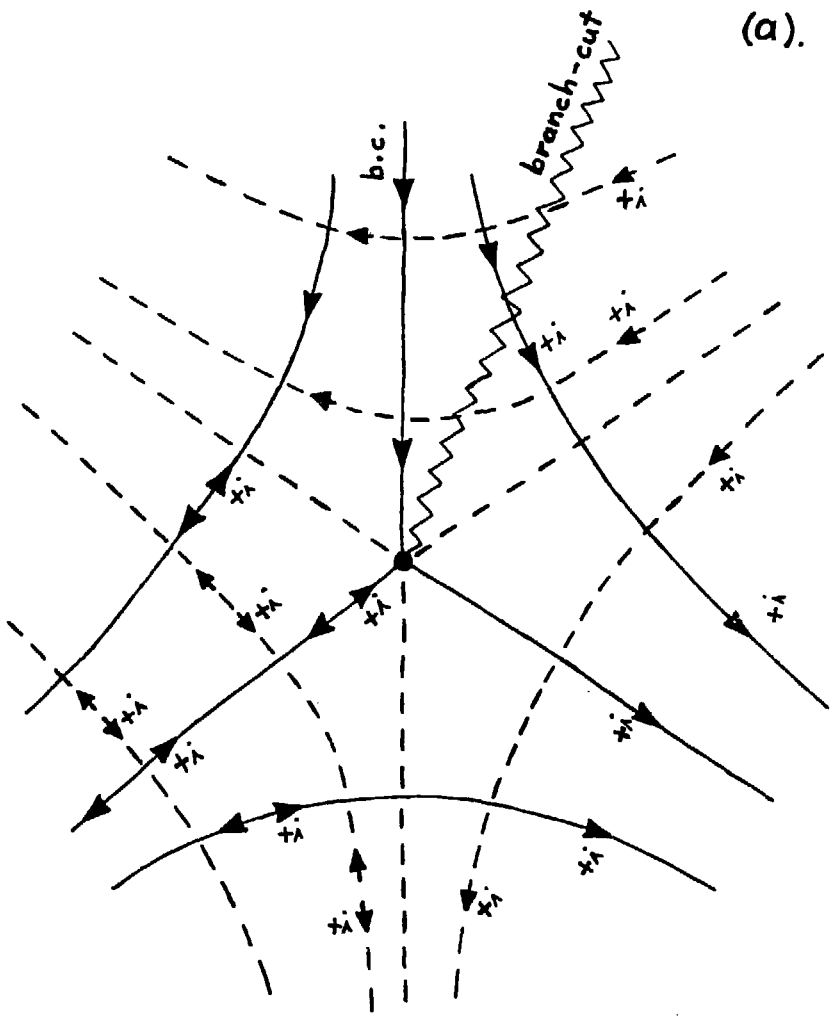

Fig. IV.1a

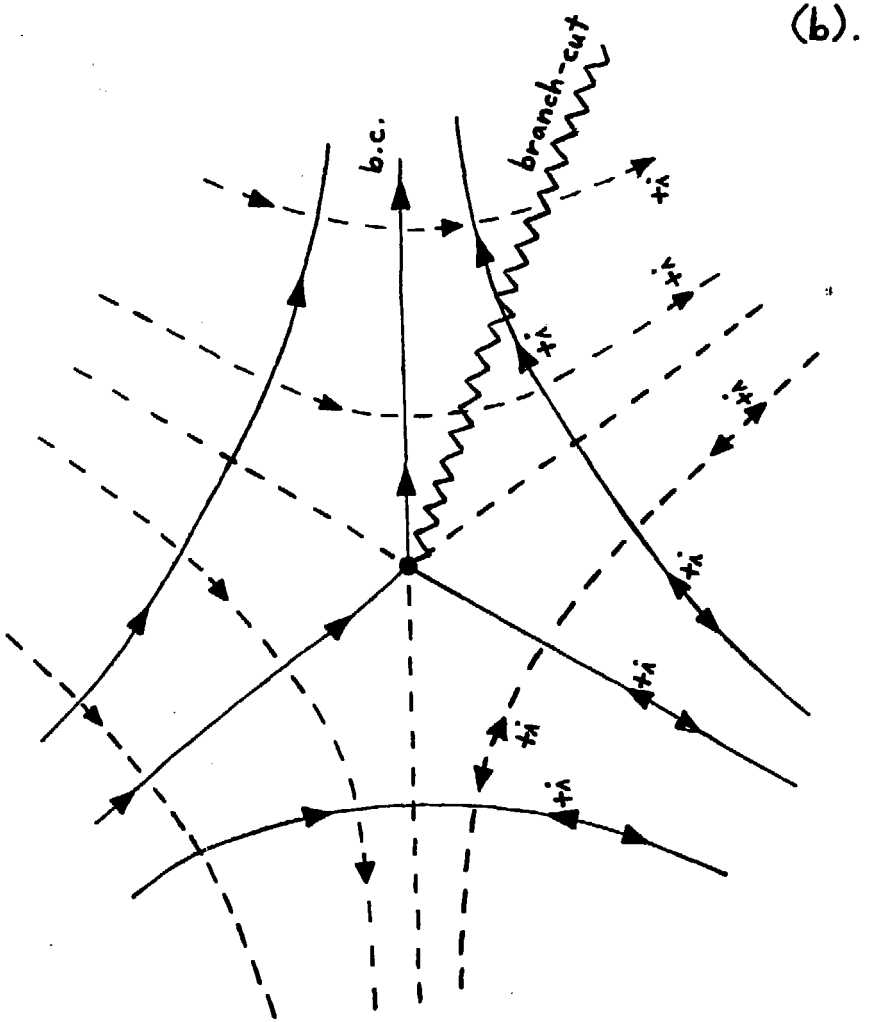

XBL 7710-6878

Fig. IV.1b

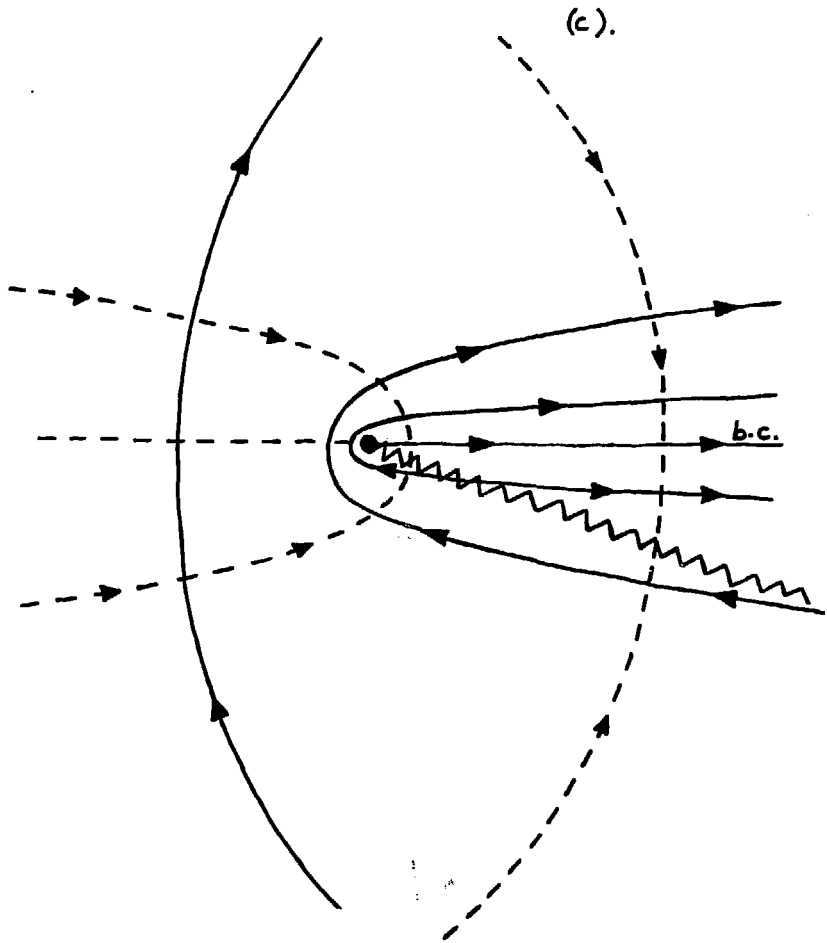

XBL 7710-6876

Fig. IV.1c

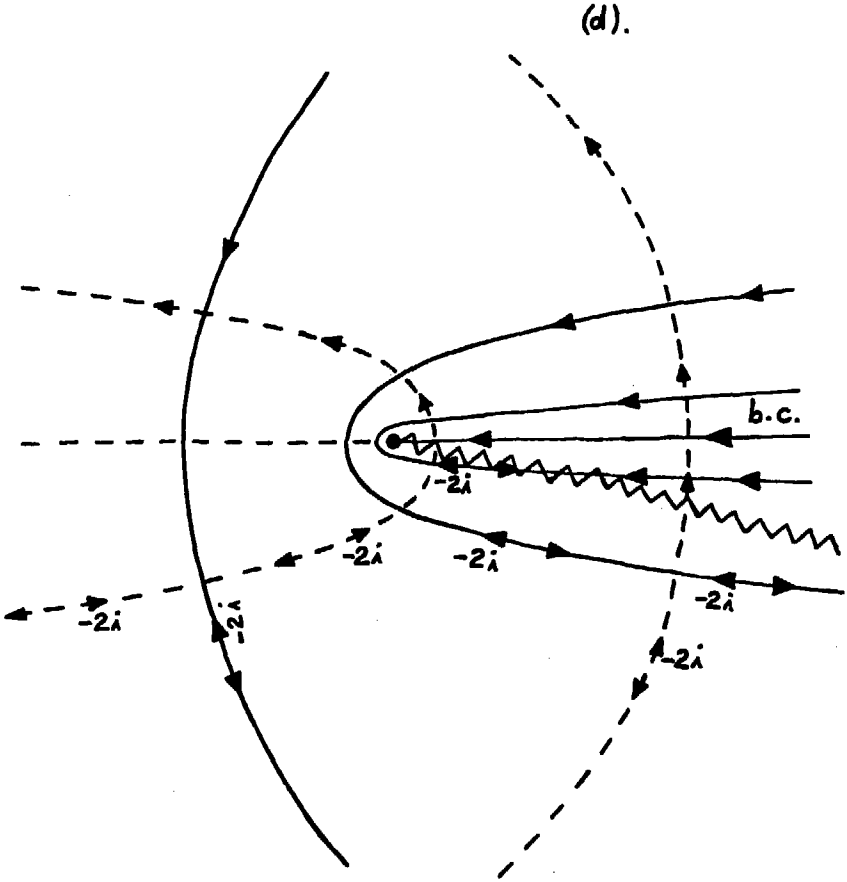

XBL 7710-6867

Fig. IV.1d

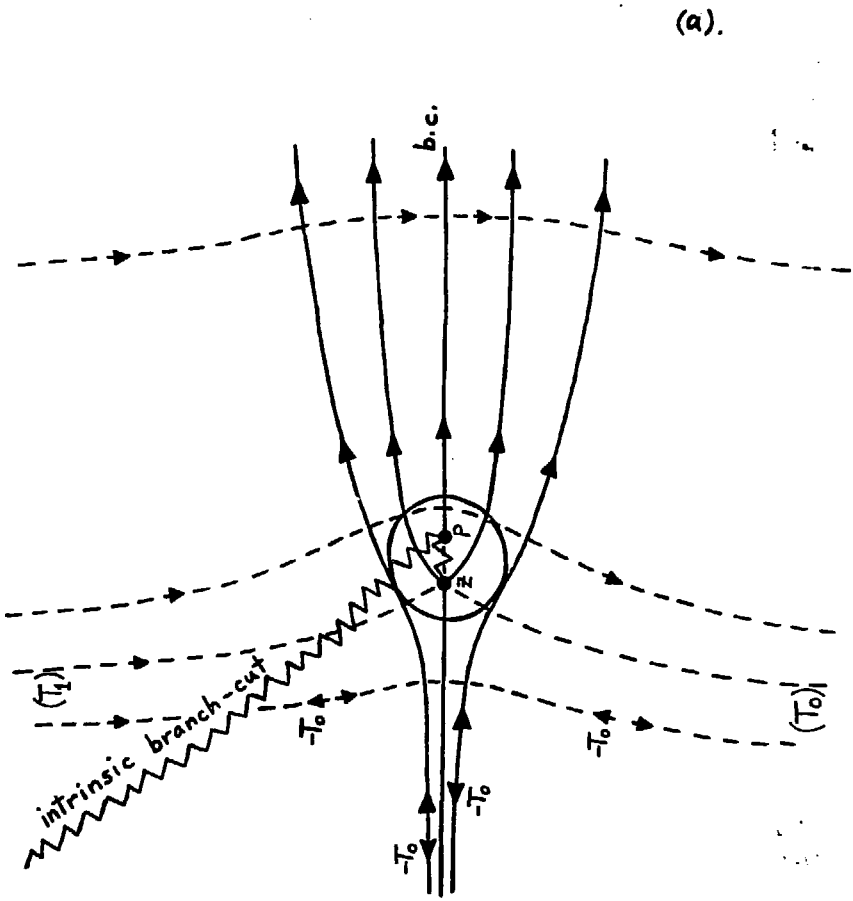

XBL 7710-6880

Fig. IV.2a

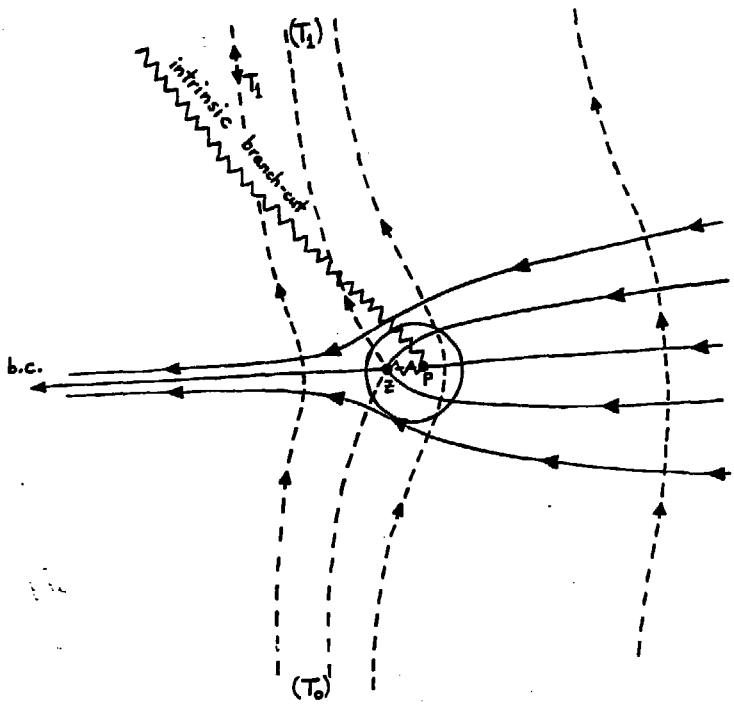

Fig. IV.2b

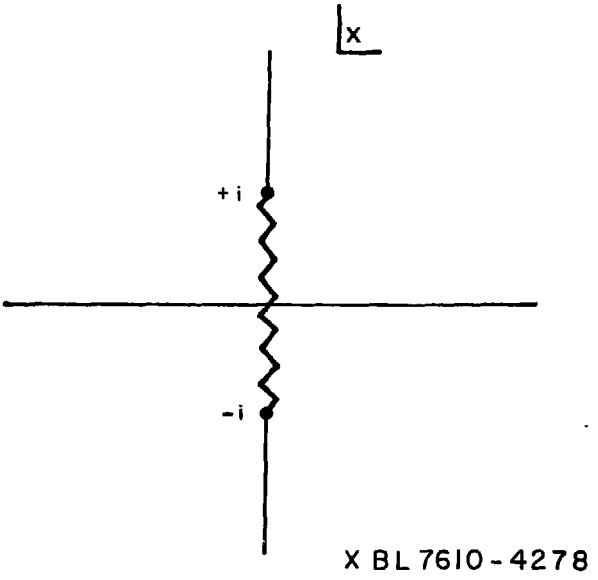

Fig. V.1

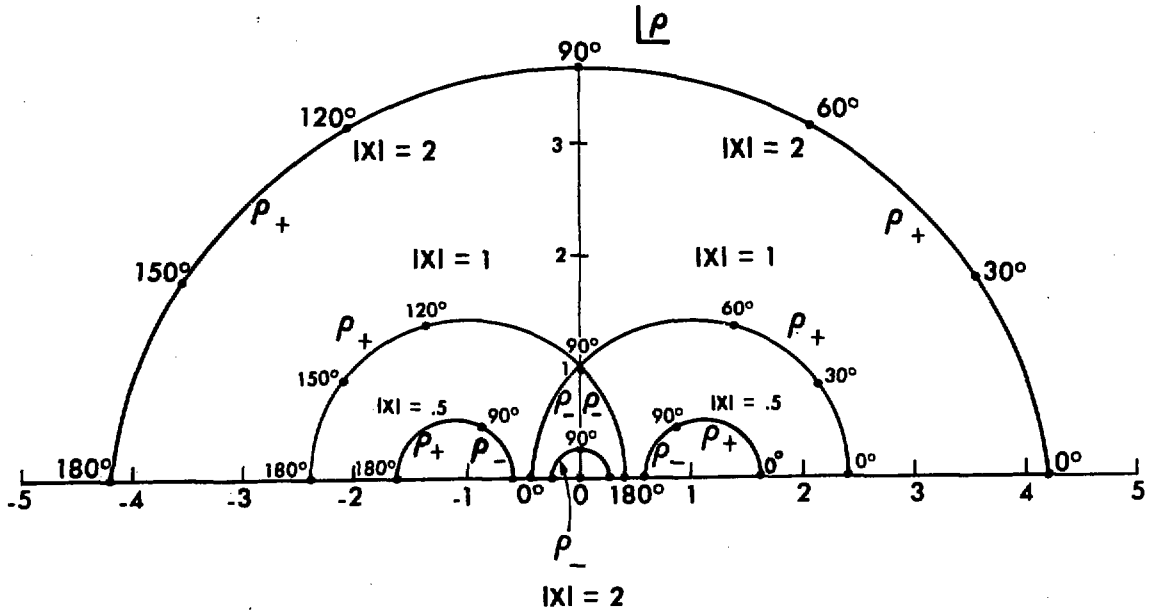

XBL7611-4421

Fig. V.2

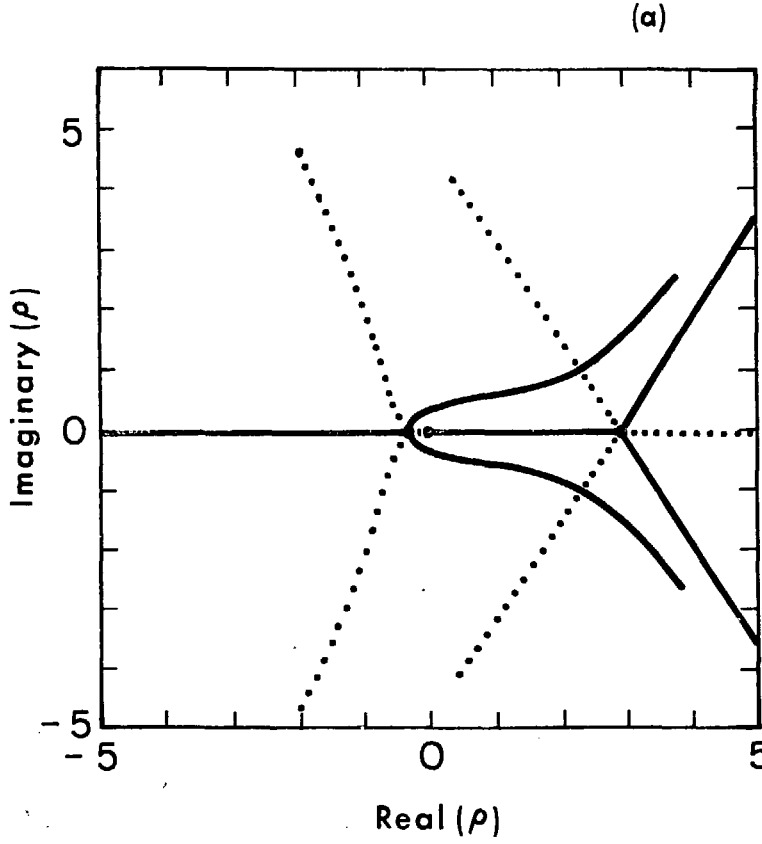

Fig. V.3a

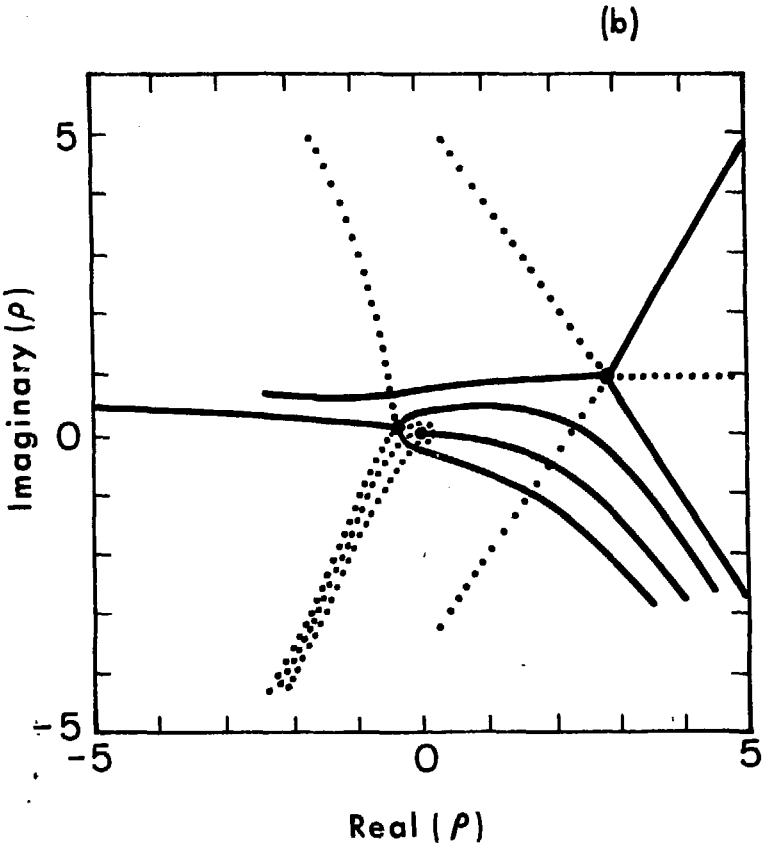

XBL7610-4199

Fig. V.3b

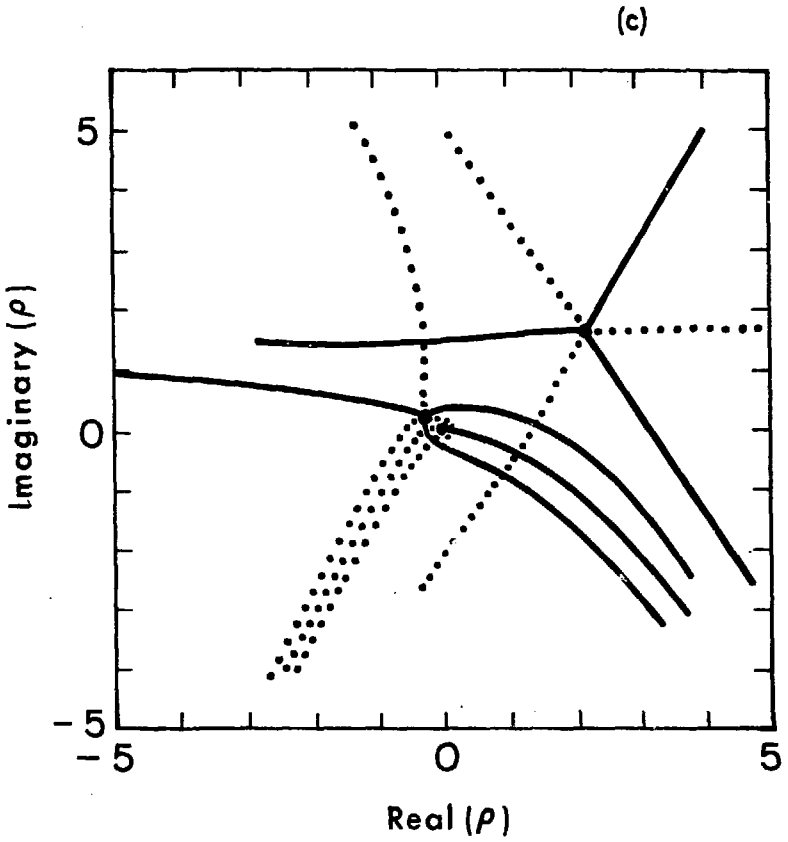

XBL7610-4203

Fig. V.3c

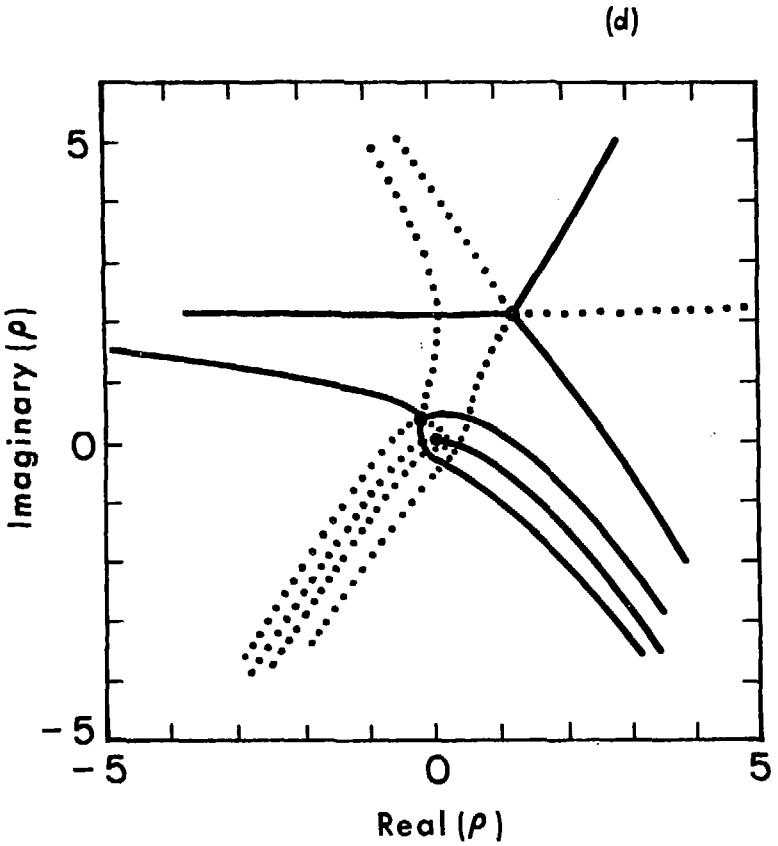

XBL7610-4204

Fig. V.3d

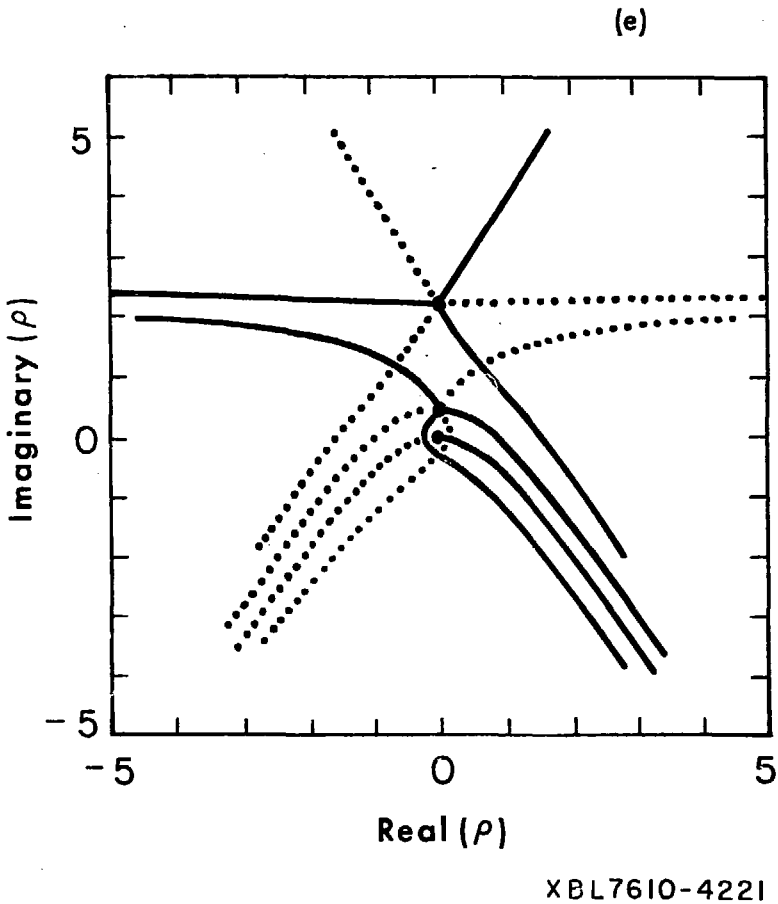

Fig. V.3e

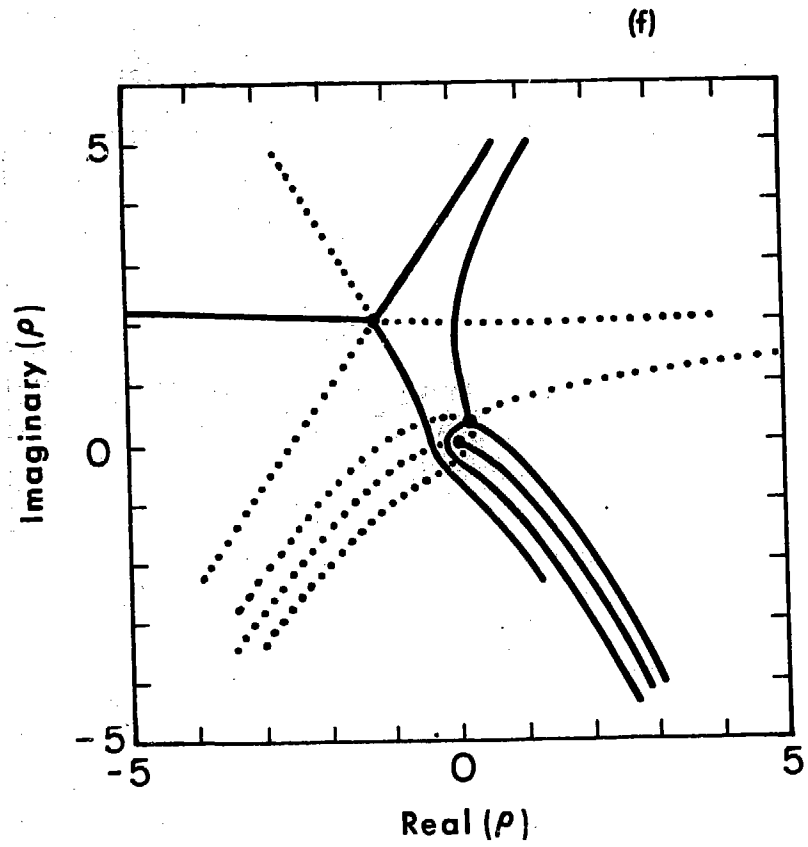

XBL7610-4190

Fig. V.3f

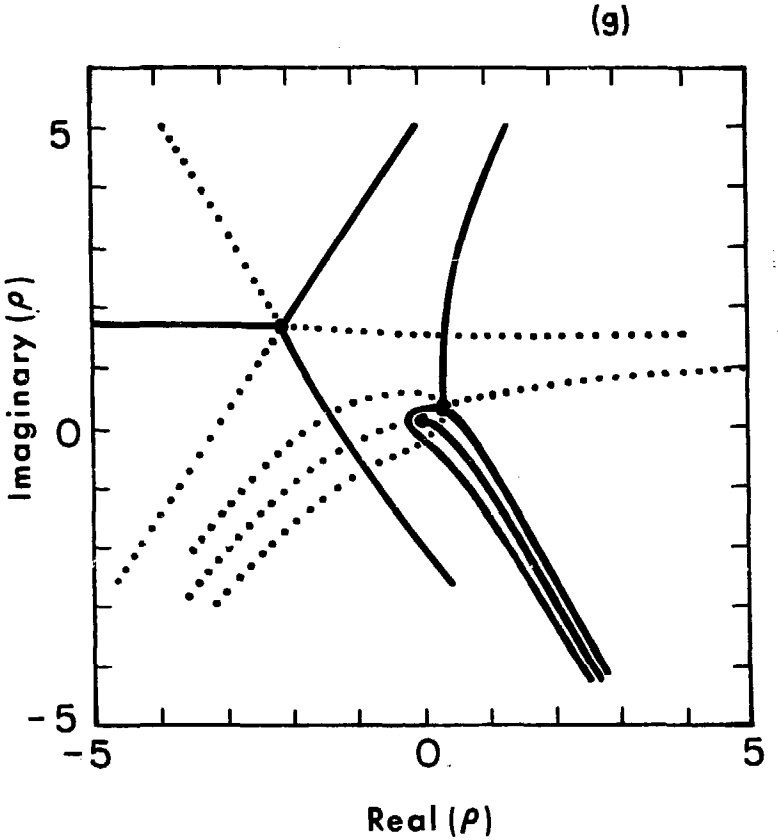

Fig. V.3g

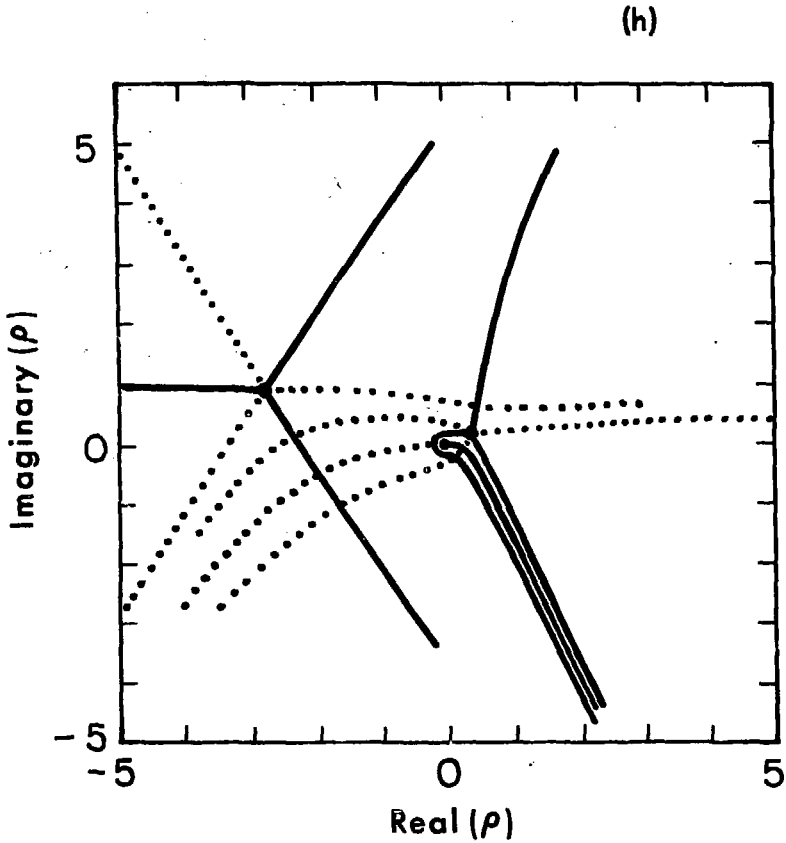

XBL7610-4193

Fig. V.3h

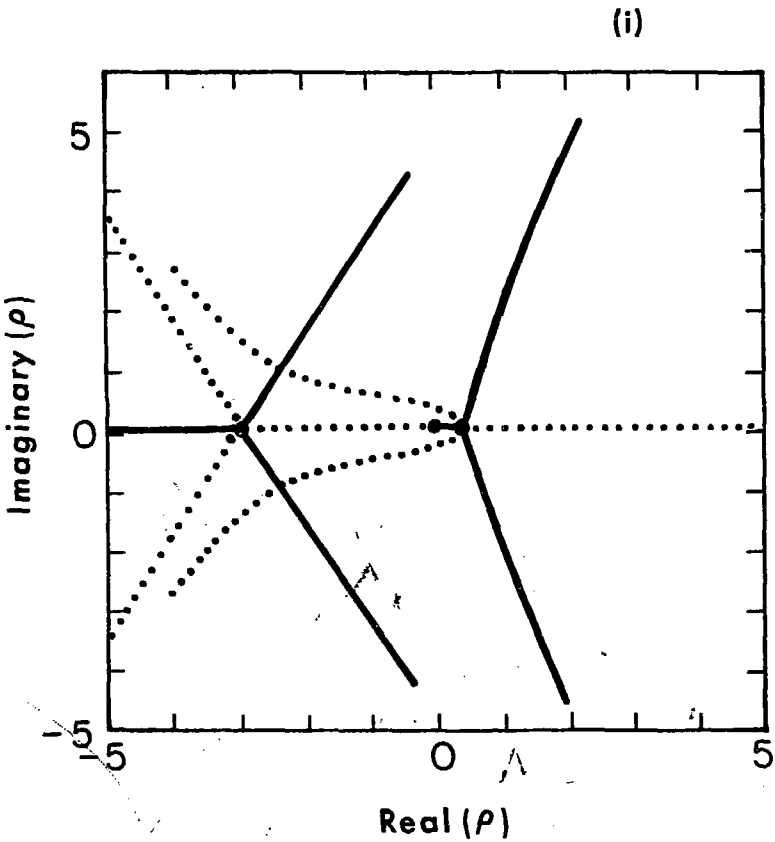

Fig. V.3i

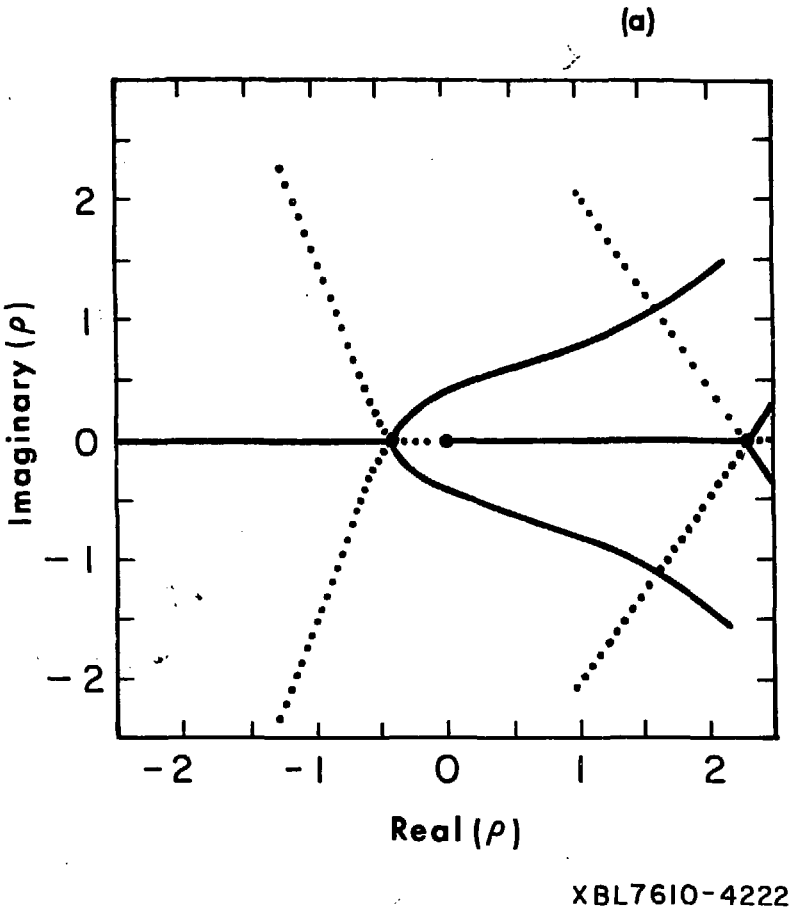

Fig. V.4a

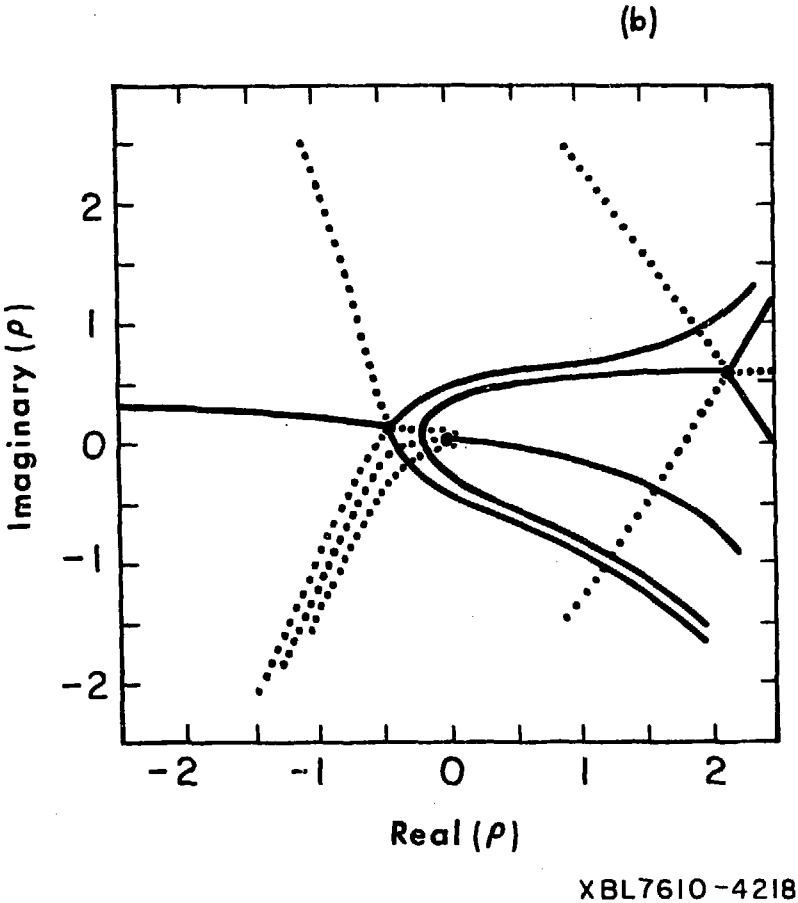

Fig. V.4b

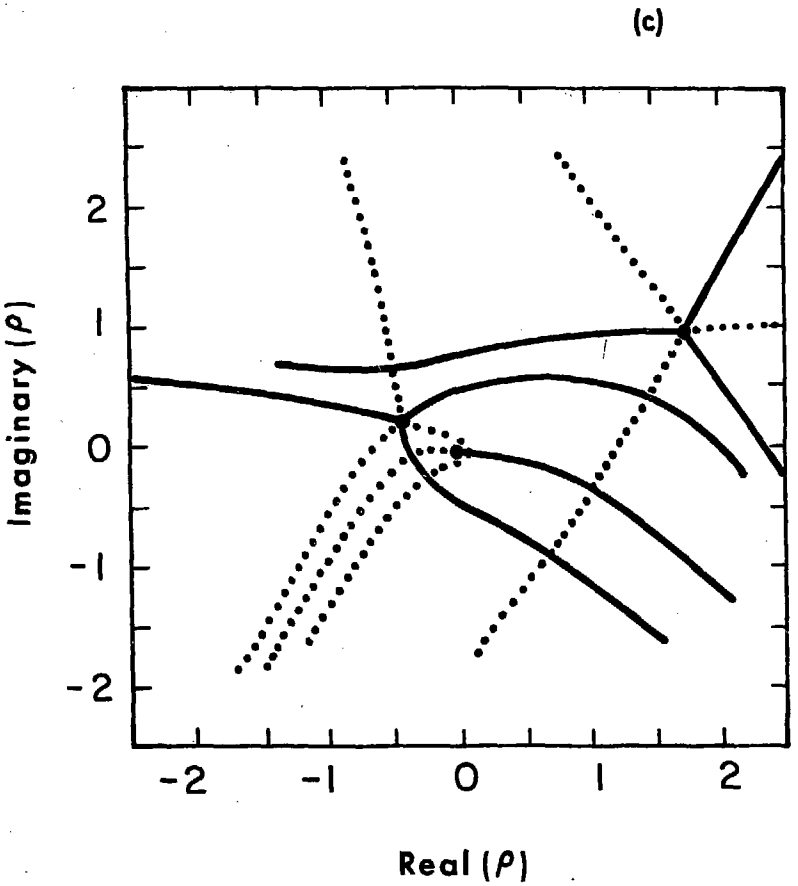

Fig. V.4c

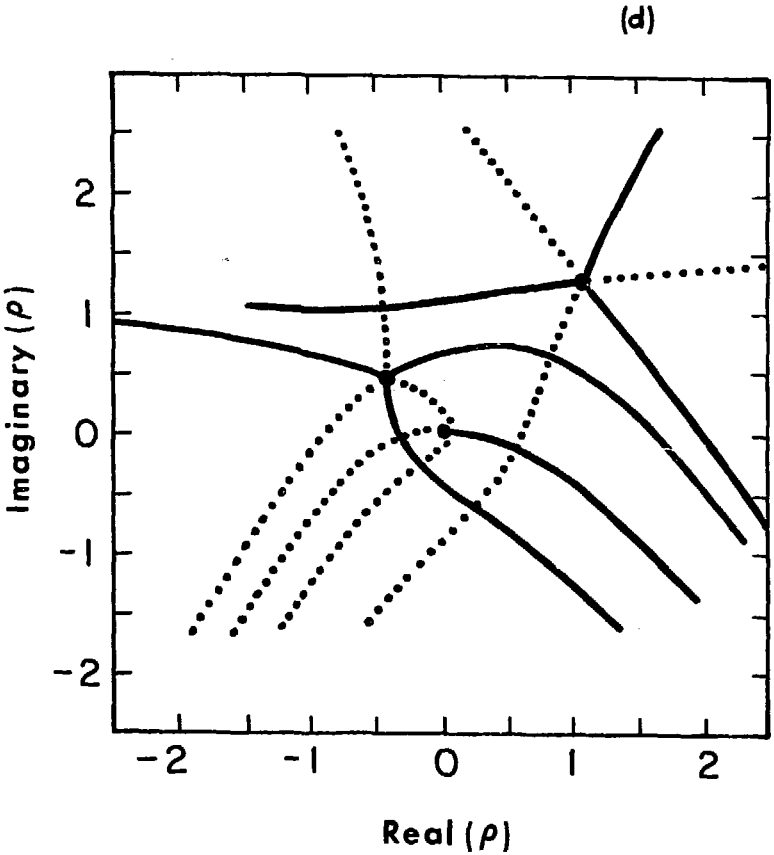

Fig. V.4d

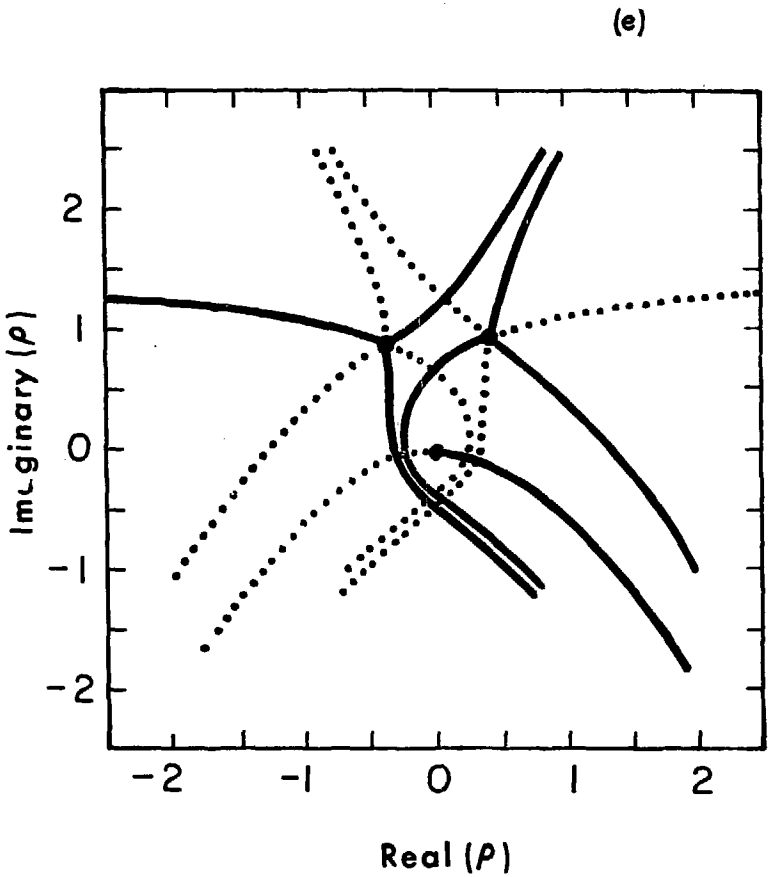

XBL7610-4215

Fig. V.4e

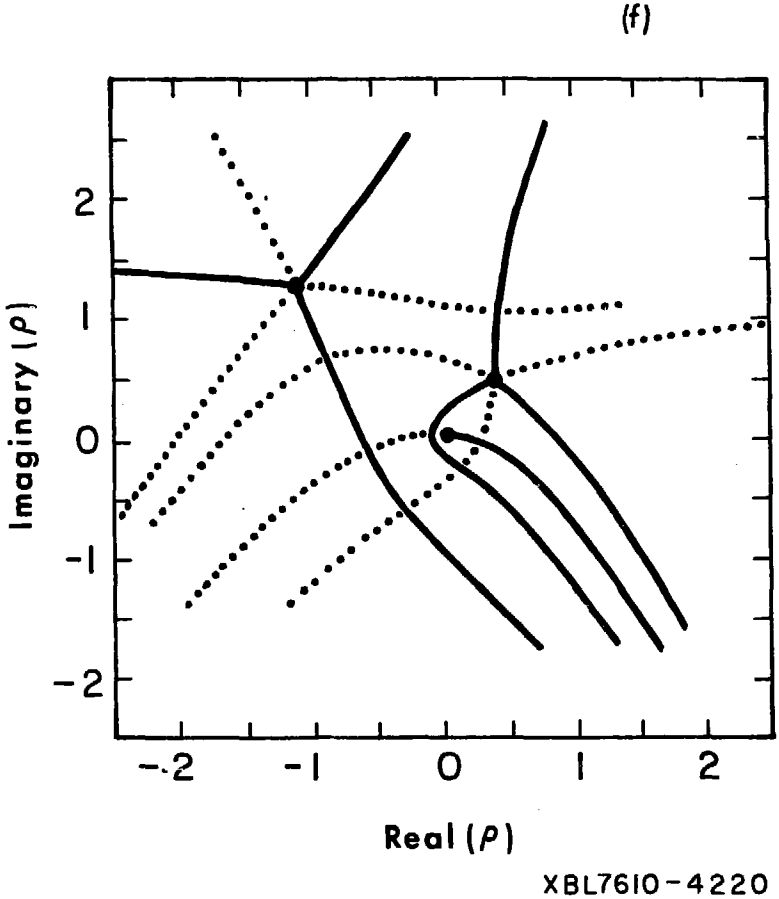

Fig. V.4f

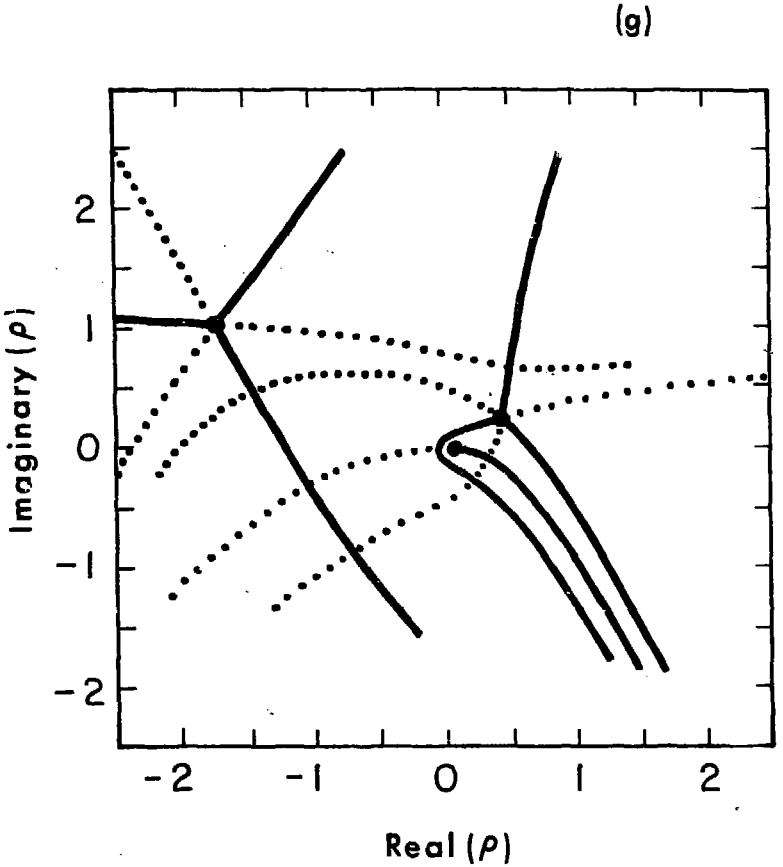

XBL7610-4216

Fig. V.4g

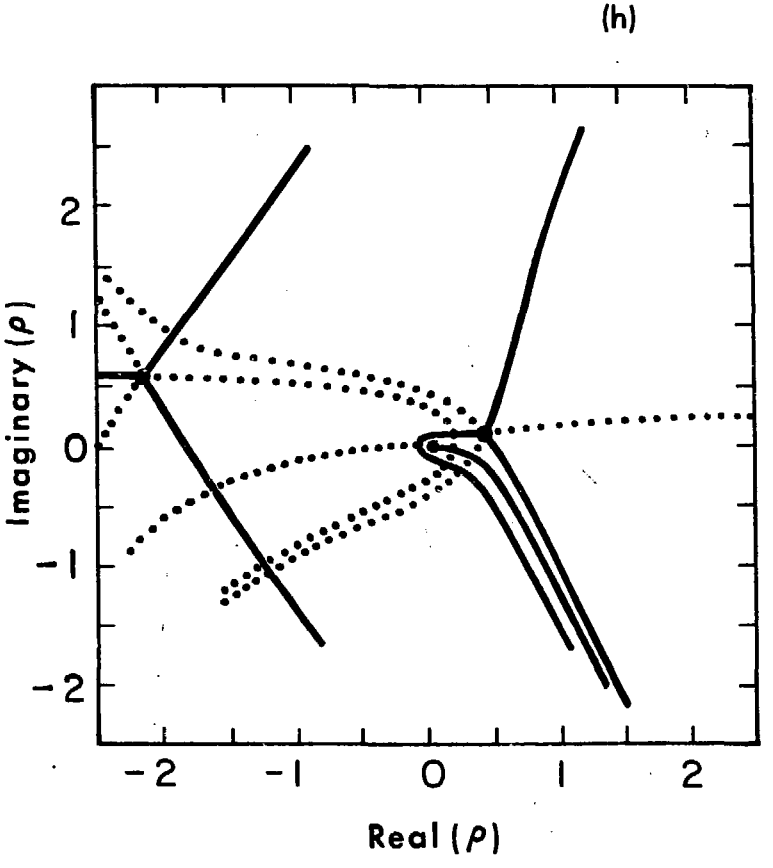

Fig. V.4h

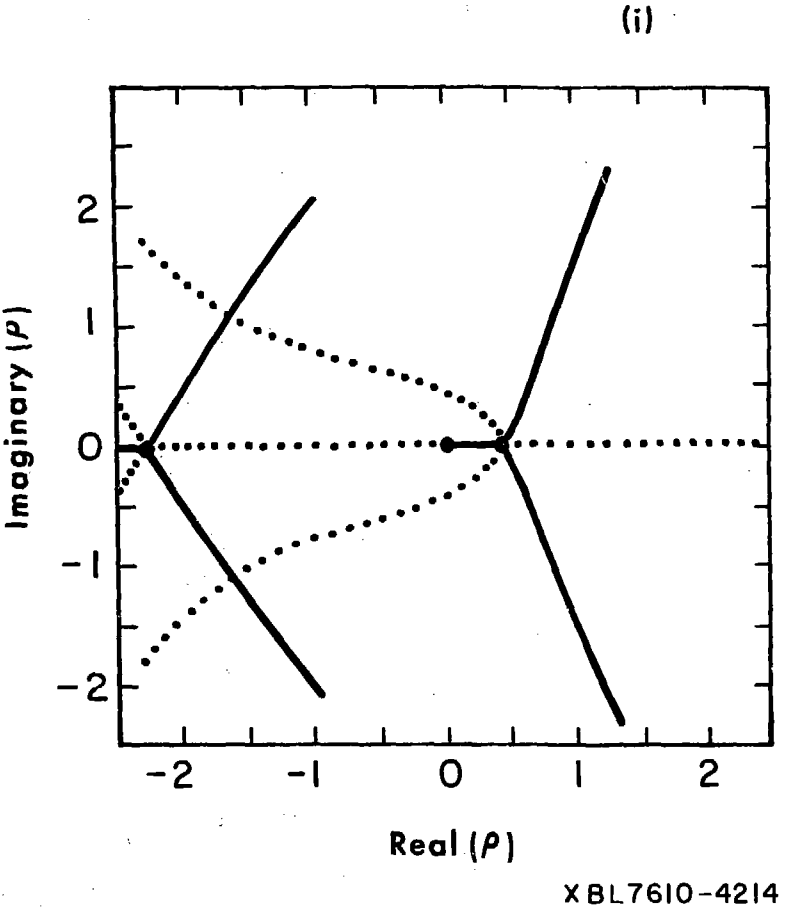

Fig. V.41

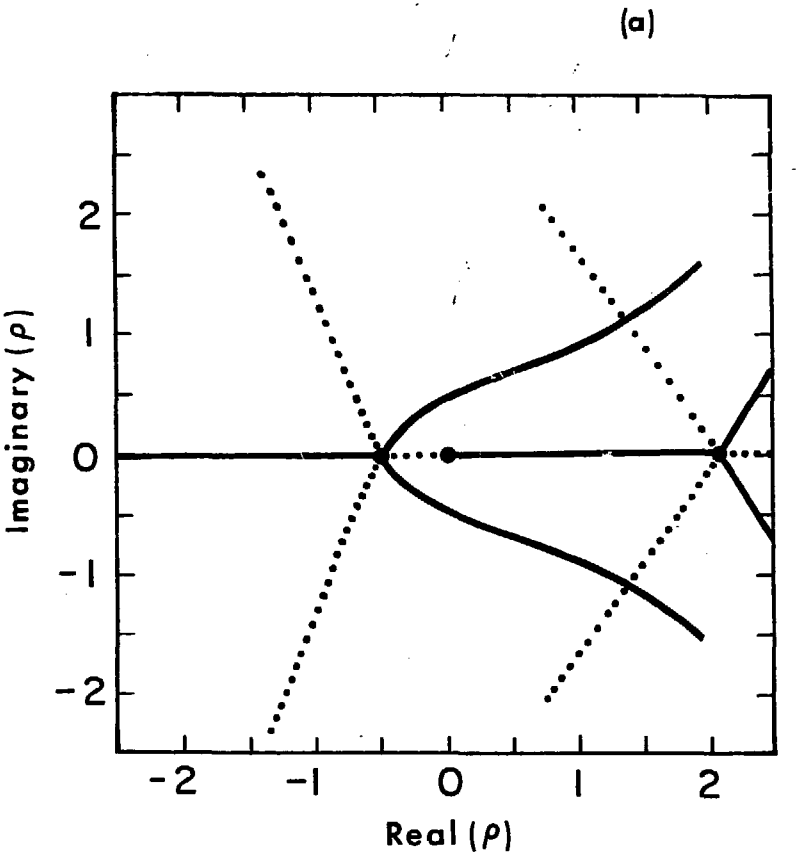

XBL 7610-4184

Fig. V.5a

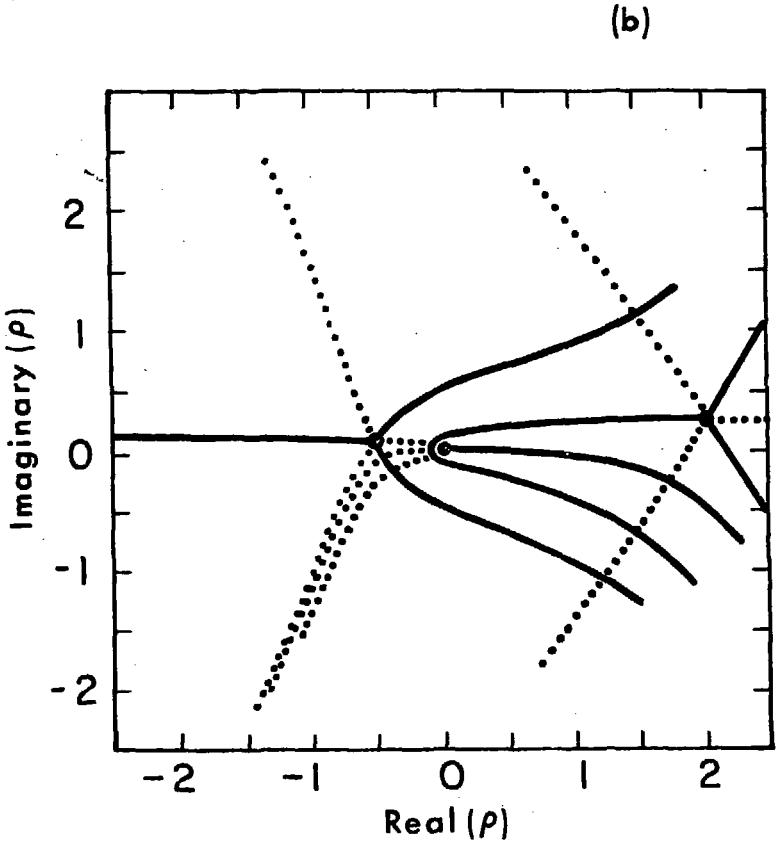

Fig. V.5b

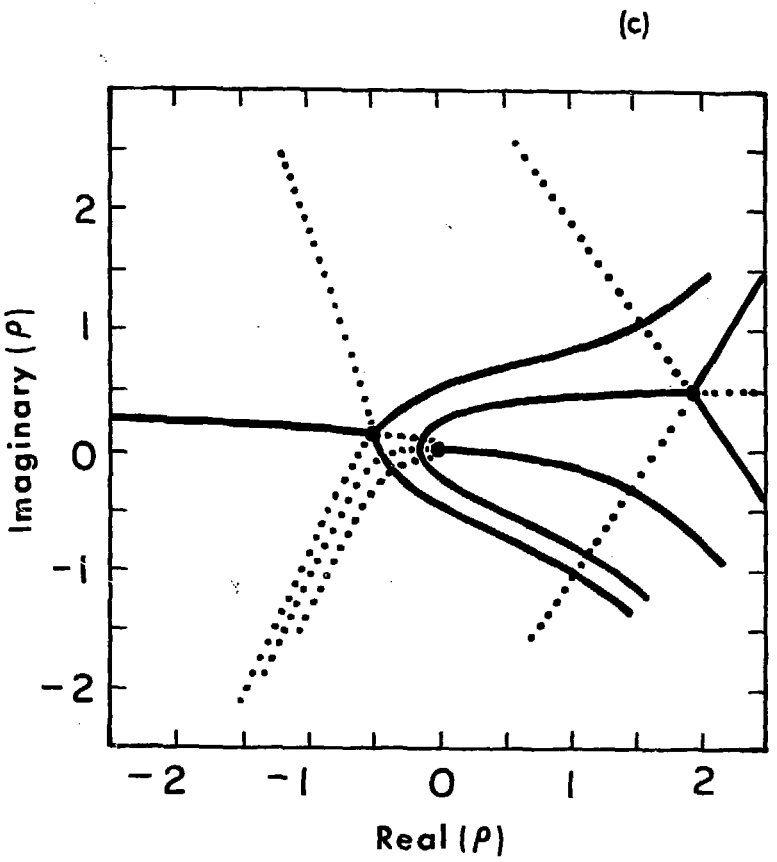

XBL 7610-4188

Fig. V.5c

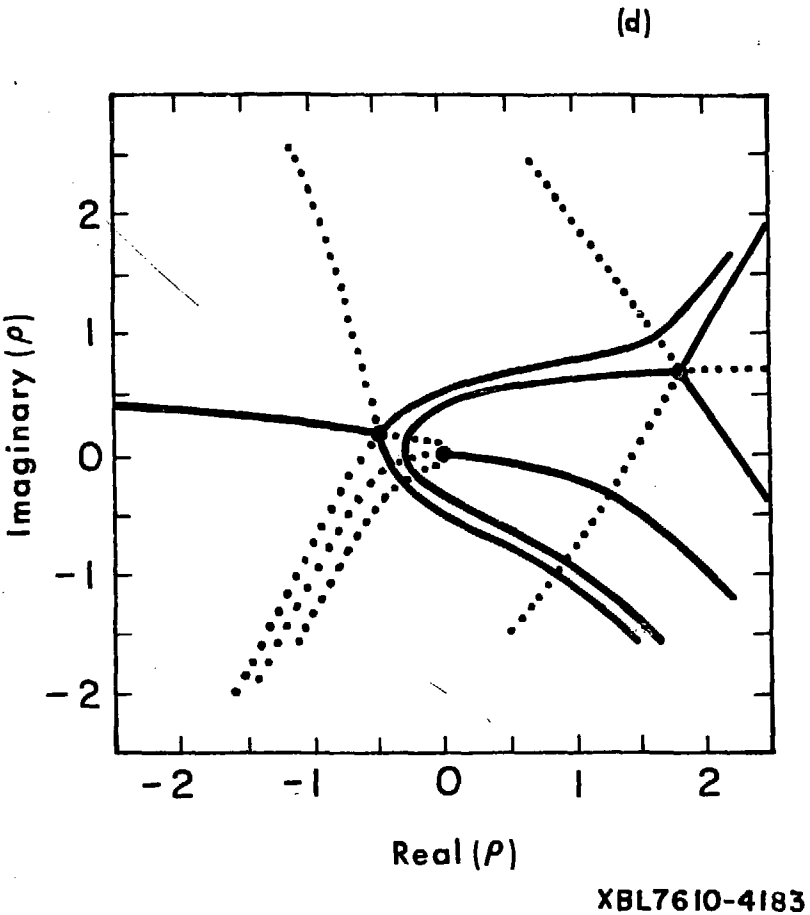

Fig. V.5d

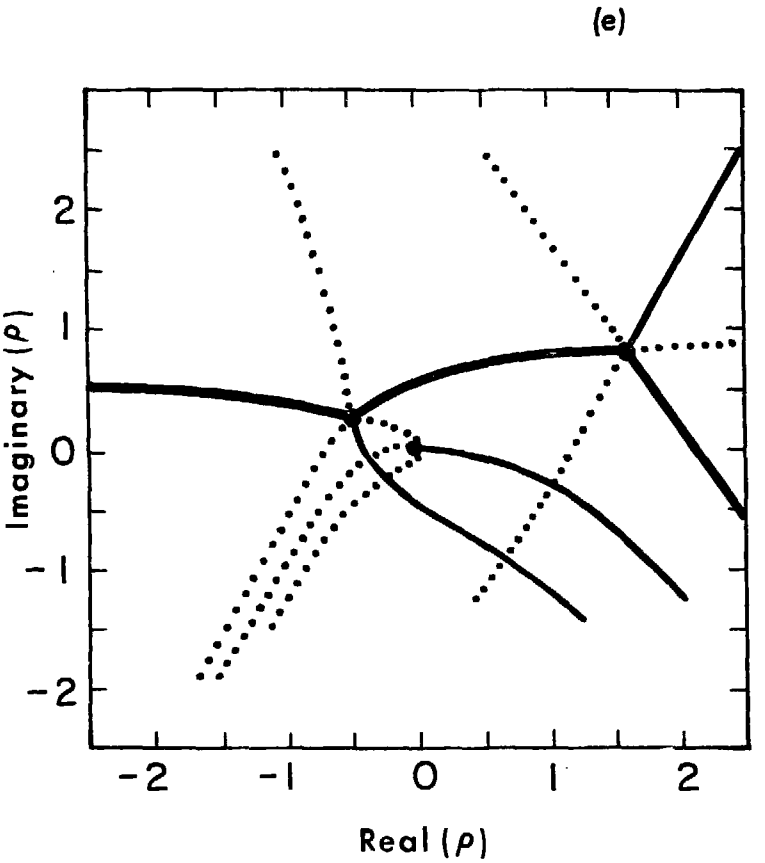

XBL 7610-4187

Fig. V.5e

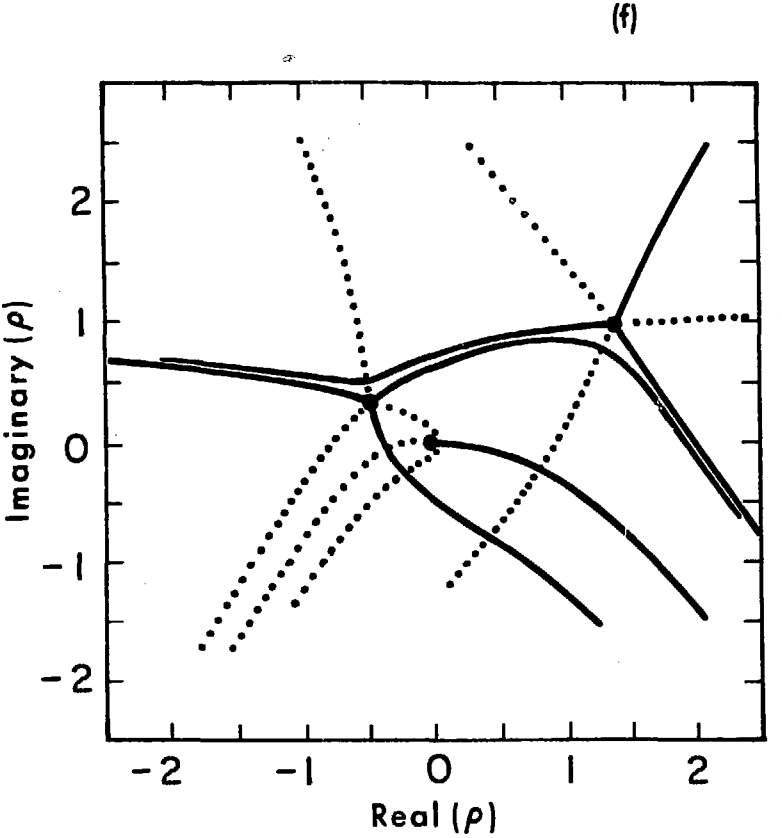

XBL 7610-4186

Fig. V.5f

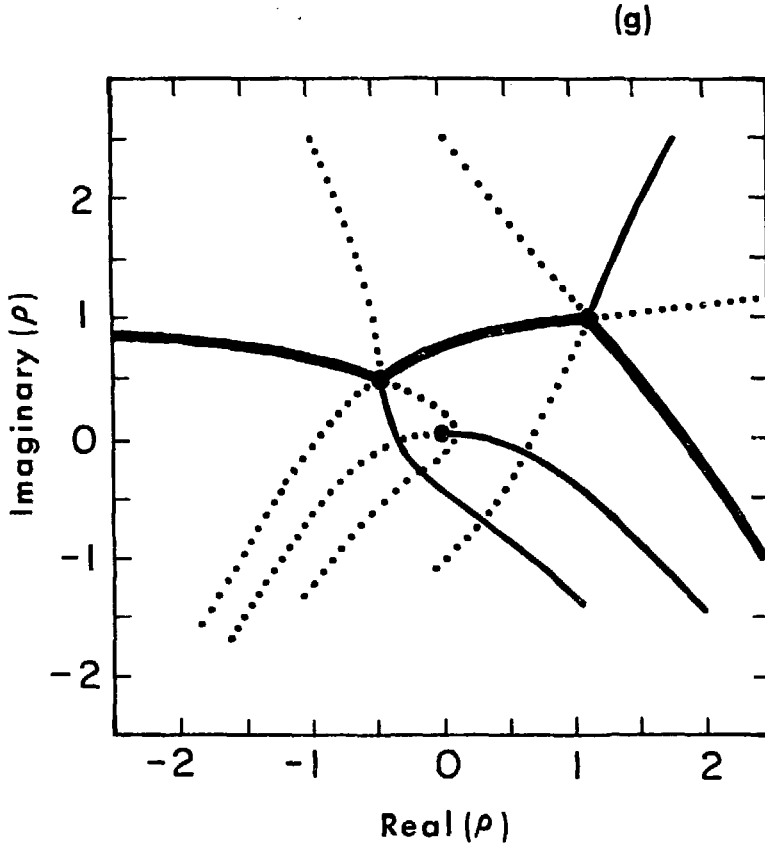

XBL 7610-4192

Fig. V.5g

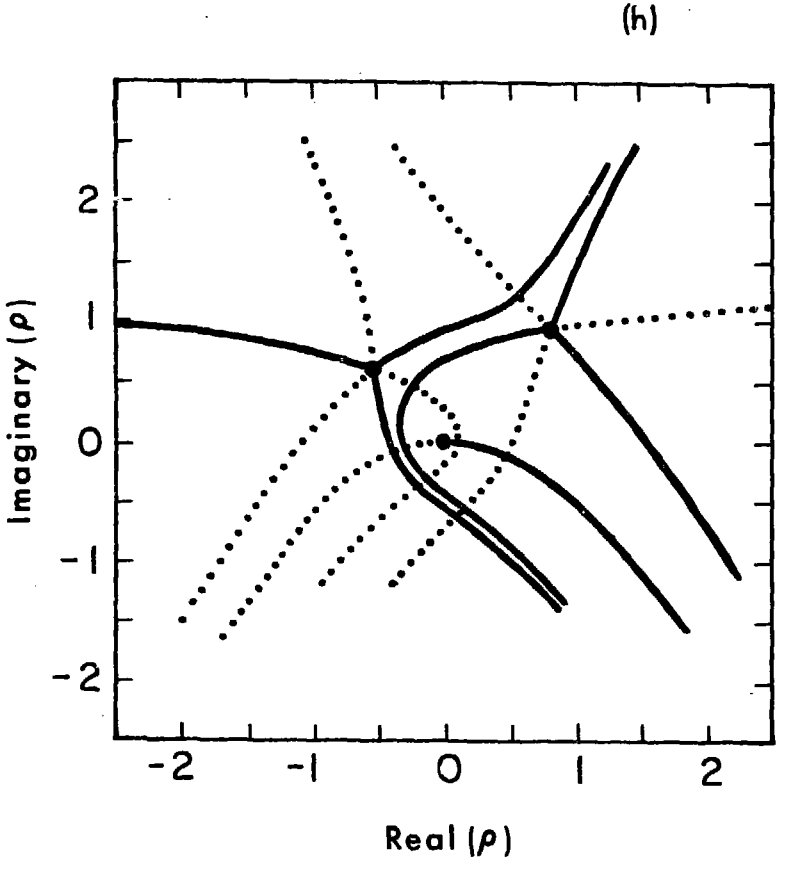

XBL 7610 - 4194

Fig. V.5h

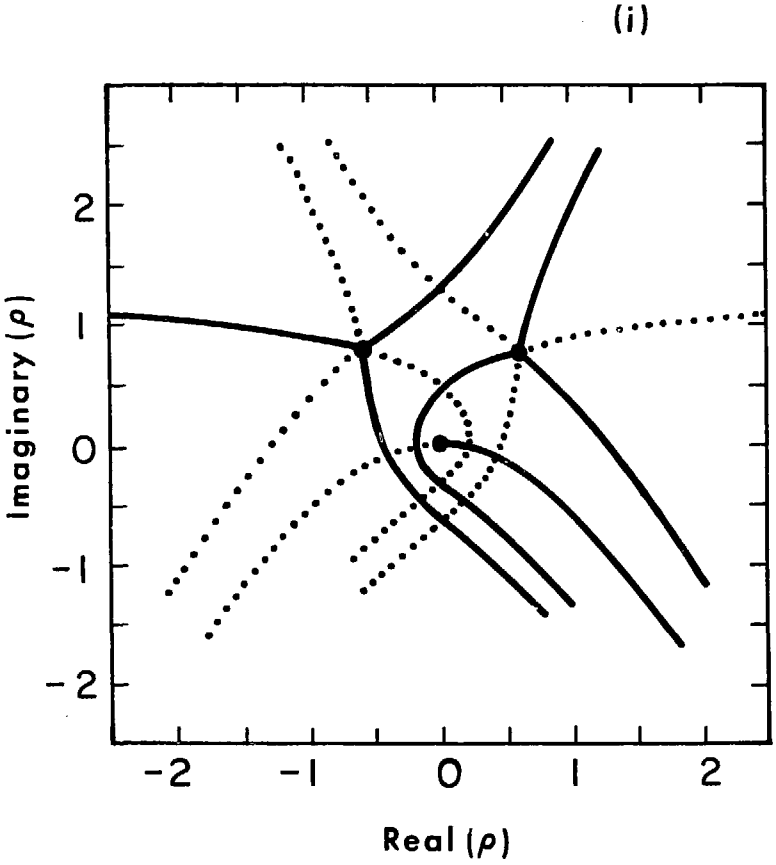

Fig. V.5i

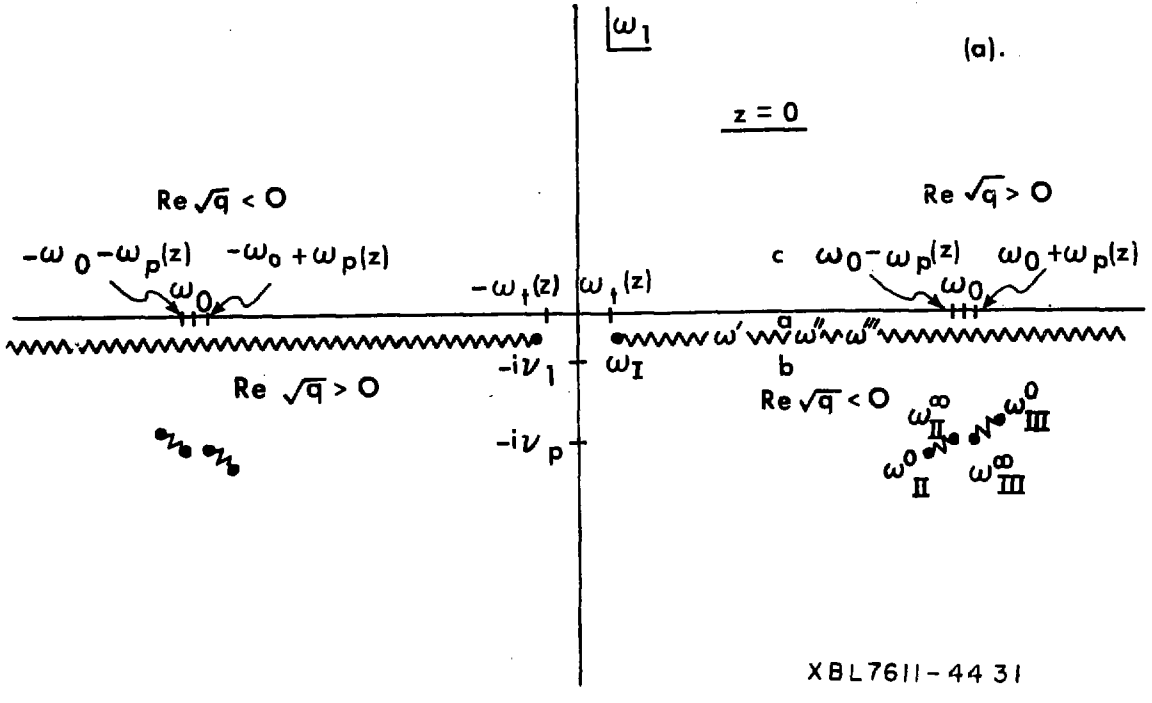
ω_1
(a).
z = 0
Re $\sqrt{q}$ < O
Re $\sqrt{q}$ > O
$-\omega_0 - \omega_p(z)$
$-\omega_0 + \omega_p(z)$
ω_0
$-\omega_t(z)$
$\omega_t(z)$
c
$\omega_0 - \omega_p(z)$
$\omega_0 + \omega_p(z)$
ω_0
ω'
a
ω''
ω'''
b
$-i\nu_1$
ω_I
Re $\sqrt{q}$ > O
Re $\sqrt{q}$ < O
ω^∞_{II}
ω^0_{III}
$-i\nu_p$
ω^0_{II}
ω^∞_{III}
XBL7611-4431

Fig. V.6a

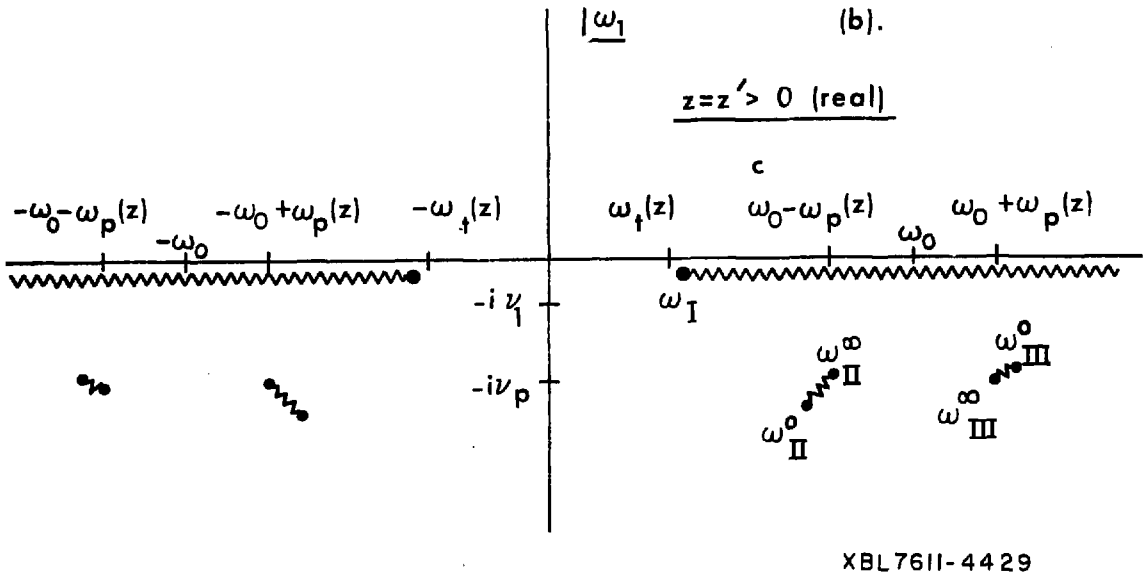
$|\omega_1$
(b).
$z=z' > 0$ (real)
c
$-\omega_0-\omega_p(z)$
$-\omega_0+\omega_p(z)$
$-\omega_t(z)$
$-\omega_0$
$\omega_t(z)$
$\omega_0-\omega_p(z)$
ω_0
$\omega_0+\omega_p(z)$
$-i\nu_1$
$-i\nu_p$
ω_I
ω^∞_{II}
ω^o_{II}
ω^o_{III}
ω^∞_{III}
XBL7611-4429

Fig. V.6b

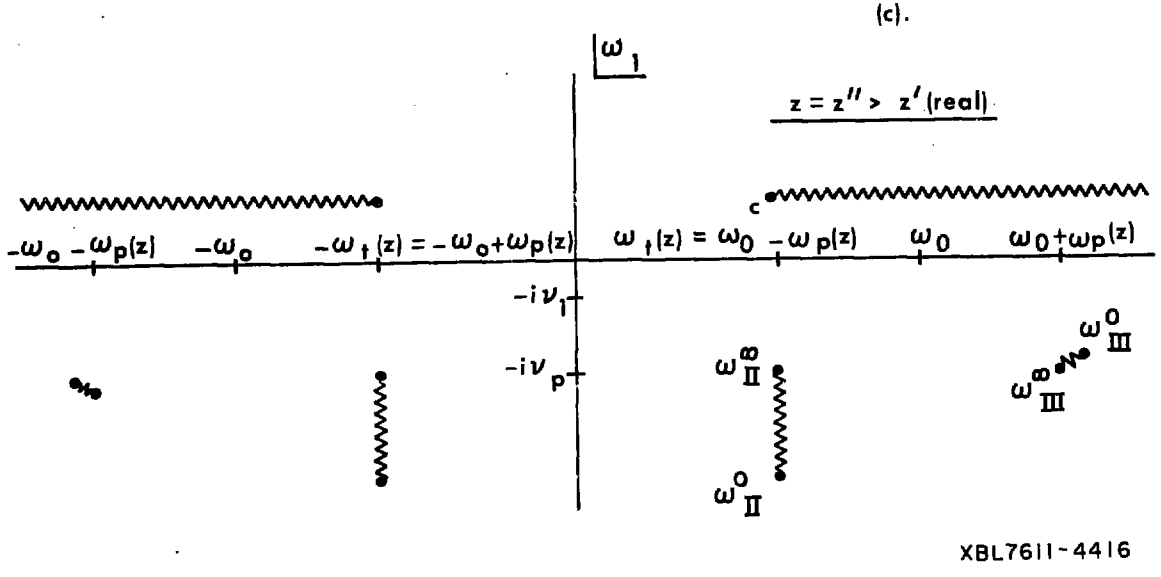
(c).
ω_1
$z = z'' > z'$ (real)
c
$-\omega_o - \omega_p(z)$
$-\omega_o$
$-\omega_1(z) = -\omega_o + \omega_p(z)$
$\omega_1(z) = \omega_0 - \omega_p(z)$
ω_0
$\omega_0 + \omega_p(z)$
$-i\nu_1$
$-i\nu_p$
ω^∞_{II}
ω^o_{II}
ω^o_{III}
ω^∞_{III}
XBL7611-4416

Fig. V.6c

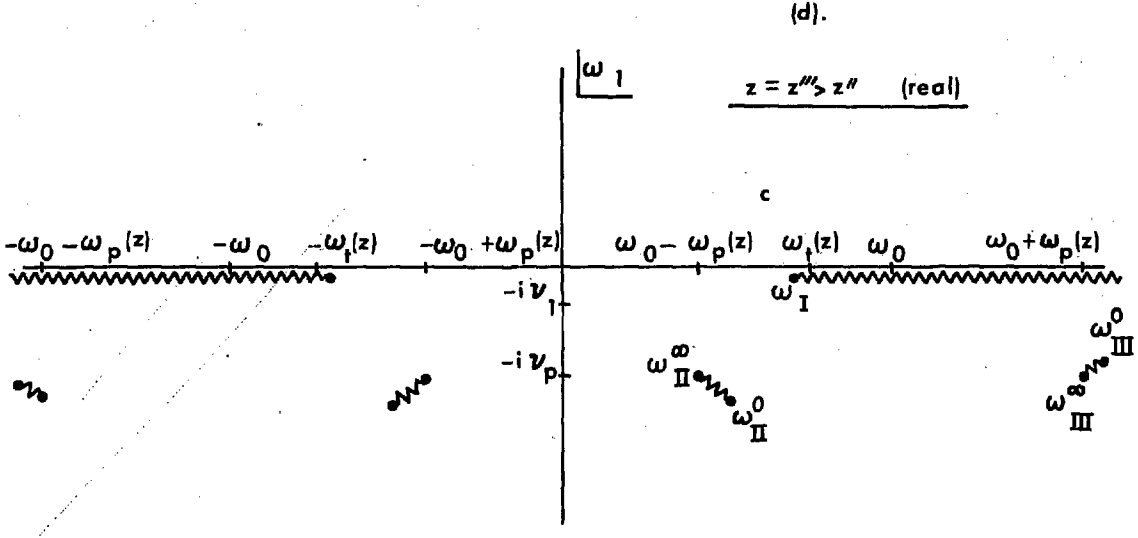

Fig. V.6d XBL 7611-4417

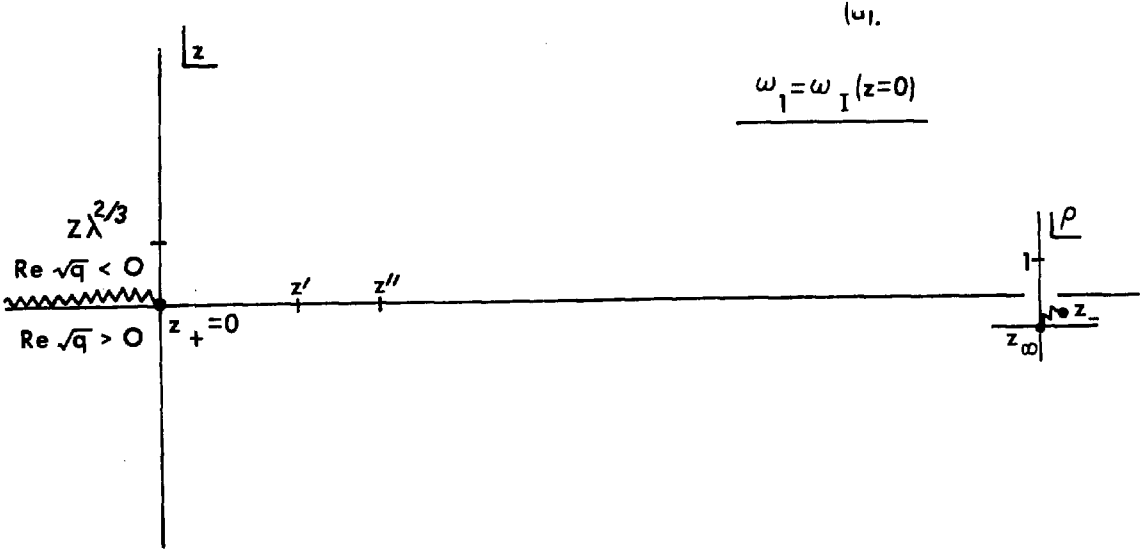

Fig. V.7a

XBL 7611-4430

(b).

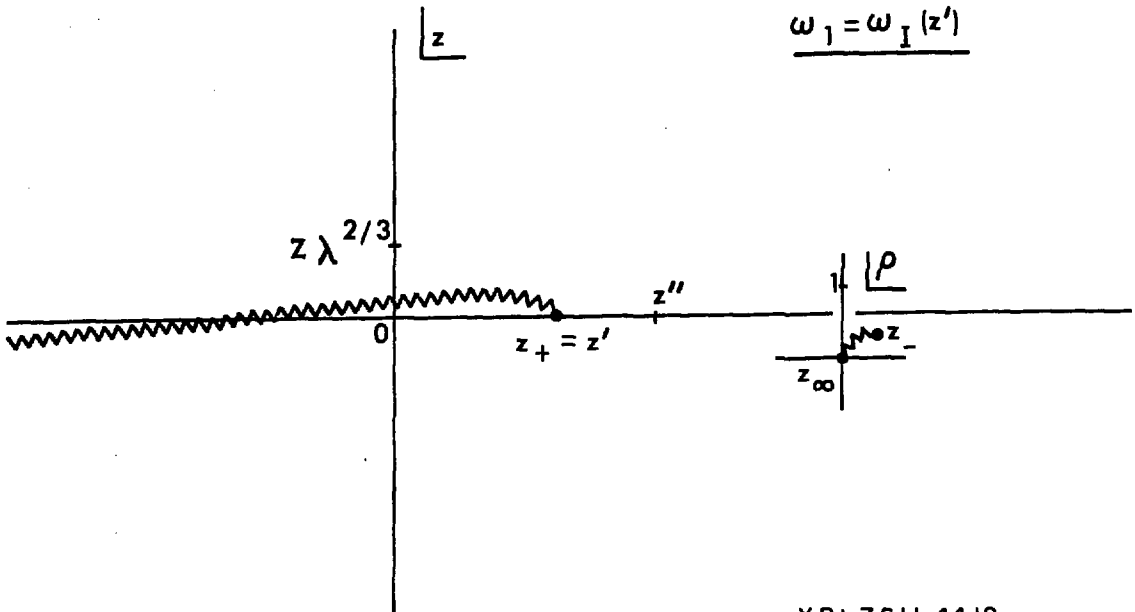

XBL7611-4418

Fig. V.7b

(c).

$\omega_1 = \omega_I(z'')$

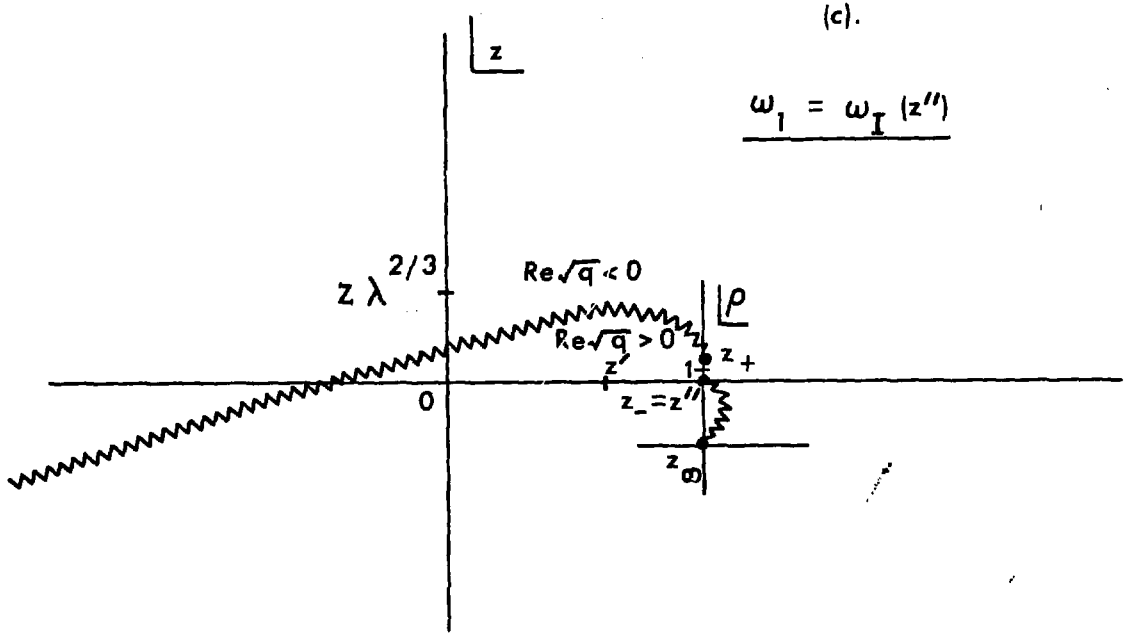

XBL 7611-4419

Fig. V.7c

(d).

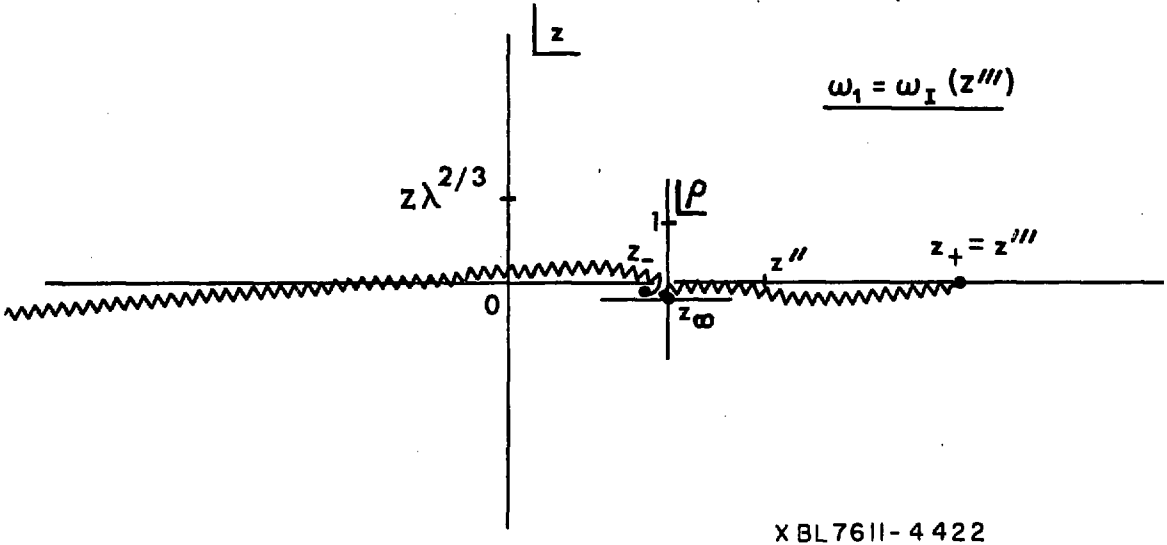

XBL7611-4422

Fig. V.7d

(e).

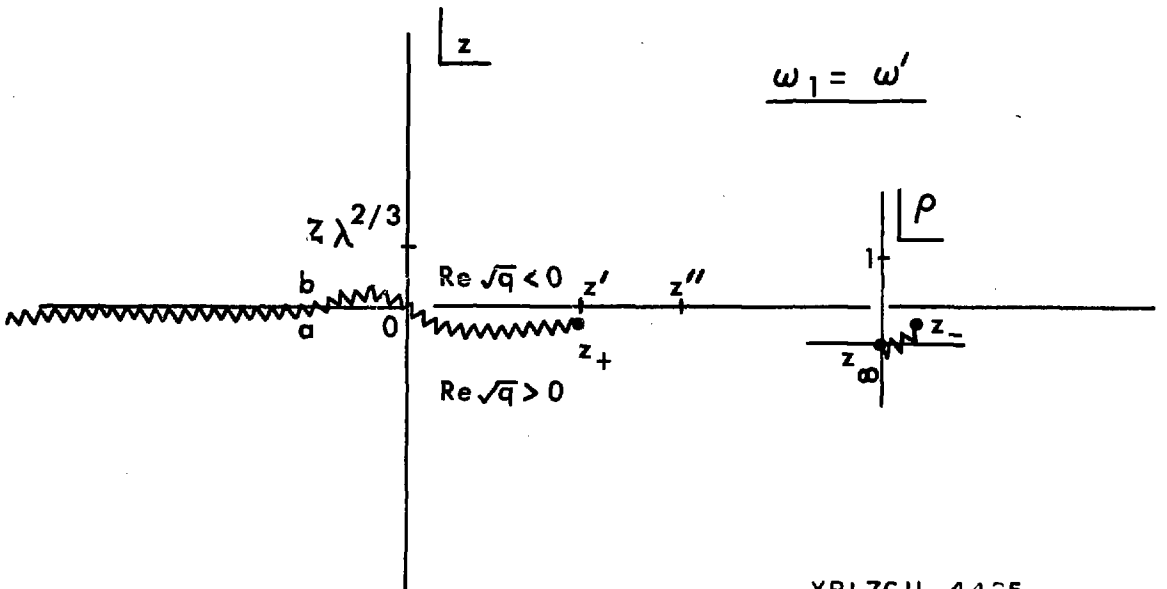

XBL7611-4425

Fig. V.7e

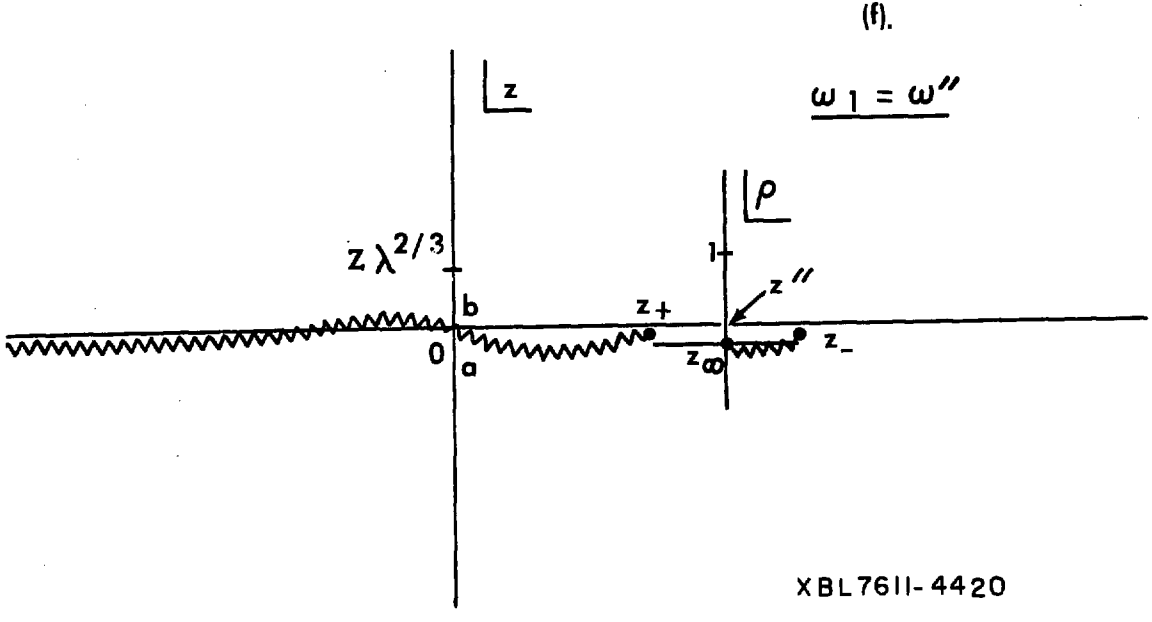

Fig. V.7f

(g).

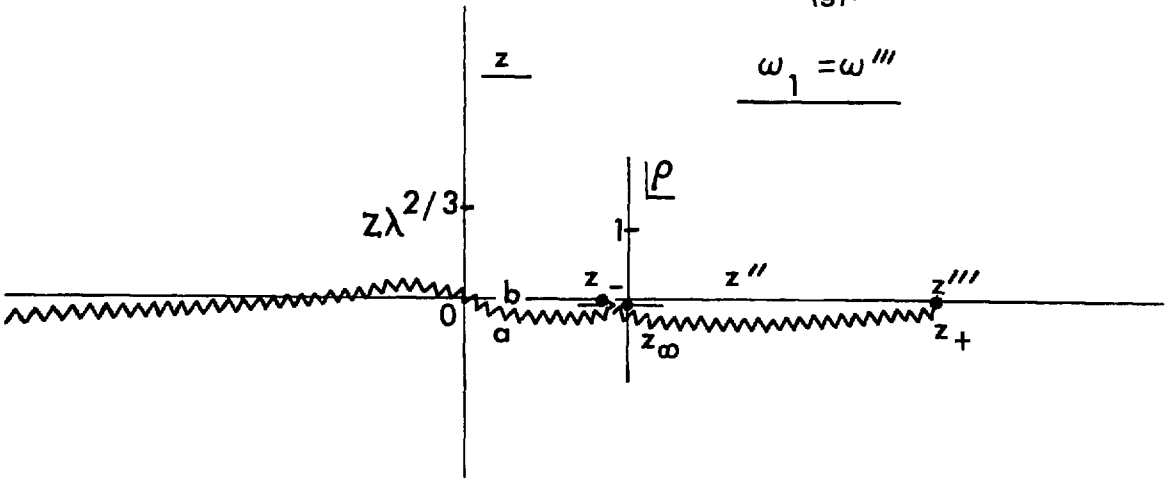

Fig. V.7g

XBL7611-4428

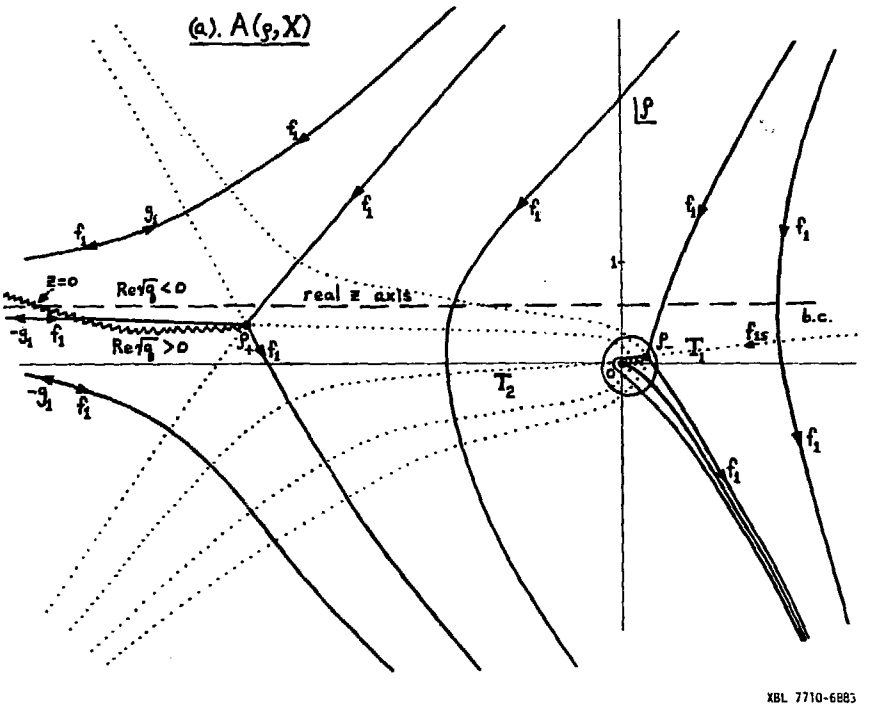

Fig. V.8a

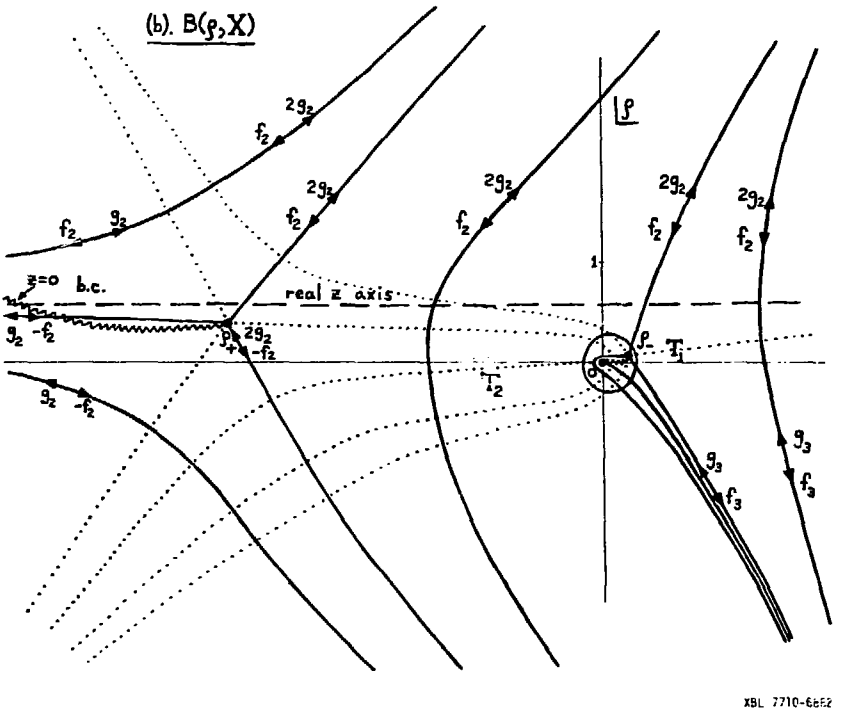

Fig. V.8b

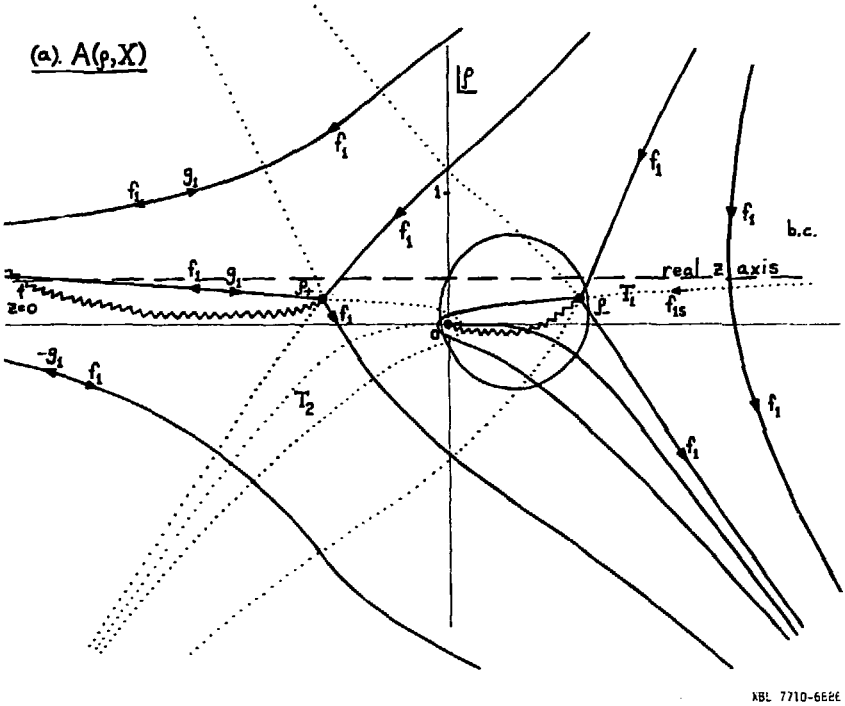

Fig. V.9a

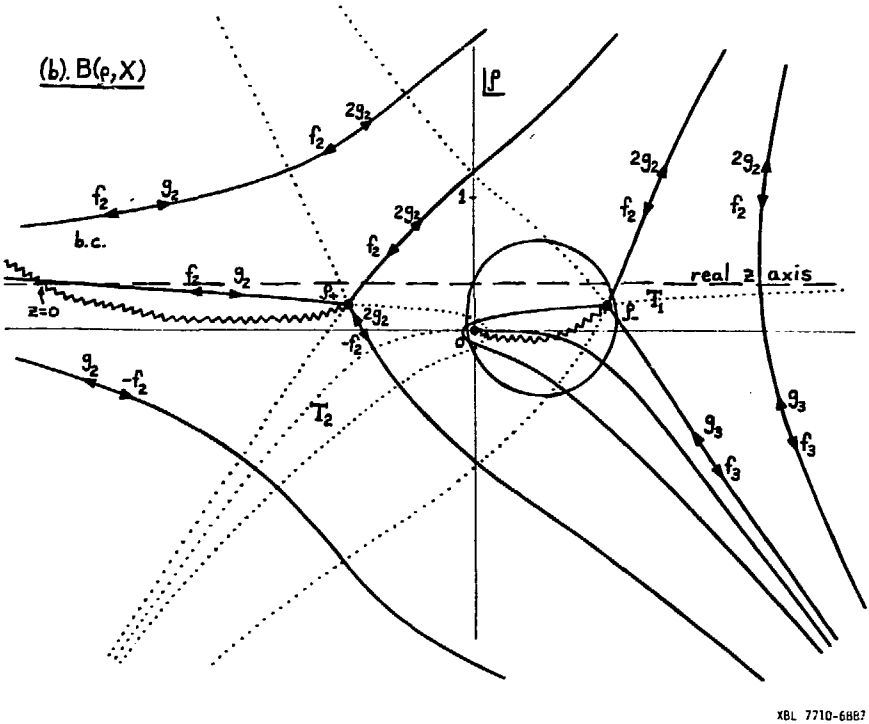
(b). B(ρ,X)
|ρ
b.c.
real z axis
z=0
1
0
f_2
g_2
$2g_2$
$-f_2$
ρ_+
ρ_-
T_1
T_2
g_3
f_3
XBL 7710-6887

Fig. V.9b

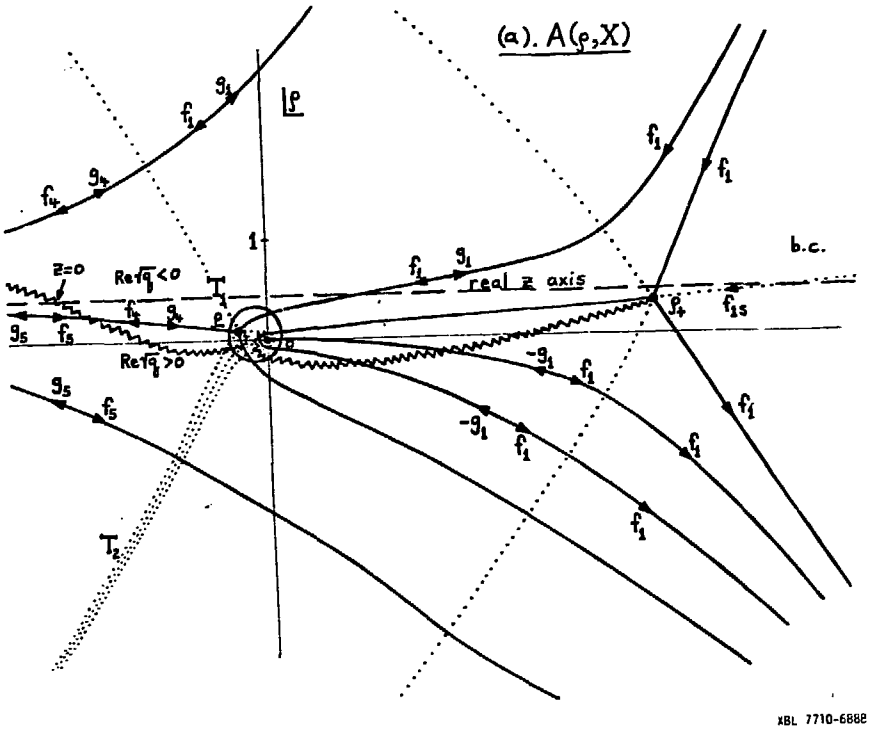

Fig. V.10a

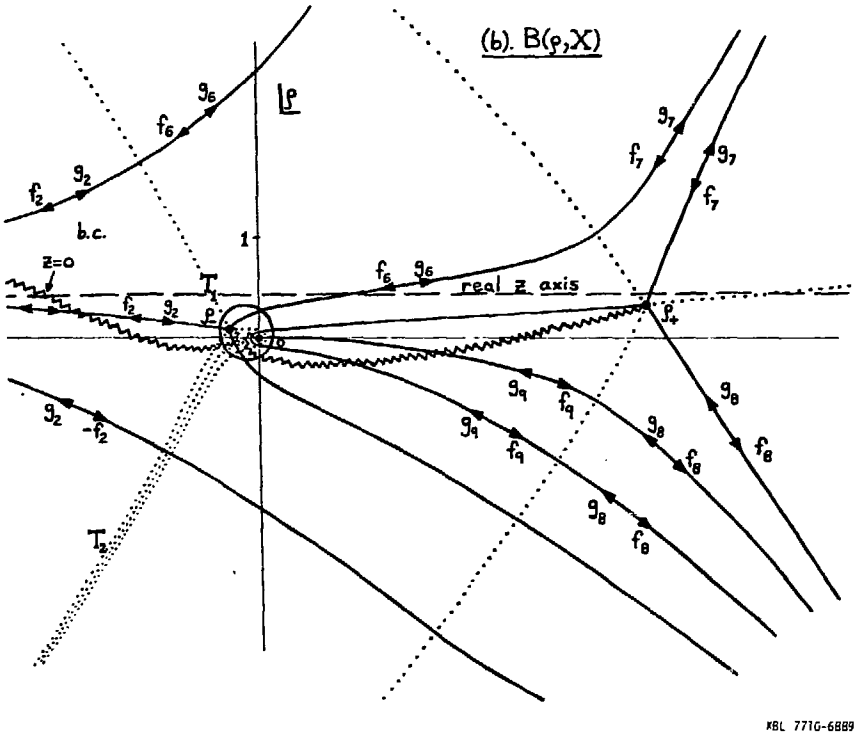
(b). B(ρ,X)
|ρ
1
b.c.
z=0
real z axis
ρ+
ρ-
T1
T2
f2
g2
f6
g6
f7
g7
f8
g8
f9
g9
XBL 7710-6889

Fig. 10b

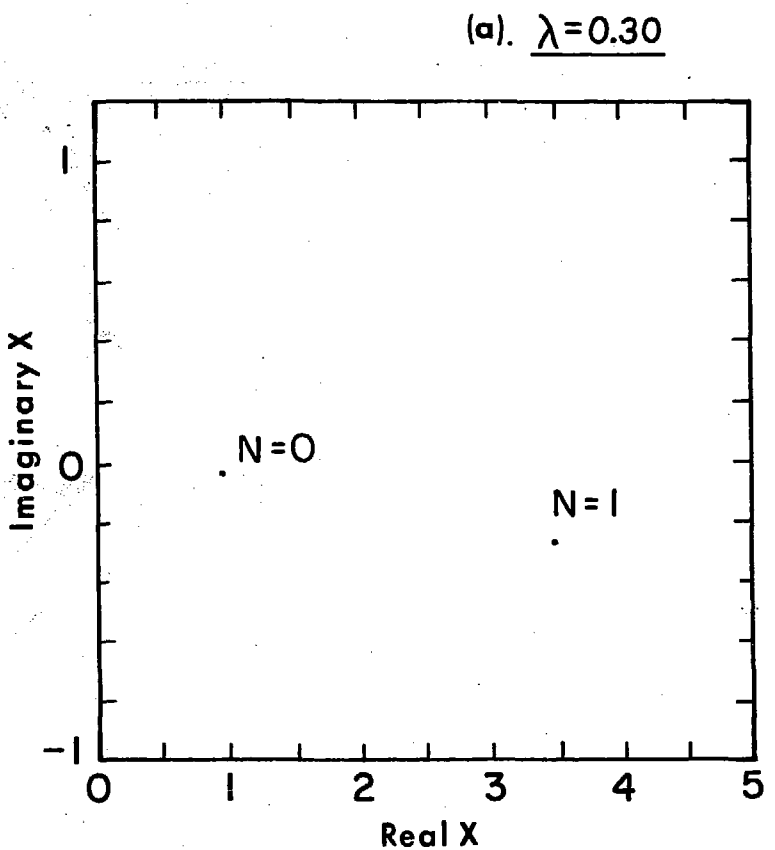

XBL 7610-4201

Fig. V.11a

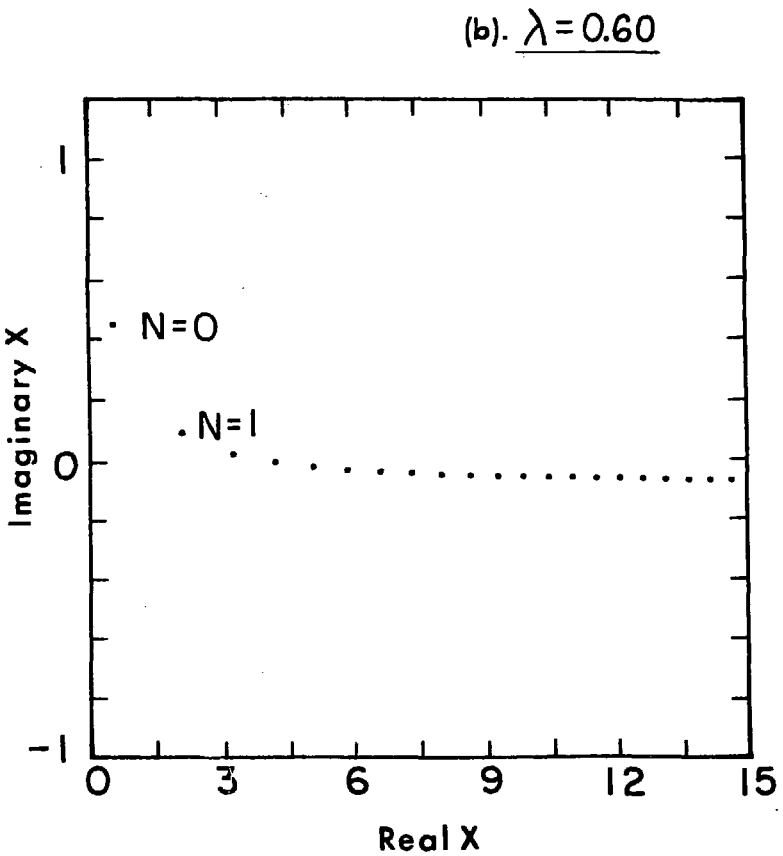

Fig. V.11b XBL 7610-4202

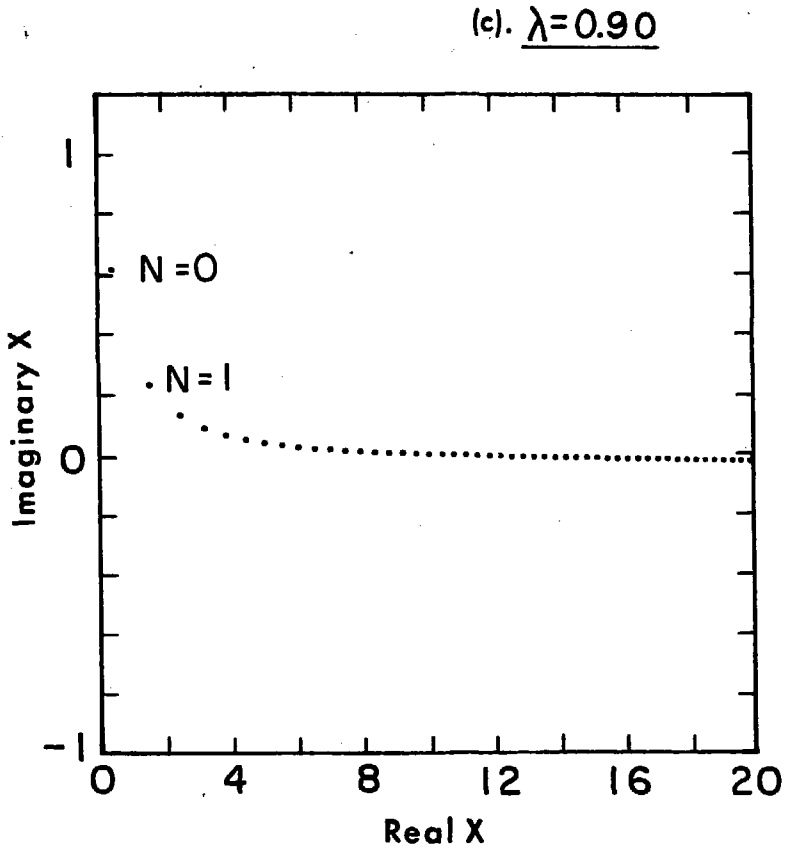

XBL7610-4189

Fig. V.11c

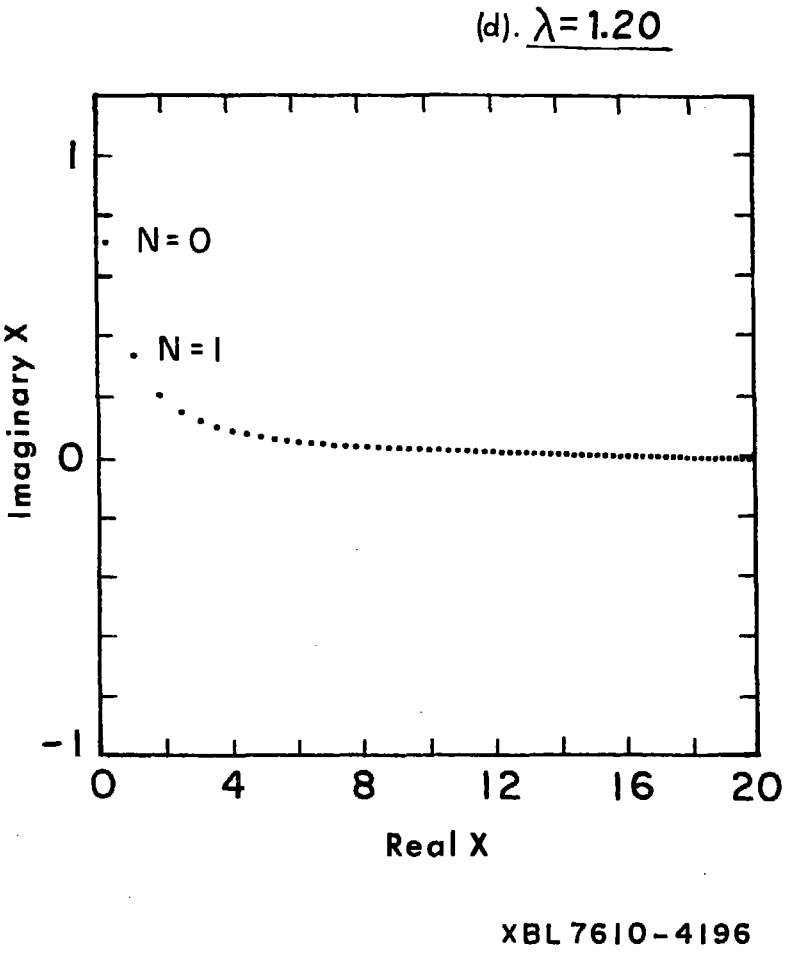

Fig. V.11d

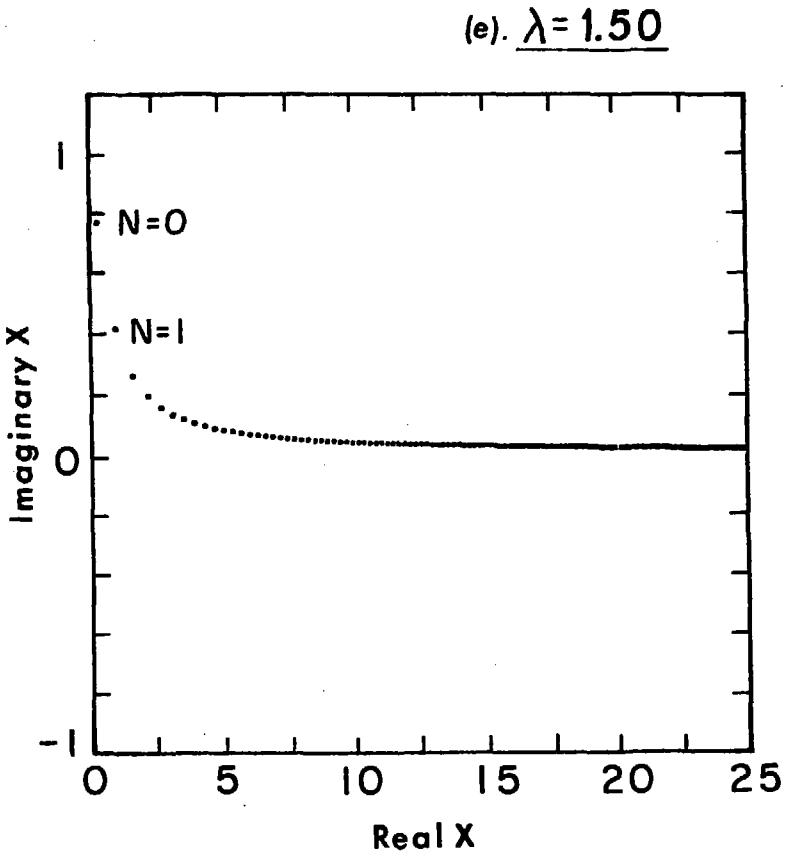

XBL7610-4191

Fig. V.11e

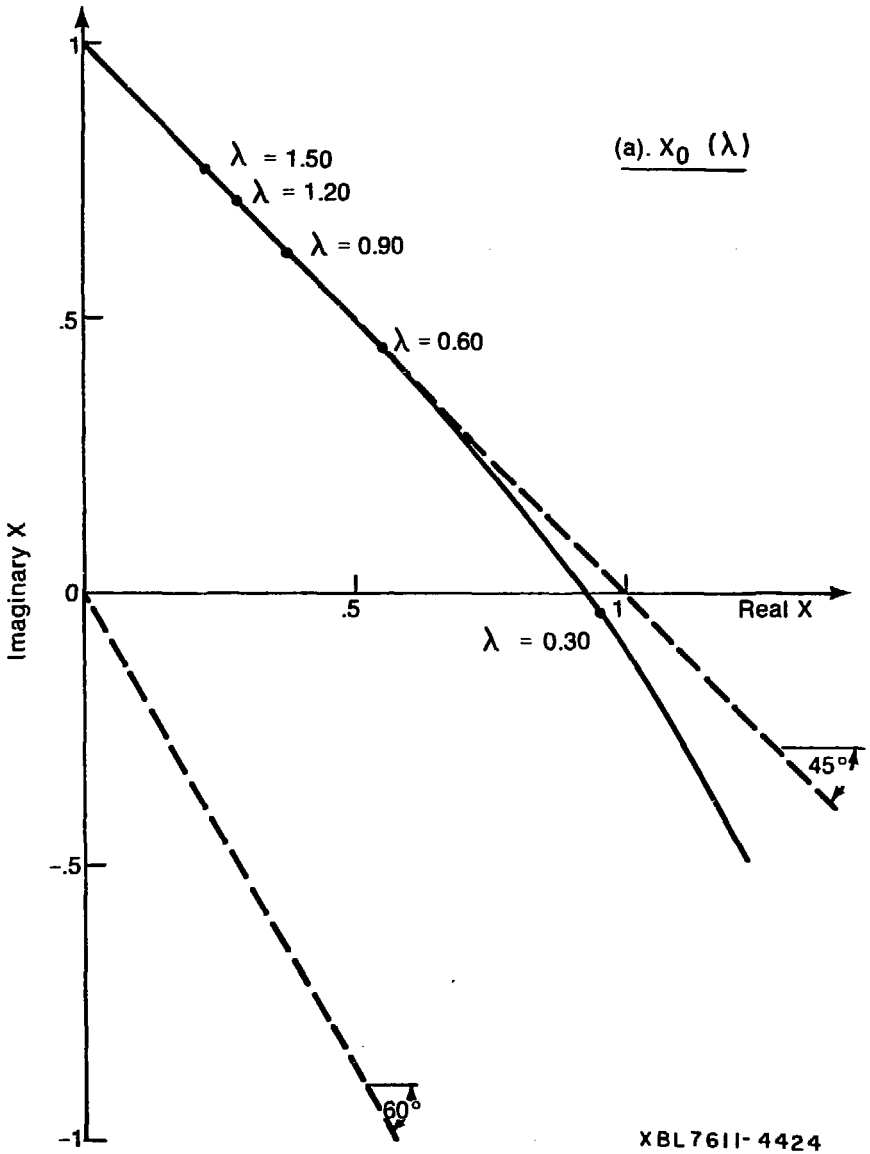
(a). X_0 (λ)
λ = 1.50
λ = 1.20
λ = 0.90
λ = 0.60
λ = 0.30
1
.5
0
-.5
-1
.5
1
Real X
Imaginary X
45°
60°
XBL7611-4424

Fig. V.12a

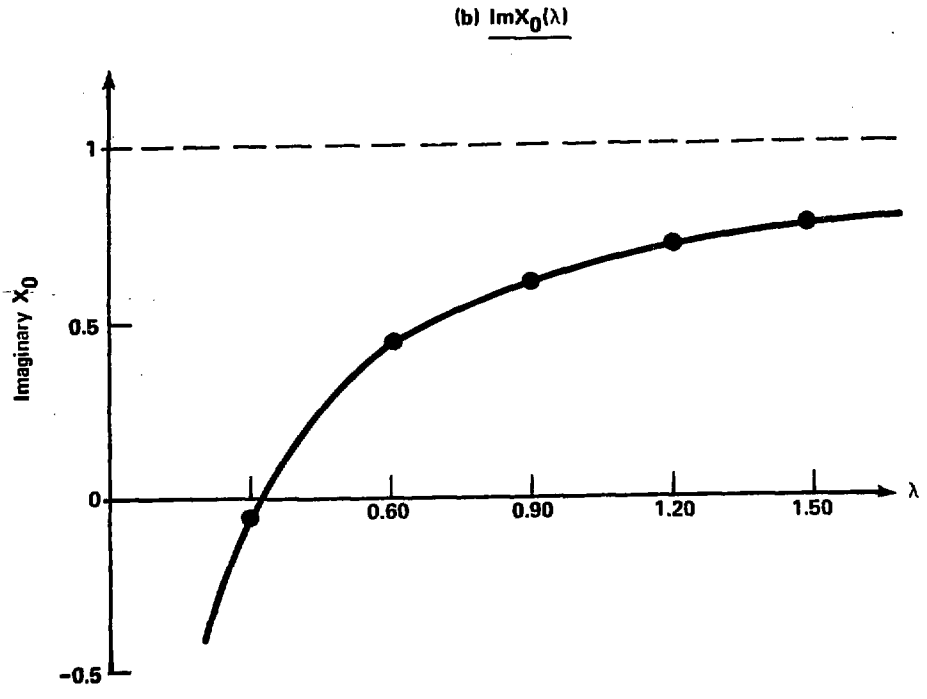

XBL7610-4283

Fig. V.12b

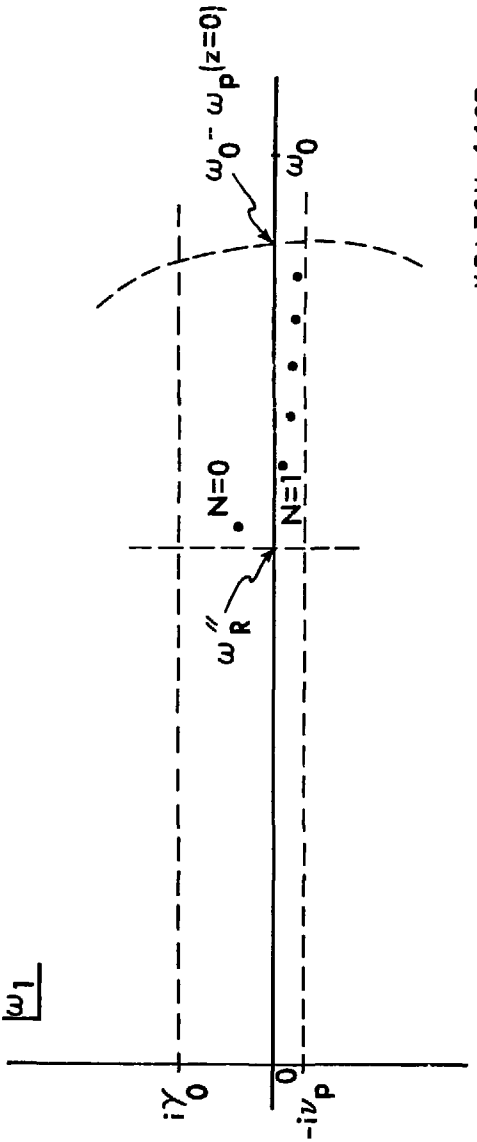

XBL7611-4427

Fig. V.13

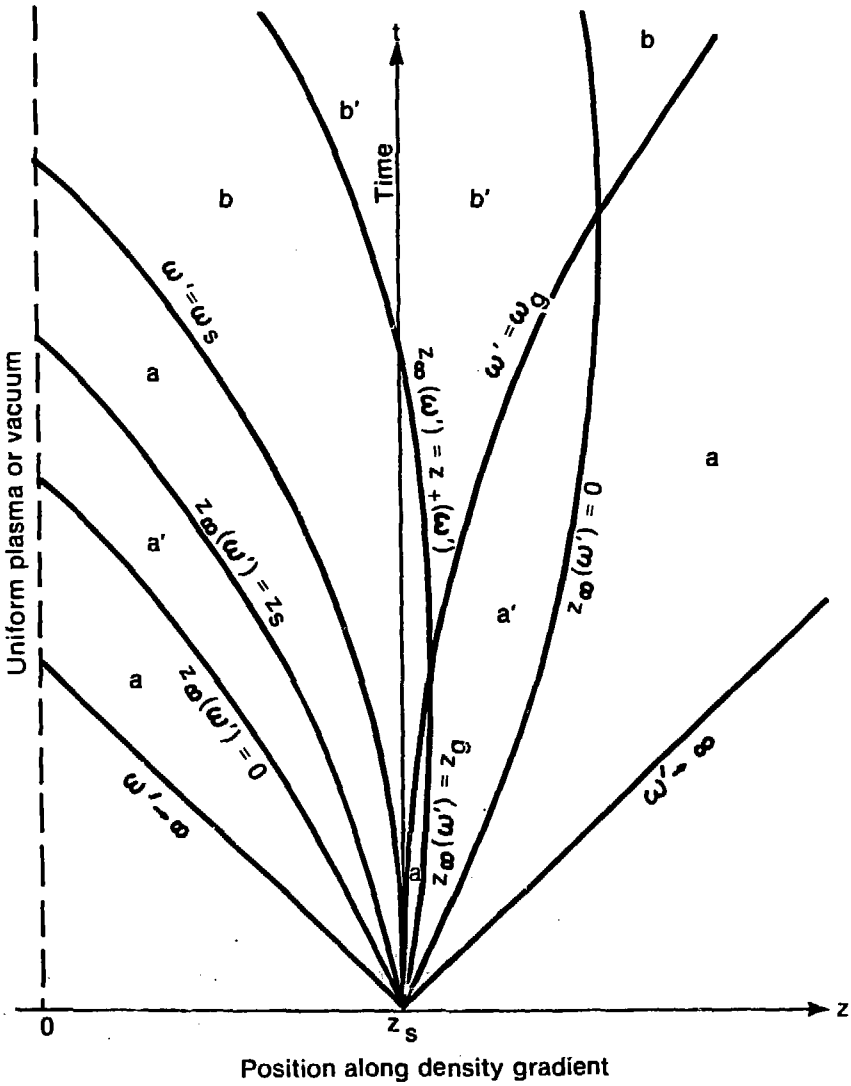

Fig. V.14

XBL7611-4423

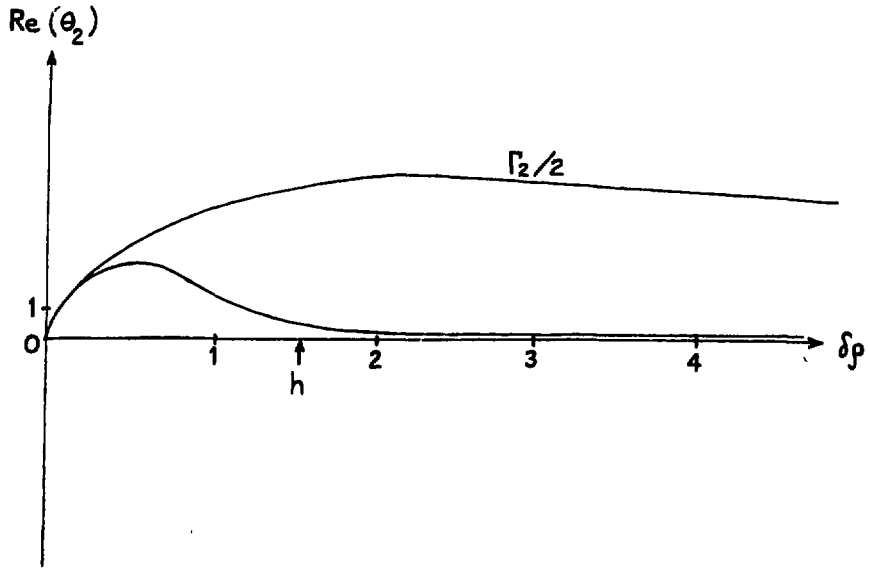

Fig. V.15

XBL 7710-6869